PIEZOELECTRIC FIBER COMPOSITES FOR STRUCTURAL ACTUATION

by

Aaron Alton Bent

B.Eng., Technical University Of Nova Scotia (1991)

Submitted to the Department of Aeronautics and Astronautics in Partial Fulfillment of the Requirement for the Degree of

MASTER OF SCIENCE

at the

MASSACHUSETTS INSTITUTE OF TECHNOLOGY

January 1994

Signature of Author_____
Department of Aeronautics and Astronautics
January 14, 1994

Certified by_____
Professor Nesbitt W. Hagood
Department of Aeronautics and Astronautics
Thesis Supervisor

Accepted by_____
Professor Harold Y. Wachman
Chairman, Department Graduate Committee

Piezoelectric Fiber Composites for Structural Actuation

by

Aaron Alton Bent

Submitted to the Department of Aeronautics and Astronautics
on January 14, 1994 in partial fulfillment of the requirements for the
Degree of Master of Science in Aeronautics and Astronautics

ABSTRACT

Composites with transversely aligned piezoelectric fibers in an epoxy matrix were developed toward the goal of highly distributed structural actuation and sensing. These active composites have addressed the need for anisotropic actuation in a form that reduced the many problems inherent in current monolithic ceramic systems. Response of the composites was predicted through the advancement of five micro-electromechanical models. These models include three Uniform Fields approaches and two elasticity approaches, based on the Self Consistent Scheme and Finite Element Method. These models predicted the effective material properties of the piezoelectric fiber composite for in-plane structural loading problems. Comparison of the models showed good agreement and established a good understanding of the dominant material system design-level issues that needed to be addressed in the program.

Conformable piezoelectric fiber composites were manufactured to investigate the various material level issues. The composites were manufactured using many of the materials and procedures utilized in the graphite/epoxy composite industry. Specimens were manufactured by hand, cured, electroded, and poled to produce active composite test articles. Testing of these articles provided experimental effective material properties, which were compared to models. Good agreement was seen between the predicted and tested piezoelectric and dielectric properties. The mechanical properties exhibited the correct trends predicted by the models, but better constituent material characterization must be carried out before conclusions may be drawn in this area.

At the structural mechanics level, an investigation was made into the field of planar structural actuation with anisotropic active materials. The mechanisms for creating anisotropic actuators were discussed, and the impact of anisotropy was shown at the individual lamina level and at the laminated structure level. Models for laminated structures

were developed using an augmented Classical Laminated Plate Theory incorporating induced stress terms to accommodate anisotropic actuator materials. A twist-extension coupled laminate was used to exemplify how twist can be directly induced into isotropic host structures using anisotropic actuation. Four anisotropic actuators with different material anisotropies were compared using this example. Finally, a laminate incorporating piezoelectric fiber composite actuators was manufactured and tested. Excellent agreement was found between the predicted and experimental response.

Thesis Supervisor: Dr. Nesbitt W. Hagood

Title: Professor of Aeronautics and Astronautics

Acknowledgements

This work was supported by a grant from the Office of Naval Research (grant # N00-14-92-J-4067), with Dr. Wallace Smith serving as technical monitor. We thank them for their support on this project.

The work that this thesis spans is almost two years, although my time here has been closer to two and a half. There are a large number of people who have influenced not only the way I do things, but also a little of who I am. For this reason, I wish to spend a moment to thank those who have helped me along the way.

Being a member of two labs, each of which had a very different focus, has certainly proved interesting. At times it was difficult; there were twice as many meetings, twice as many talks to give, and of course twice as many socials. The natural advantage is that there are twice as many great people to share ideas with and who offer their support. Both the Space Engineering Research Center (SERC) and the Technology Laboratory for Advanced Composites (TELAC) are filled with great people whose strong drive and committment inspired me to always keep working toward my own goals. I wish to thank the directors of both labs, Professor Ed Crawley and Professor Paul Lagace, for their generosity, and their willingness to accept me as a part of their labs.

A warm thankyou goes out to those people who have not only helped me along the way, but who have also been good friends. This includes (but is not necessarily limited to!) Debbie Bowser, Ping Lee, Becky Badertscher, and Albert Supple who have always made things a little easier, and Narendra Bhat who spent many hours helping me sort out one problem or another. Thanks goes out to Lenny Rigione of the Ceramics Processing Research Laboratory (CPRL/MIT), and to Rich Perilli and Tim McClure of the Microelectronics Technology Central Facility (MTCF/MIT), who always made sure that our jobs got done fast when we needed it yesterday. Of course, thanks also to my wonderful UROP helpers Jim Miskel, Zachira Catsro, and Lisa Cohen, who have contributed greatly to my research project and the quality of this thesis.

The people I worked with everyday in the Active Materials group played perhaps the largest part in shaping my experience at MIT. Since so much of my time was actually spent *here*, we saw a lot of one another. We not only went to meetings, gave lab tours, and did experiments together, but we also ate, exercised, watched movies, went hiking, and moved furniture together. It is wonderful to see a group whose spirit is strong. At one time or another we have each sought the help of the others, and the help has always been there. This has been true, whether for a small question or something much larger. I don't

know if I've ever known a group of people as supportive and giving as this one. Thanks guys.

A very special member of the Active Materials group is my advisor, Professor Nesbitt Hagood. He has provided for me, what has been one of the most phenomenal learning experiences in my life. It hasn't always been easy, but it is true that the greatest learning comes from the greatest challenges. In the past two years, I have grown immensely. Certainly the knowledge and understanding have increased, but working with Nesbitt has given much more than that. I have learned to expect more from my work and of myself, and to appreciate the satisfaction that comes from doing a good job. He has given me the freedom to try my own ideas, and the opportunity to experience new situations that many others don't get. There is a great feeling from knowing that someone has the trust in your abilities to make important decisions and help shape the direction of the work. It is an experience that I would never trade.

Finally, I would especially like to thank my family who have been behind me all the way. Thank you to my parents, Sharon Palmer and Foster Bent, who taught me the joy of learning and exploring the wonders of the world at a young age. Their greatest gift to me was making me realize that they would support and love me no matter what road I chose to take in my life. And to Ann Corkum, the most important person in my life, thank you for all the countless sacrifices you have made for us in the past two years. Your unwavering support and understanding has been far more than I could have ever asked for. Your presence in my life has filled my heart and made everday a special one.

Contents

List of Figures

List of Tables

1.0 Introduction

1.1 Motivation

Actuation and sensing is a vital component in the application of controlled structures. Sensors provide information about the structure's state, which may be fed back through a control algorithm to create the appropriate response enacted on the structure by the actuator. More recently, active materials have seen increased application in this area, replacing the traditional electromechanical means for actuation and sensing. Applications of active materials such as shape memory alloys, magnetostrictives, and piezoelectric have given investigators a new means for controlled structures technology.

Piezoelectrics are perhaps the most widely used of the active materials. Their high stiffness gives them high actuation authority, and they can be easily controlled through an applied voltage. They also have high bandwidth, which allows a greater range of applications. Piezoelectrics have typically been utilized as actuators in vibration suppression systems in structures. Coupled electromechanical models of beam and plate structures that incorporate piezoelectrics have been developed. These models have been successfully applied to the problems of piezoelectric passive damping[1] and self-sensing actuation of piezoelectric active structures[2]. Experimental results in closed-loop control of structural vibration[3-7], aeroelastic response[8,9], and acoustic transmission of plates and shells[10,11] have demonstrated the feasibility of active structural control using piezoelectric actuators and sensors.

Despite the past successes, these studies have highlighted the difficulties with piezoelectric materials in structural applications. These difficulties exist at two distinct levels: the material level issues and the structural level issues. The material issues include difficulties inherent in the piezoelectric materials themselves, associated with the generic properties of brittle ceramic materials. Integration into structural applications provide further difficulties, especially when working toward the goal of highly distributed, large scale actuation and sensing.

The material level issues are apparent when working with piezoelectric materials. As with any sintered ceramic, the material is very brittle and easily damaged. Typical applications of piezoelectrics to structures involve very thin monolithic ceramic wafers which do not conform to irregular surfaces, and are often broken during bonding to the structure. A further difficulty is the lead-based nature of piezoceramic, which creates good stiffness properties, but may add a significant penalty to the total structural mass. Distribution of the ceramic into a soft polymer material to form an active composite may

provide a solution to these material issues. This would replace the need for single monolithic pieces of ceramic. If the ceramic in the composite was fine enough, the specific strength would be much higher, and approach the strength of the unflawed ceramic. This would create a lighter and more conformable actuator that would be robust to the structural environment.

Monolithic ceramic actuators also suffer difficulties at the structural level. Conventional means of actuation has usually necessitated bonding the piezoelectric wafers to the outer surface of the structure [3,6]. Future applications will more likely embed the wafers in between regular graphite/epoxy plies in composite structures[7,12]. Incorporation of the monolithic ceramic in the structure can create stress concentrations and significantly reduce the overall strength of the composite[12]. Furthermore, for each actuator embedded, graphite/epoxy must be removed both for the ceramic and for the leads which must deliver electric field. Scaling up of the technology to large structures would require a prohibitive number of leads and inclusions[13]. The introduction of an active layer, in the form of a piezoceramic/polymer composite, would create a strong cohesive structural unit. The active layer could span the entire structure, and be cured into the composite, producing a structure with integrated actuators and sensors. With a single actuator/sensor, only a single electrode is needed, and power could be delivered to the edge of the structure without removing material.

Another issue that spans both the material and structural aspects of actuation is material orthotropy. Presently, it is difficult to distinguish and actuate only a single component of in-plane strain using monolithic ceramics. Due to its isotropic nature, the material actuates all normal components of in-plane strain equally. There is potential for controlling structural deflections independently, in different directions, using high stiffness anisotropic actuators. The current methods require a tailored composite host[14], or complex piezoelectric attachment techniques[15]. This could be simply accomplished using a single uniaxial actuation ply. The anisotropic actuation allows more efficient control of independent structural deflection shapes and could greatly enhance structural control performance. In particular, torsion could be easily induced in even isotropic hosts through the use of different actuator orientations, or a bimorph arrangement of the anisotropic actuators.

Thus, there is a need for conformable distributed actuator/sensor materials which can be easily incorporated into composites and still retain much of the actuation capability of the original ceramic. Continuous PZT fiber composites have been suggested to satisfy this need. The technology now exists to produce continuous piezoelectric fibers with diameters less than 120 microns, and as small as 5-10 microns [16]. These fibers,

when combined with an epoxy matrix, will provide active composite plies that will eventually replace the present monolithic actuators in many applications. Conformability, strength integrity, and anisotropic actuation will now be available to the designer for upcoming structural actuation and sensing needs.

1.2 Objectives

The objective for this project is to study a new technology for highly distributed structural actuation and sensing. This new approach needed to improve on the weaknesses of the current methods without introducing complexities that might otherwise deter its use. Thus, the focus became twofold. The first was to develop the ability to predict effective material properties given the individual phase properties, and carry out design studies to answer questions to key issues. The second was to develop the ability to manufacture the actuator/sensor composite from its constituent materials, and determine the best materials and processes to meet the criteria.

The ultimate goal is to enable large scale structural control applications by controlling the shape and vibration of composite structures using active laminates incorporating electroceramic fiber-reinforced composite plies.

1.3 Background

Piezoelectric fiber composites for structural actuation has its roots in several related research fields. Composite manufacturing and modeling has been evolving for several decades and provides an excellent starting point for the generalization required by active composites. Active composites themselves have been developed in many forms, primarily for ultrasonic transducer applications. The uniqueness of the present objectives will necessitate an understanding of these concepts, but with an emphasis on new methods and materials to achieve the goals of planar actuation.

Three main areas can be identified that are key in the background to development of PFC's: development of actuation materials in the area of adaptive structures, manufacture of active composites for ultrasonic applications, and traditional composite modeling methods. Each of these has a wealth of previous research, some of which is relevant to this problem. The following three sections briefly describe these works.

1.3.1 Active Materials for Adaptive Structures Applications

There is a wide range of active materials that could be used for the active element in a composite. Most of these materials are well established and understood, as many of them were developed 20 years ago or more. However, a few new materials are still

emerging. Some of these materials are obviously better suited for the structural actuation application than others, due to the particular activating field, availability, or ease of use. Specifically, ceramic actuators have been shown to be well suited for structural actuation and sensing applications. Some possibilities include piezoelectrics, electrostrictives, and shape memory ceramics. All of these materials offer high actuation authority through their high Young's modulus. All are easily controlled by the application of an electric field, and due to their quick response speed, these ceramic materials are excellent for high bandwidth actuators. Unfortunately, all are lead based, resulting in a very high density, and all are brittle in the monolithic form.

Electrostrictive materials (PMN or Lead Magnesium Niobate is the most common) are similar to piezoelectrics in that they are a lead-based ceramic, actuated with an electric field. However, the similarities end there. Electrostriction is a nonlinear effect, where the resulting strain depends on the square of the applied electric field. This nonolinearity can increase the difficulty in modeling. Not only are electrostrictive materials dependent on field, they are very sensitive to temperature fluctuations, requiring either a still more complex model or an isothermal environment. Electrostrictives, however, have very low hysteresis, providing high set-point accuracy[17], and the achievable strain levels are relatively high - up to ~0.1%.

Another potential material is shape memory ceramics. At high electric field levels, the ceramic undergoes a phase transition from antiferroelectric to ferroelectric, accompanied by a net volume change in the material. Large strains are observed (on the order of 0.2% to 1%), and the material exhibits the shape memory effect, as it remains in a meta-stable phase after the field is removed. Materials which utilize this phase transformation of antiferroelectric to ferroelectric where explored by Berlincourt[18] in the early 1960's, but are only now being considered for possible use as structural actuators [19]. Despite the exciting possibilities, shape memory ceramics are very difficult to model, requiring rate laws to represent the degree of polarization in the ferroelectric material.

Piezoelectric ceramics are ferroelectric materials that exhibit linear strain relationships with electric field at low field levels. The linear field relationship and small dependence on temperature enable easy modeling of piezoelectrics. PZT materials are also widely used, easily available, and have a whole family of types from which to choose. However, the strain associated with piezoelectrics has a large amount of hysteresis, limiting the applications to those in the dynamic range. The peak strain is also much lower than the shape memory ceramics, approximately 0.1% in the poling

direction). Nonetheless, the ease of use and modeling afforded by piezoelectric ceramics has made them the material of choice for piezoelectric fiber composites.

1.3.2 Active Composites for Ultrasonic Transducers

The purpose of manufacturing composites is almost always to produce a new material with properties superior in some fashion to those of either starting material. The addition of a second phase instantly increases the number of parameters available to customize the material. Not only can the designer specify the materials, but also their relative amounts, shapes, orientations, and manufacturing methods. In this way, it is possible to make use of the best attributes of each material to get a structural characteristic not achievable previously.

Some excellent improvements have been realized with composites. For example, structural composites have made use of strong stiff fibers and softer epoxy matrix materials. The combination guarantees strength and stiffness through the fibers while the matrix provides load transfer capability, shear properties, and conformability. Particles have also been used as the additional phase in various matrix materials to optimize for properties such as permittivity, thermal expansion, and electrical or thermal conductivity.

Composites with active elements have also been optimized to achieve better properties. Two good examples are hydrophones and ultrasonic transducers used in medical imaging. Both are made with piezoelectric ceramic material suspended in a soft epoxy matrix. The introduction of the matrix material [20] reduces the density of the transducer giving better acoustic coupling to water and better buoyancy. The increased compliance not only allows conforming to curved shapes, but increases resistance to mechanical shock and increase damping in the device. In the case of the medical imaging transducer, the two phases allow tailoring to match electrical impedance to the drive electronics and acoustic impedance to that of tissue.

The combination of piezoelectric ceramics with another phase has been coined "piezocomposite." There are many different variations, with the above examples being only two. Key to the discussion on the various types of combinations is the connectivity of each phase[20]. This indicates the manner in which the material is connected along any one axis, and greatly influences the overall properties. The connectivity is indicated by two numbers, the first of which indicates the number of directions of ceramic continuity while the second indicates the same for the second phase. Thus, PZT particles in a matrix is an example of 0-3 composite, while PZT rods in a matrix would be a 1-3 composite. Hydrophones and ultrasonic transducers are typically 1-3 composites.

There are a great many methods of fabrication. For 1-3 "rod" composites, three techniques that have been commonly used include rod alignment, dice-and-fill, and a lamination process, all of which are described in greater detail in Ref[21]. However, none of these techniques produce composites which can be used as structural elements. The rods are aligned out-of-plane of the structure and are incapable of carrying in-plane loads. Thus, the manufacturing process to be developed for the current work must move towards techniques comparable to those in standard graphite-epoxy manufacturing.

One such move in that direction has been attempted by Waller and Safari [22], through a patented technique known as "relic processing." Templates of woven carbon fiber were covered with PZT by soaking the template in a precursor solution. Heat treatment was used to burn out the carbon, leaving a hollow piezoceramic relic of the same form as the original template. The relic is sintered, then impregnated with polymer using a vacuum to gently pull the polymer into the fiber array. Good results were obtained for some of these composites, but there were some difficulties as well. For example, the sintered relic was very fragile and not easy to handle. Also, it was necessary to sand the composites to obtain piezoelectric connectivity between the electrodes. Finally, no modeling to predict these properties was carried out, nor was there any measurements of mechanical properties. Thus, there is still a significant amount of work to be done in carrying over the expertise developed for the acoustic devices to the area of structural actuation.

1.3.3 Modeling of Composites

The third area that this project draws upon is modeling of traditional composites. Composites have been modeled to predict the overall properties, knowing the properties of the materials that comprise the composite. Many methods have been developed that predict effective Young's modulus, Poisson's ratio, shear modulus, thermal expansion coefficients, conductivity, and many more. These models are continually being developed in an attempt to find a better way to represent the bulk response of a diphasic material. Typically, models have been derived for mechanical properties, or for electrical (transport) properties. Modeling of multi-field materials that are coupled electrically and mechanically can be done through a generalization of the techniques that were developed for the single field models. Only recently have investigators begun to develop the ability to predict coupled material response.

A good overview of the field of effective mechanical response is given in Jones [23]. Here, various modeling methods are described for determining the effective material stiffness constants. Probably the most basic approach is the Mechanics of

Materials approach, which uses the one-dimensional parallel and series spring analogy for the effective longitudinal and transverse stiffness, respectively. Gross approximations are made regarding the fields within the structure and the geometry of the fibers, resulting in a low estimate of the transverse properties.

Elasticity models such as those presented by Hermans[24], Hashin and Rosen[25], and Whitney and Riley[26] attempt to improve on the transverse property prediction. These models are a boundary value problem and involve solving for the stress/strain fields within a typical fiber and its surrounding matrix such that the fields are consistent with those of the bulk material. Considerations of fiber contiguity (fibers touching in some locations) and packing geometry next lead researches to consider semi-empirical methods. Perhaps the most widely used are the Halpin-Tsai relations. This method is an elasticity technique that gives bounds for the moduli depending on whether the fibers are isolated and resin contiguous, or, fibers contiguous and the matrix isolated. The principle is very similar to the discussion of connectivity given in the previous section.

Models have also been pursued for effective transport properties. These include the permittivity, permeability, heat conductivity, and electric conductivity. (The solution for one of these yields the solution for all of them, as the problems are analogous). A brief but excellent summary of the available models is presented in [27]. Interestingly enough, many of the methods used in the mechanical modeling have also been applied to the electrical models. A parallel series approach is taken by Thornborough and Pears[28] to model the effective conductivity, but with a somewhat arbitrary method of specifying geometry fractions. A multitude of researchers utilized some form of the consistent fields elasticity approach, with variations on geometry and equivalent volume fractions, to yield the effective conductivity.

Some of the more noted works were conducted for particulate composites and include authors such as Lord Rayleigh[29], Landauer[30], Kerner[31], and Hashin[32]. An extension to fibrous composites was done by Farmer and Covert [33] using methods similar to the elasticity approach by Hashin for particulate composites. Variational methods by Hashin and Shtrikman[34] give bounds to the particulate problem that correspond to the curves by Kerner and by Hashin. Finally, a discrete numerical technique termed boundary collocation was employed by Han and Cosner [35] that matches the boundary conditions in the problem only at discrete locations in the representative volume element.

Extending these methods to the coupled field analysis is a non-trivial matter. As section 2.2 will show, there now exists two governing equations to describe the electrical and mechanical field distributions in a piezoelectric material. These equations are

coupled to one another through the piezoelectric coefficients. Simplifications in the geometry or the field distributions can and have been made to allow the solution of these problems. There are also certain classes of problems where the mechanical and electrical problems decouple due to the choice of loading and poling directions. In these cases, the two problems may be solved separately and are only coupled through the constitutive equations.

Key research in these area of modeling has been performed by only a few researchers. Newnham et al.[20] seem to be the first to apply the parallel-series approach to piezocomposites. They developed one-dimensional models that largely ignored material coupling in other directions and made assumptions as to the relative stiffness and volume fractions of the two phases. Nonetheless, the work made important points as the governing factors that contributed to the bulk properties. An extension of this work to the three-dimensional spherical inclusion problem was done by Banno[36]. He again made many of the same approximations. The move to fibrous composites was made by Smith and Auld[37] to determine the effective stiffness, dielectric, and coupling coefficients for 31 connectivity rod composites in ultrasonic transducers.

Elasticity approaches to piezoelectric problems are extremely rare. Two such models are given in Pak[38] and Honein et al.[39] for the anti-plane piezoelectricity problem. In this problem, the authors consider a piezoelectric inclusion in an infinite media with far-field applied electric field and out-of-plane shear. Due to the particular geometry and loads, the problem is coupled only through the piezoelectric material constitutive relations, and a closed form solution is possible. Pak uses a series expansion for the displacement and electric fields, while Honein et al. use complex potentials and conformal mapping to produce a solution. A further elasticity model has recently been developed by Sottos[40].

1.4 The General Approach to Piezoelectric Fiber Composites

The difficulties associated with monolithic ceramic actuators were outlined in the Motivation section of this chapter, and include poor conformability, strength, and reliability. These derive from the more fundamental issue of a segmented system, where the ceramic elements are actually intrusive to the overall structure. A new, more systemic approach is needed for the development of structural actuation and sensing on a large scale. Such a solution is shown in Figure 1.1. Rather than embedding single actuator/sensors into the structure, a continuous active ply may be incorporated between standard graphite/epoxy composite plies. An interlaminar electrode acts as an interface between plies and delivers electric field to the active component. Following cure, this

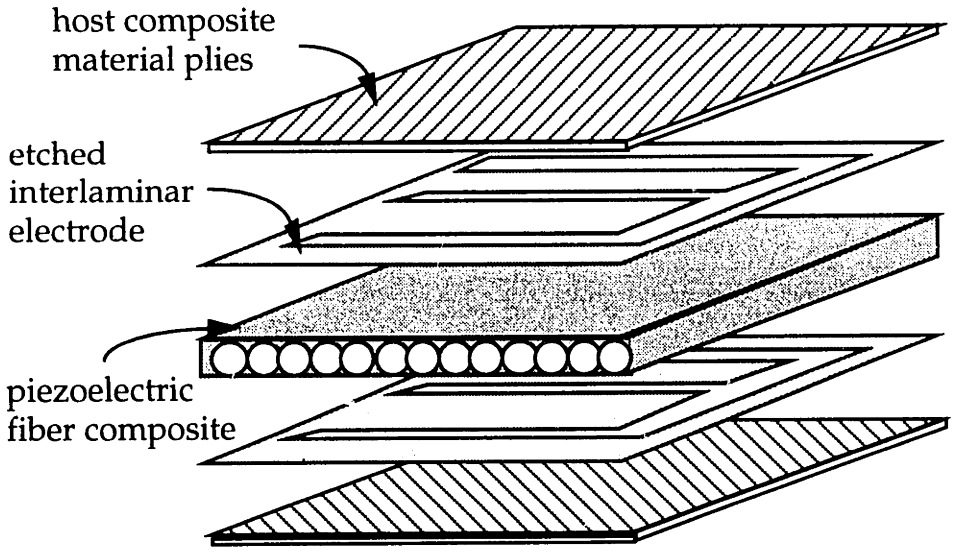

Figure 1.1: General approach to built-up active structures

active ply becomes a part of the structure, preserving the continuity, and creating an integrated built-up structure.

The active subply is electroded on the top and bottom surfaces (Figure 1.2), so that poling aligns the dipoles through the composite thickness (3-direction). After poling, an applied field results in primary strain in the 3-direction, and strain in-plane (1- and 2-directions) due to the transverse piezoelectric effect. In the built-up structure these electrodes would have to be insulated from adjacent graphite epoxy plies, but may have to be porous to allow resin flow. Resin flow is necessary for compacting of the laminate during cure and to create a bond with the active sub ply.

The problem then becomes the need to develop a method by which sensor/actuator material can be distributed within a matrix to create active composite plies. In the past, configurations for ultrasonic transducers have ranged from PVDF film and particulate ceramics where the ceramic has no connectivity in any direction, to replamine ceramics with ceramic connectivity in all 3 directions. A brief overview of this field was given in the previous section. Structural actuation and sensing, unlike previous acoustic applications, must couple to structural stresses and strains which are typically in-plane and transverse to the thickness. To actuate transverse structural deflections, the ceramic connectivity should be in the plane of the structure. The chosen configuration features the electroceramic in fiber form, which results in a fiber composite material of uniaxial actuation and in-plane sensing. Such a configuration is shown in Figure 1.2. This option is particularly attractive since it allows tailoring of anisotropic actuation in

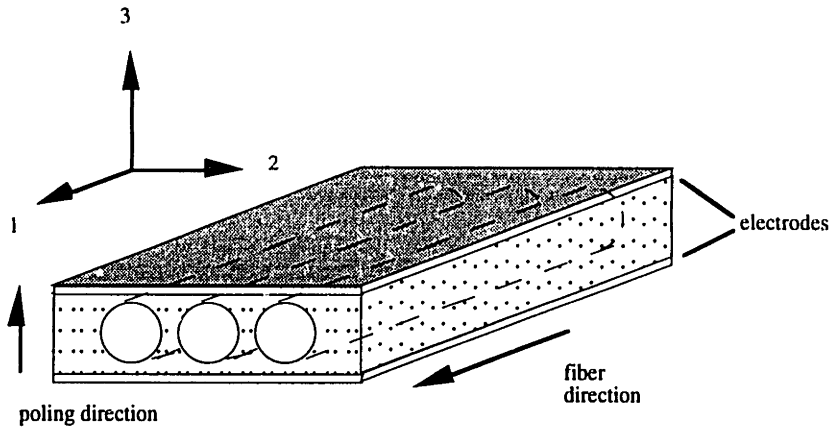

Figure 1.2: Piezoceramic fibers in active composite sub ply

the plane of the structure. Such anisotropic actuation is essential for inducing twist in laminated structures, and is an important property for aeroelastic surface control.

Manufacturing techniques for the piezoceramic fibers have been established and piezoceramic fibers have been produced in diameters small enough to incorporate into a structural ply. Although, at present, these fibers are typically fabricated at a fixed length, several novel techniques including PZT relic processing[22] and sol-gel processing[16] hold promise of continuous fibers for future applications. Eventually, such continuous fibers will allow processing similar to that of conventional graphite/epoxy composites, where pre-impregnated plies can be laid-up with varying ply angles.

1.5 Key Design Issues

There are several major issues that are integral to the design of the active structure. These may be separated into two general categories: issues at the material level, and issues at the structural level. Issues at the material level deal primarily with the active subply, and its constitutive phase materials. Integration into a larger, built-up structure is also a concern and makes up the structural level issues. These issues are presented here because they motivate some of the decisions made early in the design process, and help to outline the difficulties facing the development of this new technology.

1.5.1 Material Issues

The benefits of composite materials is to provide tailorable properties whose attributes are advantageous over those of each material type alone. Obviously, the effective mechanical and electrical properties will lie somewhere between those of the

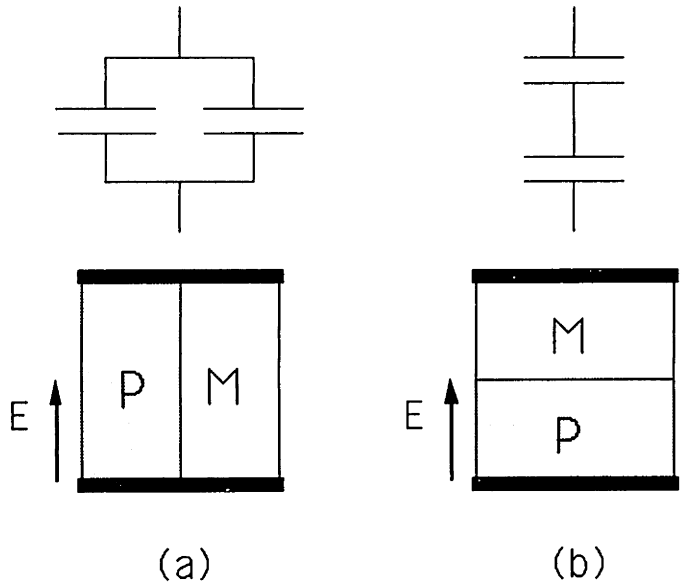

Figure 1.3: Two one-dimensional cases for material connectivity in piezoceramic (p) and matrix (m) combinations

two phases, and it is the job of modeling to provide a better idea of where this may be. More often than not, however, the design is actually a tradeoff. The favorable properties of a particular material are inevitably lessened as more of the second material is introduced. In this instance, the high piezoelectric properties are traded for a more conformable anisotropic actuator.

How the tradeoff occurs is largely governed by the relative sizes of the various properties. Although a large mismatch between the properties increases the range of tailoring possibilities, it also presents certain difficulties that are not always obvious. The materials being combined here are strongly mismatched. The polymer may be 20-100 times more compliant, and have a dielectric between 500 and 1000 times less than the piezoelectric ceramic.

The effect of this stiffness mismatch is not hard to predict: the much stiffer ceramic will govern the behavior in any direction it has connectivity (ie., along the fibers), but the polymer will have a much larger influence in the other directions (transverse to the fibers). The importance of the dielectric mismatch is not as obvious, but can be illustrated with a simple example.

Figure 1.3 shows two possible cases of simple one-dimensional material connectivity between the electrodes. Ignoring stress coupling, the problem becomes that of two capacitors in either parallel or series. From a basic physics text, it is possible to write the electric field in the piezoelectric, Ep, as a ratio of the electric field applied, $\overline{E}$. For the parallel case, Figure 1.3 (a), it is obvious that

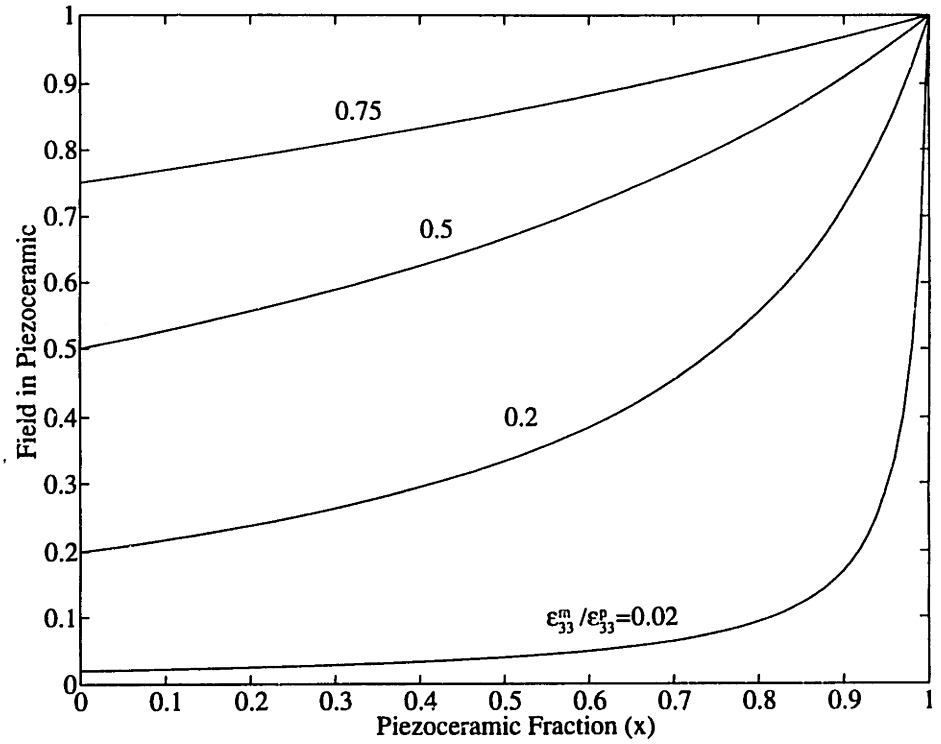

Figure 1.4: Effect of dielectric mismatch in two-phase materials

$$\frac{E^p}{\overline{E}} = 1 \tag{1.1}$$

That is, the field applied to the whole material is also that applied to the piezoelectric, by virtue of the electrodes. Thus, the piezoelectric will have the full field available to it for actuation. In the series case (Figure 1.3 (b)), however, the electric field in the piezoelectric is not that of the overall field:

$$\frac{E^p}{\overline{E}} = \frac{\varepsilon_3^m / \varepsilon_3^p}{\varepsilon_3^m / \varepsilon_3^p x + (1-x)} \tag{1.2}$$

where x is the ratio of piezoceramic thickness to total thickness. The field in the piezoelectric is some fraction of the overall field, and is dependent on both the amount of piezoelectric (x) and the dielectric mismatch ($\varepsilon_3^m/\varepsilon_3^p$). A plot of the field is shown in Figure 1.4 and it quickly becomes apparent that the dielectric mismatch between materials has a significant effect. For high mismatches, very little of the electric field actually reaches the piezoelectric, drastically reducing the potential for actuation.

This example serves to highlight one of the key issues in the design of a composite actuator, and much of the effort has been directed toward maximizing the actuation through lower dielectric mismatch. In Chapter 4.0, a study is described that

deals with modifying the matrix material in order to increase its dielectric, thus, reducing the dielectric mismatch. Chapter 6.0 outlines the manufacturing techniques and describes methods used to maximize the percentage of piezoelectric between the electrodes.

1.5.2 Structural Issues

Application of the piezoelectric fiber composites will see the incorporation of the active subply into regular graphite/epoxy plies, creating the built-up active structure. For successful integration, it will be necessary to consider issues of material compatibility, strength, load transfer, and overall reliability. One critical zone that influences all of these aspects will be the interface joining the graphite/epoxy plies with the active composite. Since this interface will include the interlaminar electrode, it is important to consider how the choice of electrode will affect the structure.

The interlaminar electrode serves the primary purpose of delivering electric field to the active composite. As such, it must include a layer of highly conductive material (i.e. a metal). Initially, the electrode material could consist of metal vapor-deposited onto the active composite surface. This would be sufficient for studies of the active composite response, but may not serve well for incorporation into other plies. The graphite fibers are also conductive and may provide paths that will short-circuit the applied fields.

This problem can be overcome by using sheets of metalized polyimide (available as thin as 0.5 mil) as an insulating electrode. The polyimide substrate would serve to electrically separate the two conducting materials. Another benefit of these types of electrodes is the possibility for etching the metal, so that certain electrode patterns may be utilized. Some novel electrode patterns been advantageous in active vibration suppression [41] and in improving transverse actuation anisotropy [42]. It is unlikely that patterned electrodes could be applied onto the active composite through a vapor deposition process.

The majority of the reliability and strength of the final integrated composite will depend on the adhesion at the interlaminar surface. Loads will be transferred between the adjoining plies through the interface layer. An incompatible electrode material will promote poor adhesion, and tend to delaminate under low loads. One way to encourage better adhesion will be to cure the active and passive composites together (co-cure), and allow the resins to cure to one another. This occurs in regular graphite/epoxy composites, and creates a very strong bond between the adjoining plies through this interface layer. The only difficulty here will be the electrode layer separating the plies. A possible solution is to finely perforate the polyimide/metal sheets with very small holes. This will

maintain the electrical conductivity, but allow the resins to flow between the various plies and create a strong integrated structure.

1.6 Overview of Thesis

This first chapter has served as an introduction into piezoelectric fiber composites. It provided a motivation for the study and showed how this new direction can make vast improvements over the current actuation technology. The near and long term goals were summarized with an emphasis on the main thrust for the present study. The Background section provided a framework for building upon these goals by discussing previous research in related areas as they pertain to the materials, composite manufacturing process, and material modeling. The general approach to built-up active structures followed, whose geometry is driven by the technology's purpose: the need to couple to in-plane structural behavior. Finally, some of the difficulties and key design issues were highlighted, providing a path in the development of piezoelectric fiber composites.

Chapter 2.0 deals with the mechanics of piezoelectric materials in order to lay the foundation for future modeling of piezoelectric fiber composites. Equations of elasticity and electrostatics for describing the field distributions in matter are presented. The coupling among elastic and electric fields is introduced through a development of the constitutive relations from the energy considerations. The reduced problems of plane stress and modified plane strain are derived, starting from the basic forms of the presented relationships. These reduced relations are utilized in future chapters.

Chapter 3.0 develops the models for predicting the bulk composite response using the foundation built in Chapter 2.0. Two different approaches to modeling, Mechanics of Materials and Elasticity, are used to determine the effective properties of the fibrous composite. Assumptions are validated through comparing the various models, and the tradeoffs occurring between the two phases are shown in design curves. Finally, a return is made to the key design issues first dealt with in section 1.5. These issues are discussed in light of the new models presented.

Chapter 4.0 centers around the matrix material and the importance of its properties to the processing and bulk properties of the composite. In particular, material mismatches introduced in section 1.5.2 and discussed in section 3.6 are once again dealt with here. However, the emphasis is on how the matrix material may be modified to make it optimal for combining with piezoelectric fibers. High dielectric particulate and surface modifying agents are added to the matrix material to make a hybrid matrix with new stiffness and dielectric properties. Experimental results for hybrid matrix materials are compared to various simple transport and elasticity models.

Chapter 5.0 investigates the mechanics of anisotropic actuation. The concept of induced stress actuation is introduced and related to actuation of structures through Classical Laminated Plate Theory. A special twist-extension laminate is chosen to exemplify anisotropic actuation in isotropic substrate structures and highlight a comparison of available and hypothetical anisotropic actuators. This laminate example is carried over experimentally in Chapters 6.0 and 7.0.

Chapter 6.0 outlines the manufacturing techniques for piezoelectric fiber composites. Preliminary manufacturing findings are summarized and used to define the needs for a successful process. The properties that are important in a manufactured specimen with respect to uniformity and geometrical arrangement are also defined. Next, the manufactured procedure is detailed from mold setup and lay-up techniques, to the actual curing process. Electroding and poling are described in the final steps of sample preparation prior to testing. Finally, some more recent methods of manufacturing are described for the manufacture of the fiber composites used in the twist-extension laminate.

Chapter 7.0 presents the experimental methods used for the testing of piezoelectric fiber composites and the results obtained from the testing. The first part of the chapter describes the methods used to determine the effective mechanical, electrical, and piezoelectric properties of the fiber composite. The results are shown and discussed with reference to one of the Uniform Fields models. The last section details the testing and results of the twist-extension coupled laminate.

Chapter 8.0, the final chapter, closes the thesis with a summary of the presented work.

2.0 Introduction to Piezoelectric Materials

2.1 Overview

Chapter 1.0 provided the motivation for the study of piezoelectric fiber composites, and outlined the improvements that can be derived form the development of this new technology. A necessary step in this development is the modeling of active composite response, which is given in Chapter 3.0. However, prior to dealing with the interaction of the various material phases, it is necessary to understand the mechanics of piezoelectric materials. Chapter 2.0 sets the stage for further analysis of active composites that incorporate piezoelectric materials.

The chapter begins by presenting the equations that govern the distribution of electric and elastic fields in matter. These are complemented by the necessary boundary conditions to describe the constraints at the material interfaces. Piezoelectric materials are introduced next, with a description of the piezoelectric conventions and material characteristics. Relationships between the field variables given in the field equations are derived from the energy considreations, and reduced to the well known constitutive relations. This is generalized to matrix notation for easier manipulations in later sections. Various constitutive forms are presented, with an example that shows relationships between several of the forms. Finally, special forms of these relations are developed that describe the reduced problems of plane stress and modified plane strain. The relations shown in this chapter may be applied also to non-active materials.

2.2 Analysis of Continuum in Matter

The term micro mechanics, as defined by Jones[23], is "the study of composite material wherein the interaction of the constituent materials is examined in detail as part of the definition of the behavior of the heterogeneous composite material." The present work considers micro mechanics in a more general sense, whereby a model of the material provides relations that govern the response of that material. This model may be derived in an analytical or empirical manner. If empirical, then the properties are simply measured. If analytical, then the material is studied at a level where it appears heterogeneous and it is necessary to consider the interaction between the individual pieces. (For a composite, these would be the matrix and fiber; for a crystalline material, this would be the individual crystal grain structures.) Either method may be used to obtain the model for the material's response. In the current work, the models for the piezoelectric and matrix materials are

assumed known through empirical methods. These models are represented by the material's constitutive relation. However, the model of the *composite* response is found both analytically (Chapter 3.0) and empirically (Chapter 6.0).

How the fields vary from location to location within a body necessitates a continuum mechanics viewpoint. Stresses and strains cannot distribute themselves randomly, but are subject to the constraints of equilibrium and compatibility. Likewise, equations of electrostatics govern the distribution of electrical fields and charges. The proper combination of elasticity and electrostatics, with the introduction of the material constitutive equations, provides the coupled governing equation for the piezoelectric problem, presented in Chapter 3.0.

The first step is to consider the equations that govern the field distributions within a body.

2.2.1 Mechanical and Electrical Field Relations

Electric Field Equations:

The following equations of electrostatics, given in Tiersten[43], govern the distribution of charge and electric field within a homogeneous body. The charge distribution is described by the charge flux, **D**, also known as the electrical displacement. Its distribution is given by:

$$\text{div}\mathbf{D} = \nabla \cdot \mathbf{D} = \rho_f \tag{2.1}$$

where ρ_f is the net free charge of the body, and ∇(del) is the first order operator,

$$\nabla = \mathbf{e}_1 \frac{\partial}{\partial x_1} + \mathbf{e}_2 \frac{\partial}{\partial x_2} + \mathbf{e}_3 \frac{\partial}{\partial x_3} \tag{2.2}$$

The electric field distribution can be similarly defined as:

$$\text{curl}\mathbf{E} = \nabla \times \mathbf{E} = 0 \tag{2.3}$$

These two equations are the primary equations of electrostatics. Further analysis requires a relationship between the two field variables. For a simple media of dielectric ε, this is

$$\mathbf{D} = \varepsilon \mathbf{E} \tag{2.4}$$

This is also known as the electrical constitutive relationship for the material. This may be combined with equation (2.1) to give Gauss' Law for dielectrics:

$$\nabla \cdot \mathbf{E} = \frac{\rho_f}{\varepsilon} \tag{2.5}$$

Equations (2.3) and (2.5) now uniquely describe the distribution of electric fields within a body of dielectric ε. Solution of the problem is often presented through the use of the field potential equation, which defines the electric field in terms of a scalar potential function, Φ, which satisfies equation (2.3).

$$\mathbf{E} = -\nabla\Phi \tag{2.6}$$

Combining equations (2.5) and (2.6) provides the familiar Poisson's equation:

$$\nabla^2\Phi = -\frac{\rho_f}{\varepsilon} \tag{2.7}$$

The appropriate boundary conditions are found by considering the junction of two materials, a and b. Air may be treated as a limiting case for his problem. The derivation is not given here, but may be found in Ref[43]. The boundary conditions are:

$$\begin{aligned} \mathbf{n}\cdot(\mathbf{D}_b - \mathbf{D}_a) = \sigma \quad &\rightarrow \quad \mathbf{D}_b^{normal} = \mathbf{D}_a^{normal} \\ \mathbf{n}\times(\mathbf{E}_b - \mathbf{E}_a) = 0 \quad &\rightarrow \quad \Phi_b = \Phi_a \end{aligned} \tag{2.8}$$

where $\mathbf{n}$ is the outward normal vector, and subscript a and b represent the two materials. The first boundary condition states that the normal components of the electrical displacement must remain constant across the boundary interface. The second shows that the scalar potential along the boundary of each material must be equal. These boundary conditions, applied to the solution of equation (2.7), allow for the solution of the electrical field distribution in dielectric materials.

Elastic Field Equations:

A similar approach may be taken for the elastic field distribution in materials. The distribution of forces is governed by the stress equilibrium equation [43]:

$$\nabla \cdot \mathbf{T} = -\mathbf{f} + \rho\ddot{\mathbf{u}} \tag{2.9}$$

where $\mathbf{T}$ is the vector of material stresses, $\mathbf{f}$ the body forces, and $\ddot{\mathbf{u}}$ the vector of second derivative displacements. Constraints are placed on the resulting strains so that they describe an admissible displacement field. These conditions are given by the equations of compatibility, for which a single vector form is not available. Instead, it may be given in tensor form:

$$\frac{\partial^2 S_{nk}}{\partial x_m \partial x_l} + \frac{\partial^2 S_{ml}}{\partial x_n \partial x_k} - \frac{\partial^2 S_{nl}}{\partial x_m \partial x_k} - \frac{\partial^2 S_{km}}{\partial x_l \partial x_n} = 0 \tag{2.10}$$

These two equations are the primary equations of elasticity. A further analysis requires a relationship between the stresses and strains, which come from a knowledge of

the material constitutive relationships. A typical problem in elasticity allows some simplification from a full three dimensional analysis. In these cases, it is possible to consider derivation of the governing differential equation in terms of a single potential, just as was done in the electrostatics problem. At the present level, this is not possible, and will be discussed in Chapter 3.

Just as the electric field could be related to a potential function through a differential relationship, the strains may be related to the displacements through the following:

$$S_{ij} = \frac{1}{2}(u_{i,j} + u_{j,i}) \tag{2.11}$$

The boundary conditions may be stated for the full elasticity problem. These can also be simplified to represent a reduced problem.

$$\begin{aligned} t_i &= T_{ij} n_j = \hat{t}_i \\ u_i &= \hat{u}_i \end{aligned} \tag{2.12}$$

The first boundary condition states that the tractions, t, which may be found from the components of stress T_{ij} and the outward normal n_j, must be equal to the prescribed traction, $\hat{t}_i$. The second boundary condition specifies that the displacements u_i at the boundary must be equal to the prescribed displacements, $\hat{u}_i$. In both cases, the prescribed conditions may be defined by the presence of a second material.

2.2.2 Piezoelectric Materials

Material Conventions

Piezoelectric materials, like all poled ferroelectric ceramics, are transversely isotropic. That is, one plane of the material is isotropic, while the out-of-plane direction has properties different from the other two. This anisotropy is caused by the poling of the material, which aligns the dipoles in a specific direction. Prior to poling, the material is isotropic and actually exhibits no piezoelectric effect. By the convention given in Ref[44], the plane of isotropy is labeled the 1-2 plane, and the out-of-plane direction is always labeled the 3 direction (Figure 2.1). Thus it is along the 3 direction that the dipoles align, causing an increase in the material compliance, dielectric, and piezoelectric constants.

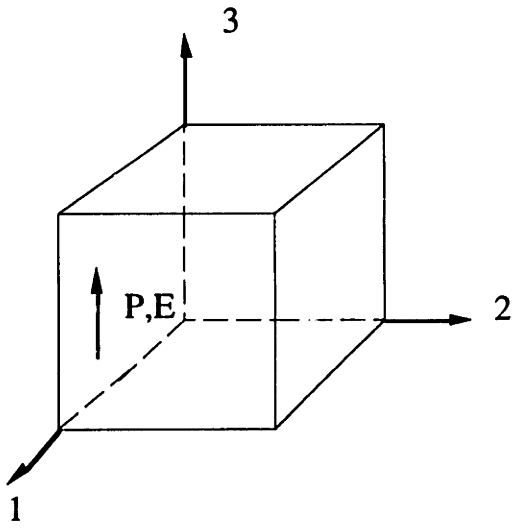

Figure 2.1: Material axes definitions for piezoelectric crystals

The poling process occurs through the application of a high electric field, aligning the dipoles as shown in Figure 2.2. During the poling process, the alignment causes strains to occur in all three directions. If a sufficiently high field was used, much of the strain will remain, even after the field is removed. Further application of an electric field in the same polarity will cause elongation in the 3 direction, accompanied by a shortening in the 1 and 2 directions. A field in the opposite direction will produce equivalent strain, but of the opposite sign. However, a high field of polarity opposite to the original poling field will tend to depole the material and begin poling in the other direction.

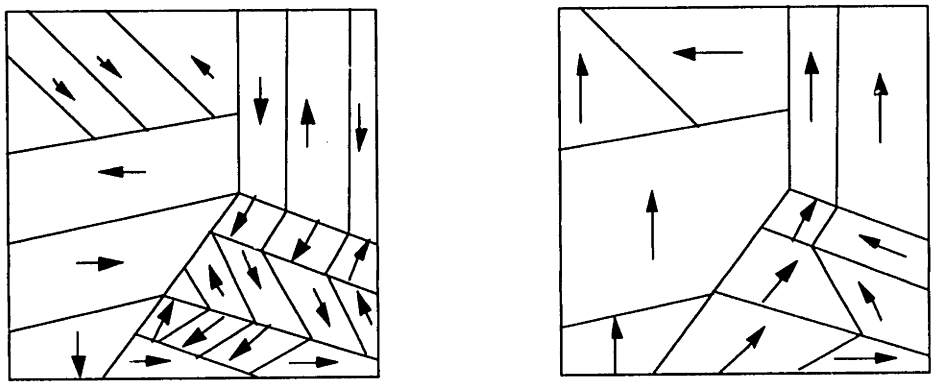

Figure 2.2: Alignment of material crystal dipoles due to application of polarization field, from Ref[45].

Constitutive Relations

The following development of the constitutive relations is given in more detail in Ref[46]. The derivation is based on a consideration of the total contribution to an increase in strain energy of a system by a change in the equations of state of that system. For piezoelectric materials, this includes both electrical and elastic contributions[1]:

$$dU = T_{ij}dS_{ij} + E_k dD_k \tag{2.13}$$

where T_{ij} are the material stresses, S_{ij} the material strains, E_k the electrical field, and D_k the electrical displacement. A change in the dependent state variables is made through a Legendre transformation. The resulting energy expression is defined as Gibb's Free Energy, G:

$$G = U - T_{ij}S_{ij} - E_k D_k \tag{2.14}$$

Taking the derivative of Gibb's energy produces the following

$$dG = dU - T_{ij}dS_{ij} - S_{ij}dT_{ij} - D_k dE_k - E_k dD_k \tag{2.15}$$

and after simplification,

$$dG = -S_{ij}dT_{ij} - D_k dE_k \tag{2.16}$$

Examining the change in the free energy with respect to a field variable, with all others held constant, defines the relationships between the states. The following variables are defined as the dependent equations of state:

$$\begin{aligned} D_k &= \left(\frac{dG}{dE_k}\right)_S \qquad E \ \text{constant} \\ T_{ij} &= \left(\frac{dG}{dS_{ij}}\right)_E \qquad S \ \text{constant} \end{aligned} \tag{2.17}$$

and the following relationships are found for the state variables:

$$\begin{aligned} dT_{ij} &= \left(\frac{dT_{ij}}{dS_{kl}}\right)_E dS_{kl} - \left(\frac{dT_{ij}}{dE_k}\right)_S dE_k \\ dD_i &= \left(\frac{dD_i}{dS_{kl}}\right)_E dS_{kl} + \left(\frac{dD_i}{dE_k}\right)_S dE_k \end{aligned} \tag{2.18}$$

For piezoceramic materials, the assumption of small deformations permits the linear form of the above, providing further simplification. The terms relating the

[1] Isothermal case

independent and dependent field variables are defined by the following well known material constants:

$$c_{ijkl}^{E} = \left(\frac{dT_{ij}}{dS_{kl}}\right) \quad e_{ikl} = \left(\frac{dT_{ij}}{dE_k}\right) \quad \varepsilon_{ik}^{S} = \left(\frac{dD_i}{dE_k}\right) \tag{2.19}$$

The stiffness tensor, c_{ijkl}^{E}, relates the stress and strain fields for a constant electric field. The electric displacement and electric field are related through the dielectric tensor, ε_{ik}^{S}. Coupling of the mechanical and electrical fields is represented through the piezoelectric induced stress tensor e_{ikl}. The constitutive relations may then be summarized in the following form:

$$\begin{aligned} \mathbf{D}_i &= \varepsilon_{ik}^{S}\mathbf{E}_k + \mathbf{e}_{ikl}\mathbf{S}_{kl} \\ \mathbf{T}_{ij} &= -\mathbf{e}_{kij}\mathbf{E}_k + \mathbf{c}_{ijkl}^{E}\mathbf{S}_{kl} \end{aligned} \tag{2.20}$$

Constitutive Forms:

These tensors (Eqn 2.19) may be more conveniently written in matrix form through the use of Voight notation convention. The mechanical fields can be represented by 6 independent components, while the electrical fields are represented by 3:

$$\mathbf{D} = \begin{Bmatrix} D_1 \\ D_2 \\ D_3 \end{Bmatrix} \quad \mathbf{E} = \begin{Bmatrix} E_1 \\ E_2 \\ E_3 \end{Bmatrix} \quad \mathbf{S} = \begin{Bmatrix} S_{11} \\ S_{22} \\ S_{33} \\ 2S_{23} \\ 2S_{13} \\ 2S_{12} \end{Bmatrix} = \begin{Bmatrix} S_1 \\ S_2 \\ S_3 \\ S_4 \\ S_5 \\ S_6 \end{Bmatrix} \quad \mathbf{T} = \begin{Bmatrix} T_{11} \\ T_{22} \\ T_{33} \\ T_{23} \\ T_{13} \\ T_{12} \end{Bmatrix} = \begin{Bmatrix} T_1 \\ T_2 \\ T_3 \\ T_4 \\ T_5 \\ T_6 \end{Bmatrix} \tag{2.21}$$

The matrix form of equation 2.20 becomes:

$$\begin{Bmatrix} \mathbf{D} \\ \mathbf{T} \end{Bmatrix} = \begin{bmatrix} \varepsilon^{S} & \mathbf{e} \\ -\mathbf{e}_t & \mathbf{c}^{E} \end{bmatrix} \begin{Bmatrix} \mathbf{E} \\ \mathbf{S} \end{Bmatrix} \tag{2.22}$$

where the superscripts S and E denote the constant mechanical and electrical field boundary conditions, and t indicates matrix transpose. Since there are four field variables, there are actually four separate forms of the constitutive equations for piezoelectric materials, standardized by Ref[44]. These are the following:

Form 1:

In tensor form:

$$D_i = \varepsilon_{ik}^S E_k + e_{ikl} S_{kl}$$
$$T_{ij} = -e_{kij} E_k + c_{ijkl}^E S_{kl} \tag{2.23}$$

In matrix form:

$$\begin{Bmatrix} \mathbf{D} \\ \mathbf{T} \end{Bmatrix} = \begin{bmatrix} \boldsymbol{\varepsilon}^S & \mathbf{e} \\ -\mathbf{e}_t & \mathbf{c}^E \end{bmatrix} \begin{Bmatrix} \mathbf{E} \\ \mathbf{S} \end{Bmatrix} \tag{2.24}$$

Form 2:

In tensor form:

$$D_i = \varepsilon_{ik}^T E_k + d_{ikl} T_{kl}$$
$$S_{ij} = d_{kij} E_k + s_{ijkl}^E T_{kl} \tag{2.25}$$

In matrix form:

$$\begin{Bmatrix} \mathbf{D} \\ \mathbf{S} \end{Bmatrix} = \begin{bmatrix} \boldsymbol{\varepsilon}^T & \mathbf{d} \\ \mathbf{d}_t & \mathbf{s}^E \end{bmatrix} \begin{Bmatrix} \mathbf{E} \\ \mathbf{T} \end{Bmatrix} \tag{2.26}$$

Form 3:

In tensor form:

$$E_i = \beta_{ik}^T D_k - g_{ikl} T_{kl}$$
$$S_{ij} = g_{kij} D_k + s_{ijkl}^D T_{kl} \tag{2.27}$$

In matrix form:

$$\begin{Bmatrix} \mathbf{E} \\ \mathbf{S} \end{Bmatrix} = \begin{bmatrix} \boldsymbol{\beta}^T & -\mathbf{g} \\ \mathbf{g}_t & \mathbf{s}^D \end{bmatrix} \begin{Bmatrix} \mathbf{D} \\ \mathbf{T} \end{Bmatrix} \tag{2.28}$$

Form 4:

In tensor form:

$$E_i = \beta_{ik}^S D_k - h_{ikl} S_{kl}$$
$$T_{ij} = -h_{kij} D_k + c_{ijkl}^D S_{kl} \tag{2.29}$$

In matrix form:

$$\begin{Bmatrix} \mathbf{E} \\ \mathbf{T} \end{Bmatrix} = \begin{bmatrix} \boldsymbol{\beta}^S & -\mathbf{h} \\ -\mathbf{h}_t & \mathbf{c}^D \end{bmatrix} \begin{Bmatrix} \mathbf{D} \\ \mathbf{S} \end{Bmatrix} \tag{2.30}$$

Simple matrix algebra provides relationships between the material property constants of the various forms. The two most utilized of the above are forms 1 and 2, because the electric field is an independent variable in these. Piezoelectric materials are

often used in this capacity, where the electric field is either applied or short circuited (zero). For these two forms, the following relationships may be derived. From form 2, solve for the stress:

$$\mathbf{T} = (\mathbf{s}^E)^{-1}\mathbf{S} - (\mathbf{s}^E)^{-1}\mathbf{d}_t\mathbf{E} \tag{2.31}$$

Substitute into the equation for D,

$$\mathbf{D} = \mathbf{d}(\mathbf{s}^E)^{-1}\mathbf{S} - \mathbf{d}(\mathbf{s}^E)^{-1}\mathbf{d}_t\mathbf{E} + \boldsymbol{\varepsilon}^T\mathbf{E} \tag{2.32}$$

and, compare to form 1:

$$\mathbf{c}^E = (\mathbf{s}^E)^{-1} \quad \mathbf{e} = \mathbf{d}\mathbf{c}^E \quad \boldsymbol{\varepsilon}^S = \boldsymbol{\varepsilon}^T - \mathbf{d}\mathbf{c}^E\mathbf{d}_t \tag{2.33}$$

These first relationship shows that the short circuit stiffness ($\mathbf{c}^E$) is simply the inverse of the short circuit compliance ($\mathbf{s}^E$). The second relation demonstrates that the induced piezoelectric stress depends on the magnitude of both the stiffness and the piezoelectric free strain ($\mathbf{d}$) constants. This is similar to the induced thermal 'stress' due to a clamped thermal expansion. The final relation shows that the clamped dielectric is smaller than the free dielectric.

A second set of relations may be derived by considering the other equation contained in form 2. Solving for the electric field gives

$$\mathbf{E} = (\boldsymbol{\varepsilon}^T)^{-1}\mathbf{D} - (\boldsymbol{\varepsilon}^T)^{-1}\mathbf{d}\mathbf{T} \tag{2.34}$$

Substitute into equation for S:

$$\mathbf{S} = \mathbf{s}^E\mathbf{T} + \mathbf{d}_t(\boldsymbol{\varepsilon}^T)^{-1}\mathbf{D} - \mathbf{d}_t(\boldsymbol{\varepsilon}^T)^{-1}\mathbf{d}\mathbf{T} \tag{2.35}$$

and, compare to form 3:

$$\boldsymbol{\beta}^T = (\boldsymbol{\varepsilon}^T)^{-1} \quad \mathbf{g} = (\boldsymbol{\varepsilon}^T)^{-1}\mathbf{d} \quad \mathbf{s}^D = \mathbf{s}^E - \mathbf{d}_t(\boldsymbol{\varepsilon}^T)^{-1}\mathbf{d} \tag{2.36}$$

The above shows relationships for the various electrical properties and their inverses. The third of these is important and demonstrates that the material is less compliant with open circuit electrical boundary conditions.

The primary form to be used in the study of the effective material constants is form 2, where the electric field and stress are the independent variables. This has been chosen because these independent variables are the ones most easily controlled in both physical experiments, and hypothetical experiments for analysis. The full matrix form for piezoelectric materials is presented:

$$\begin{Bmatrix} S_1 \\ S_2 \\ S_3 \\ S_4 \\ S_5 \\ S_6 \end{Bmatrix} = \begin{bmatrix} s_{11}^E & s_{12}^E & s_{13}^E & 0 & 0 & 0 \\ s_{12}^E & s_{11}^E & s_{13}^E & 0 & 0 & 0 \\ s_{13}^E & s_{13}^E & s_{33}^E & 0 & 0 & 0 \\ 0 & 0 & 0 & s_{55}^E & 0 & 0 \\ 0 & 0 & 0 & 0 & s_{55}^E & 0 \\ 0 & 0 & 0 & 0 & 0 & s_{66}^E \end{bmatrix} \begin{Bmatrix} T_1 \\ T_2 \\ T_3 \\ T_4 \\ T_5 \\ T_6 \end{Bmatrix} + \begin{bmatrix} 0 & 0 & d_{31} \\ 0 & 0 & d_{31} \\ 0 & 0 & d_{33} \\ 0 & d_{15} & 0 \\ d_{15} & 0 & 0 \\ 0 & 0 & 0 \end{bmatrix} \begin{Bmatrix} E_1 \\ E_2 \\ E_3 \end{Bmatrix}$$

$$\begin{Bmatrix} D_1 \\ D_2 \\ D_3 \end{Bmatrix} = \begin{bmatrix} 0 & 0 & 0 & 0 & d_{15} & 0 \\ 0 & 0 & 0 & d_{15} & 0 & 0 \\ d_{31} & d_{31} & d_{33} & 0 & 0 & 0 \end{bmatrix} \begin{Bmatrix} T_1 \\ T_2 \\ T_3 \\ T_4 \\ T_5 \\ T_6 \end{Bmatrix} + \begin{bmatrix} \varepsilon_{11}^T & 0 & 0 \\ 0 & \varepsilon_{11}^T & 0 \\ 0 & 0 & \varepsilon_{33}^T \end{bmatrix} \begin{Bmatrix} E_1 \\ E_2 \\ E_3 \end{Bmatrix} \quad (2.37)$$

This same description may be used for the polymer phase with two exceptions: all d_{ij} are zero (no coupling), and the material properties are isotropic ($s_{11} = s_{33}$, $s_{13} = s_{12}$, etc.). During later derivations, compliances and dielectrics for the polymer phase can be distinguished from those of the piezoelectric by their lack of superscripts which otherwise indicate the mechanical and electrical boundary conditions (see notation in the Appendix).

2.3 Reduced Problems in Piezoelectric Materials

Up to this point, the constitutive equations have been presented for the response for a three dimensional structure, without assumptions of either plane stress or strain. Modeling in subsequent chapters will require the constitutive relations for a reduced problem. Chapter 3.0 deals with electromechanical modeling of piezoelectric fiber composites, and will need the formulation for a modified plane strain problem. Chapter 5.0 will make use of the plane stress constitutive relations for modeling the response of structures that incorporate piezoelectric fiber composites. This first subsection examines the simple plane stress assumption, and how they must be enforced with respect to the constitutive relations. The following subsection details the modified plane strain assumption.

2.3.1 The Plane Stress Problem

Typical applications of piezoelectric fiber composites will include plate and shell structures with and without various substrate materials (aluminum, glass, graphite/epoxy, etc.). In this case, an important assumption is made about the state of stress in the material.

Namely, the normal stress through the thickness and its corresponding shear stresses are zero:

$$T_3 = T_4 = T_5 = 0 \tag{2.38}$$

This is the common Kirchoff assumption in simple plate and shell theory[47]. To apply this condition, the constitutive equations must be in the compliance form (i.e. with stress as the independent field variable). After reduction, the constitutive equations are as follows:

$$\begin{Bmatrix} D_3 \\ S_1 \\ S_2 \\ S_6 \end{Bmatrix} = \begin{bmatrix} \varepsilon_{33}^T & d_{31} & d_{32} & 0 \\ d_{31} & s_{11}^E & s_{12}^E & 0 \\ d_{32} & s_{12}^E & s_{22}^E & 0 \\ 0 & 0 & 0 & s_{66}^E \end{bmatrix} \begin{Bmatrix} E_3 \\ T_1 \\ T_2 \\ T_6 \end{Bmatrix} \tag{2.39}$$

The remaining strains S_3, S_4, and S_5 are not necessarily zero[2]. but may be calculated after the primary system is solved. Note that the above form includes a more general case of anisotropy, both piezoelectrically ($d_{32} \neq d_{31}$) and mechanically ($c_{22} \neq c_{11}$) than that for monolithic PZT.

In some cases it may be important to represent the piezoelectric properties in a form other than that used to enforce the plane stress assumptions. A common alternate form is form 2, given below:

$$\begin{Bmatrix} D_3 \\ T_1 \\ T_2 \\ T_6 \end{Bmatrix} = \begin{bmatrix} \varepsilon_{33}^S & e_{31} & e_{32} & 0 \\ -e_{31} & c_{11}^E & c_{12}^E & 0 \\ -e_{32} & c_{12}^E & c_{22}^E & 0 \\ 0 & 0 & 0 & c_{66}^E \end{bmatrix}^* \begin{Bmatrix} E_3 \\ S_1 \\ S_2 \\ S_6 \end{Bmatrix} \tag{2.40}$$

where e_{ij} are the piezoelectric induced stress constants. This form provides the mechanical stress terms as the dependent variable. Such an expression is important when modeling the response of a structure to a load applied by an actuator, and will be used in the subsequent sections. As the comparison of the two above forms has shown:

$$\mathbf{c}^{E^*} = (\mathbf{s}^{E^*})^{-1} \quad \mathbf{e}^* = \mathbf{d}^* \mathbf{c}^{E^*} \quad \boldsymbol{\varepsilon}^{S^*} = \boldsymbol{\varepsilon}^{T^*} - \mathbf{d}^* \mathbf{c}^{E^*} \mathbf{d}_t^* \tag{2.41}$$

Since the relations are based on the plane stress assumptions, the above constants (designated with a '*' to show plane stress) will *not* have a one-to-one correspondence to those constants derived from a fully three dimensional analysis. The relationship between the full three-dimensional constants to those above are given below:

---

[2] S_4 and S_5 are zero, however, for the piezoelectric fiber composite problem

$$c_{11}^{E^*} = c_{11}^E - \frac{c_{13}^{E\,2}}{c_{33}^E} \quad c_{12}^{E^*} = c_{12}^E - \frac{c_{13}^E c_{23}^E}{c_{33}^E} \quad c_{22}^{E^*} = c_{22}^E - \frac{c_{23}^{E\,2}}{c_{33}^E} \quad c_{66}^{E^*} = c_{66}^E$$

$$e_{31}^* = e_{31} - \frac{c_{13}^E e_{33}}{c_{33}^E} \quad e_{32}^* = e_{32} - \frac{c_{23}^E e_{33}}{c_{33}^E} \quad \varepsilon_{33}^{S^*} = \varepsilon_{33}^S + \frac{e_{33}^2}{c_{33}^E} \tag{2.42}$$

2.3.2 The Modified Plane Strain Problem

Consider a body of arbitrary cross-section, such as in Figure 2.3, with geometry and loading invariant along its length (x_1 direction). Assume that this body has constitutive equations of piezoelectric material with axes aligned along the geometry as shown. Since elastic symmetry exists in orthogonal axes, plane sections will remain plane with loading. However, this body is not necessarily infinite in length so that, although there is no variable dependence on x_1, the problem is not one of pure plane strain. Strain along the x_1 direction exists, and is very important, especially in the piezoelectric problem. These type of conditions are not unique and are often termed the "modified plane strain" analyses [25, 26][3]. Given the present assumptions, S_5 , S_6 and D_1 must be zero. This is true since the out-of plane loads , T_5 , T_6 and E_1 are assumed zero.

With strain in the x_1 direction constant, it is possible to re-write the constitutive equations in a form that considers S_1 an independent variable. In this way, it appears as an applied loading. From above, using the formulation for S_1, solve for T_1:

$$\begin{aligned} S_1 &= d_{31}E_3 + s_{11}T_1 + s_{12}T_2 + s_{13}T_3 \\ T_1 &= \frac{1}{s_{11}}S_1 - \frac{d_{31}}{s_{11}}E_3 - \frac{s_{12}}{s_{11}}T_2 - \frac{s_{13}}{s_{11}}T_3 \end{aligned} \tag{2.43}$$

In this new form, stress is the dependent variable in the 1 direction. Applying this relationship to the remaining equations, and renaming the material constants to simplify leaves:

$$\begin{aligned} T_1 &= \beta_d S_1 - \beta_a T_2 - \beta_b T_3 - \beta_c E_3 \\ S_2 &= \beta_{15}E_3 + \beta_{11}T_2 + \beta_{12}T_3 + \beta_a S_1 \\ S_3 &= \beta_{56}E_3 + \beta_{12}T_2 + \beta_{22}T_3 + \beta_b S_1 \\ S_4 &= \beta_{14}E_2 + \beta_{66}T_4 \\ D_2 &= \beta_{44}E_2 + \beta_{14}T_4 \\ D_3 &= \beta_{55}E_3 + \beta_{15}T_2 + \beta_{56}T_3 + \beta_c S_1 \end{aligned} \tag{2.44}$$

---

[3] Contrast this to Lekhnitskii [48] who refers to "generalized plane strain" as those problems where cross sections warp, but all identically, caused by more general anisotropy (non orthogonal elastic axes).

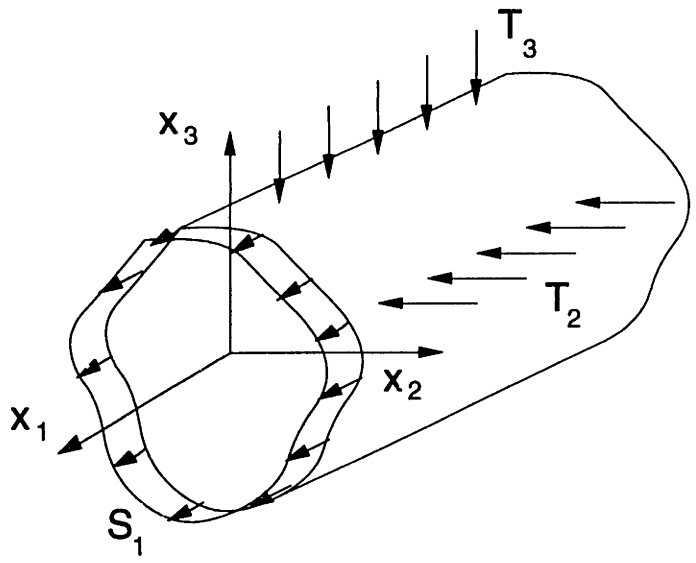

Figure 2.3: Modified plane strain axis and load definitions

where the modified plane strain material constants are:

$$\beta_a = \frac{s_{12}^E}{s_{11}^E} \quad \beta_b = \frac{s_{13}^E}{s_{11}^E} \quad \beta_c = \frac{d_{31}}{s_{11}^E} \quad \beta_d = \frac{1}{s_{11}^E}$$

$$\beta_{15} = \frac{d_{31}(s_{11}^E - s_{12}^E)}{s_{11}^E} \quad \beta_{56} = \frac{d_{33}s_{11}^E - d_{31}s_{13}^E}{s_{11}^E} \quad \beta_{55} = \frac{\varepsilon_{33}^T s_{11}^E - d_{31}^2}{s_{11}^E} \quad \beta_{14} = d_{15}$$

$$\beta_{11} = \frac{s_{11}^{E\,2} - s_{12}^{E\,2}}{s_{11}^E} \quad \beta_{12} = \frac{(s_{11}^E - s_{12}^E)s_{13}^E}{s_{11}^E} \quad \beta_{22} = \frac{s_{11}^E s_{33}^E - s_{13}^{E\,2}}{s_{11}^E} \quad \beta_{44} = \varepsilon_{11}^T \quad \beta_{66} = s_{55}^E$$

(2.45)

2.4 Summary

Chapter 2.0 has provided an introduction into the mechanics of piezoelectric materials. Understanding these materials relies not only on the material property relations, but also a knowledge of the principles that govern fields within the materials. In this chapter, both were presented, beginning with the equations of elasticity and electrostatics, and their accompanying boundary conditions. The property relations of piezoelectric materials were also presented, both in full form, and in reduced forms for particular problems. These components provide all the necessary pieces that comprise a solution to fields in continuum.

The stage is now set for the modeling of piezoceramic fiber composites in Chapter 3.0.

3.0 Modeling Piezoelectric Fiber Composites

3.1 Overview

The design of active structures and the answers to key issues in the microstructure require the ability to predict effective material properties. Although materials are easily characterized through experimental procedures, only isotropic materials are well served by this method. The introduction of two and three phase materials prompts us to look for ways to predict, rather than measure the bulk properties. Purely experimental results, although important for a qualitative understanding, are too narrow to be applied to the endless combinations of matrix and filler.

Largely beginning in the 1960's, mechanical models were investigated to find the overall stiffness, and electrical analogy models were developed for various transport properties. The two types of models were independent, as coupling between the fields did not exist in any of the constituent phases. With the introduction of piezoelectric crystals, the need for multi-field analysis to predict effective properties became apparent. This chapter details the various modeling techniques used to predict effective properties. In the background, the method of determining macroscopic properties from a microscopic look at the geometry, or micro-electromechanical modeling is presented. Following this, three individual modeling techniques are described and their results shown for material parameters in the region of interest. Finally, the various models are compared to validate assumptions, and provide insight into the problem.

3.2 Background

Constitutive relations provide a means for relating complementary mechanical and electrical fields within a homogeneous material. The constitutive equations for piezoelectric and for epoxy are two such examples. The response of each monolithic material is straightforward, with the understanding that the fields are the same at each location. Heterogeneous materials, however, are subject to localized behavior occurring within the material phases. The constitutive equations then become a way to describe the averaged response of the material, using mechanical and electrical fields that are uniform only in a macroscopic sense.

The manner in which these averaged, or effective, properties are found involve understanding the mechanisms at the micro level. At this level, the individual phases can be distinguished and form, ideally, a series of repeating elements called representative volume elements (R.V.E.). It is the response of these individual elements that determines

the response of the overall structure. In turn, the macroscopic loads and boundary conditions applied to the overall structure are reflected at the microscopic level.

There are numerous methods to determine the effective properties, all of which fall into two general categories: Mechanics of Materials and Elasticity Approaches. A model from each of these categories is presented in this chapter. The Mechanics of Materials method is characterized by largely simplifying assumptions in the way the field distributions are treated and with the geometry of the internal micro structure. Elasticity Approaches use equations of elasticity and electrostatics to govern the field distributions, and as such, are much more complicated than a Mechanics of Materials approach. For this reason, the geometry is often simplified to make a solution possible. Numerical elasticity models, such as the finite element, use a discrete description of field distributions within the material. The results are usually very good and the method allows accurate representation of the internal geometry. One downfall in an implicit method such as this one, however, is the lack of a closed form solution that allows physical insight into the dominant parameters. Nonetheless, it provides a means to validate previous assumptions and a basis for comparing the various models.

As pointed out above, each model takes a different approach to representing the problem at the micro structure level. It is possible to define three main elements that must be considered in the modeling approach:

1. The individual phases and their constitutive properties
2. A method for governing the field distributions in the material
3. Reference to the microstructure geometry

It is the manner in which each is dealt with that differentiates the various approaches to modeling. These three elements are discussed further below, and a comparison of the models to be presented here is shown in Table 3.1.

Material Phases and Constitutive Properties

All of the models consider the fiber and matrix material phases, as shown in the figure depicting the microstructure (Fig. 3.1). The Self Consistent Fields model also introduces a third phase, representing the smeared effective properties of the composite. Obviously, these properties are initially unknown, and are determined through the solution of the elasticity problem. The constitutive equations of the material phases are also necessary, for they relate the different field variables of a material at every point within the

Table 3.1: Comparison of models developed in chapter 3

CFUF: Closed Form Uniform Fields
NUF: Numerical Uniform Fields
DUF: Discrete Uniform Fields
SCF: Self Consistent Fields
FEM: Finite Element Method

MODEL TYPE	CFUF Mech Matls	NUF Mech Matls	DUF Mech Matls	SCF Elasticity	FEM Elasticity
Section	3.3	3.3	3.3	3.4	3.5
Consistent Fields	no	no	no	yes	yes
Closed Form	yes	no	no	yes	no
RVE Type	a	a	b	c	b
Model Considers:					
size, orientation	yes	yes	yes	yes	yes
shape	no	no	yes	yes	yes
contiguity	no	no	no	no	no
packing geom	no	no	yes	no	yes

body. For the Mechanics of Materials models, where the fields are assumed uniform throughout the phases, the constitutive relations also describe the materials response everywhere in the body. However, models which describe field distributions through a continuum approach, such as the Elasticity models, utilize the constitutive relations to couple the field equations. The Self Consistent Fields requires a third constitutive relation, which is introduced for the effective material. The degree of anisotropy for this material is higher than that for the piezoelectric material because it represents the composite relations.

Governing Field Distributions

Field distributions within matter are governed by the electric and elastic field equations presented in section 2.2.1. For a material of infinite extent, these materials will simply describe a uniform distribution. However, for any problem describing the interaction of materials with disimilar material properties and complex geometries, the fields within the phases will no longer be uniform. Such is the case for any of the models here, because they examine the composite at the microstructure level where phase boundaries are apparent. The Uniform Fields models (CFUF and NUF), however, make the assumption that the fields within each of the materials is actually constant. The consequence of such an assumption is discussed when comparing the models (section 3.6). The Discrete Uniform

Fields (DUF) model also assumes uniform fields, but the microstructure is discertized, so that the fields vary in a discrete manner across the materials.

The elasticity approaches incorporate at least some level of the field distributions. The Self Consistent (SCF) assumes uniform fields within the fiber, but models varying fields within the matrix material. The Finite Element Method (FEM) allows for fully varying field distribution within each phase.

Microstructure Geometry

Another way in which models are very different is in the way the microstructure of the composite is represented. The actual geometry is a unidirectional, continuous fiber composite lamina. Several of these lamina will eventually be bonded together to produce the built-up active structure, but only one lamina needs to be analyzed. Once the orthotropic properties have been found, Classical Laminated Plate Theory can be used to find the overall structure properties from a summation of the individual ply properties.

Due to the unidirectional fibers, the composite has no geometrical variation in the direction along the fibers. Thus, although physically a 3-D problem, the problem can be represented with a two dimensional model by examining the microstructure perpendicular to the fibers, as shown previously in Figure 2.3. Strains and stresses still occur along the fiber direction but do not vary with this direction. This class of problem is often termed modified plane strain and is independent of the assumptions in the various modeling approaches. This type of problem was introduced in section 2.3.2.

Zooming in on the microstructure of an actual composite would reveal randomly distributed fibers packed in various arrangements. Since it is impossible to model random geometry, representative volume elements are used to capture the interaction between a typical fiber and its surrounding matrix. Volume elements can vary widely between the various models and may or may not consider all of the following attributes: size and orientation of fibers, shape of fibers, packing geometry, and contiguity between fibers. Size and orientation of fibers is considered in all the models discussed here, with the size of fiber accounted for with the volume fraction of fiber, v_f. This is simply a volume ratio of fiber to total volume in the representative volume element, and is equal to the overall percentage of fiber in the bulk material.

The other attributes of the volume element, however, are not the same and are indicative of the different approaches. For example, the shape of the fiber may be simplified to a square, such as in the case of the Mechanics of Materials approach shown as RVE (a) of Fig 3.1. Another consideration involves the volume element packing. Two

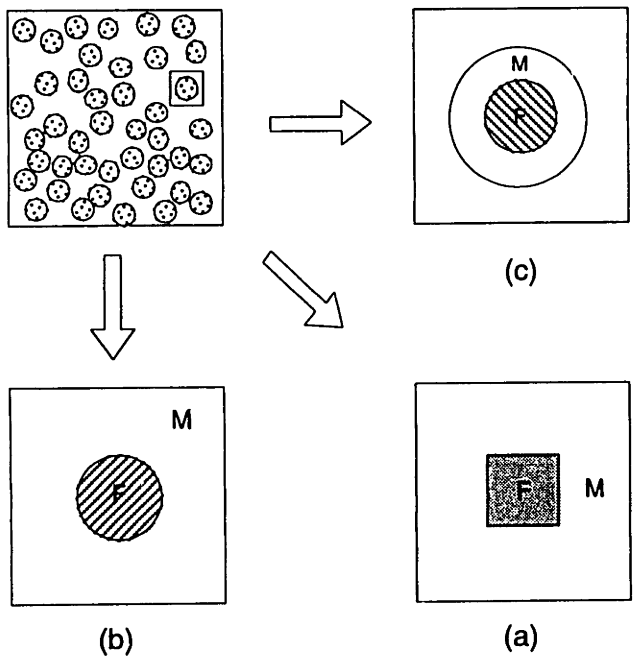

Figure 3.1: Two dimensional representation of micro structure in fibrous composite for three types of Representative Volume Elements: (a) CFUF and NUF, (b) DUF and FEM, and (c) SCF.

common packing arrangements, square and rectangular, are shown in Figure 3.2. A square array assumes that the amount of matrix material is equal around the fiber. In this way, a composite with equal spacing of fibers in the 2 and 3 directions can be represented using only the volume fraction. This is likely a correct representation of any composite where the thickness of the ply is much larger (>10 times) than the fiber diameter, and manufacturing does not create a preferred direction. For this reason, all the models developed in this chapter will utilize the square packing array, so that they will best represent a multi-fiber layer composite. This provides a good basis for comparison between the models, given in section 3.6. The other packing arrangement, the rectangular array, has the added freedom of specifying unequal amounts of matrix around the fiber. This can be used to model composites with manufacturing that causes preferred directional spacing, such as the techniques used to manufacture the mono-fiber layer composites, outlined in section 5.3. In this case, the Uniform Fields models and Finite Element models may be adapted to allow such rectangular packing. Other such differences that distinguish the models will be further discussed in the development of each. Throughout, it may be useful for the reader to refer to the summary chart (Table 3.1) that compares the various models.

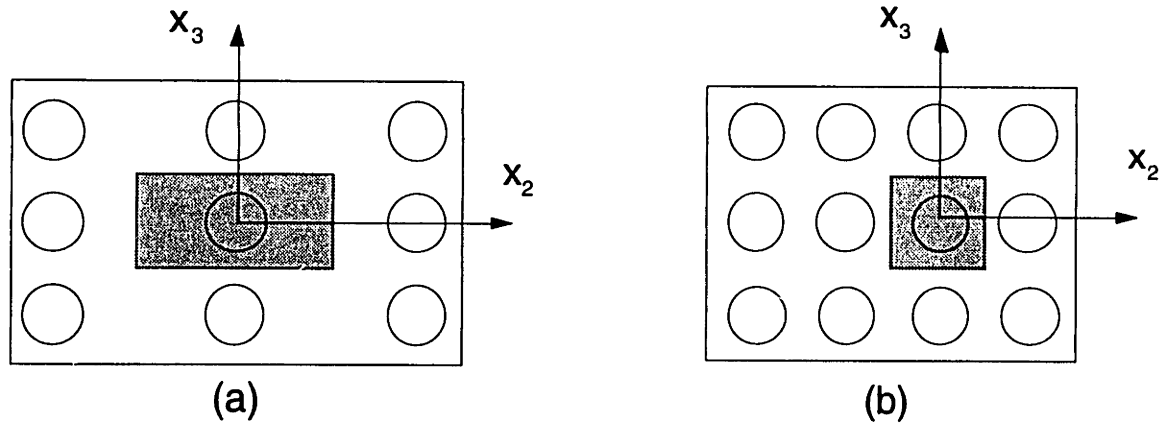

Figure 3.2: Representative Volume Elements for rectangular (a) and square (b) packing arrays

Assumptions

Before continuing on to discuss each model individually, it is important to state the assumptions. These assumptions are irrespective of the model, and can be divided into two groups: material assumptions and structural assumptions. For the materials themselves, it is assumed that the two phases are in good contact and are perfectly bonded everywhere. That is, there is negligible effects due to interfacial phenomena such as poor wetting and water adsorption. In addition to this, deformations and electric fields are considered small enough that the linear forms of the constitutive equations (Eq 2.3) adequately describe the field relationships. This is likely the case due to the practical limits set on deformations and fields by the low failure strain and dielectric breakdowns, respectively, of the material. Finally, it is assumed that all the piezoelectric materials are uniformly polarized in the 3 axis direction. This is not exactly true because the polarization will be directed along the field lines present in the fiber. As some of the models show, this is not completely accurate. However, as it turns out, the field lines are close enough to uniform in the fiber that the assumption is a good one.

The structural assumptions deal with the response of the composite as a whole. Although the composite is three dimensional in nature, there is no variation in geometry or properties along the fiber length. If this composite is "long" (i.e. 1 direction dimension large compared to the others), then there will also be no variation in electrical or mechanical fields with this dimension[4] . Thus, since this composite problem is dependent only on the

[4] Away from the ends

coordinates describing the location in a plane perpendicular to the fiber, the formulation in section 2.3.2 for the modified plane strain problem is applicable here.

It is important to understand that strain along the fiber does exist, and is central to the discussion of piezoelectric fiber composites. Away from the ends, each plane of fiber and matrix acts as a disk and remains a plane after loads are applied. Out of plane shear stresses and strains, therefore, do not exist, and all loads are in the plane of the structure except the normal load, T_1. In a physical sense, this situation must occur or there will be a large accumulation of out-of-plane displacement over the length of the material. To guarantee such a situation, the composite element must be long. The effect of the ends will create local warping out of plane around the fiber, and the local existence of shear stresses due to the three dimensional stress equilibrium conditions. High percentages of fibers and small spatial scales reduce such an effect.

3.3 Uniform Fields Models

3.3.1 Introduction to Uniform Fields

The class of model used here is a *Uniform Fields* approach, where the mechanical and electrical fields are assumed uniform within each of the material phases. Several previous researchers have utilized this technique for modeling both particulate[36], and rod composites[37]. Of particular relevance is this last work, that looked at the problem of finding the effective material properties for an ultrasound transducer where piezoceramic rods are embedded through the thickness of the composite (Figure 3.3). Both the poling and electric field direction are aligned with the ceramic rod, so that the composite is transversely isotropic in nature. In the present work, a higher degree of anisotropy is present because the direction of poling is perpendicular to the direction of fibers, rather than along the fiber length.

The *Uniform Fields* approach is developed through a generalization of the *Mechanics of Materials* method which deals with purely mechanical system responses. A good description of this model is given in Ref[23]. The basic premise can be expressed through a mechanical spring analogy where the fiber is a spring of high stiffness, and the matrix material is a spring with low stiffness. Effective stiffness in directions along the fiber and perpendicular to the fiber are found by addition of these springs in parallel and series, respectively. Naturally, a parallel addition gives a system response dominated by the stiff fiber phase, while the series addition gives a response more dependent on the matrix phase.

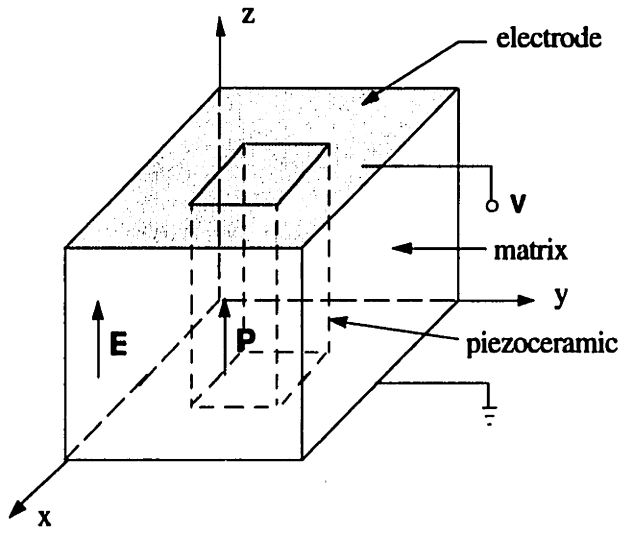

Figure 3.3: Representative volume element of rod composite [37].

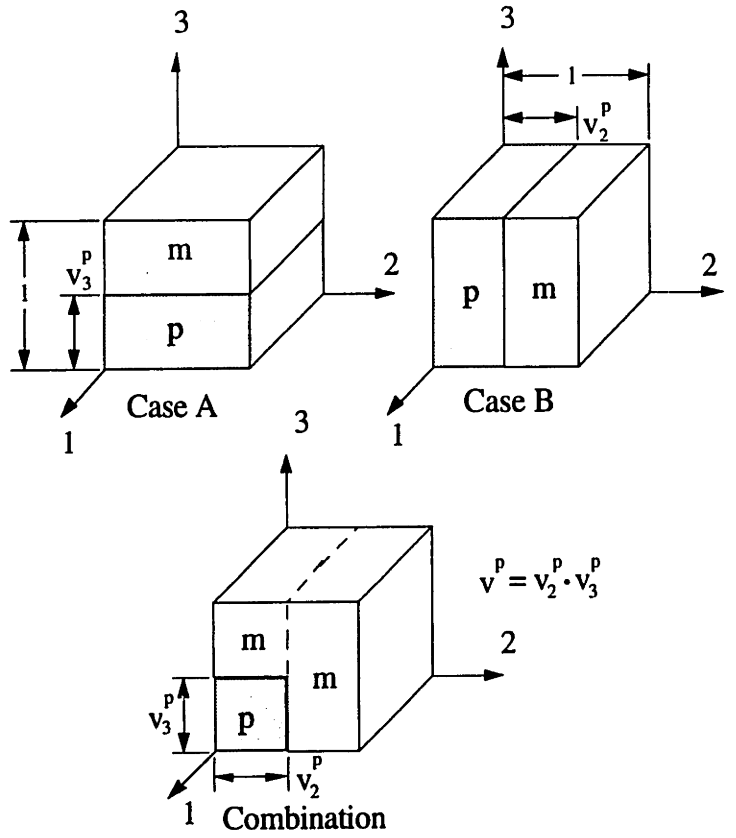

Fig. 3.4: Representation of the possible phase geometry in the piezoceramic fiber problem (p - piezoceramic, m - matrix)

Typically, longitudinal mecnanical properties have shown good agreement with predictions based on a parallel model. This is understandable, since the fibers are continuous in the longitudinal direction and ensure an essentially uniform strain. In contrast, transverse properties are underestimated using the series model. The assumption of equal stresses in both phases is inaccurate. This has been shown in classic studies of stress concentrations around a hole or inclusion in a plate subjected to far-field applied loads.

Some improvements in the modeling of transverse properties can be realized by using a combination model. The combination model can be described as a generalization of the mechanics of materials approach for which the parallel and series models are bounds. Here, columns of matrix are modeled in parallel with columns of matrix and fiber that are in series with each other. The possibility now exists for adjusting two fiber volume fractions. A volume fraction value of one in either direction will result in effective properties predicted by the series or parallel models alone. A generalization of this method to electrical-mechanical coupled fields is the focus of this section.

As with any model, the objective is to find the response of the material as a whole, so that the description of the material may be represented by properties of an effective homogeneous media. The basis of this model, as the name implies, is that all of the fields are uniform in the individual phases. This is assumed true, even at the microstructure level. The stress, strain, electric field, and electrical displacement in any one direction can be represented by a single average value. As previously mentioned, this description has been used successively in the past[37], and its accuracy depends largely on the spatial scale of the phase distributions. For finely distributed phases, it is likely that these assumptions will provide a good estimate of the response in an averaged sense.

These assumptions make it possible to treat the piezocomposite in an efficient manner. Although the ply is actually three dimensional, there is no geometrical variation along the fibers (the 1-direction). This leaves two possible descriptions of the piezoelectric and matrix phases: one with material connectivities in the 1- and 2-directions, and the second with connectivities in the 1- and 3-directions. The uniform field assumption makes it possible to refer to the phases without regard to the individual coordinates of the distributed material. Thus, the same effect is obtained if all the piezoceramic were grouped together and represented as one area. This provides the interpretation given in Figure 3.4 Each of the two cases, A and B, act as building blocks for the combination model and are examined separately.

3.3.2 Fully Coupled Analysis

Case A Combination

The geometry and loading for case A is shown in Figure 3.5. Looking more closely at this case, the internal stresses, strains and electric fields can be understood through the application of the previous assumptions. In the 1-direction, the average strain must be equal to the strain in each of the ceramic and matrix.

$$\overline{S}_1 = S_1^p = S_1^m \tag{3.1}$$

The average stress, however, is some combination of stresses in the two phases. The contribution of each material to the average stress is in proportion to the fraction of each in the 1-direction. This is apparent from a free body diagram. Thus,

$$\overline{T}_1 = v_3^p T_1^p + v_3^m T_1^m \tag{3.2}$$

where v_3^p is the fraction of piezoceramic measured across the element in the 3-direction. Stresses and strains in the 2-direction, and in-plane shear are treated in the same manner. In the 3-direction, the average stress $\overline{T}_3$ must be equal to the stress in the matrix,

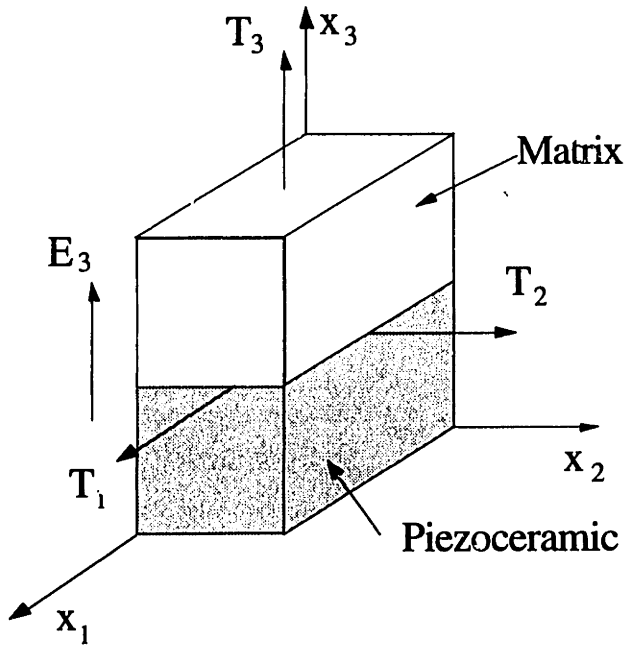

Figure 3.5: Case A material combination for the Uniform Fields models

and therefore, also in the ceramic. The average strain will be an addition of strains provided by each phase, again in proportion to the amount of each material:

$$\overline{T}_3 = T_3^p = T_3^m \tag{3.3}$$

$$\overline{S}_3 = v_3^p S_3^p + v_3^m S_3^m . \tag{3.4}$$

The average electrical displacement (units of charge per unit area) must be equal to that in the matrix and in the ceramic. Finally, the voltage applied across the specimen in the 3 direction must be equal to the sums of voltage across each phase. Since the voltage is the product of electric field and thickness, the expressions obtained are

$$\overline{D}_3 = D_3^m = D_3^p \tag{3.5}$$

$$\overline{E}_3 = v_3^p E_3^p + v_3^m E_3^m \tag{3.6}$$

The uncoupled problem of out-of-plane shear strains and transverse electric fields is not of interest , and is therefore ignored here. Solution for the effective properties involves the constitutive equations (2.37) for both materials, and the conditions imposed by equations (3.1) to (3.6). The procedure involves the simultaneous solution of a large number of equations through elimination of the non-averaged field variables. A more unified approach is possible if the conditions are assembled into matrices.

$$\begin{Bmatrix} \overline{T}_1 \\ \overline{T}_2 \\ \overline{S}_3 \\ \overline{T}_6 \\ \overline{E}_3 \end{Bmatrix} = v_3^p \begin{Bmatrix} T_1 \\ T_2 \\ S_3 \\ T_6 \\ E_3 \end{Bmatrix}_p + v_3^m \begin{Bmatrix} T_1 \\ T_2 \\ S_3 \\ T_6 \\ E_3 \end{Bmatrix}_m \tag{3.7}$$

$$\begin{Bmatrix} \overline{S}_1 \\ \overline{S}_2 \\ \overline{T}_3 \\ \overline{S}_6 \\ \overline{D}_3 \end{Bmatrix} = \begin{Bmatrix} S_1 \\ S_2 \\ T_3 \\ S_6 \\ D_3 \end{Bmatrix}_p = \begin{Bmatrix} S_1 \\ S_2 \\ T_3 \\ S_6 \\ D_3 \end{Bmatrix}_m \tag{3.8}$$

Note that there are only two types of conditions, those that average the field variables in proportion to each material phase, and those that provide for equal fields carried across the phase. The constitutive equations are then rewritten in the following form:

$$\begin{Bmatrix} T_1 \\ T_2 \\ S_3 \\ T_6 \\ E_3 \end{Bmatrix}_{p,m} = \begin{bmatrix} a_{11} & a_{12} & a_{13} & 0 & a_{15} \\ a_{12} & a_{11} & a_{13} & 0 & a_{15} \\ -a_{13} & -a_{13} & a_{33} & 0 & a_{35} \\ 0 & 0 & 0 & a_{44} & 0 \\ a_{15} & a_{15} & -a_{35} & 0 & a_{55} \end{bmatrix}_{p,m} \begin{Bmatrix} S_1 \\ S_2 \\ T_3 \\ S_6 \\ D_3 \end{Bmatrix}_{p,m} = \mathbf{A}_{p,m} \begin{Bmatrix} S_1 \\ S_2 \\ T_3 \\ S_6 \\ D_3 \end{Bmatrix}_{p,m} \tag{3.9}$$

where the a_{ij} are given in the Appendix. Substitution of (3.9) into (3.7) averages all of the necessary fields in one step.

$$\begin{Bmatrix} \overline{T}_1 \\ \overline{T}_2 \\ \overline{S}_3 \\ \overline{T}_6 \\ \overline{E}_3 \end{Bmatrix} = v_3^p \mathbf{A}_p \begin{Bmatrix} S_1 \\ S_2 \\ T_3 \\ S_6 \\ D_3 \end{Bmatrix}_p + v_3^m \mathbf{A}_m \begin{Bmatrix} S_1 \\ S_2 \\ T_3 \\ S_6 \\ D_3 \end{Bmatrix}_m \tag{3.10}$$

Finally, applying (3.8) equates the necessary field variables, leaving:

$$\begin{Bmatrix} \overline{T}_1 \\ \overline{T}_2 \\ \overline{S}_3 \\ \overline{T}_6 \\ \overline{E}_3 \end{Bmatrix} = \left(v_3^p \mathbf{A}_p + v_3^m \mathbf{A}_m \right) \begin{Bmatrix} \overline{S}_1 \\ \overline{S}_2 \\ \overline{T}_3 \\ \overline{S}_6 \\ \overline{D}_3 \end{Bmatrix} \tag{3.11}$$

The last equation describes the averaged response to uniform averaged inputs, thus the term in the parenthesis contains all the effective properties. If the final step

is to rewrite the effective constitutive equations and return to the original forms, the following describes the Case A combination of piezoceramic and matrix:

$$\begin{Bmatrix} \bar{S}_1 \\ \bar{S}_2 \\ \bar{S}_3 \\ \bar{S}_6 \\ \bar{D}_3 \end{Bmatrix} = \begin{bmatrix} s_{11} & s_{12} & s_{13} & 0 & d_{31} \\ s_{12} & s_{22} & s_{13} & 0 & d_{31} \\ s_{13} & s_{13} & s_{33} & 0 & d_{33} \\ 0 & 0 & 0 & s_{66} & 0 \\ d_{31} & d_{31} & d_{33} & 0 & \varepsilon_{33} \end{bmatrix}_A \begin{Bmatrix} \bar{T}_1 \\ \bar{T}_2 \\ \bar{T}_3 \\ \bar{T}_6 \\ \bar{E}_3 \end{Bmatrix} \tag{3.12}$$

Since our interest is in the ply properties:

$$\begin{Bmatrix} \bar{S}_1 \\ \bar{S}_2 \\ \bar{S}_6 \\ \bar{D}_3 \end{Bmatrix} = \begin{bmatrix} s_{11} & s_{12} & 0 & d_{31} \\ s_{12} & s_{11} & 0 & d_{31} \\ 0 & 0 & s_{66} & 0 \\ d_{31} & d_{31} & 0 & \varepsilon_{33} \end{bmatrix}_A \begin{Bmatrix} \bar{T}_1 \\ \bar{T}_2 \\ \bar{T}_6 \\ \bar{E}_3 \end{Bmatrix} \tag{3.13}$$

where:

$$s_{11}^A = \frac{s_{11}v_3^m(\bar{\varepsilon}(s_{12}^E + s_{11}^E) - 2d_{31}^2 v_3^m)(s_{12}^E - s_{11}^E) + v_3^p(\bar{\varepsilon}s_{11}^E - v_3^m d_{31}^2)(s_{12}^2 - s_{11}^2)}{(-\bar{s}_{12} + \bar{s}_{11})(\bar{\varepsilon}(\bar{s}_{12} + \bar{s}_{11}) - 2d_{31}^2 v_3^{m^2})} \tag{3.14}$$

$$s_{12}^A = -\frac{s_{12}v_3^m(\bar{\varepsilon}(s_{12}^E + s_{11}^E) - 2d_{31}^2 v_3^m)(s_{12}^E - s_{11}^E) + v_3^p(\bar{\varepsilon}s_{12}^E - v_3^m d_{31}^2)(s_{12}^2 - s_{11}^2)}{(-\bar{s}_{12} + \bar{s}_{11})(\bar{\varepsilon}(\bar{s}_{12} + \bar{s}_{11}) - 2d_{31}^2 v_3^{m^2})} \tag{3.15}$$

$$s_{66}^A = \frac{s_{66}^E s_{66}}{v_3^p s_{66} + v_3^m s_{66}^E} \tag{3.16}$$

$$d_{31}^A = \frac{d_{31}v_3^p\varepsilon_{33}(s_{12} + s_{11})}{\bar{\varepsilon}(\bar{s}_{12} + \bar{s}_{11}) - 2d_{31}^2 v_3^{m^2}} \tag{3.17}$$

$$\varepsilon_{33}^A = \varepsilon_{33}\frac{\varepsilon_{33}^T(\bar{s}_{12} + \bar{s}_{11}) - 2d_{31}^2 v_3^m}{\bar{\varepsilon}(\bar{s}_{12} + \bar{s}_{11}) - 2d_{31}^2 v_3^{m^2}} \tag{3.18}$$

and

$$\bar{\varepsilon} = \varepsilon_{33}v_3^p + \varepsilon_{33}^T v_3^m \tag{3.19}$$

$$\bar{s}_{11} = s_{11}v_3^p + s_{11}^E v_3^m \tag{3.20}$$

$$\bar{s}_{12} = s_{12}v_3^p + s_{12}^E v_3^m \tag{3.21}$$

Case B Combination

Combining properties for the Case B geometry (Figure 3.6) is done in a completely analogous manner as Case A. The differences come about from the differing connectivity

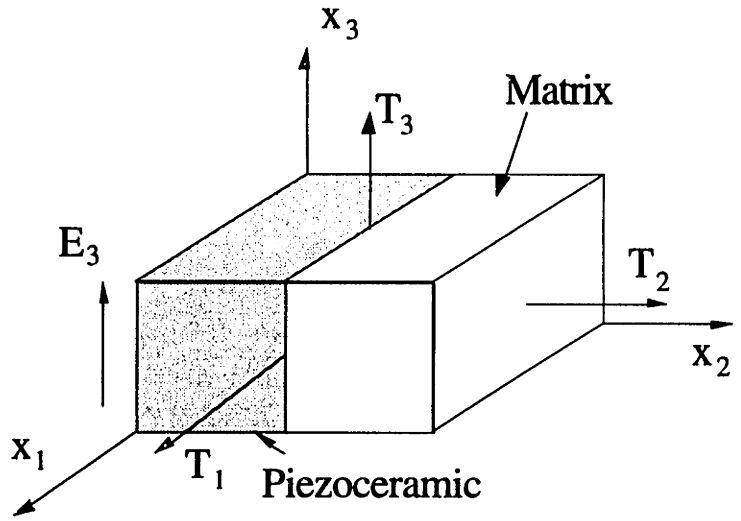

Figure 3.6: Case B material combination for the Uniform Fields models

in the two cases. This is reflected in the different set of field variables that are equal in the two phases. In this case, strains in the piezoceramic and matrix are equal for the 1 and 3 directions, stresses are equal in the 2 and 6 (in-plane shear) directions, and electric field is maintained the same across the materials in the 3 direction. Thus,

$$\begin{Bmatrix} \overline{S}_1 \\ \overline{T}_2 \\ \overline{S}_3 \\ \overline{T}_6 \\ \overline{E}_3 \end{Bmatrix} = \begin{Bmatrix} S_1 \\ T_2 \\ S_3 \\ T_6 \\ E_3 \end{Bmatrix}_p = \begin{Bmatrix} S_1 \\ T_2 \\ S_3 \\ T_6 \\ E_3 \end{Bmatrix}_m \tag{3.22}$$

The remaining field variables are averaged according to the fraction of each phase:

$$\begin{Bmatrix} \overline{T}_1 \\ \overline{S}_2 \\ \overline{T}_3 \\ \overline{S}_6 \\ \overline{D}_3 \end{Bmatrix} = v_2^p \begin{Bmatrix} T_1 \\ S_2 \\ T_3 \\ S_6 \\ D_3 \end{Bmatrix}_p + v_2^m \begin{Bmatrix} T_1 \\ S_2 \\ T_3 \\ S_6 \\ D_3 \end{Bmatrix}_m \tag{3.23}$$

where v_2^p is the fraction of piezoceramic measured across the case B element in the 2-direction. Rewriting the constitutive equations in the appropriate form gives

$$\begin{Bmatrix} T_1 \\ S_2 \\ T_3 \\ S_6 \\ D_3 \end{Bmatrix}_{p,m} = \begin{bmatrix} b_{11} & b_{12} & b_{13} & 0 & b_{15} \\ -b_{12} & b_{11} & b_{23} & 0 & b_{25} \\ b_{13} & -b_{23} & b_{33} & 0 & b_{35} \\ 0 & 0 & 0 & b_{44} & 0 \\ -b_{15} & b_{25} & -b_{35} & 0 & b_{55} \end{bmatrix}_{p,m} \begin{Bmatrix} S_1 \\ T_2 \\ S_3 \\ T_6 \\ E_3 \end{Bmatrix}_{p,m} = \mathbf{B}_{p,m} \begin{Bmatrix} S_1 \\ T_2 \\ S_3 \\ T_6 \\ E_3 \end{Bmatrix}_{p,m} \tag{3.24}$$

where the b_{ij} are again left to the Appendix. Applying both conditions (3.22, 3.23) yields:

$$\begin{Bmatrix} \overline{T}_1 \\ \overline{S}_2 \\ \overline{T}_3 \\ \overline{S}_6 \\ \overline{D}_3 \end{Bmatrix} = \left(v_2^p \mathbf{B}_p + v_2^m \mathbf{B}_m \right) \begin{Bmatrix} \overline{S}_1 \\ \overline{T}_2 \\ \overline{S}_3 \\ \overline{T}_6 \\ \overline{E}_3 \end{Bmatrix} \tag{3.25}$$

Finally, rewriting the effective constitutive equations in the original form and simplifying to only the ply properties results in the case B effective properties:

$$\begin{Bmatrix} S_1 \\ S_2 \\ S_6 \\ D_3 \end{Bmatrix} = \begin{bmatrix} s_{11} & s_{12} & 0 & d_{31} \\ s_{12} & s_{22} & 0 & d_{32} \\ 0 & 0 & s_{66} & 0 \\ d_{31} & d_{32} & 0 & \varepsilon_{33} \end{bmatrix}_B \begin{Bmatrix} T_1 \\ T_2 \\ T_6 \\ E_3 \end{Bmatrix} \tag{3.26}$$

where:

$$s_{11}^B = \frac{s_{11}^E v_2^p (s_{11}^2 - s_{12}^2) + s_{11} v_2^m (s_{11}^E s_{33}^E - s_{13}^{E\,2})}{\overline{s}_{11}\overline{s}_{33} - \overline{s}_{13}^2} \tag{3.27}$$

$$d_{31}^B = v_2^p \frac{d_{31}(s_{11}\overline{s}_{33} - s_{12}\overline{s}_{13}) + d_{33} v_2^m (s_{12} s_{11}^E - s_{11} s_{13}^E)}{\overline{s}_{11}\overline{s}_{33} - \overline{s}_{13}^2} \tag{3.28}$$

and

$$\overline{s}_{11} = s_{11} v_2^p + s_{11}^E v_2^m \tag{3.29}$$

$$\overline{s}_{13} = s_{12} v_2^p + s_{13}^E v_2^m \tag{3.30}$$

$$\overline{s}_{33} = s_{11} v_2^p + s_{33}^E v_2^m \tag{3.31}$$

The remaining effective property terms are too long to be expressed here, and are left for the Appendix.

3.3.3 General Methodology

Both case A and B follow the same approach in obtaining effective material properties in terms of a general methodology which can be applied to cases of any connectivity. It involves two main steps. The first is to recognize those field variables that are equal in both phases as independent variables and reorganize the constitutive equations from (Eqn 2.37) to be functions of those variables.

$$\begin{Bmatrix} \mathbf{M} \\ \mathbf{E} \end{Bmatrix}^{D} = \begin{bmatrix} c_1 & c_2 \\ c_2 & c_3 \end{bmatrix} \begin{Bmatrix} \mathbf{M} \\ \mathbf{E} \end{Bmatrix}^{I} \tag{3.32}$$

where D and I represent dependent and independent field variables of the mechanical (M) and electrical type (E). The second step is to substitute these constitutive relations into the general form of the phase averaging equations:

$$\begin{Bmatrix} \overline{\mathbf{M}} \\ \overline{\mathbf{E}} \end{Bmatrix}^{D} = v^{p} \begin{Bmatrix} \mathbf{M} \\ \mathbf{E} \end{Bmatrix}_{p}^{D} + v^{m} \begin{Bmatrix} \mathbf{M} \\ \mathbf{E} \end{Bmatrix}_{m}^{D} \tag{3.33}$$

Since the independent field variables in each phase are equal to each other, and to the average field:

$$\begin{Bmatrix} \overline{\mathbf{M}} \\ \overline{\mathbf{E}} \end{Bmatrix}^{D} = \left(v^{p} \begin{bmatrix} c_1 & c_2 \\ c_2 & c_3 \end{bmatrix}_{p} + v^{m} \begin{bmatrix} c_1 & c_2 \\ c_2 & c_3 \end{bmatrix}_{m} \right) \begin{Bmatrix} \overline{\mathbf{M}} \\ \overline{\mathbf{E}} \end{Bmatrix}^{I} \tag{3.34}$$

As previoulsy mentioned, cases A and B serve as building blocks for the Combination Model. Each separate case predominantly captures some aspects of the overall response. For example, Case A alone is able to capture the dominant terms in the effective elastic constants s_{11}^{eff} and s_{33}^{eff}, as well as the effective dielectric ε_{33}^{eff} and longitudinal piezoelectric free strain constant, d_{31}^{eff}. Case B, however, better captures transverse effects like the transverse compliance s_{22}^{eff} and free strain d_{32}^{eff}. Together the two cases are combined to give the combination model. In this way, the combination model captures all effects and coupling, and more nearly represents the actual geometry.

To derive the combination model using the cases already developed, the properties of the ceramic (phase p) in Case B are replaced with the effective properties from Case A. In this way, Case B becomes the combination of matrix (phase m) with an effective piezoceramic/matrix slice (phase A) from Case A. To actually carry this out, the following substitutions would be made in the equations for Case B (Eq 3.27, 3.28, and those given in Appendix A):

$$
\begin{aligned}
s_{11}^{E} &\leftarrow s_{11}^{A} \\
s_{12}^{E} &\leftarrow s_{12}^{A} \\
s_{22}^{E} &\leftarrow s_{22}^{A} \\
&\vdots \\
d_{31}^{E} &\leftarrow d_{31}^{A}
\end{aligned}
\tag{3.35}
$$

Except for the in-plane shear, this gives unwieldy equations for which the important dominating terms are impossible to identify algebraically. In fact, the full analysis is better suited to numerical computation of the effective constants. This has been done for all effective properties, and the results for the ply properties have been plotted in section 3.6, where all of the models are compared.

3.3.4 Closed Form Solutions:

A numerical solution, although complete in the sense that all coupling terms are included, does not provide insight into the mechanics of the response. It would be advantageous to have closed form solutions to give another means for evaluating the effective constants of the combination model. The question is, to what level of approximation must the analysis be taken to allow a tractable solution?

Returning to the original cases, A and B, the next logical assumption is to ignore induced stresses caused by differing Poisson's ratios in the two materials. For example, the induced stresses T_2 and T_3 are assumed zero for a load applied in the 1- direction, T_1. This is likely a good approximation, especially when the loads are applied along the 1-direction, due to the large fiber and matrix mismatch in stiffness.

In order to neglect the induced stresses, it is necessary to equate, a priori, two of the stresses to zero *within* each phase, not just the averaged stress. In addition to eliminating the induced stresses, this allows only a limited set of effective properties to be found for any particular loading. In order to find all of the effective properties, it is necessary to apply a series of hypothetical tests. The various loading cases are shown in Figure 3.7. The premise for each is an applied stress in one direction, zero stress within both phases in the other two directions, and an applied electric field, E_3. Note that the electric field is applied in all cases to maintain the electrical coupling terms.

This procedure is carried out here for the first loading case shown in Figure 3.7, the longitudinal test. The first step is to write the constitutive equations (Eq 2.3) to reflect the lack of mechanical coupling. For each phase, T_2 and T_3 are zero, so that the only applied loads are T_1 and E_3. The corresponding strains in the constitutive equation are removed as well and kept separate. Equation 2.37 becomes:

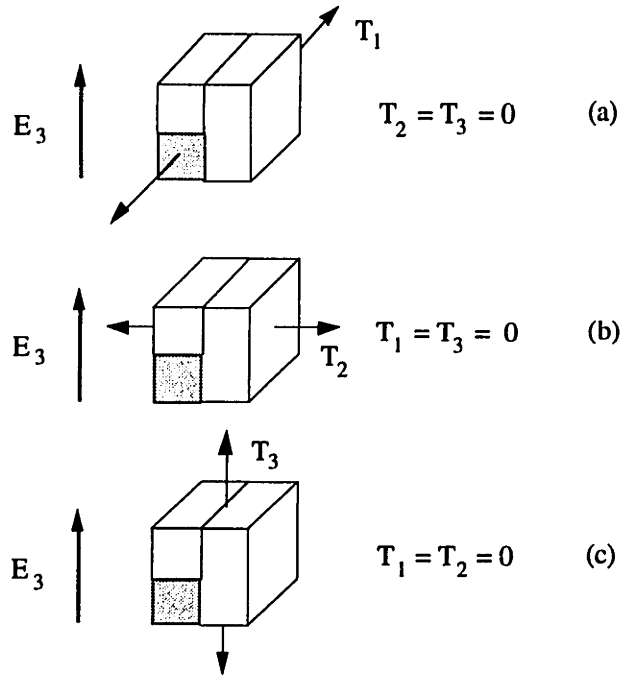

Figure 3.7: Loading configurations for the closed form combination model.

$$\begin{Bmatrix} S_1 \\ D_3 \end{Bmatrix}_{p,m} = \begin{bmatrix} s_{11}^E & d_{31} \\ d_{31} & \varepsilon_3^T \end{bmatrix}_{p,m} \begin{Bmatrix} T_1 \\ E_3 \end{Bmatrix}_{p,m} \tag{3.36}$$

Since the in-plane shear is completely uncoupled from all other loading, its form is not affected by this approximation and equation (Eq 3.10) still applies. Case A is applied first. The pertinent conditions are taken from (Eq 3.7) and (Eq 3.8):

$$\begin{Bmatrix} \overline{T}_1 \\ \overline{E}_3 \end{Bmatrix} = v_3^p \begin{Bmatrix} T_1 \\ E_3 \end{Bmatrix}_p + v_3^m \begin{Bmatrix} T_1 \\ E_3 \end{Bmatrix}_m \tag{3.37}$$

$$\begin{Bmatrix} \overline{S}_1 \\ \overline{D}_3 \end{Bmatrix} = \begin{Bmatrix} S_1 \\ D_3 \end{Bmatrix}_p = \begin{Bmatrix} S_1 \\ D_3 \end{Bmatrix}_m \tag{3.38}$$

Rewriting the constitutive equations results in

$$\begin{Bmatrix} T_1 \\ E_3 \end{Bmatrix}_{p,m} = \begin{bmatrix} a'_{11} & a'_{12} \\ a'_{12} & a'_{22} \end{bmatrix}_{p,m} \begin{Bmatrix} S_1 \\ D_1 \end{Bmatrix}_{p,m} \tag{3.39}$$

where, for the piezoceramic,

$$a'_{11} = \frac{\varepsilon_3^T}{s_{11}^E \varepsilon_3^T - d_{31}^2} \quad a'_{12} = -\frac{d_{31}}{s_{11}^E \varepsilon_3^T - d_{31}^2} \quad a'_{22} = \frac{s_{11}^E}{s_{11}^E \varepsilon_3^T - d_{31}^2} \tag{3.40}$$

Setting d_{31} to zero and removing the superscripts in the above will give corresponding terms for the matrix material. Note that the a'_{ij} given here *do not* have a one-to-one correspondence with the a_{ij} in equation 3.9.

These relations are substituted into the conditions (Eq 3.37) and are combined and inverted, as before, to give the effective constitutive equations in the original form:

$$\begin{Bmatrix} \overline{S}_1 \\ \overline{D}_3 \end{Bmatrix} = \begin{bmatrix} s_{11} & d_{31} \\ d_{31} & \varepsilon_3 \end{bmatrix}_{A'} \begin{Bmatrix} \overline{T}_1 \\ \overline{E}_3 \end{Bmatrix} \tag{3.41}$$

where A' represents the effective properties in this case A combination with no induced stress coupling. From this, the following effective properties are extracted:

$$d_{31}^{A'} = \frac{d_{31} s_{11} v_3^p \varepsilon_{33}}{(v_3^p \varepsilon_{33} + v_3^m \varepsilon_{33}^T)(s_{11} v_3^p + s_{11}^E v_3^m) - d_{31}^2 v_3^{m^2}} \tag{3.42}$$

$$s_{11}^{A'} = \frac{s_{11}(s_{11}^E (v_3^p \varepsilon_{33} + v_3^m \varepsilon_{33}^T) - v_3^m d_{31}^2)}{(v_3^p \varepsilon_{33} + v_3^m \varepsilon_{33}^T)(s_{11} v_3^p + s_{11}^E v_3^m) - d_{31}^2 v_3^{m^2}} \tag{3.43}$$

The dielectric constant, $\varepsilon_{33}^{A'}$, is taken from the vertical load test (Figure 3.7c), which provides the most compact form of the equation. To find $s_{12}^{A'}$, it is necessary to return to the unused portion of the original constitutive equations and extract the expression for $\overline{S}_2$. In case A,

$$\overline{S}_2 = S_2^p = S_2^m \tag{3.44}$$

Thus, from the original constitutive equations (Eq 2.37) with $T_2^{p,m} = T_3^{p,m} = 0$, there are two possible expressions for S_2

$$\overline{S}_2 = S_2^p = s_{12}^E T_1^p + d_{31} E_3^p \tag{3.45}$$

or,

$$\overline{S}_2 = S_2^m = s_{12} T_1^m$$

Substitutions for the fields in the two phases are made from (3.39), giving either:

$$s_{12}^{A'} = \frac{s_{11}(s_{12}^E (v_3^p \varepsilon_{33} + v_3^m \varepsilon_{33}^T) - v_1^m d_{31}^2)}{(v_3^p \varepsilon_{33} + v_3^m \varepsilon_{33}^T)(s_{11} v_3^p + s_{11}^E v_3^m) - d_{31}^2 v_3^{m^2}} \tag{3.46}$$

or

$$s_{12}^{A'} = \frac{s_{12}(s_{11}^E (v_3^p \varepsilon_{33} + v_3^m \varepsilon_{33}^T) - v_1^m d_{31}^2)}{(v_3^p \varepsilon_{33} + v_3^m \varepsilon_{33}^T)(s_{11} v_3^p + s_{11}^E v_3^m) - d_{31}^2 v_3^{m^2}} \tag{3.47}$$

This difficulty arises from the fact that the assumption of equal strains in the matrix and ceramic can no longer exactly hold because components due to the induced stresses have been neglected. However, the two terms will produce nearly identical results because the following is true for the nearly equal Poisson's ratios in the two materials:

$$s_{11}s_{12}^E \approx s_{12}s_{11}^E \tag{3.48}$$

Also important is the fact that the coupling term $v_1^m d_{31}^2$ is comparatively small. This term represents the effect of matrix clamping on the fiber properties, and is multiplied by either the s_{11}^E or s_{12}^E terms, depending on the the test case from which the effective property comes. Effective compliance s_{12} is the only ply property for which this inconsistency appears, and from this point on, equation (3.48) is used.

Case B is developed in the same manner as case A, with T_2 and T_3 remaining zero. The constitutive equations remain the same as (3.24), and from (3.22) and (3.23) the needed conditions on the field variables become:

$$\begin{Bmatrix} \overline{T}_1 \\ \overline{D}_3 \end{Bmatrix} = v_2^p \begin{Bmatrix} T_1 \\ D_3 \end{Bmatrix}_p + v_2^m \begin{Bmatrix} T_1 \\ D_3 \end{Bmatrix}_m \tag{3.49}$$

$$\begin{Bmatrix} \overline{S}_1 \\ \overline{E}_3 \end{Bmatrix} = \begin{Bmatrix} S_1 \\ E_3 \end{Bmatrix}_p = \begin{Bmatrix} S_1 \\ E_3 \end{Bmatrix}_m \tag{3.50}$$

Reorganizing the constitutive equations is straightforward and results in:

$$\begin{Bmatrix} T_1 \\ D_3 \end{Bmatrix}_{p,m} = \begin{bmatrix} b'_{11} & b'_{14} \\ -b'_{14} & b'_{44} \end{bmatrix}_{p,m} \begin{Bmatrix} S_1 \\ E_3 \end{Bmatrix}_{p,m} \tag{3.51}$$

where,

$$b'_{11} = \frac{1}{s_{11}^E} \quad b'_{14} = -\frac{d_{31}}{s_{11}^E} \quad b'_{44} = \frac{s_{11}^E \varepsilon_{33}^T - d_{31}^2}{s_{11}^E} \tag{3.52}$$

Substituting into (3.49), and returning the effective constitutive equations to the original form gives:

$$\begin{Bmatrix} S_1 \\ D_3 \end{Bmatrix} = \begin{bmatrix} s_{11} & d_{31} \\ d_{31} & \varepsilon_3 \end{bmatrix}_{B'} \begin{Bmatrix} \overline{T}_1 \\ \overline{E}_3 \end{Bmatrix} \tag{3.53}$$

Again, to determine the effective s_{12}, it is necessary to return to the unused part of the original constitutive equations. For case B, the condition for S_2 is:

$$\overline{S}_2 = v_2^p S_2^p + v_2^m S_2^m \tag{3.54}$$

Substituting for the strains in the matrix and piezoelectric gives:

$$\overline{S}_2 = v_2^p (s_{11}^E T_1^p + d_{31} E_3^p) + v_2^m (s_{12} T_1^m) \tag{3.55}$$

Stresses T_1^p and T_1^m can be found in the reorganized constitutive equations (3.51), and since E_3 is an independent variable the following equation is derived

$$\overline{S}_2 = \frac{s_{12}^E s_{11} v_2^p + s_{12} s_{11}^E v_2^m}{s_{11} v_2^p + s_{11}^E v_2^m} \overline{T}_1 \tag{3.56}$$

Summarizing:

$$s_{11}^{B'} = \frac{s_{11} s_{11}^E}{s_{11} v_2^p + s_{11}^E v_2^m} \tag{3.57}$$

$$s_{12}^{B'} = \frac{s_{12}^E s_{11} v_2^p + s_{12} s_{11}^E v_2^m}{s_{11} v_2^p + s_{11}^E v_2^m} \tag{3.58}$$

$$d_{31}^{B'} = \frac{s_{11} v_2^p d_{31}}{s_{11} v_2^p + s_{11}^E v_2^m} \tag{3.59}$$

Closed Form Combination Model

Combining Cases A and B may be accomplished by replacing the piezoceramic properties in case B with the effective case A material properties. If the other two tests shown in Figure 3.7 are carried out in a similar manner, all the ply properties can be found for the closed form Combination Model. These are given below:

Longitudinal test:

$$d_{31}^{eff} = \frac{d_{31} v_2^p v_3^p \varepsilon_{33} s_{11}}{\left(\overline{s}_1 v_2^p + s_{11}^E v_2^m\right)\overline{\varepsilon} - v_3^m d_{31}^2 \left(v_2^p v_3^m + v_2^m\right)} \tag{3.60}$$

$$s_{11}^{eff} = \frac{s_{11}(s_{11}^E \overline{\varepsilon} - v_3^m d_{31}^2)}{\left(v_2^p \overline{s}_1 + s_{11}^E v_2^m\right)\overline{\varepsilon} - v_3^m d_{31}^2 \left(v_2^p v_3^m + v_2^m\right)} \tag{3.61}$$

$$s_{12}^{eff} = \frac{\left(s_{11} s_{12}^E v_2^p + s_{12} s_{11}^E v_2^m\right)\overline{\varepsilon} - v_3^m d_{31}^2 \left(s_{11} v_2^p + s_{12} v_2^m\right)}{\left(\overline{s}_1 v_2^p + s_{11}^E v_2^m\right)\overline{\varepsilon} - v_3^m d_{31}^2 \left(v_2^p v_3^m + v_2^m\right)} \tag{3.62}$$

Transverse test:

$$s_{22}^{eff} = s_{11} \frac{\left(\overline{s}_1 v_2^m + s_{11}^E v_2^p\right)\overline{\varepsilon} - d_{31}^2 v_3^m \left(v_2^p + v_2^m v_3^m\right)}{\overline{s}_1 \overline{\varepsilon} - d_{31}^2 {v_3^m}^2} \tag{3.63}$$

$$d_{32}^{eff} = \frac{d_{31} v_2^p v_3^p \varepsilon_{33} s_{11}}{\overline{s}_1 \overline{\varepsilon} - {v_3^m}^2 d_{31}^2} \tag{3.64}$$

Vertical test:

$$\varepsilon_{33}^{eff} = \varepsilon_{33} \frac{\left(s_{11} v_2^p + v_2^m \overline{s}_2\right)\left(v_2^p \varepsilon_{33}^T + v_2^m \overline{\varepsilon}\right) - v_2^m v_3^p d_{33}^2 \left(v_3^m v_2^m + v_2^p\right)}{\overline{\varepsilon}\left(s_{11} v_2^p + \overline{s}_2 v_2^m\right) - v_2^m v_3^m v_3^p d_{33}^2} \tag{3.65}$$

In-plane shear modulus:

$$s_{66}^{eff} = \frac{s_{66}^{E} s_{66} v_2^p + s_{66}\left(v_3^p s_{66} + v_3^m s_{66}^{E}\right) v_2^m}{v_3^p s_{66} + v_3^m s_{66}^{E}} \tag{3.66}$$

where:

$$\bar{\varepsilon} = \left(v_3^p \varepsilon_{33} + v_3^m \varepsilon_{33}^{T}\right) \tag{3.67}$$

$$\bar{s}_1 = \left(s_{11} v_3^p + s_{11}^{E} v_3^m\right) \tag{3.68}$$

$$\bar{s}_2 = \left(s_{33}^{E} v_3^p + s_{11} v_3^m\right) \tag{3.69}$$

Note that the effective in-plane shear compliance (s_{66}^{eff}) is completely uncoupled from any electrical effects. This is a result of poling perpendicular to the in-plane shear.

In each equation, the coupling terms are easy to identify. The compliance constants now contain electrical terms, and the strain-to-voltage and dielectric constants contain mechanical terms. A closer examination of the d_{31}^{eff} constant provides insight into the factors that contribute to the actuation along the fibers. If the equations are normalized by s_{11}^{E} and ε_{33}^{T},the expression involving d_{31}^{eff} becomes

$$\frac{d_{31}^{eff}}{d_{31}} = \frac{v_2^p v_3^p \left(\frac{\varepsilon_{33}}{\varepsilon_{33}^{T}}\right)\left(\frac{s_{11}}{s_{11}^{E}}\right)}{\left(v_2^p \left(\frac{\bar{s}_1}{s_{11}^{E}}\right) + v_2^m\right)\left(\frac{\bar{\varepsilon}}{\varepsilon_{33}^{T}}\right) - k_{31}^2 v_3^m \left(v_2^p v_3^m + v_2^m\right)} \tag{3.70}$$

where k_{31} is the familiar material coupling factor given by:

$$k_{31}^2 = \frac{d_{31}^2}{s_{11}^{E} \varepsilon_3^{T}} \tag{3.71}$$

The actuation capability is a direct function of the elastic and dielectric mismatch ratios located in the numerator of the above equation. Higher mismatches in dielectric are detrimental to the actuation, as the term $\varepsilon_{33}/\varepsilon_{33}^{T}$ becomes very small. Improved actuation benefits from a high mismatch in compliance s_{11}/s_{11}^{E}, because the matrix material is soft and does not clamp the fibers. These mismatch ratios also contribute to the denominator terms, but in a less direct manner. The material coupling factor serves as an indication of the ability of the piezoelectric material to exchange electrical and mechanical energy. Since all other terms are positive in the denominator of equation 3.70, larger values of k_{31}^2 lead to better effective actuation capability. PZT-5H type ceramic has a relatively high k_{31}^2 (0.15) compared to other piezoceramics, but the term that contains it is still small compared to the other denominator term. This is a direct consequence of the high dielectric mismatch

between the fiber and matrix. Lowering the mismatch is likely to be a key issue in future work.

3.3.5 Discretization Model

Overall, the combination model is well represented by the closed form equations. The use of the numerical solution seems unnecessary for the material property regimes of interest. There is, however, one facet of the modeling that has yet to be addressed, for which the numerical solution will be well suited. Up to this point, the models have ignored the details of the actual phase geometry and assumed a square piezoceramic fiber. This was necessary to allow description of the ceramic fraction through the use of only two variables, v_2^p and v_3^p. However, through the numerical solution, cases A and B can be applied any number of times, suggesting that a discretized approach may be possible.

Such an approach could be used to model circular fibers. The method involves dividing the matrix/fiber element into thin rectangular slices which can be added together to give a discrete version of a circular fiber. Due to symmetry, a quarter model is adequate to represent the volume element, shown in Figure 3.8.

Note that the volume element is not necessarily square. Slices of matrix and fiber are combined using the case A equations, and then each of these slices are combined through applying the case B geometry equations. The previous definitions of volume fractions, v_2^p and v_3^p are retained to deal with the individual slices. However, to deal with the overall circular nature of the problem, define a width line fraction, x_2, and a thickness line fraction, x_3. These line fractions give the maximum percentage of fiber for a line drawn across the volume element in each of the two directions. Note that the actual volume fraction will be some value lower than the product of the two line fractions and that the maximum possible volume fraction is actually $\pi/4$, and not one.

The following is a summary of the steps used for finding the effective properties using the discretizing method:

- Divide the element into N slices of fiber and matrix of width

$$dx = \frac{x_2}{N} \tag{3.72}$$

- Find the volume fraction of fiber in each slice by finding the average height, h, at each slice:

$$h = \frac{h_1 + h_2}{2} \tag{3.73}$$

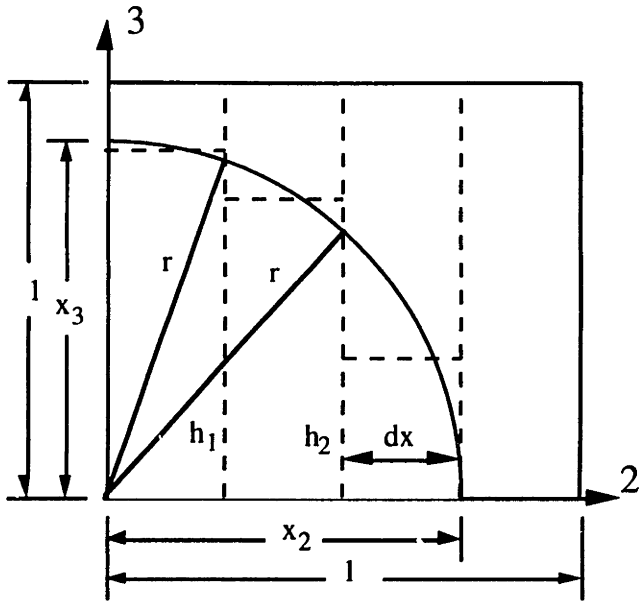

Figure 3.8: Volume element for the discretization model

where h_1 and h_2 are found from the geometry of the element.

- Rewrite the constitutive equations in the form for Case A combination. For the i^{th} slice, apply Case A to matrix and fiber:

$$\mathbf{A}_i = h_i \mathbf{A}_p + (1 - h_i)\mathbf{A}_m \tag{3.74}$$

- This provides the effective constitutive equations for the i^{th} slice. These are rewritten in the original form to give s_{11}^A, s_{12}^A, etc.
- Rewrite the constitutive equations in the form for Case B combination. Each slice is then combined with the others and the final column of pure matrix using:

$$\mathbf{B}_{tot} = \sum_i^N \mathbf{B}_i dx + (1 - x_2)\mathbf{B}_m \tag{3.75}$$

- Rearranging $\mathbf{B}_{tot}$ to the original form of the constitutive equations will yield the final effective properties.

These effective properties represent the fully coupled combination model, now with discrete slices that model the circular geometry in the true specimen. The *Uniform Field* assumption still applies within each slice, but the individual slices imply slightly inconsistent fields at the boundaries. In a sense, fields are allowed to vary (discretely) across the volume element. This type of model is expected to provide better agreement with experimental measurements. The reason for this stems from the fact that the current

specimens have only one fiber layer across the thickness. The dielectric and strain-to-voltage constants are extremely sensitive to the amounts of matrix above and below the fiber, and the averaged thickness in the square fiber models is simply not adequate in this case. For this reason, experimental results are compared to this discretized model.

This is not to say that the models based on square fibers are of limited usefulness. On the contrary, these models will be valuable for piezoceramic fiber composites with multi-fiber layers through the thickness. In these cases, the homogeneous nature of the *Uniform Field* model will be better represented in the composite, and the volume fractions will be a statistical measure of the number of fibers in each direction. These models will form the basis for comparison with other models, such as self-consistent approaches and energy methods to determine effective properties. Note also that the Uniform Field models are able to account for volume fractions above $\pi/4$, where the fibers may be in a hexagonal packing arrangement. The discretized model cannot, and merely represents an extension of the current models to better represent the present experimental geometry.

3.4 Self Consistent Scheme

3.4.1 Introduction

The Self Consistent Scheme (SCS) as a means for evaluating effective material constants has been around since 1946, when Polder and van Santen [49] first considered the problem of effective permeability of a particulate composite material. The actual naming of the method as Self Consistent, however, is attributed to Hill [50] and refers to a model where a fiber is assumed to behave as though it were embedded in an effective media of infinite extent. The properties of this effective material are chosen to lead to a solution that is consistent between the material phases. Since that time, the terms self consistent, concentric cylinders (spheres), doubly embedded cylinders (spheres), and cylinders (spheres) assemblage model have all been used to describe the various microstructure and approaches taken to model the effective properties for fibrous (particulate) composites. Often the terms are misused, and there are important differences discerning the two basic approaches to elasticity solutions.

Self Consistent Approach

When Hill first introduced the term Self Consistent Scheme [50] in 1965, he proposed to model a particulate composite by solving a boundary value problem of a single inclusion of radius 'a' in an infinite effective media, subject to far-field applied loads (Fig. 3.9 (a)). Solution of the boundary problem provided the material constants for the composite. Hill admits the work was based on an earlier application of this method to the modeling of polycrystalline aggregates by Hershey [51], which is a different problem than that of a two-phase composite. He states, however, that "not withstanding this difference in viewpoint, the entire [present] analysis is found to remain structurally close to that for a crystal aggregate." A fellow researcher, Hashin [52] was less convinced, and suggested that a better approach would be to consider the matrix material as another material phase in the boundary value problem. Thus, the element to be modeled was an inclusion surrounded by matrix material, which was subsequently surrounded by an infinite effective material (Fig. 3.9 (b)). This was termed the Generalized Self Consistent Scheme[5].

[5] Also known as the doubly embedded model

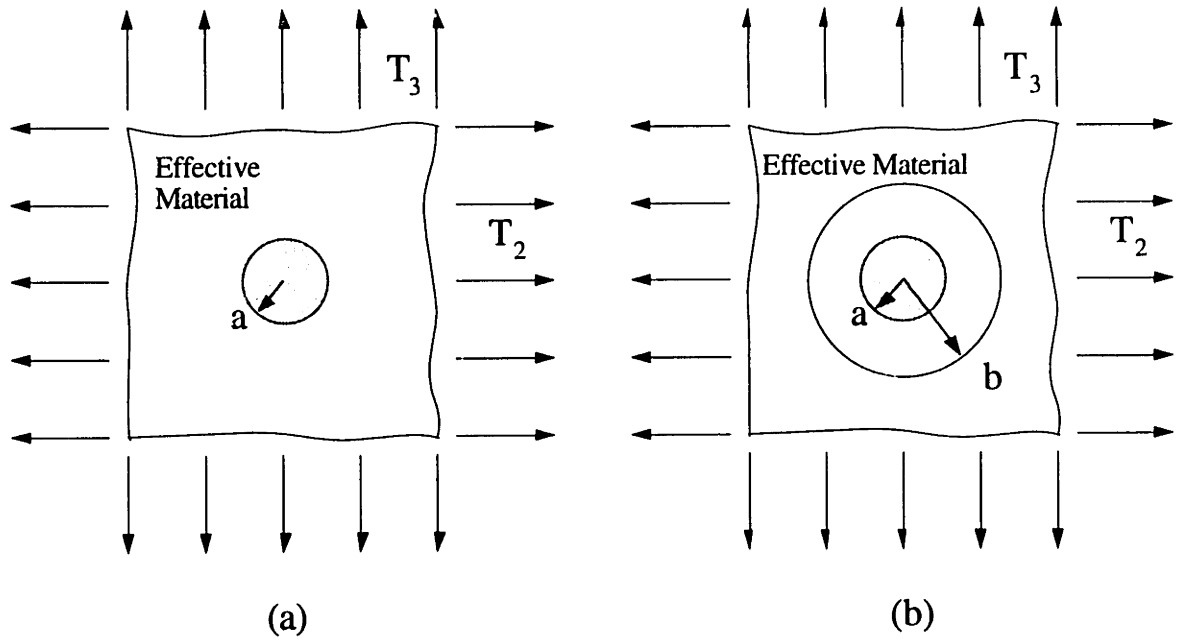

Figure 3.9: Representative Volume Elements of (a) Self Consistent and (b) Generalized Self Consistent

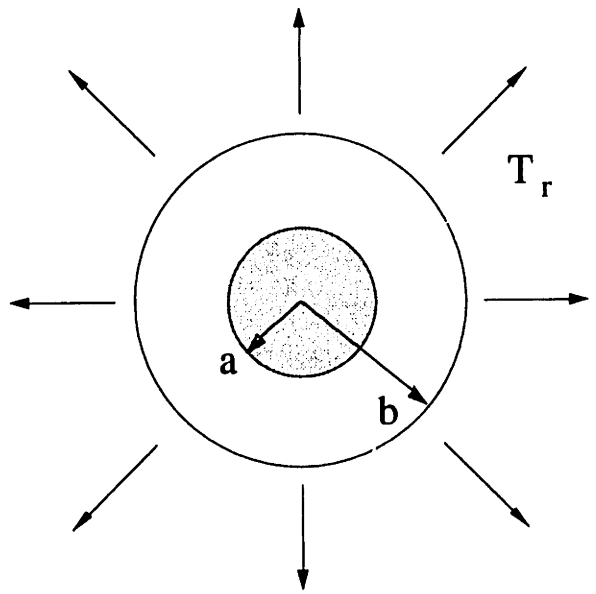

Figure 3.10: Typical repeating element for fibrous or particulate composite (concentric model)

Repeating Element Approach

A very different approach was undertaken at approximately the same time for the solution of effective properties. The difference lies not in the modeling techniques (i.e. direct vs. variational approaches), but with the volume element and boundary conditions chosen. These differences in models virtually always were founded in disagreements with the manner in which the composite microstructure could be best represented. Instead of modeling an inclusion encapsulated in an infinite effective media, this approach was to model the response of a repeating element of the composite and equate its response with that of the overall composite. Such a repeating element is shown in Figure 3.10, where the matrix material surrounds a fiber or particulate material. Another repeating element example is the one used in the Uniform Fields or Finite Element models. The rationale behind this approach was that the entire composite is made up of these repeating elements, each of which behaves in the same manner, so that it is only necessary to analyze a single one.

The difference may seem slight, however, the principle is significantly different. In the Self Consistent Scheme, the loads were applied far field, at infinity. In the repeating element approach, the conditions experienced by the composite macroscopically are applied to the repeating element itself. Models by Whitney & Riley [26], Hill [53], and Hashin & Rosen [25], all utilize this element. In Whitney & Riley and Hill, the effective properties are found by equating the total strain energy of the element (due to applied macroscopic loads) to the strain energy in the matrix and fiber. Hashin & Rosen use the principles of minimum and complementary potential energy to determine bounds on the effective constants. These bounds correspond for the special case of randomly distributed cylinders of varying size, where each cylinder has the same proportion of fiber/matrix volume.[6]

Both methods have been successful in generating reasonable estimates of the various effective material constants. Hashin, in a more recent survey paper [54], however, cautions the user of the Self Consistent or Generalized Self Consistent approaches. He states that the basic premise violates the MMM principle[7] , where dimensions at each level must be substantially larger than the one prior to it. The embedding of the inclusion in an effective media is meaningless since "the latter are averages of the former", and that it is incorrect to have varying elastic (electric) fields in the equivalent body.

---

[6] For fibers, this is called the concentric cylinders assemblage (for particulate, concentric spheres)

[7] Micro-Mini-Macro

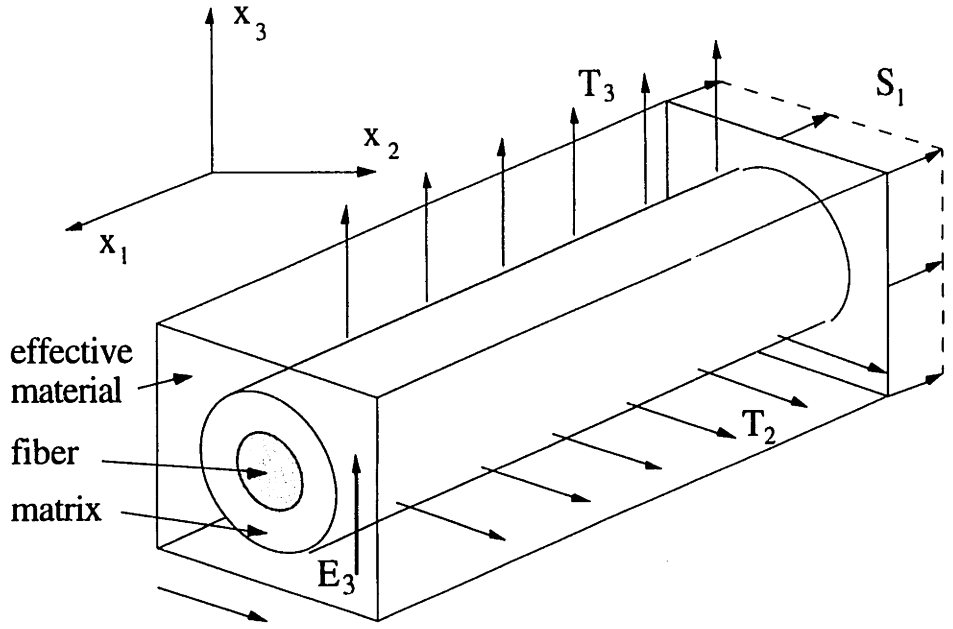

Figure 3.11: Present approach to Self Consistent Scheme for piezoelectric fiber composite

Current Approach

A variation of both approaches is suggested for the present analysis. Consider a repeating element, as in Figure 3.11, that represents a fiber surrounded by an appropriate amount of matrix material, and whose response is typical of the entire composite. However, rather than use energy summations or weighted averages (as in Uniform Fields), use the idea that this element is surrounded by many more of these elements that will have the same response as the modeled element. These other elements will appear as a homogeneous material with unknown effective properties, just as in the standard Self Consistent. The key difference lies in the interpretation of the effective media. Just as in the true Self Consistent, the effective material will have material properties equal to the properties that describe the macroscopic response of the composite. However, the effective material here is truly homogenous, so that everywhere the fields are uniform and equal to those predicted by the macroscopic response. The introduction of the repeating element inclusion should not effect the field distributions or cause varying fields within this effective material.

The appropriate conditions that fulfill this point of view translate into assuming the far-field boundary conditions are applied at the matrix/effective material interface, rather than at infinity. Thus, the initial problem is similar to the repeating element approach. The

notion of the surrounding effective material, although the role it plays is passive, is convenient for establishing the premise of effective response. In this way, the model is similar to Self Consistent approach. Here, the boundary value problem is still solved subject to the consistent fields requirement at the outer interface, but the (bi)harmonic equations do not apply in the effective material. Due to its similarity in general and the presence of an effective material, the term "Self Consistent" is kept to describe this new method.

3.4.2 Analysis of Piezoelectric Continuum

This section continues from the mechanical and electric field equations introduced in section 2.2.1. The conditions of modified plane strain that describe the piezoelectric fiber composites problem are enforced upon these equations to reduce the order of the problem.

Electrical Problem:

The equation governing charge distribution in matter was given in equation 2.1. This can be thought of as the electrical equivalent of elastic equilibrium, and may be expressed in tensor form[43] as

$$D_{i,i} = 0 \tag{3.76}$$

or,

$$\frac{\partial D_2}{\partial x_2} + \frac{\partial D_3}{\partial x_3} = 0 \tag{3.77}$$

since field variables are invariant in the longitudinal (1) direction. The net free charge, ρ_f, may be set to zero in the interior. The electrically equivalent compatibility conditions are given by equation 2.3, and summarized as

$$\varepsilon_{ijk} E_{j,k} = 0 \tag{3.78}$$

where ε_{ijk} is an anti-symmetric tensor ($\varepsilon_{123} = \varepsilon_{231} = \varepsilon_{312} = 1$, and $\varepsilon_{132} = \varepsilon_{321} = \varepsilon_{213} = -1$, all others zero). Reducing this set of three equations results in only one non-zero equation

$$\frac{\partial E_2}{\partial x_3} - \frac{\partial E_3}{\partial x_2} = 0 \tag{3.79}$$

which can be satisfied by the scalar potential Φ defined in equation 2.6.

Elastic Problem:

The equilibrium equations, which were defined in equation 2.9 may also be expressed in the following tensor form:

$$\frac{\partial T_{ij}(t)}{\partial x_j} + P_i(t) = \rho \frac{\partial^2 u_i}{\partial t^2} \tag{3.80}$$

The above equation generates three equations of equilibrium. Ignoring time dependence and body forces, and remembering that derivatives with respect to dimension x_1 are zero, equilibrium equations become:

$$\begin{aligned} \frac{\partial T_2}{\partial x_2} + \frac{\partial T_4}{\partial x_3} &= 0 \\ \frac{\partial T_4}{\partial x_2} + \frac{\partial T_3}{\partial x_3} &= 0 \end{aligned} \tag{3.81}$$

Conditions of compatibility arise from the fact that six strains are derived from only three displacements, indicating that the strains are inter-dependent [47]. The tensor equation from equation 2.10 generates six equations of compatibility. Since all out-of-plane strains (S_5 , S_6) are zero, and there is no dependence of strains on the x_1 direction, only one compatibility equation remains:

$$\frac{\partial^2 S_2}{\partial x_3^2} + \frac{\partial^2 S_3}{\partial x_2^2} = \frac{\partial^2 S_4}{\partial x_2 \partial x_3} \tag{3.82}$$

which is satisfied by the strain-displacement relations given in equation 2.11.

Stress and Electric Potential Functions:

One possible formulation of the combined problem is done using two functions defined in terms of the independent variables, T and E. For the stress problem, the components can be expressed in terms of a single stress function, F, that exactly satisfies equilibrium (Eqn 3.81):

$$T_2 = \frac{\partial^2 F}{\partial x_3^2} \quad T_3 = \frac{\partial^2 F}{\partial x_2^2} \quad T_4 = \frac{\partial^2 F}{\partial x_3 \partial x_2} \tag{3.83}$$

In the electrical problem, it is possible to represent the electric fields by the electric function, Φ:

$$E_2 = -\frac{\partial \Phi}{\partial x_2} \quad E_3 = -\frac{\partial \Phi}{\partial x_3} \tag{3.84}$$

This function is more commonly known as the electric potential. Note that the definition above exactly satisfies equation 3.79.

All that remains is to formulate the two remaining field equations (3.77) and (3.82) in terms of the stress and electric functions. To achieve this, the modified plane strain constitutive equations (2.44) are substituted into (3.77) and (3.82), so that the equations are written solely in terms of T and E (with the exception of S_1). The like terms are grouped together and replaced with the above defined functions. Then,

$$\begin{aligned} L_4F + L_3\Phi + L_aS_1 &= 0 \\ L_3F + L_2\Phi + L_bS_1 &= 0 \end{aligned} \tag{3.85}$$

where the L_i terms are linear differential operators defined as:

$$\begin{aligned} L_4 &= \beta_{11}\frac{\partial^4}{\partial x_3^4} + (2\beta_{12} + \beta_{16})\frac{\partial^4}{\partial x_3^2 \partial x_2^2} + \beta_{22}\frac{\partial^4}{\partial x_2^4} \\ L_3 &= -\beta_{15}\frac{\partial^3}{\partial x_3^3} + (-\beta_{56} + \beta_{14})\frac{\partial^3}{\partial x_3 \partial x_2^2} \\ L_2 &= \beta_{55}\frac{\partial^2}{\partial x_3^2} + \beta_{44}\frac{\partial^2}{\partial x_2^2} \\ L_a &= \beta_a\frac{\partial^2}{\partial x_3^2} + \beta_b\frac{\partial^2}{\partial x_2^2} \\ L_b &= -\beta_c\frac{\partial}{\partial x_3} \end{aligned} \tag{3.86}$$

The modified plane strain material constants were given in equation 2.45. Since S_1 does not vary with x_2 or x_3, $L_aS_1 = L_bS_1 = 0$ and the problem becomes two coupled fourth order differential equations in two variables:

$$\begin{aligned} L_4F + L_3\phi &= 0 \\ L_3F + L_2\phi &= 0 \end{aligned} \tag{3.87}$$

where coupling is caused by the L_3 operator.

Analogy to Coupled Purely Mechanical Problems:

The appearance of the third order differential operator, L_3, creates coupling of the electrical and mechanical problems. This operator exists due to the existence of the piezoelectric constants:

$$L_3 = -\beta_{15}\frac{\partial^3}{\partial x_3^3} + (-\beta_{56} + \beta_{14})\frac{\partial^3}{\partial x_3 \partial x_2^2} \tag{3.88}$$

where

$$\beta_{15} = \frac{\left(s_{11}^E - s_{12}^E\right)d_{31}}{s_{11}^E}$$

$$\beta_{56} = \frac{d_{33}s_{11}^E - d_{31}s_{13}^E}{s_{11}^E} \qquad (3.89)$$

$$\beta_{14} = d_{15}$$

For materials without coupling parameters the two equations would be uncoupled, leaving the two problems to be solved independently.

Interestingly enough, there exists another situation whereby the problems are again coupled, this time for purely mechanical reasons. Materials of a degree of anisotropy high enough to couple the extensional and shear strains will also exhibit coupling of the above nature. An example of such a material is one that has non-orthogonal material principal axes. Lekhnitskii [48] gives the complete problem formulation for a material of arbitrary anisotropy. In such a case, the operator L_3 would have the complementary differentials

$$\frac{\partial^3}{\partial x_3^2 \partial x_2} \quad \text{and} \quad \frac{\partial^3}{\partial x_2^3} \qquad (3.90)$$

These do not appear in the piezoelectric problem because the poling process creates a preferred direction, leaving the 'd' matrix virtually unpopulated for electric fields other than those in the poling direction.

Special Cases:

The coupled problem is a difficult one to solve. Even through complex variable techniques, Lekhnitskii [48], provides solutions to similar problems for only very special cases of materials with rectilinear anisotropy. These include stress distribution around elliptical and circular cavities in materials, and stresses in an infinite plate with circular core. In all cases, the solutions are found for problems which are uncoupled arising from assumptions of isotropy, or special geometry and loading. Is it possible to make some similar assumptions to the current problem to allow easier solution?

The first possibility is to assume isotropy in the piezoelectric. Compliance in the 2 and 3 directions are typically 20% different for short-circuit conditions, allowing for the possibility that the in-plane properties may be made isotropic. However, it is easy to show that the very important piezoelectric stress terms ($\mathbf{e} = \mathbf{c}^E\mathbf{d}$) are very sensitive to small changes of compliance, resulting in errors from 25% to 50% with assumptions of isotropy.

In addition to this, the material has strong electrical anisotropy and can never be assumed electrically isotropic. Furthermore, the governing equations still remain coupled.

One possible assumption may be that the fields are uniform in the materials. Such an assumption was used in all the *Uniform Fields* approaches presented in section 3.3. This not only uncouples the problem but ignores the continuum derived governing equations and relies on constitutive equations and combining rules above (All derivatives are zero, so that there is no continuum problem to solve).

A less drastic assumption is one of uniform fields, but only in the fiber material. It has been shown in various studies [48,55] that the stress distributions must be uniform for an inclusion in an infinite material. This is the well known 'inclusion problem' and holds for even anisotropic cores. One can assume that for matrix materials with less than infinite extent (i.e. other adjacent fibers), these fields will not be exactly uniform, but may be close. This approach is taken here.

This leaves only the matrix material to be considered. The matrix is non-active, therefore $L_3 = 0$, and the problem is uncoupled. In addition, the material is exactly isotropic so that there is a simplification of material parameters that leads to a further simplifying of the governing equations. Since

$$\begin{aligned} & s_{11} = s_{22} \\ & s_{12} = s_{13} \qquad \rightarrow \qquad \beta_{11} = \beta_{22} \\ & s_{55} = 2(s_{11} - s_{12}) \qquad \beta_{55} = 2(\beta_{11} - \beta_{12}) \end{aligned} \tag{3.91}$$

and the problem becomes:

$$\begin{aligned} \nabla^4 F &= 0 \\ \nabla^2 \Phi &= 0 \end{aligned} \tag{3.92}$$

Thus, the electrical and mechanical equations are in the familiar harmonic and biharmonic forms, for which solutions are well known.

3.4.3 Boundary Conditions and General Approach

The premise of the self consistent, described in the previous section. relies on finding the response of the material to a given set of inputs in order to determine the effective material properties. Those applied loads are the longitudinal strain, S_1, the transverse stresses, T_2 and T_3, and the electric field, E_3, as shown in Figure 3.11. As will be explained later, these four loads allow derivation of the entire three-dimensional material property matrix for the fully orthotropic effective material.

The coupled governing equations (Eqn. 3.87) for the piezoelectric material are difficult to solve, and an approximation was made as to the field distribution inside the piezoelectric fiber. Both the electric and elastic fields are assumed to be uniform within the center (piezoelectric) cylinder. This will be a good assumption, as the Finite Element model will show, especially at lower volume fractions. For a cylinder embedded in an infinite medium these fields are exactly uniform, even if the cylinder is elastically anisotropic [55]. However, since the surrounding matrix sheath is not infinite, the fields will be somewhat non-uniform. This nonuniformity, no matter how slight, will pose some difficulties when the problem is rigorously formulated. In the present analysis, the problem will be overconstrained, and it will be necessary to ignore some of the less important boundary constraints. The solution of the overall problem is first summarized as follows:

1. Examine the elastic problem:

(a) Assume stresses are known in the fiber:

$$T_2,\ T_3,\ T_4$$

Transform stresses to polar coordinates:

$$T_r,\ T_\theta,\ T_{r\theta}$$

(b) Solve boundary value problem ($\nabla^4 F = 0$) in the matrix, subject to stresses at the fiber/matrix interface, and subject to uniform "macroscopic" stresses, $\overline{T}_2$ and $\overline{T}_3$ on the matrix/effective material interface:

r = a:

$$T_r^m = T_r^f \quad \text{and} \quad T_{r\theta}^m = T_{r\theta}^f$$

r = b:

$$T_r^m = T_r^{eff} \quad \text{and} \quad T_{r\theta}^m = T_{r\theta}^{eff}$$

where a and b are the fiber and matrix outer diameters (same as shown in Figure 3.9 (b)). This provides a description of stresses throughout the matrix and fiber as functions of fiber stresses , T_2 T_3, T_4 and applied stresses $\overline{T}_2$ and $\overline{T}_3$.

(c) Determine strains S_r, S_θ, and $S_{r\theta}$ in the matrix and fiber using constitutive equations.

(d) Integrate strains to determine displacements u_r and u_θ in both materials.

(e) Equate displacements at boundaries to generate 3 equations relating unknowns (E_2, E_3, T_2, T_3, T_4) to applied loads ($\overline{T}_2$, $\overline{T}_3$, $\overline{E}_3$, $\overline{S}_1$):

r = a:

$$u_r^m = u_r^f \qquad u_\theta^m = u_\theta^f$$

2. Examine the electric problem:

(a) Assume electric fields are known in the fiber:

$$E_2,\ E_3$$

Transform fields to polar coordinates:

$$E_r,\ E_\theta$$

(b) Solve boundary value problem ($\nabla^2\Phi = 0$) for the matrix, subject to electric potential boundary conditions at the fiber/matrix interface and the matrix/effective material interface:

r = a:

$$\Phi^m = \Phi^f$$

r = b:

$$\Phi^m = \Phi^{eff}$$

(c) Determine the electrical displacements, D_r, in the matrix and fiber using constitutive equations.

(d) Equate the electrical displacements to generate 2 equations relating unknowns (E_2, E_3, T_2, T_3, T_4) to applied loads ($\overline{T}_2$, $\overline{T}_3$, $\overline{E}_3$, $\overline{S}_1$):

r = a:

$$D_r^m = D_r^f$$

3. Solve the system of 5 equations for 5 unknowns:

(a) Solve for the assumed stresses and electric fields in the fiber in terms of the applied loads, $\overline{T}_2$, $\overline{T}_3$, $\overline{E}_3$, $\overline{S}_1$.

Up to this point, the problem has been formulated in exactly the same manner as the repeating-element approach. The loads have been applied to the exterior of the matrix sheath (the matrix/effective material interface) without regard to the effective material. This was possible because the macroscopic loads applied ($\overline{T}_2$, $\overline{T}_3$, $\overline{E}_3$, $\overline{S}_1$ and $\overline{T}_4 = \overline{E}_2 = 0$) were the independent variables in the analysis, and the complementary macroscopic fields ($\overline{T}_1$, $\overline{S}_2$, $\overline{S}_3$, $\overline{S}_4$, $\overline{D}_2$, $\overline{D}_3$) did not appear. Thus, it was not necessary to specify the nature of the relationship between these field variables, and the problem has been kept general.

At this stage, there are several options that may be pursued. One typical approach, as discussed in section 3.4.1, is to equate the strain energy of the repeating element with that of an effective material that undergoes the macroscopically uniform deformations due to the macroscopic applied loads. However, the approach used here, is the use of an effective material surrounding the repeating element, as in the traditional self consistent. Here, the fields are consistent between the matrix/effective material interface as well as the fiber/matrix interface. The enforcing of these consistent fields brings into the analysis the unknown effective material constants through the effective material constitutive equations. Solution of a final system of equations determines the effective constants for the piezoelectric fiber composite.

4. Examine the effective material:

(a) Formulate the fully orthotropic constitutive equations for the effective material in the same manner as for the other two materials (Eqn. 2.43-2.45).

(b) Determine strains S_r, S_θ, and $S_{r\theta}$ in the effective material using constitutive equations.

(c) Integrate strains to determine displacements, and equate displacements in matrix and effective material:

r = b:

$$u_r^m = u_r^{eff} \qquad u_\theta^m = u_\theta^{eff}$$

(d) Determine electrical displacements , D_r, in the effective material using constitutive equations.

(e) Equate electrical displacements in matrix and effective material:

r = b:

$$D_r^m = D_r^{eff}$$

(f) There remains only one applied load whose complementary field has not been used. This is the applied strain loading, $\overline{S}_1$. During the problem formulation, this strain was written as an independent variable with the constraint that it is uniform across the entire volume element. To accomplish this load requires a special stress, $\overline{T}_1$, which may be found from a force summation. This summation is simply a requirement that the overall longitudinal force of the repeating element must be equal to that of the effective material:

$$\overline{T}_1^{eff} A_{elem} = \int_{A_{elem}} (T_1^f + T_i^m) dA$$

(g) The equations generated in steps (c), (e), and (f) describe a system of equations for the effective material constants in terms of the matrix and fiber material constants and the volume fraction. Solution of this system is done simply by a matrix inversion.

3.4.4 Self Consistent Analysis

The section follows the problem summary given in the previous section and elaborates on the steps given there. The first step is to examine the elastic problem:

1. The Elastic Problem:

For the time being, assume that the stresses within the fiber cylinder are known. Since they are to describe uniform fields, they can be immediately written as follows:

$$T_2^f = T_2 \qquad T_3^f = T_3 \qquad T_4^f = T_4 \tag{3.93}$$

The stresses T_2 and T_3 are the normal stresses in the 2 and 3 axis directions. The stress T_4 is the shear stress in the 2-3 plane. Since all boundary conditions are to be imposed in the polar coordinate domain, the stresses are converted to polar coordinates:

$$T_r^f = \left(\frac{T_2 + T_3}{2}\right) + \left(\frac{T_2 - T_3}{2}\right)\cos 2\theta + T_4 \sin 2\theta$$

$$T_\theta^f = \left(\frac{T_2 + T_3}{2}\right) - \left(\frac{T_2 - T_3}{2}\right)\cos 2\theta - T_4 \sin 2\theta \qquad (3.94)$$

$$T_{r\theta}^f = -\left(\frac{T_2 - T_3}{2}\right)\sin 2\theta + T_4 \cos 2\theta$$

Macroscopic loads are applied to the overall body through the effective material sheath. These stresses are also uniform. In this material, only the normal stresses are applied[8].

$$T_2^{eff} = \overline{T}_2 \quad T_3^{eff} = \overline{T}_3 \quad T_4^{eff} = 0 \qquad (3.95)$$

These are also transformed to polar coordinates:

$$\overline{T}_r = \left(\frac{\overline{T}_2 + \overline{T}_3}{2}\right) + \left(\frac{\overline{T}_2 - \overline{T}_3}{2}\right)\cos 2\theta$$

$$\overline{T}_\theta = \left(\frac{\overline{T}_2 + \overline{T}_3}{2}\right) - \left(\frac{\overline{T}_2 - \overline{T}_3}{2}\right)\cos 2\theta \qquad (3.96)$$

$$\overline{T}_{r\theta} = 0$$

These two materials surround the matrix and provide the boundary conditions for the biharmonic problem in the matrix material. The general solution of the biharmonic problem ($\nabla^4 F = 0$) is an infinite series:

$$\begin{aligned} F = {} & a_0 \log r + b_0 r^2 + c_0 r^2 \log r + d_0 r^2\theta + a_0'\theta \\ & + \frac{a_1}{2} r\theta \sin\theta + (b_1 r^3 + a_1' r^{-1} + b_1' r \log r)\cos\theta \\ & - \frac{c_1}{2} r\theta \cos\theta + (d_1 r^3 + c_1' r^{-1} + d_1' r \log r)\sin\theta \\ & + \sum_{n=2}^{\infty} (a_n r^n + b_n r^{n+2} + a_n' r^{-n} + b_n' r^{-n+2})\cos n\theta \\ & + \sum_{n=2}^{\infty} (c_n r^n + d_n r^{n+2} + c_n' r^{-n} + d_n' r^{-n+2})\sin n\theta \end{aligned} \qquad (3.97)$$

---

[8] The shear stress and transverse electric field are part of an uncoupled system that may be determined separately

However, the fields in the matrix will only be a function of terms that are of the same order as the materials surrounding it (i.e. constant and 2θ terms). Higher order terms will drop out, as will the lower $\cos\theta$ and $\sin\theta$ terms. Other terms are inadmissible, such as the θ terms denoted by the a_0', a_1, c_1 constants. These are used to model singularities and do not apply here. The elastic fields in the matrix material may be described by the reduced potential with renamed constants:

$$F = a_0 \log r + b_0 r^2 + \left(a_2 r^2 + b_2 r^4 + c_2 \frac{1}{r^2} + d_2\right)\cos 2\theta + \left(e_2 r^2 + f_2 r^4 + g_2 \frac{1}{r^2} + h_2\right)\sin 2\theta \tag{3.98}$$

From this stress potential comes the stresses within the matrix:

$$T_r^m = \frac{a_0}{r^2} + 2b_0 + \left(-2a_2 - 6\frac{c_2}{r^4} - 4\frac{d_2}{r^2}\right)\cos 2\theta + \left(-2e_2 - 6\frac{g_2}{r^4} - 4\frac{h_2}{r^2}\right)\sin 2\theta$$

$$T_\theta^m = \frac{-a_0}{r^2} + 2b_0 + \left(2a_2 + 12b_2 r^2 + 6\frac{c_2}{r^4}\right)\cos 2\theta + \left(2e_2 + 12f_2 r^2 + 6\frac{g_2}{r^4}\right)\sin 2\theta$$

$$T_{r\theta}^m = \left(2a_2 + 6b_2 r^2 - 6\frac{c_2}{r^4} - 2\frac{d_2}{r^2}\right)\sin 2\theta + \left(-2e_2 - 6f_2 r^2 + 6\frac{g_2}{r^4} + 2\frac{h_2}{r^2}\right)\cos 2\theta \tag{3.99}$$

Since the stresses are "known" in the two materials surrounding the matrix, these stresses act as boundary conditions for the matrix boundary value problem. The appropriate conditions for stress equilibrium on the interfaces are:

$$T_r^m = T_r^f \quad \text{and} \quad T_{r\theta}^m = T_{r\theta}^f \quad \text{at} \quad r = a$$
$$T_r^m = \overline{T}_r \quad \text{and} \quad T_{r\theta}^m = \overline{T}_{r\theta} \quad \text{at} \quad r = b \tag{3.100}$$

Solution for the constants is straightforward and results in:

$$a_0 = \frac{a^2 b^2}{b^2 - a^2}\left[\left(\frac{T_2 + T_3}{2}\right) - \left(\frac{\overline{T}_2 + \overline{T}_3}{2}\right)\right]$$

$$b_0 = \frac{1}{2\left(b^2 - a^2\right)}\left[-a^2\left(\frac{T_2 + T_3}{2}\right) + b^2\left(\frac{\overline{T}_2 + \overline{T}_3}{2}\right)\right]$$

$$
\begin{aligned}
a_2 &= \frac{b^2\left(4a^4+a^2b^2+b^4\right)}{2\left(a^2-b^2\right)^3}\left(\frac{\overline{T}_2-\overline{T}_3}{2}\right)-\frac{a^2\left(4a^4+a^2b^2+b^4\right)}{2\left(a^2-b^2\right)^3}\left(\frac{T_2-T_3}{2}\right)\\
b_2 &= -\frac{a^2b^2}{\left(a^2-b^2\right)^3}\left[\left(\frac{\overline{T}_2-\overline{T}_3}{2}\right)-\left(\frac{T_2-T_3}{2}\right)\right]\\
c_2 &= \frac{a^4b^4\left(a^2+b^2\right)}{2\left(a^2-b^2\right)^3}\left[\left(\frac{\overline{T}_2-\overline{T}_3}{2}\right)-\left(\frac{T_2-T_3}{2}\right)\right]\\
d_2 &= -\frac{a^2b^2\left(a^4+a^2b^2+b^4\right)}{\left(a^2-b^2\right)^3}\left[\left(\frac{\overline{T}_2-\overline{T}_3}{2}\right)-\left(\frac{T_2-T_3}{2}\right)\right]\\
e_2 &= -\frac{a^2\left(a^4+a^2b^2+4b^4\right)}{2\left(a^2-b^2\right)^3}T_4\\
f_2 &= \frac{a^2b^2}{\left(a^2-b^2\right)^3}T_4\\
g_2 &= -\frac{a^4b^4\left(a^2+b^2\right)}{2\left(a^2-b^2\right)^3}T_4\\
h_2 &= \frac{a^2b^2\left(a^4+a^2b^2+b^4\right)}{\left(a^2-b^2\right)^3}T_4
\end{aligned}
\qquad (3.101)
$$

The stresses throughout the fiber and matrix are now known as a function of the macroscopic applied loads and the assumed stresses in the fiber. To eliminate these latter terms, and be able to describe the problem solely in terms of the applied loads, it is necessary to also match the displacements at the two interfaces. The displacements are derived from an integration of complementary fields, the strains. Once again, the fields need to be converted to polar coordinates to allow matching of boundary conditions along the circular interface. The transformation for the strain matrix is given by

$$
\begin{Bmatrix} S_r \\ S_\theta \\ S_{r\theta} \end{Bmatrix} = \mathbf{R}_S \begin{Bmatrix} S_2 \\ S_3 \\ S_4 \end{Bmatrix} \qquad (3.102)
$$

where $\mathbf{R}_S$ is the second order transformation matrix given in section 5.2.2. The Cartesian strains can then be replaced by the independent field variables (E_2, E_3, $\overline{S}_1$, T_2, T_3, T_4) through the constitutive equations for each material. In this way, the strain can also be written as functions of the same loads as the equations developed thus far.

In the matrix material, the strains are simply:

$$S_r^m = \beta_{11}^m T_r^m + \beta_{12}^m T_\theta^m + \beta_a^m S_1$$
$$S_\theta^m = \beta_{12}^m T_r^m + \beta_{22}^m T_\theta^m + \beta_a^m S_1 \qquad (3.103)$$
$$S_{r\theta}^m = \beta_{66}^m T_{r\theta}^m$$

It is possible to show that these strains satisfy compatibility. The polar form of the two dimensional compatibility equation is given in REF[48]:

$$\frac{\partial^2 S_r}{\partial \theta^2} - r\frac{\partial S_r}{\partial r} + r\frac{\partial^2 (rS_{r\theta})}{\partial r^2} - \frac{\partial^2 (rS_{r\theta})}{\partial r \partial \theta} = 0 \qquad (3.104)$$

Introduction of the stresses (Eqn. 3.99) into the polar constitutive equations (Eqn. 3.103) will satisfy the above compatibility. The next step is the determination of the displacements. The strain-displacement relations in polar coordinates are:

$$S_r = \frac{\partial u_r}{\partial r}$$
$$S_\theta = \frac{u}{r} + \frac{1}{r}\frac{\partial u_\theta}{\partial \theta} \qquad (3.105)$$
$$S_{r\theta} = \frac{1}{r}\frac{\partial u_r}{\partial \theta} + \frac{\partial u_\theta}{\partial r} - \frac{u_\theta}{r}$$

from which the displacements are found by integration:

$$u_r = \int S_r dr + F_\theta$$
$$u_\theta = \int (r\varepsilon_\theta - u) d\theta - \int F_\theta d\theta + G_r \qquad (3.106)$$

where F_θ and G_r are constants of integration that are functions of θ only and r only, respectively. To determine these constants of integration, the above displacements may be substituted into the final equation in equation 3.105 for $S_{r\theta}$ and compared to the value of $S_{r\theta}$ in equation. 3.103. The following differential equation is found for the constants:

$$\frac{1}{r}\frac{\partial F_\theta}{\partial \theta} + \frac{\partial G_r}{\partial r} + \frac{1}{r}\int F_\theta d\theta - \frac{1}{r} G_r = 0 \qquad (3.107)$$

The only solutions that satisfy the above are:

$$F_\theta = H\sin\theta + K\cos\theta \qquad \text{and} \qquad G_r = J_r \qquad (3.108)$$

Conditions of symmetry force H and K to be zero, because the first order θ terms do not preserve the geometry and loading symmetries. The term G_r must also be zero because it represents a rotation of the material element about the 1-axis, which again

violates symmetry. These arguments are true for both the fiber and matrix displacements. For an applied macroscopic shear load, $\overline{T}_4$, these terms may not necessarily be zero[9] .

For the matrix material, the following terms comprise the displacement:

constant:

$$u_r^m = -\frac{a^2}{b^2-a^2}\left(\frac{T_2+T_3}{2}\right)\left[\beta_{11}^m\left(\frac{b^2}{r}+r\right)\right]+$$
$$\frac{b^2}{b^2-a^2}\left(\frac{\overline{T}_2+\overline{T}_3}{2}\right)\left[\beta_{11}^m\left(\frac{a^2}{r}+r\right)+\beta_{12}^m\left(\frac{-a^2}{r}+r\right)\right]+r\beta_{a}^m S_1$$
$$u_\theta^m = 0$$

cos2θ:

$$u_r^m = \left[\beta_{11}^m\left(-2a_2 r+2\frac{c_2}{r^3}+4\frac{d_2}{r}\right)+\beta_{12}^m\left(2a_2 r+4b_2 r^3-2\frac{c_2}{r^3}\right)\right]\cos 2\theta$$
$$u_\theta^m = -\left[\beta_{11}^m\left(2e_2 r+6f_2 r^3+2\frac{g_2}{r^3}-2\frac{h_2}{r}\right)+\beta_{12}^m\left(-2e_2-2f_2 r^3-2\frac{g_2}{r^3}-2\frac{h_2}{r}\right)\right]\cos 2\theta \qquad (3.109)$$

sin2θ:

$$u_r^m = \left[\beta_{11}^m\left(-2e_2 r+2\frac{g_2}{r^3}+4\frac{h_2}{r}\right)+\beta_{12}^m\left(2e_2 r+4f_2 r^3-2\frac{g_2}{r^3}\right)\right]\sin 2\theta$$
$$u_\theta^m = -\left[\beta_{11}^m\left(2a_2 r+6b_2 r^3+2\frac{c_2}{r^3}-2\frac{d_2}{r}\right)+\beta_{12}^m\left(-2a_2-2b_2 r^3-2\frac{c_2}{r^3}-2\frac{d_2}{r}\right)\right]\sin 2\theta$$

Since the fiber material is rectangularly orthotropic, the polar constitutive equations are somewhat less concise, and have an angular dependence:

$$S_r^f = \left(\frac{S_2^f+S_3^f}{2}\right)+\left(\frac{S_2^f-S_3^f}{2}\right)\cos 2\theta+\frac{S_4^f}{2}\sin 2\theta$$
$$S_\theta^f = \left(\frac{S_2^f+S_3^f}{2}\right)-\left(\frac{S_2^f-S_3^f}{2}\right)\cos 2\theta-\frac{S_4^f}{2}\sin 2\theta \qquad (3.110)$$
$$S_{r\theta}^f = S_4\cos 2\theta-(S_2-S_3)\sin 2\theta$$

where

$$S_2^f+S_3^f = E_3\left(\beta_{15}^f+\beta_{56}^f\right)+T_2\left(\beta_{11}^f+\beta_{12}^f\right)+T_3\left(\beta_{12}^f+\beta_{22}^f\right)$$

9 The shear modulus s_{44}^{eff} is not of interest here, since the application is of planar structures

$$S_2^f - S_3^f = E_3\left(\beta_{15}^f - \beta_{56}^f\right) + T_2\left(\beta_{11}^f - \beta_{12}^f\right) + T_3\left(\beta_{12}^f - \beta_{22}^f\right) \qquad (3.111)$$

$$S_4^f = \beta_{14}^f E_2 + \beta_{66}^f T_4$$

Integration for the displacements in the fiber gives:

constant:

$$u_r^f = \frac{r}{2}\left[E_3\left(\beta_{15}^f + \beta_{56}^f\right) + T_2\left(\beta_{11}^f + \beta_{12}^f\right) + T_3\left(\beta_{12}^f + \beta_{22}^f\right) + S_1\left(\beta_a^f + \beta_b^f\right)\right]$$

$$u_\theta^f = 0$$

cos2θ:

$$u_r^f = \frac{r}{2}\left[E_3\left(\beta_{15}^f - \beta_{56}^f\right) + T_2\left(\beta_{11}^f - \beta_{12}^f\right) + T_3\left(\beta_{12}^f - \beta_{22}^f\right) + S_1\left(\beta_a^f - \beta_b^f\right)\right]\cos 2\theta$$

$$u_\theta^f = \frac{r}{2}\left[\beta_{14}^f E_2 + \beta_{66}^f T_4\right]\cos 2\theta \qquad (3.112)$$

sin2θ:

$$u_r^f = \frac{r}{2}\left[\beta_{14}^f E_2 + \beta_{66}^f T_4\right]\sin 2\theta$$

$$u_\theta^f = -\frac{r}{2}\left[E_3\left(\beta_{15}^f - \beta_{56}^f\right) + T_2\left(\beta_{11}^f - \beta_{12}^f\right) + T_3\left(\beta_{12}^f - \beta_{22}^f\right) + S_1\left(\beta_a^f - \beta_b^f\right)\right]\sin 2\theta$$

The next step is to equate the displacements in the fiber and matrix at r=a. This gives 5 equations, which when added to the 2 from the electric problem gives 7 equations in only 5 unknowns (E_2, E_3, T_2, T_3, T_4). An examination of the displacement equations reveals that two of the displacement terms for the fiber (3.112) are redundant, while two for the matrix (3.109) are *almost* redundant. When the displacements are equated, the equations for the u_θ displacements are almost exactly the same as those for u_r.

This derives from the fact that the fields were assumed uniform within the fiber, when actually they will be slightly nonuniform due to the finite extent of the surrounding material (matrix). The fields within the fiber need additional terms to describe the variations, and it is possible (although lengthy) to show that an infinite series is necessary to rigorously formulate the problem. However, the uniform assumption is close to the actual distributions so that the extra terms were originally ignored. Had the matrix been infinite in dimension, these equations would likely be redundant, and the uniform fields would exactly describe the fiber distribution, as predicted by Eshelby [55].

The extra equations act to overconstrain the problem. The decision at this point was to ensure the most important equations are satisfied. Here, the radial displacements u_r are more fundamental to the problem, as loads are applied in the transverse direction. The tangential displacements, u_θ, are not as important, and ignoring them will result (potentially) in slight interface sliding. However, these equations are very similar to those for the radial displacement, so that this sliding will be very small. The equations are summarized in equation 3.126.

2. The Electric Problem:

Uniform electric fields are assumed in the fiber material:

$$E_2^f = E_2 \qquad \text{and} \qquad E_3^f = E_3 \tag{3.113}$$

In order to enforce the electrical boundary conditions, the fields will need to be written in polar coordinates. Since electric fields are first order tensors, transformations are carried out using a first order transformation matrix, R_E, whose form is given in section 5.2.2.

$$\begin{Bmatrix} E_r \\ E_\theta \end{Bmatrix} = R_E \begin{Bmatrix} E_2 \\ E_3 \end{Bmatrix} \tag{3.114}$$

The transformation gives:

$$\begin{aligned} E_r^f &= E_2 \cos\theta + E_3 \sin\theta \\ E_\theta^f &= -E_2 \sin\theta + E_3 \cos\theta \end{aligned} \tag{3.115}$$

One of the boundary conditions to be satisfied for this electrical problem is that of equal scalar potentials along the interface. The potential is related to the fields through

$$E_r = -\frac{\partial \Phi}{\partial r} \qquad \text{and} \qquad E_\theta = -\frac{1}{r}\frac{\partial \Phi}{\partial \theta} \tag{3.116}$$

Integration of equation 3.115 reveals the potential in the fiber to be:

$$\Phi^f = -rE_2 \cos\theta - rE_3 \sin\theta \tag{3.117}$$

The macroscopic loads are applied to the overall body through the effective material surrounding the matrix. These applied loads are uniform:

$$E_2^{eff} = 0 \qquad E_3^{eff} = \bar{E}_3 \tag{3.118}$$

Note that the macroscopic electric field is restricted to be only in the 3 axis direction, due to the electrode placement on the composite. However, transverse fields,

E_2, may exist in the fiber or matrix material. Transforming these fields to polar coordinates and integrating for the potential gives:

$$\begin{aligned} E_r^{eff} &= \bar{E}_3 \sin\theta \\ E_\theta^{eff} &= \bar{E}_3 \cos\theta \\ \Phi^{eff} &= -\bar{E}_3 r \sin\theta \end{aligned} \tag{3.119}$$

The electric field distribution within the matrix is governing by the harmonic equation $\nabla^2\Phi = 0$. The general solution is an infinite series, but the matrix potential will only contain terms similar to that in the two phases surrounding it. Thus, the potential in the matrix is described as:

$$\Phi^m = \left(a_1 r + \frac{b_1}{r}\right)\cos\theta + \left(c_1 r + \frac{d_1}{r}\right)\sin\theta \tag{3.120}$$

The electric potential at the matrix boundaries must be equal to that of the surrounding materials. Thus, the potentials in equations 3.117 and 3.119 serve as boundary conditions for the matrix problem. The conditions are:

$$\begin{aligned} \Phi^m &= \Phi^f \qquad \text{at } r = a \\ \Phi^m &= \Phi^{eff} \qquad \text{at } r = b \end{aligned} \tag{3.121}$$

Solution of the above equations provides the values of the constants $a_1 \ldots d_1$ in terms of the fiber and macroscopic effective fields:

$$\begin{aligned} a_1 &= \frac{a^2}{b^2 - a^2} E_2 & b_1 &= \frac{a^2}{b^2 - a^2} E_3 - \frac{b^2}{b^2 - a^2} \bar{E}_3 \\ c_1 &= -\frac{a^2 b^2}{b^2 - a^2} E_2 & d_1 &= -\frac{a^2 b^2}{b^2 - a^2} E_3 + \frac{a^2 b^2}{b^2 - a^2} \bar{E}_3 \end{aligned} \tag{3.122}$$

The electric fields are now known through the fiber and matrix in terms of the same field variables. Enforcing the second boundary condition of equal electrical displacement will allow the problem to be described solely in terms of the applied macroscopic loads. The polar electrical displacements may be written using the transformation:

$$\begin{Bmatrix} D_r \\ D_\theta \end{Bmatrix} = R_E \begin{Bmatrix} D_2 \\ D_3 \end{Bmatrix} \tag{3.123}$$

$$D_r = D_2 \cos\theta + D_3 \sin\theta$$

The Cartesian electrical displacements are related to the stresses and electric fields through the constitutive equations. For the matrix:

$$D_r^m = \beta_{44}^m E_r^m = \beta_{44}^m \left[-\left(a_1 - \frac{b_1}{r} \right) \cos\theta - \left(c_1 r - \frac{d_1}{r} \right) \sin\theta \right] \qquad (3.124)$$

and for the fiber:

$$D_r^f = (\beta_{44}^f E_2 + \beta_{14}^f T_4)\cos\theta + (\beta_{55}^f E_3 + \beta_{15}^f T_2 + \beta_{56}^f T_3 + \beta_c^f S_1)\sin\theta \quad (3.125)$$

Equating the electrical displacements at r=b gives two equations (one from $\sin\theta$ and one from $\cos\theta$) of the 5 total needed to determine the 5 unknowns (E_2, E_3, T_2, T_3, T_4) in terms of the applied macroscopic loads ($\overline{T}_2$, $\overline{T}_3$, $\overline{E}_3$, $\overline{S}_1$).

3. Solve the System of Equations:

The 5 equations are best summarized in matrix form. The terms from the matrix material, $a_0 \ldots h_2$, have been combined and condensed as much as possible:

$$\begin{bmatrix} A_{11} & A_{12} & A_{13} & 0 & 0 \\ A_{21} & A_{22} & A_{23} & 0 & 0 \\ A_{31} & A_{32} & A_{33} & 0 & 0 \\ 0 & 0 & 0 & A_{44} & A_{45} \\ 0 & 0 & 0 & A_{54} & A_{55} \end{bmatrix} \begin{Bmatrix} T_2 \\ T_3 \\ E_3 \\ T_4 \\ E_2 \end{Bmatrix} = \begin{bmatrix} D_{11} & D_{12} & D_{13} & 0 \\ D_{21} & D_{22} & D_{23} & 0 \\ D_{31} & 0 & 0 & D_{41} \\ 0 & 0 & 0 & 0 \\ 0 & 0 & 0 & 0 \end{bmatrix} \begin{Bmatrix} \overline{S}_1 \\ \overline{T}_2 \\ \overline{T}_3 \\ \overline{E}_3 \end{Bmatrix} \quad (3.126)$$

where the terms A_{ij} and D_{ij} are given in the Appendix.

Note that the separate equations in the matrix describe two separate, uncoupled systems. The first of these involves fields T_2, T_3, and E_3, which may be named the normal system. The second set involves T_4 and E_2, or the shear system. These two problems are uncoupled. Furthermore, for the applied macroscopic loads, there is no forcing in the shear system. Thus, the fields within the fiber, T_4 and E_2, must be zero. The remaining, normal, system may be reduced to:

$$\begin{bmatrix} A_{11} & A_{12} & A_{13} \\ A_{21} & A_{22} & A_{23} \\ A_{31} & A_{32} & A_{33} \end{bmatrix} \begin{Bmatrix} T_2 \\ T_3 \\ E_3 \end{Bmatrix} = \begin{bmatrix} D_{11} & D_{12} & D_{13} & 0 \\ D_{21} & D_{22} & D_{23} & 0 \\ D_{31} & 0 & 0 & D_{34} \end{bmatrix} \begin{Bmatrix} \overline{S}_1 \\ \overline{T}_2 \\ \overline{T}_3 \\ \overline{E}_3 \end{Bmatrix} \qquad (3.127)$$

The system is easily solved:

$$\begin{Bmatrix} T_2 \\ T_3 \\ T_4 \end{Bmatrix} = A^{-1} D \begin{Bmatrix} \overline{S}_1 \\ \overline{T}_2 \\ \overline{T}_3 \\ \overline{E}_3 \end{Bmatrix} = C \begin{Bmatrix} \overline{S}_1 \\ \overline{T}_2 \\ \overline{T}_3 \\ \overline{E}_3 \end{Bmatrix} \qquad (3.128)$$

4. Examine the Effective Material:

The effective material will have orthotropy of higher degree than the piezoelectric or matrix materials. Since the constitutive equations for the effective material will be needed, the next task is to determine the modified plane strain property relations. This follows the discussion accompanying equations 2.43-2.45. Note that the following are *not* the same as those equations for the piezoelectric.

$$\begin{aligned}
\bar{S}_2 &= \beta_{11}^{eff}\bar{T}_2 + \beta_{12}^{eff}\bar{T}_3 + \beta_{15}^{eff}\bar{E}_3 + \beta_a^{eff}\bar{S}_1 \\
\bar{S}_3 &= \beta_{12}^{eff}\bar{T}_2 + \beta_{22}^{eff}\bar{T}_3 + \beta_{56}^{eff}\bar{E}_3 + \beta_b^{eff}\bar{S}_1 \\
\bar{D}_3 &= \beta_{15}^{eff}\bar{T}_2 + \beta_{56}^{eff}\bar{T}_3 + \beta_{55}^{eff}\bar{E}_3 + \beta_c^{eff}\bar{S}_1 \\
\bar{T}_1 &= -\beta_a^{eff}\bar{T}_2 - \beta_b^{eff}\bar{T}_3 + \beta_c^{eff}\bar{E}_3 + \beta_d^{eff}\bar{S}_1
\end{aligned} \tag{3.129}$$

where

$$\beta_a = \frac{s_{12}^E}{s_{11}^E} \quad \beta_b = \frac{s_{13}^E}{s_{11}^E} \quad \beta_c = \frac{d_{31}}{s_{11}^E} \quad \beta_d = \frac{1}{s_{11}^E} \quad .$$

$$\beta_{15} = d_{32} - \frac{d_{31}s_{12}^E}{s_{11}^E} \quad \beta_{56} = \frac{d_{33}s_{11}^E - d_{31}s_{13}^E}{s_{11}^E} \quad \beta_{55} = \frac{\varepsilon_{33}^T s_{11}^E - d_{31}^2}{s_{11}^E} \tag{3.130}$$

$$\beta_{11} = s_{22}^E - \frac{s_{12}^{E\,2}}{s_{11}^E} \quad \beta_{12} = s_{23}^E - \frac{s_{12}^E s_{13}^E}{s_{11}^E} \quad \beta_{22} = \frac{s_{11}^E s_{33}^E - s_{13}^{E\,2}}{s_{11}^E}$$

The independent field variables ($\bar{T}_2$, $\bar{T}_3$, $\bar{E}_3$, $\bar{S}_1$) in the above equations are the macroscopic, uniform loads applied to the effective material. In accordance with the premise of the model, these formed some of the boundary conditions at the matrix outer boundary. The resulting complementary fields ($\bar{S}_2$, $\bar{S}_3$, $\bar{D}_3$, $\bar{T}_1$) must match between the matrix and the effective material at r=b. These complementary fields are related to the applied loads through the above constitutive equations. In this manner, the effective material constants become introduced to the problem, and may be solved for. The mechanical boundary conditions are satisfied by equating displacements at the interface. Displacements for the matrix are known (Eqn 3.109). Displacements for the effective material may be found in the same manner as for the fiber, where the polar strains are integrated to determine the polar displacements. The radial displacement of the effective material is:

constant:

$$u_r^{eff} = \frac{r}{2}\left[(\beta_{15}+\beta_{56})\bar{E}_3 + (\beta_a+\beta_b)\bar{S}_1 + (\beta_{11}+\beta_{12})\bar{T}_2 + (\beta_{12}+\beta_{22})\bar{T}_3\right] \quad (3.131)$$

<u>cos2θ</u>:

$$u_r^{eff} = \frac{r}{2}\left[(\beta_{15}-\beta_{56})\bar{E}_3 + (\beta_a-\beta_b)\bar{S}_1 + (\beta_{11}-\beta_{12})\bar{T}_2 + (\beta_{12}-\beta_{22})\bar{T}_3\right]\cos 2\theta$$

Once again, only the radial displacements of the materials are used. Equating the displacements of the matrix and effective material at r=b gives two equations, where the fields in the matrix that *were* described in terms of the assumed fiber fields (T_2, T_3, and E_3) can be replaced with the macroscopic loads solved for in equation 3.128. This is summarized shortly, in equation 3.133.

The electrical boundary conditions are satisfied by equating the radial electrical displacements at the interface. The electrical displacement for the matrix is given in equation 3.124. The electrical displacement for the effective material follows from the constitutive equations (Eqn 3.130) after converting to polar coordinates:

$$D_r^{eff} = \left[\beta_{55}^{eff}\bar{E}_3 + \beta_c^{eff}\bar{S}_1 + \beta_{15}^{eff}\bar{T}_2 + \beta_{56}^{eff}\bar{T}_3\right]\sin\theta \quad (3.132)$$

The result of satisfying the final boundary conditions is three equations that relate fields in the effective material, that are a function of the macroscopic loads and effective material constants, to fields in the matrix, that are functions of the macroscopic loads and material constants for the matrix and fiber. They appear as follows:

$$\begin{bmatrix} (\beta_{11}+\beta_{12}) & (\beta_{12}+\beta_{22}) & (\beta_{15}+\beta_{56}) & (\beta_a+\beta_b) \\ (\beta_{11}-\beta_{12}) & (\beta_{12}-\beta_{22}) & (\beta_{15}-\beta_{56}) & (\beta_a-\beta_b) \\ \beta_{15} & \beta_{56} & \beta_{55} & \beta_c \end{bmatrix}_{eff} \begin{Bmatrix} \bar{T}_2 \\ \bar{T}_3 \\ \bar{E}_3 \\ \bar{S}_1 \end{Bmatrix} = \begin{bmatrix} M_{11} & M_{12} & M_{13} & M_{14} \\ M_{21} & M_{22} & M_{23} & M_{24} \\ M_{31} & M_{32} & M_{33} & M_{34} \end{bmatrix} \begin{Bmatrix} \bar{T}_2 \\ \bar{T}_3 \\ \bar{E}_3 \\ \bar{S}_1 \end{Bmatrix}$$

(3.133)

This final matrix allows for the simple solution of (all but one of) the effective material properties by comparing corresponding matrix terms. The final effective material constant

$$\beta_d^{eff} = \frac{1}{s_{11}^{eff}} \quad (3.133)$$

cannot be found from looking at the solution to the in-plane (2-3 axis) problem. Instead, it must be determined by considering the longitudinal response of the matrix/fiber element, and comparing it to the response of the effective material. Since the applied macroscopic load in the 1 axis was the uniform longitudinal strain, $\bar{S}_1$, the complementary

field is the axial stress, $\overline{T}_l$. Thus, the responses are compared by equating the total longitudinal stress T_l in the matrix and fiber element, to the macroscopic stress $\overline{T}_l$ developed by the same longitudinal strain $\overline{S}_l$ in the effective material. Since the stress fields vary within the matrix, they need to be averaged over the element by integration:

$$\overline{T}_l = v_f T_l^f + (1 - v_f) \perp_{A_m} \int_{A_m} T_l^m dA \tag{3.134}$$

The longitudinal stresses for the effective, fiber, and matrix materials may be found from the respective constitutive equations (Eqn 2.44 for the matrix and fiber, and Eqn 3.128 for the effective material). Finally, the effective material constants may be easily determined finterms of the modified plane strain constants, equation 3.130:

$$s_{11}^{eff} = \frac{1}{\beta_d^{eff}} \quad s_{12}^{eff} = \frac{\beta_a^{eff}}{\beta_d^{eff}} \quad s_{22}^{eff} = \beta_{11}^{eff} + \frac{\beta_a^{eff\,2}}{\beta_d^{eff}}$$

$$s_{13}^{eff} = \frac{\beta_b^{eff}}{\beta_d^{eff}} \quad s_{23}^{eff} = \beta_{12}^{eff} + \frac{\beta_a^{eff}\beta_b^{eff}}{\beta_d^{eff}} \quad s_{33}^{eff} = \beta_{22}^{eff} + \frac{\beta_b^{eff\,2}}{\beta_d^{eff}}$$

$$d_{31}^{eff} = \frac{\beta_c^{eff}}{\beta_d^{eff}} \quad d_{32}^{eff} = \beta_{15}^{eff} + \frac{\beta_a^{eff}\beta_c^{eff}}{\beta_d^{eff}} \quad d_{33}^{eff} = \beta_{56}^{eff} + \frac{\beta_b^{eff}\beta_c^{eff}}{\beta_d^{eff}} \quad \varepsilon_{33}^{eff} = \beta_{55}^{eff} + \frac{\beta_c^{eff\,2}}{\beta_d^{eff}} \tag{3.135}$$

where the effective β_{ij}^{eff}, solved from equation 3.133, are given in Appendix C.

3.5 The Finite Element Model

3.5.1 Introduction

The finite element method (FEM) is an extremely effective method to modeling structures, dynamics, and transport phenomena. It is very easy to develop models that represent simple systems and provide solutions that act as another check in calculations. It can also provide answers to the response of systems that are so complicated that finite element is the only means for such a response prediction. Popularity for this method derives from the fact that extremely accurate results can be obtained when the user designs a model that properly represents the system.

This method has been widely used for the purpose of calculating the effective material properties of multi-field media. However, the basic elements (discussed in sections 3.2 and 3.4) have not changed since the mid 1960's, and the same disagreements remain as to the ones that best represent the composite microstructure. Thus, the same assumptions that limited the analytical approaches, such as fiber contiguity and packing arrangement, still exist in the formulation of the problem for the finite element solution. The point, however, is not to use the FEM to evaluate different volume elements, but rather to confirm the approaches taken in modeling, based on a particular microstructure representation. Thus, the value of an implicit approach such as this one lies in the validation of assumptions used in the simpler models.

Few examples of finite element modeling of coupled field materials have been published [42,56], although the method is well suited to such materials. Only recently have FEM software packages been extended to include "multi-field" solids in the more general sense that allows modeling of electrical-mechanical coupled materials. Previous methods utilized directional-specific thermal expansion coefficients to approximate the piezoelectric effect. The method is classed as an elasticity type of solution because it approximately satisfies the coupled electrical-mechanical governing equations. The problem is formulated in terms of displacement and voltage degrees of freedom, so that the compatibility and potential distribution equations are exactly satisfied. The energy formulation, however, only approximately satisfies the equilibrium and charge distribution field equations through a minimization of the total potential energy. More detail about the solution procedure is given in section 3.5.3.

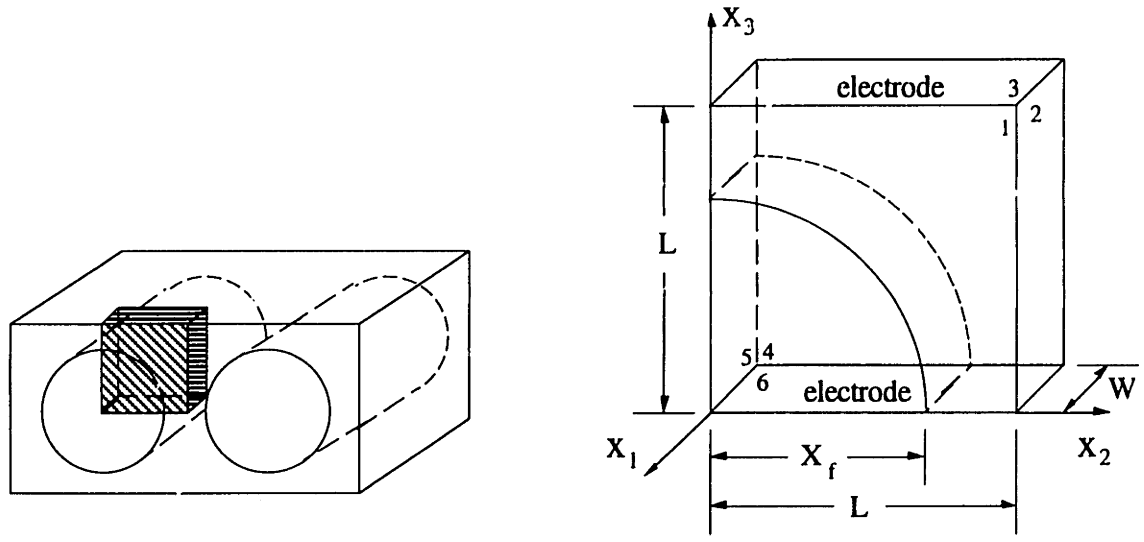

Figure 3.12: Quarter model representation of the composite microstructure for the Finite Element Method

3.5.2 Model Description

The premise behind the model is similar to the Uniform Fields approach. A repeating element is selected to represent the response of the entire composite. Again, the volume element is taken to be a representative single fiber with surrounding matrix material in proportion to the volume fraction being modeled. Due to symmetry, it is only necessary to model a quarter section of this basic element. This is shown in Figure 3.12 (a) and (b). In accordance with the discussion in 3.2, the amount of matrix surrounding the fiber is taken to be equal in the 2 and 3 axis directions. This will match the other models, and best represent a multi-fiber thickness composite. The finite element approach, like the Uniform

Table 3.2: FEM Quarter model Boundary Conditions

Face	Mechanical Boundary Conditions	Electrical Boundary Conditions
1	displacements coupled in x_1	$D_1 = 0$
2	displacements coupled in x_2	$D_2 = 0$
3	displacements coupled in x_3	voltage potential coupled
4	zero displacement in x_1	$D_1 = 0$
5	zero displacement in x_2	$D_2 = 0$
6	zero displacement in x_3	voltage potential coupled

Table 3.3: FEM Load Cases to Determine PFC Effective Material Properties

Load Case #	Mechanical Loading	Electrical Loading	Properties Obtained
1	$T = 0$ on faces 1,2,3 (zero stress)	Apply electrical field V_3 on face 3	ε_{33}^T d_{31} d_{32}
2	Apply displacement u_1 on face 1	$V_3 = 0$ on faces 3, 6 (short circuit)	s_{11}^E s_{12}^E
3	Apply displacement u_2 on face 2	$V_3 = 0$ on faces 3, 6 (short circuit)	s_{12}^E s_{22}^E

Fields models, is very flexible, and may be adapted to model geometry more appropriate to the experimental specimens.

The volume element is comprised of six faces which each have appropriate mechanical and electrical boundary conditions. The 1,2, and 3 faces are the x_1, x_2, and x_3 faces with positive (outward) direction normals. These faces are free to strain, restricted only by coupled displacements in that face's respective direction. In the 1 direction, this represents the assumption that the plane perpendicular to the fiber must remain plane after deformation[10]. In the 2 and 3 directions, this represents the requirement that the repeating element must have uniform deformations that satisfy those of the composite macroscopic response. The faces 4, 5, and 6 are the faces with negative x_1, x_2, and x_3 orientation. These represent the planes of symmetry for the quarter model, and have symmetry electrical and mechanical conditions. The electrical symmetry is enforced through equating the normal electrical displacement to zero, while the mechanical symmetry is enforced by setting all normal mechanical displacements to zero. Finally, although they are not modeled explicitly, the electrode surfaces are generated by electrically coupling the nodes on face 3 together and the nodes on face 6 together. The boundary conditions for all faces are summarized in Table 3.2. These are invariant with load case.

Like the Uniform Fields approach (especially the Closed Form model), the material properties are found by posing a series of hypothetical experiments. In the finite element method, a series of separate load cases are applied to the repeating element. For this model, only the load cases that provide the planar properties are applied, and are presented in Table 3.3. The first load case (#1) applies an electric field to the element, while all faces (1-3) are stress-free. This is accomplished by placing the potential on the top electrode to

[10] See section 2.? for a description of the PZT Fiber Composite Problem

some arbitrary voltage V_3. Given this set of loading conditions, the solution to the problem returns values of displacement (u_1, u_2) and surface charge q_s on the electrode:

Load Case #1:

From the constitutive equations,

$$\begin{Bmatrix} \overline{D} \\ \overline{S} \end{Bmatrix} = \begin{bmatrix} \varepsilon^T & d \\ d_t & s^E \end{bmatrix}_{eff} \begin{Bmatrix} \overline{E} \\ 0 \end{Bmatrix}$$

$$\varepsilon_{33}^T = \frac{\overline{D}}{\overline{E}} = \frac{q_s/(W \cdot L)}{V_3 / L} \qquad (3.136)$$

$$d_{31} = \frac{u_1/W}{V_3 / L}$$

$$d_{32} = \frac{u_2 / L}{V_3 / L}$$

where W is the depth of the model, and L is the dimension of the model in both the 2 and 3 directions. The second and third load cases involve applying known displacements u_1 and u_2 to the faces, and determining the forces developed to keep the model in equilibrium. Since the electrodes are shorted, the electrical field is macroscopically zero. The compliances are then calculated as follows:

Load Case #2:

$$\begin{Bmatrix} \overline{D} \\ \overline{S} \end{Bmatrix} = \begin{bmatrix} \varepsilon^T & d \\ d_t & s^E \end{bmatrix}_{eff} \begin{Bmatrix} 0 \\ \overline{T} \end{Bmatrix} \qquad (3.137)$$

$$s_{11}^E = \frac{S_1}{T_1}$$

$$s_{12}^E = \frac{S_2}{T_1} \qquad (3.138)$$

where:

$$T_1 = \frac{F_1}{(L \cdot L)} \quad S_1 = \frac{u_1}{W}$$

$$T_2 = 0 \qquad S_2 = \frac{u_2}{L} \qquad (3.139)$$

Load Case #3:

$$s_{12}^E = \frac{S_1}{T_2} \qquad (3.140)$$

Table 3.4: Model Statistics for Finite Element Fiber/Matrix Quarter Model

Line Fraction, X_f	# Elements	# Nodes	# Active DOFs
0.1	325	726	2177
0.3	349	758	2305
0.5	325	720	2165
0.7	254	593	1725
0.9	310	697	2081
0.95	273	624	1837
0.98	438	938	2874

$$s_{22}^{E} = \frac{S_2}{T_2}$$

where:

$$T_1 = 0 \qquad S_1 = \frac{u_1}{W}$$
$$T_2 = \frac{F_2}{(L \cdot W)} \qquad S_2 = \frac{u_2}{L} \tag{3.141}$$

Automatic mesh generation was used to discretize the quarter model. A typical mesh is shown in Figure 3.13 (a) and (b). Figure 3.13 (a) shows the front view (face 1) of the fiber/matrix quarter model for the particular fiber line fraction (X_f) of 0.90. The number of elements varied between 254 and 438, depending on the fiber line fraction. A variation in volume fraction was accomplished by setting the fiber line fraction to values between 0.1 and 0.98, corresponding to volume fractions between 0.0079 and 0.754 (the maximum for square packing is $\pi/4$, or 0.785). For each of these cases, the model statistics are summarized in Table 3.4. Higher concentrations of elements did not significantly affect the effective properties. The exploded three-dimensional view of the same model ($X_f = 0.90$) is shown in Figure 3.13 (b). From this figure, it is possible to see the element packing and the higher concentration of elements near the top electrode, where the model is most sensitive.

3.5.3 Finite Element Theory and Analysis

The finite element method for piezoelectric static and linear dynamic analysis can be found outlined in Ref[57]. The paper develops the general method of electro-elastic analysis by incorporating the effect of piezoelectrics into a finite element formulation. The basis of the theory is the variational principles, extended to the piezoelectric case. The

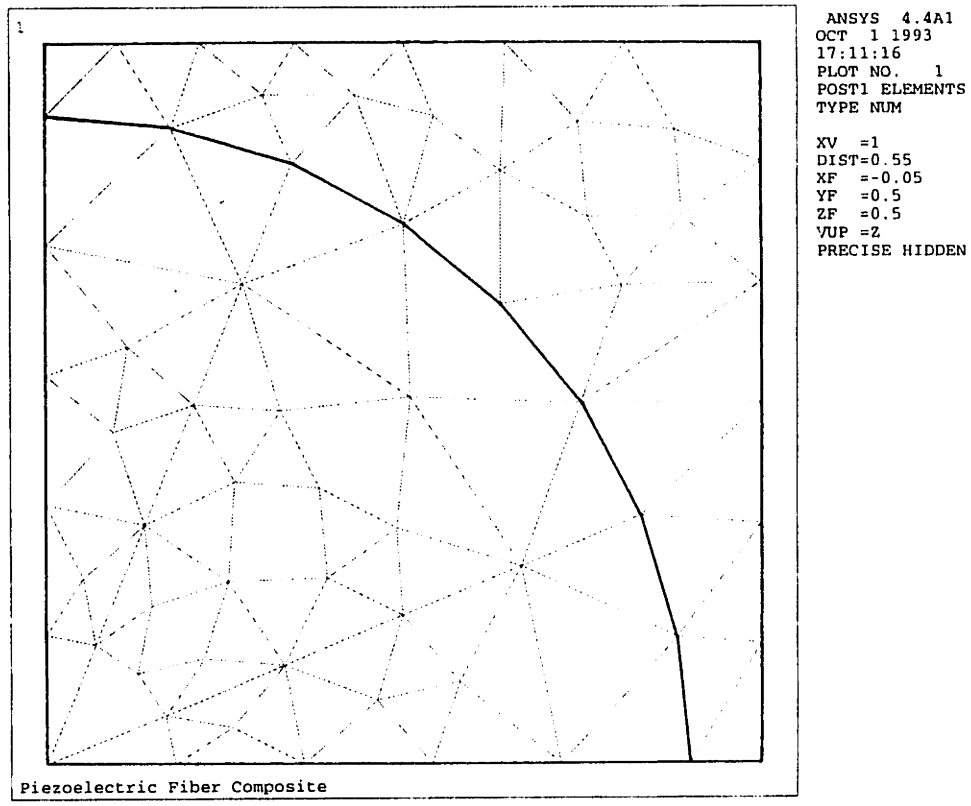

(a)

(b)

Figure 3.13: Element mesh for fiber/matrix quarter model at 0.90 line fraction ($X_f = X_1 = X_2$); (a) Front face (#1) view, (b) 3D Exploded view

authors develop a three dimensional tetrahedral element based on an assumed displacement-potential degrees of freedom, so that the formulation is an extension of the Principle of Minimum Potential Energy. It is from this theory that the elements in the chosen analysis software are derived.

Energy Formulation

The theory begins with the definition of the virtual work density:

$$\begin{aligned} \delta W &= \delta U \\ \delta W &= \{\delta \mathbf{u}\}_t \{\mathbf{F}\} - \delta\Phi\sigma \end{aligned} \tag{3.142}$$

where $\{\mathbf{u}\}$ is the displacement, Φ the electric potential, $\{\mathbf{F}\}$ the mechanical force density, σ the charge density, and δ the virtual quantity. To apply the principle of variations for the above formulation requires form 1 of the constitutive relations, from equation 2.23:

$$\begin{aligned} \{\mathbf{T}\} &= \left[\mathbf{c}^E\right]\{\mathbf{S}\} - [\mathbf{e}]_t \{\mathbf{E}\} \\ \{\mathbf{D}\} &= [\mathbf{e}]\{\mathbf{S}\} + \left[\varepsilon^T\right]\{\mathbf{E}\} \end{aligned} \tag{3.143}$$

Applying the principle of Minimum Potential Energy immediately produces the following matrix form:

$$\begin{aligned} &\int_{Vol} \left(\{\delta\mathbf{S}\}_t \left[\mathbf{c}^E\right]\{\mathbf{S}\} - \{\delta\mathbf{S}\}_t [\mathbf{e}]_t \{\mathbf{E}\} - \{\delta\mathbf{E}\}_t [\mathbf{e}]\{\mathbf{S}\} - \{\delta\mathbf{E}\}_t \left[\varepsilon^T\right]\{\mathbf{E}\} - \{\delta\mathbf{u}\}_t \{\overline{\mathbf{F}}\} + \delta\Phi\overline{\sigma}_B \right) dV \\ &- \int_{A1} \{\delta\mathbf{u}\}_t \{\overline{\mathbf{T}}\} dA + \int_{A2} \delta\Phi\overline{\sigma}_A dA - \{\delta\mathbf{u}\}\{\mathbf{P}\} + \delta\Phi\mathbf{Q} = 0 \end{aligned}$$

(3.144)

where the prescribed quantities are: $\{\overline{\mathbf{F}}\}$, the body force, $\{\overline{\mathbf{T}}\}$ the surface traction, $\{\mathbf{P}\}$ the point force, $\overline{\sigma}^B$ the body charge, $\overline{\sigma}^A$ the surface charge, and $\mathbf{Q}$ the point charge. The integrals are performed over the volume (vol), and the surfaces A1 and A2 which denote those areas where tractions and charge are prescribed, respectively.

To formulate the relations for a finite element method, it is necessary to describe the displacements and potentials through the nodal degrees of freedom $\mathbf{u}_i$ and V_i, and the interpolation functions $\mathbf{N}_u$ and $\mathbf{N}_V$:

$$\begin{aligned} \{\mathbf{u}\} &= [\mathbf{N}_u]\{\mathbf{u}_i\} \\ V &= [\mathbf{N}_V]\{V_i\} \end{aligned} \tag{3.145}$$

The prescribed body and surface forces (or charges) may be expressed in a similar manner:

$$\{\bar{F}\} = [N_{\bar{F}}]\{\bar{F}_i\} \qquad \bar{\sigma}^B = [N_{\bar{\sigma}^B}]\{\bar{\sigma}_i^B\}$$
$$\{\bar{T}\} = [N_{\bar{T}}]\{\bar{T}_i\} \qquad \bar{\sigma}^A = [N_{\bar{\sigma}^A}]\{\bar{\sigma}_i^A\} \tag{3.146}$$

Relating the assumed displacements and potentials to the formulated strains and electric fields is described by the strain-displacement and scalar potential relations, given in section 2.2.2. In matrix form:

$$\{S\} = [B_u]\{u_i\}$$
$$\{E\} = -[B_V]\{V_i\} \tag{3.147}$$

where B_u and B_V are the linear differential operator matrices that capture the derivative relationships. Substitution of 3.145, 3.146, and 3.147 into the variational form, and evaluating for all virtual displacements yields the following two coupled equations:

$$[K_{uu}]\{u_i\} + [K_{uV}]\{V_i\} = \{F_B\} + \{F_A\} + \{F_P\}$$
$$[K_{Vu}]\{u_i\} + [K_{VV}]\{V_i\} = \{Q_B\} + \{Q_A\} + \{Q_P\} \tag{3.148}$$

The additional kinetic term $[m]\{\ddot{u}_i\}$ may be added to the first of the above equations to accommodate dynamic problems. The electro-elastic matrices for the above are defined as:

$$[K_{uu}] = \int_{vol}[B_u]_t[c^E][B_u]dV \qquad [K_{uV}] = \int_{vol}[B_u]_t[e]_t[B_V]dV$$
$$[K_{Vu}] = \int_{vol}[B_V]_t[e][B_u]dV \qquad [K_{VV}] = -\int_{vol}[B_V]_t[\varepsilon^T][B_V]dV \tag{3.149}$$
$$\{F_B\} = \int_{vol}[N_u]_t[N_{\bar{F}}]dV\{\bar{F}_i\} \qquad \{Q_B\} = -\int_{vol}[N_V]_t[N_{\bar{\sigma}^B}]dV\{\bar{\sigma}_i^B\}$$
$$\{F_A\} = \int_{Al}[N_u]_t[N_{\bar{T}}]dA\{\bar{T}_i\} \qquad \{Q_A\} = -\int_{Al}[N_V]_t[N_{\bar{\sigma}^A}]dA\{\bar{\sigma}_i^A\}$$
$$\{F_P\} = [N_u]_t\{P\} \qquad \{Q_P\} = -[N_V]_t Q$$

Solution of the problem requires an iterative technique. The coupled field interaction is introduced through the load vector with an iterative solution procedure [59] that recalculates the load at each step. For a thermal-elastic problem, the analysis requires two iterations. The first iteration solves the heat transfer problem and calculates the corresponding thermal free strain. The second iteration uses this as an input and solves the structural problem. For a coupled multi-field problem (such as piezoelectrics), a further iteration would follow, inputting the structural results from the second iteration into the re-solution of the thermal (electric potential) problem. For this case, the elastic solution lags the electric potential solution at each step. For the particular program chosen for this

analysis, the number of iterations is controlled internally by a convergence criteria that ensures convergence for each nodal degree of freedom within a specified amount.

Following solution, it is straightforward to calculate the field distributions using the constitutive relations and the interpolation functions:

$$\begin{aligned} \{\mathbf{T}\} &= \left[\mathbf{c}^{E}\right]\left[\mathbf{B}_{u}\right]\{\mathbf{u}_{i}\} + [\mathbf{e}]_{t}\left[\mathbf{B}_{V}\right]\{V_{i}\} \\ \{\mathbf{D}\} &= [\mathbf{e}]\left[\mathbf{B}_{u}\right]\{\mathbf{u}_{i}\} - \left[\varepsilon^{T}\right]\left[\mathbf{B}_{V}\right]\{V_{i}\} \end{aligned} \tag{3.150}$$

The complementary fields, T and D, will only approximately satisfy their respective governing equations.

The Electro-elastic Tetrahedral Finite Element

A commercially available finite element analysis software package , ANSYS[11] , was used for modeling of the fiber composite. This software could support multi-field elements, allowing solution of mechanical-electrical coupled materials. Both brick (8 node) and tetrahedral (10 and 4 node) elements were available, but tetrahedral elements were chosen for their flexibility in automatic mesh generation schemes. Tetrahedral elements are also less susceptible to aspect ratio difficulties, so that they work well in complicated geometry or locations of sharp corners. In particular, areas of matrix/fiber interfaces are critical, especially near the top electrode where the matrix area is very small for large fiber volume fractions.

The reference that provided the above variational formulation [57] also provides a discussion on this element type. However, a more thorough discussion, including tetrahedral elements with quadratic and cubic interpolation functions may be found in Ref[58]. The element used here is the four node element, so that the interpolation functions can describe only a linear field distribution between any two nodes.

The tetrahedral element used in this model is shown in Figure 3.14, with nodes 1..4 and corresponding opposite faces 1..4. The poling direction is defined in the z direction. For formulating the element matrices, a substantial simplification may be obtained through the use of Natural, rather than Cartesian coordinates. These coordinates are defined with respect to the element instead of a fixed, global system so that element manipulations are simplified. These natural coordinates can then be referenced to the global system.

---

[11] ANSYS, Version 4.4A, Swanson Analysis, PO Box 65, Houston, PA 15342

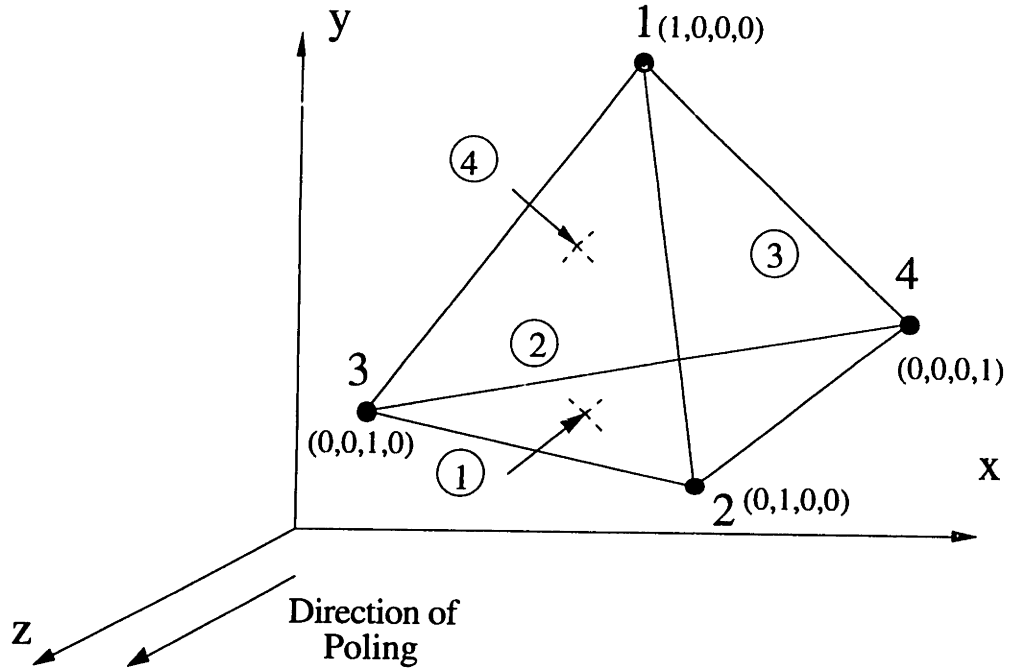

Figure 3.14: Four noded tetrahedral multi-field element used in this finite element analysis showing nodes (1..4), and element faces (1...4) defined by volume elements.

The natural coordinates are dimensionless, and describe positions through a *ratio* of quantities. For a three dimensional element, these are denoted volume coordinates. Thus, the coordinates are ratios of volumes, that when combined, describe a unique position within the element:

$$\xi_1 = \frac{\vartheta_1}{\vartheta} \quad \xi_2 = \frac{\vartheta_2}{\vartheta} \quad \xi_3 = \frac{\vartheta_3}{\vartheta} \quad \xi_4 = \frac{\vartheta_4}{\vartheta} \qquad (3.151)$$

where ϑ is the total tetrahedron volume and ϑ_i is a portion of the total volume that is subtended by some arbitrary point P and the surface $\xi_i = 0$. This is the surface opposite the vertex of node i. The combination of the four volume coordinates describe the location of point P (Figure 3.14). Using these relations it is possible to derive the formulation relating the Cartesian and volume coordinates [57,58]:

$$\begin{Bmatrix} 1 \\ x \\ y \\ z \end{Bmatrix} = \begin{bmatrix} 1 & 1 & 1 & 1 \\ x_1 & x_2 & x_3 & x_4 \\ y_1 & y_2 & y_3 & y_4 \\ z_1 & z_2 & z_3 & z_4 \end{bmatrix} \begin{Bmatrix} \xi_1 \\ \xi_2 \\ \xi_3 \\ \xi_4 \end{Bmatrix} \qquad (3.152)$$

Each node has four degrees of freedom: u, v, w, and V. Linear interpolation functions are chosen so as to describe compatible and continuous behavior in the element. From Ref[59], the following are used:

$$
\begin{aligned}
u &= u_1(2\xi_1 - 1)\xi_1 + \ldots + u_4(2\xi_4 - 1)\xi_4 \\
v &= v_1(2\xi_1 - 1)\xi_1 + \ldots + v_4(2\xi_4 - 1)\xi_4 \\
w &= w_1(2\xi_1 - 1)\xi_1 + \ldots + w_4(2\xi_4 - 1)\xi_4 \\
V &= V_1(2\xi_1 - 1)\xi_1 + \ldots + V_4(2\xi_4 - 1)\xi_4
\end{aligned}
\tag{3.153}
$$

Note that the interpolation function for the potential V is identical to that of the elastic displacements, u, v, and w. This formulation provides the basis for solution of the electro-elastic finite element problem incorporating tetrahedral multi-field elements.

3.6 Model Comparison

3.6.1 Basis for Comparison

A comparison may be made of the five models presented in sections 3.3 to 3.5. There are a number of ways these models may be compared, and it is important to justify the premise upon which each model is judged. Differences lie primarily in the volume element assumed for each of the models derived. For example, the closed form (CFUF) and numerical (NUF) uniform fields models face basic constraints due to the fact that they model round fibers as square. The Self Consistent Fields (SCF) is limiting to modeling composites with an equal distribution of fibers in every direction. The Discrete Uniform Fields (DUF), and the Finite Element Model (FEM) have more freedom in specifying the directional geometry, and can model circular fibers.

The premise upon which the models are based are that of a periodic composite structure, with square element packing such that there is an equal distribution of fibers in both directions. This is more typical of composites with a thickness significantly greater than the fiber diameter. In such cases, the spatial scale is fine enough that the assumption of square fibers in the two models is unimportant, and the composite may be described by a single parameter - the volume fraction. The basis for such a comparison is important because it will allow a common ground with which to compare future models, and eventually a comparison with piezoelectric fiber composites with multi-fiber layers. Naturally, the present models do not preclude a comparison with the current specimens, as several of the models may be adapted to better model the experimental geometry.

The comparisons made of the models will present plots of the effective material constant, nondimensionalized by the corresponding material constant of the piezoceramic. These graphs will show the effective constants plotted versus the volume fraction of fiber in the composite. The plots could also have been made as a function of line fraction; however, this quantity is not as widely recognized, and is actually more appropriate in discussion of mono-layer fiber composites. Nonetheless, the line fraction remains an important description of the geometry in some of the models.

Since the packing is a square array, the maximum theoretical volume fraction is $\pi/4$ (0.785), which occurs when the circular fibers touch the outer boundary of the volume element. This is portrayed in Figure 3.15, in the representative volume element of the Discrete Uniform Fields and Finite Element Model. In this case, the line fractions X_2 and X_3 are equal to 1. The maximum packing is not as easily specified in the remaining models. In these cases, the fiber touching the outer boundary would represent a maximum

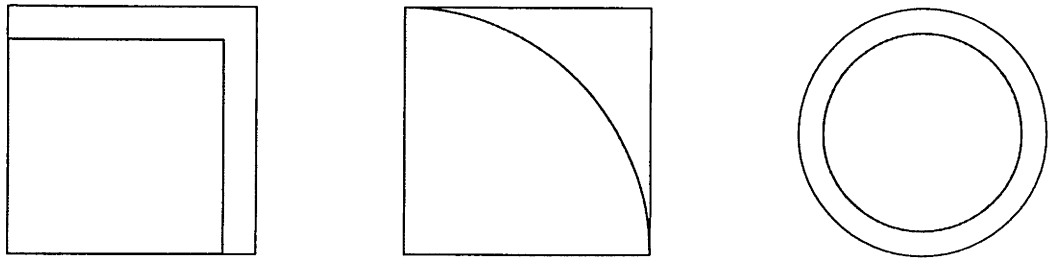

• CFUF • DUF • SCF

• NUF • FEM

$v_f = v_2 \cdot v_3 = \sqrt{\pi/4}X_2\sqrt{\pi/4}X_3$ $v_f = \pi/4\,X_2X_3$ $v_f = a^2/b^2$

Figure 3.15: Representative Volume Elements and volume fractions for five models compared in this chapter. Geometry shown for maximum fiber volume fraction.

volume fraction of 1, rather than $\pi/4$. The appropriate action is simply to enforce that the total fiber area in these models is the same as that for the first case. For the NUF and CFUF models (Figure 3.15) this is achieved by defining the parameters v_2 and v_3 as the following:

$$v_2 = v_3 = \sqrt{\pi/4}X_2 = \sqrt{\pi/4}X_3 \qquad (3.154)$$

where X_2 and X_3 are defined by the DUF and FEM model element. This is achieved in the Self Consistent Field model by setting the ratio a^2/b^2 to that of the volume fraction v_f. In this way, the maximum volume fraction in each case is $\pi/4$, and the models may now be compared on a common basis.

3.6.2 The Models Compared

Electric Potential Distribution

Before turning to the comparison of the effective composite properties, it is useful to take a look at the field distributions within the volume elements of the various models. The electric potential distributions provide an excellent illustration of how each model is fundamentally different, in both the geometry of the various phases, and how the field distributions are modeled in each of these phases. The distributions also offer an explanation for the differences that become apparent when comparing the effective properties.

The four different plots, shown in Figures 3.16 (a) through (d), are the electric potential distributions for a fiber volume fraction of $v_f = 0.9\pi/4$, and a dielectric mismatch of $\varepsilon_{33}^T/\varepsilon_{33}$ =10. Here, the lines signify values of equal potential, so that closely spaced lines indicate a large change in potential. All of the models capture the basic effect of the mismatch, shown as a field potential concentration in the matrix above the fiber, and a very reduced potential in the fiber. It is this low potential in the fiber that makes poling difficult, and high levels of actuation harder to obtain. Each model also captures the more even spacing of potential lines in the pure matrix, as the distance from the fiber is increased. These similarities capture the predominant effects that shape the effective material properties that are seen in the upcoming plots. However, significant differences exist in these models which require further understanding. These differences will define certain regimes of volume fraction where a particular model more accurately captures the macroscopic response.

The simplest models are the Closed Form and Numerical Uniform Fields approaches, shown in Figure 3.16 (a). These models are almost identical, the only difference being in the amount of elastic coupling present. Since all of these plots (a) - (d) are shown for a stiffness mismatch of s_{11}/s_{11}^E =20, there is little clamping and the problem is almost a purely electrical one. Both of these models use the combination model approach, where a slice of fiber and matrix is combined with a slice of pure matrix. The fields in each material phase is assumed uniform, so that the equipotential lines are straight. The square fiber assumption allows equal levels of potential into parts of the fiber that would normally be further away from the electrode in a circular fiber. This is approximately offset by the fact that the square fiber is moved further away from the electrode by the condition that the overall volume fraction be equal.

The Discretized Uniform Fields model (DUF) uses the combination model approach, but in a discrete manner. Many slices of matrix and fiber are added together to give a distribution of fields that vary discretely across the element. In this way, the model is able to capture the circular geometry of the fiber. This is reflected by the equipotential lines that vary within the fiber and matrix. In particular, as the fiber material becomes further from the electrode, the potential across the fiber becomes less and less. This may more accurately model the zone of fiber that is inactive, and that tends to clamp the piezoceramic during actuation, resulting in a reduced effective d_{31}^{eff}. Another benefit of this approach is obvious at the maximum packing, where the model captures the correct fiber-electrode interaction, enabling better representation of the electric and piezoelectric properties at high volume fractions (for the assumed square packing geometry).

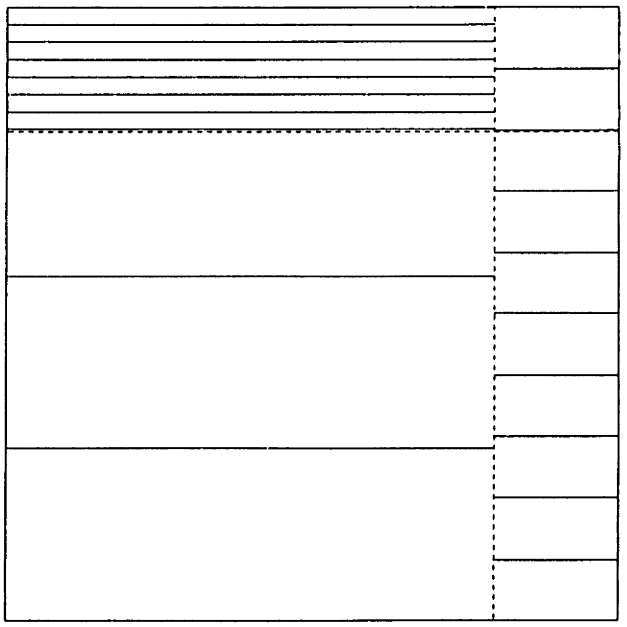

(a)

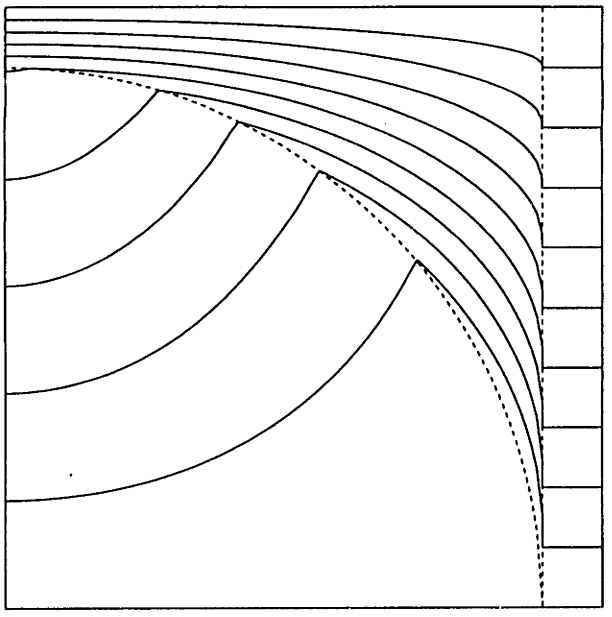

(b)

Figure 3.16: Equipotentials for fiber fraction $v_f = 0.9\,\pi/4$, and mismatch of $\varepsilon_{33}^T/\varepsilon_{33} = 10$
(a) Closed Form (CFUF), Numerical (NUF) Uniform Fields, (b) Discrete Model (DUF)

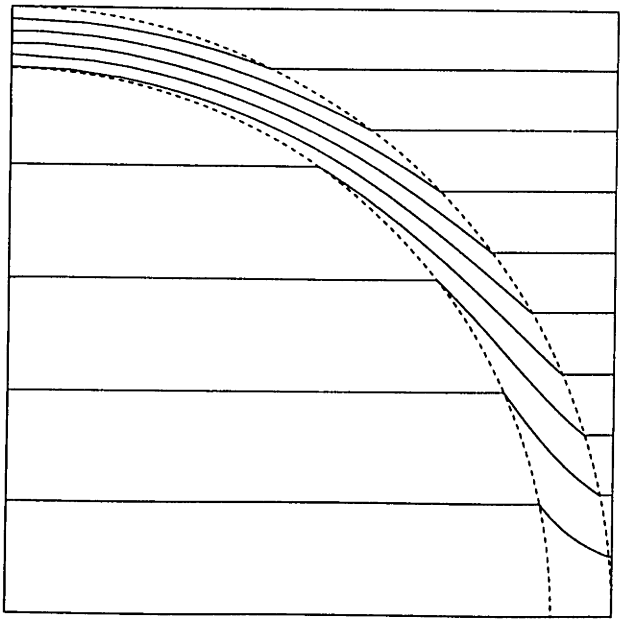

(c)

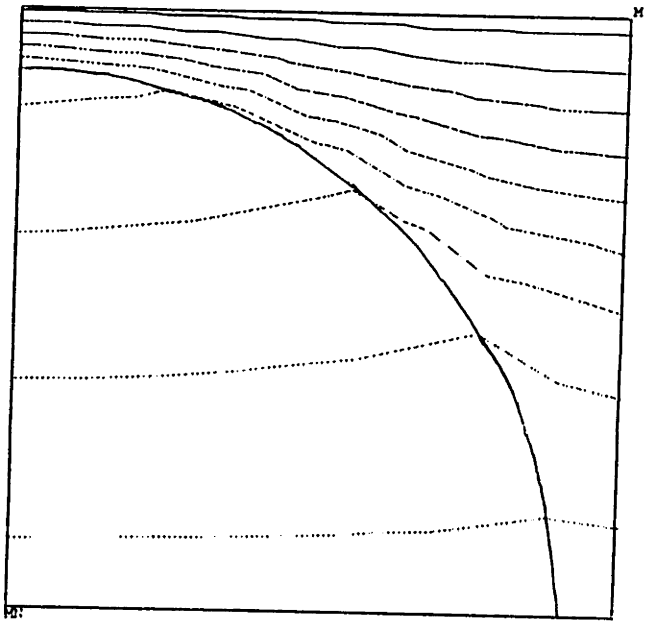

(d)

Figure 3.16: Equipotentials for fiber fraction $v_f = 0.9\pi/4$, and mismatch of $\varepsilon_{33}^T/\varepsilon_{33} = 10$
(c) Self Consistent Fields (SCF), (d) Finite Element Method (FEM)

The Self Consistent Fields model (SCF), shown in Figure 3.16 (c), is similar to the DUF model in that it can model circular fibers and allows some nonuniform field distributions. It also bears some similarity to the CFUF and NUF models because it assumes uniform fields in the fiber and has the same geometric limitation where the fiber is not touching the electrode at the maximum volume fraction. However, the field distribution *is* allowed to vary within the matrix material. This captures the concentration of elastic field within the fiber phase, where field lines are drawn into the fiber due to the field variations around it. This results in higher electric potential in the fiber than that predicted by the CFUF and NUF models which did not allow field variations. As the effective material constant comparison will show, this causes a significant increase in the dielectric and piezoelectric properties at low fiber volume fractions.

The potential distribution of the Finite Element Model (FEM), shown in Figure 3.16 (d), is likely the most accurate portrayal for the given packing geometry. This model incorporates full material coupling, and allows field variations within each material phase. Interestingly enough, some aspect of this model is represented in each of the simpler models. For example, the FEM shows almost uniform potential distributions within the fiber, validating the assumption in the CFUF, NUF, and SCF models. It also hints at the reduction in electric potential at the fiber edges that was strongly seen in the DUF model. Equipotential distributions in the matrix material are also somewhat similar between the FEM and the DUF and SCF models. Like the SCF model, the FEM will predict the concentration of potential within the fiber. However, like the DUF model, the FEM is able to correctly portray the geometry at high volume fractions.

Effective Material Constants

The previous section provided insight into the geometry of modeling differences present within each model. A better understanding of the model differences is valuable when assessing the results of the comparison of the effective material constants. This is especially important for the electrical and piezoelectric properties because the composite response is not as well understood for these as it is for the mechanical properties. The piezoelectric properties are very important to model accurately because they are used as a measure of actuation capability, and as a comparison to other material systems. In this section, the six important in-plane material properties are shown as a function of volume fraction, and are compared for the five models.

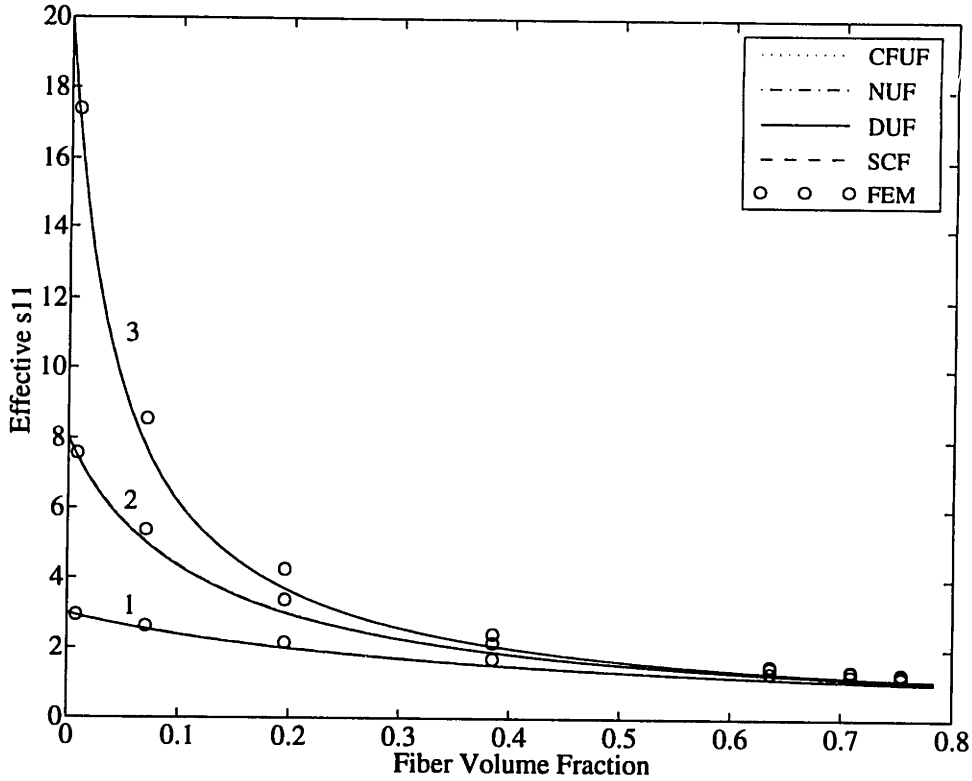

Figure 3.17: Comparison of effective nondimensionalized 11 compliance. All models are for $\varepsilon_{33}^{T}/\varepsilon_{33} = 100$, with compliance ratios s_{11}/s_{11}^{E} of 3, 8, 20 for curves 1, 2, 3.

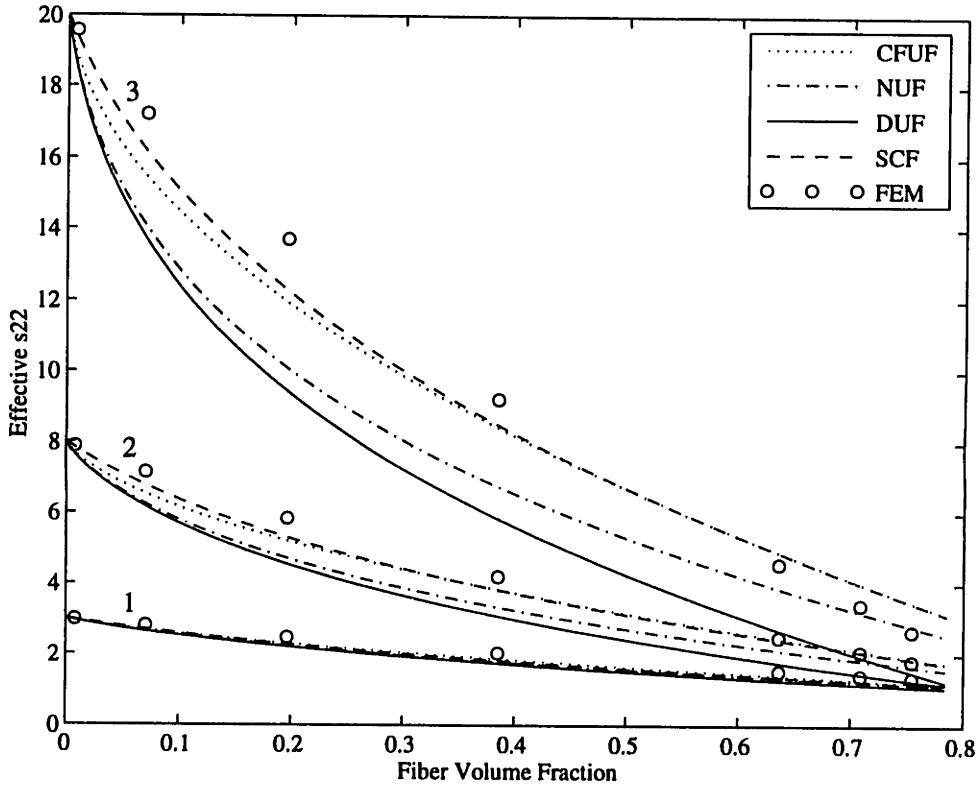

Figure 3.18: Comparison of effective nondimensionalized 22 compliance. All models are for $\varepsilon_{33}^{T}/\varepsilon_{33} = 100$, with compliance ratios s_{11}/s_{11}^{E} of 3, 8, 20 for curves 1, 2, 3.

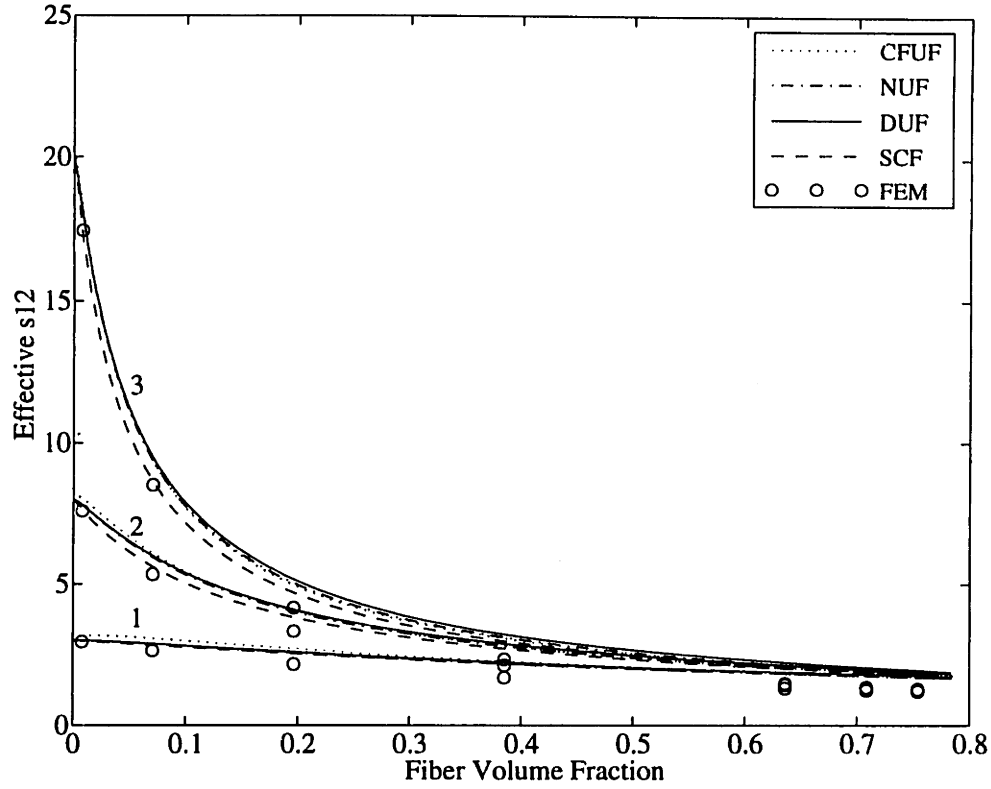

Figure 3.19: Comparison of effective nondimensionalized 12 compliance. All models are for $\varepsilon_{33}^{T}/\varepsilon_{33} = 100$, with compliance ratios s_{11}/s_{11}^{E} of 3, 8, 20 for curves 1, 2, 3.

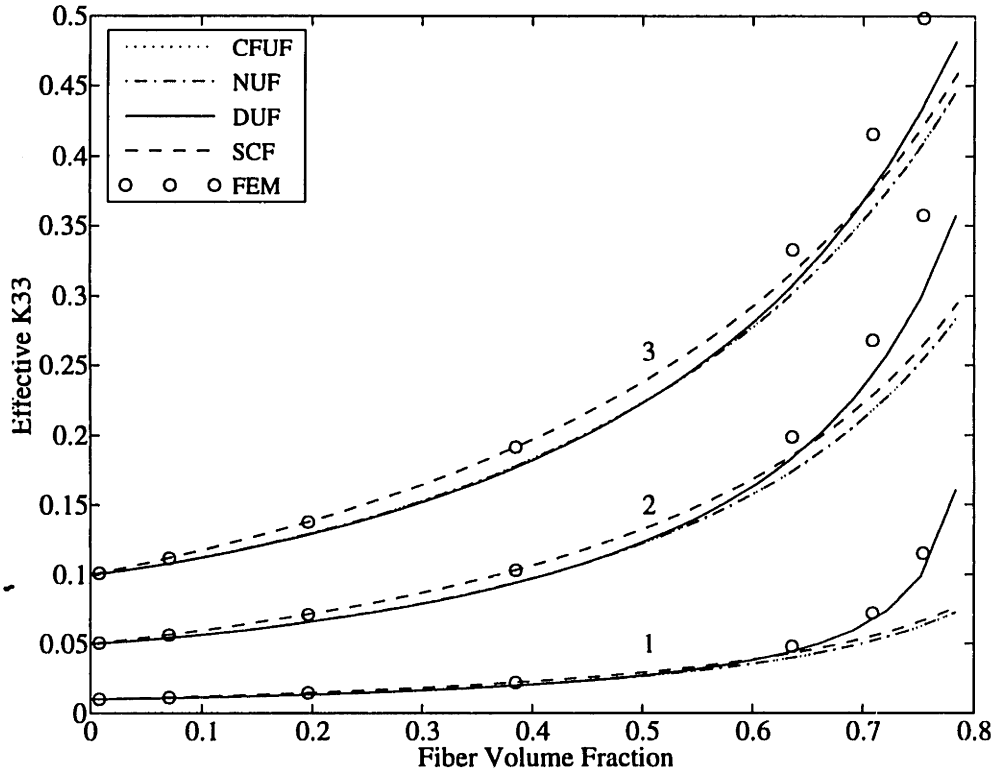

Figure 3.20: Comparison of models for effective nondimensionalized 33 dielectric. Models are for $s_{11}/s_{11}^{E} = 20$ with compliance ratios $\varepsilon_{33}^{T}/\varepsilon_{33}$ of 100,20,10 for curves 1,2,3.

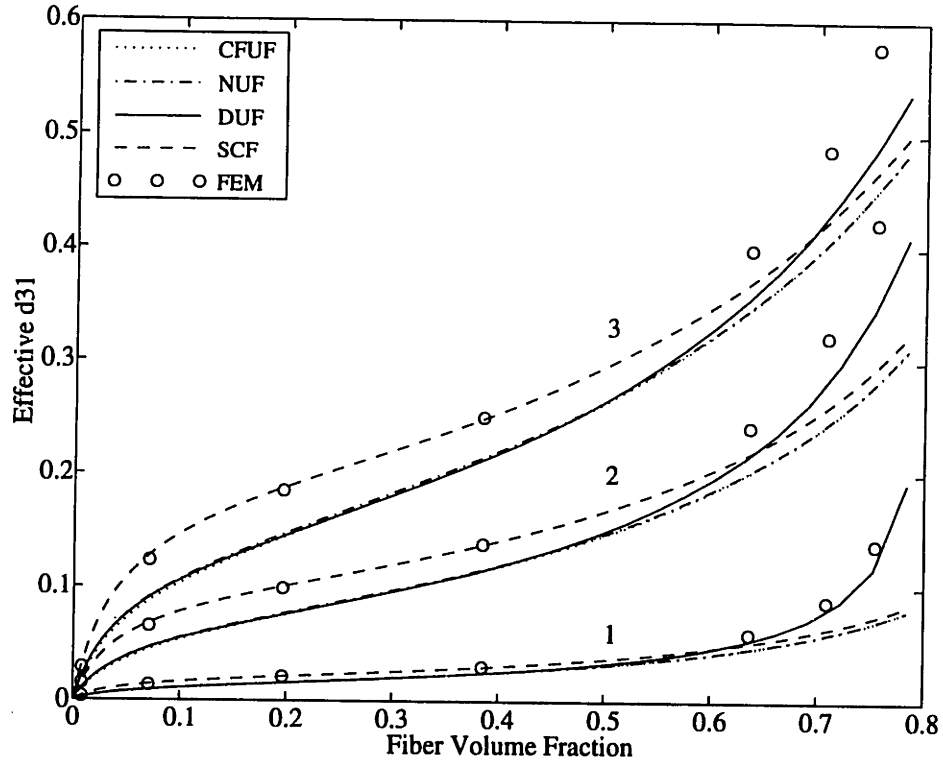

Figure 3.21: Comparison of effective nondimensionalized 31 piezoelectric free strain. All models are for $s_{11}/s_{11}^{E} = 20$ with compliance ratios $\varepsilon_{33}^{T}/\varepsilon_{33}$ of 100,20,10 for curves 1,2,3.

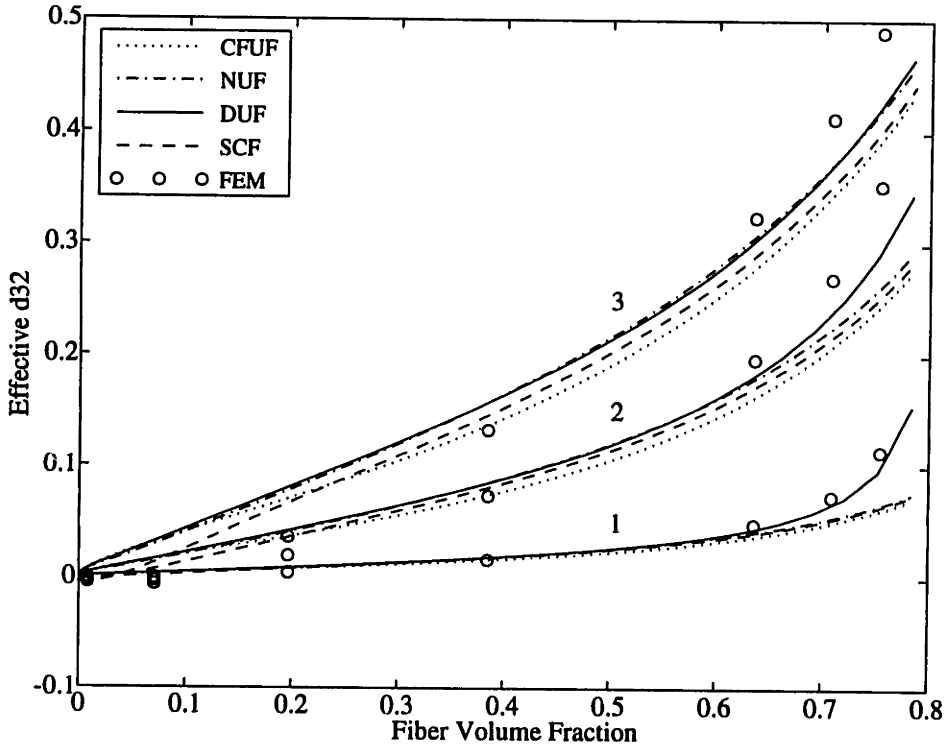

Figure 3.22: Comparison of effective nondimensionalized 32 piezoelectric free strain. All models are for $s_{11}/s_{11}^{E} = 20$ with compliance ratios $\varepsilon_{33}^{T}/\varepsilon_{33}$ of 100,20,10 for curves 1,2,3.

The first model comparison is made of the effective compliance in the longitudinal direction (insert), shown in Figure 3.17. Comparison is made for three compliance ratios [insert] of 20, 8, and 3. There is excellent agreement between all of the models, as is to be expected for longitudinal elastic property predictions in a fibrous composite. For this geometry, it is well known that even a simple mechanics of materials, two springs in parallel, give a good estimate of this property. All the plots show that a small amount of fiber reinforcement quickly reduces the compliance. The first four models directly overplot, while the FEM model is slightly more compliant. This effect is unexplained, but may simply be due to the different model constraints placed on this volume element. Overall, the good agreement acts as a check for each of the models.

The transverse compliance, s_{22}^{eff}, offers a much more varied distribution of predictions. The curves, given in Figure 3.18, are again shown for three different compliance mismatches (20, 8, and 3), and the effective compliance is nondimensionalized by s_{11}^{E}. The general trend shown here is that a much higher percentage of fibers is needed to significantly decrease the composite compliance. All of the models provide a better prediction than the simple mechanics of materials model, which would simply be a straight line between the pure matrix and fiber properties for each ratio. This method has always underestimated the transverse stiffness (overestimated the compliance). In comparing the individual models, the DUF and NUF models are overly stiff, likely because the uniform fields assumption introduces inconsistent strain fields in the phases, which have a stiffening effect. The NUF model gives essentially the same prediction as the DUF model, except that the latter can model circular fibers so that the compliance reflects touching fibers at maximum packing. The CFUF model has the same premise as the NUF model, but without the constraint of material clamping which introduces stresses in directions other than the loading axis. Thus, it predicts a more compliant system. The Self Consistent Fields (SCF) model more accurately predicts the general trend, as seen in the FEM model, with exception of high volume fractions. This is, of course, due to the geometry assumed at maximum packing. The FEM is the most compliant system throughout the majority of volume fractions, but tends to decrease sharply at the maximum volume fraction nears.

The effective s_{12}^{eff} compliance term is shown in Figure 3.19. This material parameter is similar to the longitudinal compliance in that it can be predicted by a simple Mechanics of Materials approach to within reasonable accuracy [23]. This is reflected in the close agreement between the models. There *is* a slightly larger variation between the models than for the s_{11}^{eff}, particularly in the Self Consistent Fields (SCF) and the Finite Element Method (FEM) which allow concentrations of stress within the matrix material.

Both of these models are less compliant (stiffer) throughout the range of fiber volume fractions. The FEM is the least compliant, especially at high volume fractions.

The comparison of the electrical properties begins with a discussion of the composite dielectric, ε_{33}^{eff}. In the plot of Figure 3.20, three comparisons are shown of effective dielectric for material mismatches of $\varepsilon_{33}^{T}/\varepsilon_{33}$ of 100, 20, and 10. The effective dielectric has been nondimensionalized by the piezoceramic dielectric. For effective dielectric, it is evident that a large percentage of high-dielectric fibers must be present before a large increase is seen. This is especially true at larger mismatches. All uniform field models (CFUF, NUF, and DUF) provide the same prediction, with the exception of the DUF model at high volume fractions. This model, as discussed earlier, has fiber contact with the electrode at maximum packing, while the other two do not. The FEM and SCF models exactly compare until volume fractions of about 0.5, after which the FEM model follows DUF prediction. The good comparison between the FEM and SCF is due to the accurate electric field representation in the material phases.

The effective d_{31}^{eff}, shown in Figure 3.21, almost exactly echoes the comparison for dielectric, in terms of the models that are similar. This is explained by the large dependence of the effective piezoelectric constants on the field distributions within the fiber. Like the dielectric comparison, three comparisons are made for dielectric mismatches of 100, 20, and 10 between the fiber and matrix. The compliance mismatch is held at 20 for these comparisons. Little change in effective piezoelectric constants is seen until compliance mismatches of 3 or lower[12], which is very unlikely for a piezoelectric fiber composite system. Once again, the FEM and SCF models compare very well until higher volume fraction, when the DUF model better represents the through-thickness line fraction X_3. At low volume fractions, the electric potential concentration in the fiber, as predicted by the FEM and SCF models, makes a significant departure from the other models. The difference is as much as 20% in some cases.

The final comparison to be made is that of the transverse piezoelectric free strain constant, d_{32}^{eff}, given in Figure 3.22.. This comparison is made on the same basis as that for the d_{31}^{eff} and ε_{33}^{eff} constants. The disparity between the models is much less than that for d_{31}^{eff}, with the exception of the FEM model. At high volume fraction, the FEM model breaks away from the other models, again followed by the DUF model. At low volume fractions, however, an interesting phenomenon occurs. The FEM model predicts that the sign for d_{32}^{eff} actually switches, and the plots for the three mismatch ratios cross over as the sign changes back. a positive value for d_{32}^{eff} is caused by the longitudinal contraction of the

[12] See section 4.2.2 for a brief discussion of the compliance dependence of d_{31}^{eff}.

fiber that forces the matrix to expand transversely more than the fiber contracts. For a uniform fields assumption and equal Poisson's ratios, this will not occur. However, the field concentrations in the SCF and FEM model *do* capture this phenomenon. This effect would be further enhanced in a mono-fiber layer composite because the matrix would not be constrained to move with the fiber in the vertical direction. Evidence of this is seen in the experimental results. The benefit of such a phenomenon is an increase in actuation anisotropy.

4.0 Optimization of Matrix Material Properties

4.1 Overview

Tailoring anisotropic materials includes the freedom to choose parameters at the material, lamina, and laminate levels of manufacturing. Thus, such choices also include the properties of the matrix and fibers materials. Fewer options are available with the fibers, because the choice is limited to ceramic type, the matrix material offers a much broader range from which to choose.

Matrix materials can be metal, ceramic, or organic, depending on the reinforcing material and the purpose of the composite. For the present application, an organic matrix system is chosen for the role it must play in piezoceramic fiber composites. The matrix material must support and protect the brittle fibers, and provide load transfer and load distribution between the fibers. Although the matrix is usually much lower in density, stiffness, and strength than the fibers, it is this mechanism of load transfer that is key to the composites success. It is the means by which the composite is capable of carrying load far above that allowed by the matrix alone, yet at a much reduced cost in weight.

Some of the properties desired for the matrix are obvious. The matrix material should have relatively low stiffness to minimize clamping of the piezoelectric fibers, and be non-conducting to allow the necessary voltage potential distributions between the electrodes and around each fiber. Other material properties are not so obvious. An added complexity is the addition of certain filler materials which will influence these properties and involve a tradeoff between the desired mechanical and electrical properties. An optimization of the matrix material must consider both the mechanical and electrical effects on the overall composite properties. This is the purpose of this chapter.

This chapter investigates the possibilities for influencing the properties of the composite through the matrix material. It begins with a look at the key issues that dominate the choice of material parameters, both at the manufacturing level, and at the performance level of the composite. The introduction of high dielectric filler is the focus of much of this work. Simple models are compared to experimental data to analyze the effect of the filler. Surface modifying agents are also employed as a chemical additive to vary the effects of the particulate filler. Finally, the matrix properties are summarized for use in manufacturing of the fiber composites.

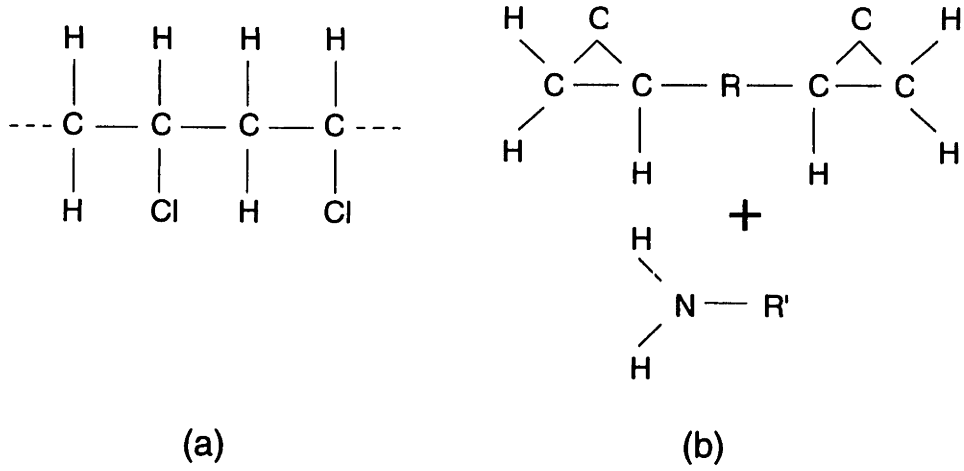

Figure 4.1: Examples of polymer types: (a) A thermoplastic, Polyvinylchloride; (b) A thermoset, two-part epoxy where R and R′ are complex polyfunctional molecules

4.2 Key Issues

There are several issues that will drive the choice for a suitable matrix material. These are primarily involved with the ability to manufacture 'good' composites, and the goal of higher actuation capability. The ability to manufacture good composites includes issues of polymer type and family, and how these will affect manufacturing. The actuation capability deals with the parameters that are favorable to high actuation. Both mechanical and electrical properties of the constituent phase materials will play a role in the level of effective composite actuation.

4.2.1 Available Polymer Materials

The basis of all polymers [60] is an organic backbone molecule of only carbon atoms to which other atoms attach. These other atoms include hydrogen, oxygen, chlorine, fluorine, sulfur, and nitrogen to name a few. Although the presence of these other atoms determine the families of polymers, the two main types of polymers, thermoplastics (TP) and thermosetting (TS) materials, depend on the structure of the carbon backbone itself.

In thermoplastics, the carbon atoms create a single chain with branches which assume a snakelike form in space. When a thermoplastic material is heated, the Van der Waals forces between the molecules weaken and the individual molecules slide and separate from each other (the material melts). The advantage of this type of polymer is that it can be injection molded, and then remelted and reused. Disadvantages, however, result for the

same reason. Although easy to fabricate, thermoplastics are not as rigid or strong as thermosets. The rigidity is very dependent on temperature and it is not uncommon to see an order of magnitude change in the modulus over 40°C. A common example of a thermoplastic is polyvinylchloride (PVC), whose basic structural group is shown in Figure 4.1 (a).

Instead of a single chain, thermosetting materials comprise a network of carbon atoms that crosslink with other carbon atoms. Unlike thermoplastics, this material uses heat and pressure to set, and cannot be remelted. Thus thermosets are generally stronger and more rigid, even at elevated temperatures. Another consideration is manufacturing. Thermosets can typically be used to manufacture at room temperatures, while thermoplastics cannot. For this reason, and others that become apparent with preliminary manufacturing, a thermosetting material is chosen as the matrix material for this project. A familiar example of a thermosetting compound is a two-part epoxy shown in Figure 4.1 (b). In this case, the actual epoxy is combined with a "hardener" material that serves to crosslink the epoxy molecules.

4.2.2 Properties for High Actuation Capability

Both mechanical and electrical properties of the matrix material will influence the actuation capability of the composite. A good measure of this capability is simply through the piezoelectric free strain constant d_{31}. Figure 4.2 shows the variation of the composite d_{31} versus volume fraction. This figure is very similar to the figures in Chapter 3.0, but now includes the influence of various stiffness ratios between fiber and matrix material as well.

Although the majority of variation in d_{31} is directly from the dielectric ratio, some influence on d_{31} can be attributed to the epoxy stiffness. However, a typical compliance for common epoxies is 20:1. At mismatches above even 8:1, very little change is seen in the actuation capability with matrix stiffness. Matrix material this soft offers very little restraint to the expanding fibers, so that the clamping effect is almost negligible. It is this assumption that enabled the solution of the closed form combination model.

Matrix dielectric, however, strongly influences the composite actuation capability. This influence comes about from the strong reliance of electric field distributions on relative dielectric. A simple one-dimensional model was presented in section 1.5.1 that clearly shows that high dielectric mismatch is detrimental to the actuation when the materials are in a series arrangement with respect to the 3 axis direction. This is echoed in Figure 4.2. The most obvious solution is the selection of a matrix material with high dielectric. Since virtually all polymers have very low dielectric constants, a method to increase the matrix

dielectric must be found. This same method, as it turns out, has the potential to greatly change the stiffness of the matrix, so that the consideration of actuation capability due to matrix stiffness becomes important.

A second concern for high actuation lies in the ability to reach full poling field levels within the fiber. The ceramic does not assume piezoelectric properties upon manufacture. Instead it is necessary to actually apply an electric field to polarize the ceramic before any piezoelectric effect may be achieved (see section 2.2.2). Thus, in order to attain the full piezoelectric properties , this field must be above the coercive field of the particular piezoceramic type. This coercive field is a strong function of temperature, so that piezoceramics are often poled at temperatures substantially above room temperature.

Figure 4.3 is a design curve for piezoelectric fiber composites, generated using the fully coupled Numerical Uniform Field (NUF) model. It shows the necessary through-thickness line fraction (X_3) that must be achieved in manufacturing, for a given matrix material dielectric. This is shown for three levels of piezoceramic coercive field, where the areas to the right of each line are regions of attainable poling levels in the fiber. The criteria set by these design curves are the ability to reach the coercive field within the fiber without reaching the breakdown field of the epoxy matrix (500 volts/mil). This is a problem due to the electric field intensification within the matrix material above the fiber at its closest approach to the electrode. This was demonstrated in the comparison of the various models (see section 3.6).

The three separate curves indicate the uncertainty of the necessary poling field in the piezoceramic. The room temperature value is approximately 17 volts/mil (7 kV/cm), but this changes significantly with temperature, decreasing to values around 12 volts/mil (5 kV/cm) or lower for 80°C poling [61]. The difficulty is that the polarization levels also depend on time, and the dependence of poling on these two parameters is not well understood. Further work is being done to quantify the phenomena. At the present, the usual method is to pole at levels above the coercive field for substantial time periods (20 min, for example) to ensure full poling.

The maximum X_3 line fraction achieved in manufacturing (without specimen sanding) has been approximately 0.98. Figure 4.3 shows that at a coercive field of 15 volts/mil, it will be necessary to have a matrix with quite a high dielectric, at least 55-57. This will require a tenfold increase over the pure epoxy, whose dielectric relative to air is around 6. Lower coercive fields require lower matrix dielectric. For a reasonable coercive field which may be attained at 80-100 °C, such as 10 volts/mil, the matrix material will need to have a dielectric in the vicinity of 35. It is not unfeasible that the coercive field may be as low as 5 volts/mil. In such a case, it would be possible to pole composites with lower

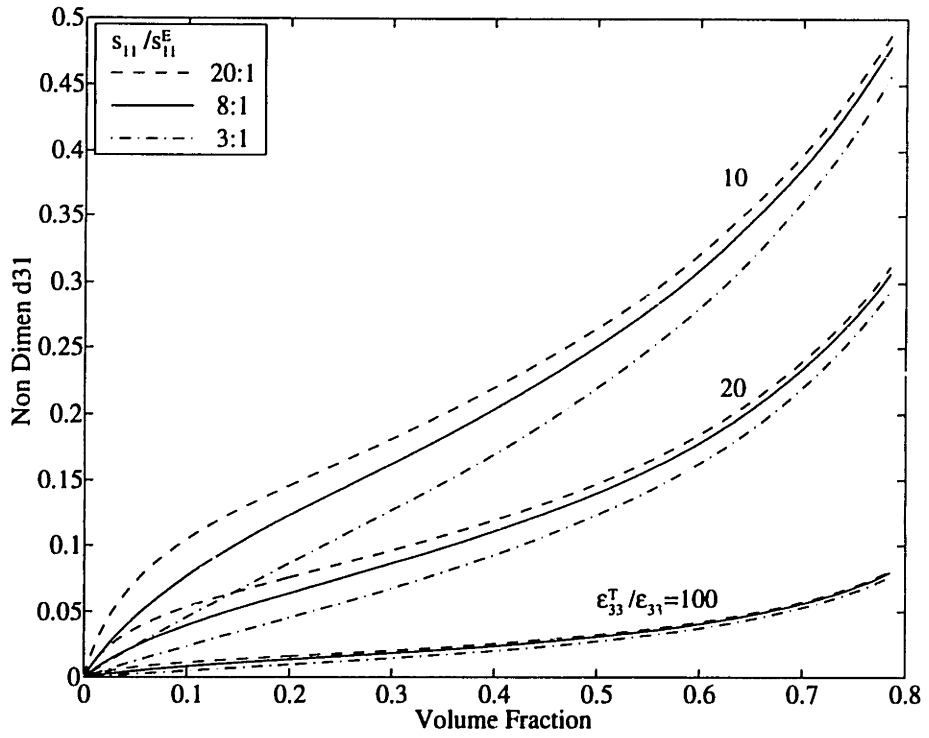

Figure 4.2: Effect of matrix dielectric and stiffness on the nondimensionalized composite d_{31} constant. Predictions made using Numerical Uniform Fields (NUF).

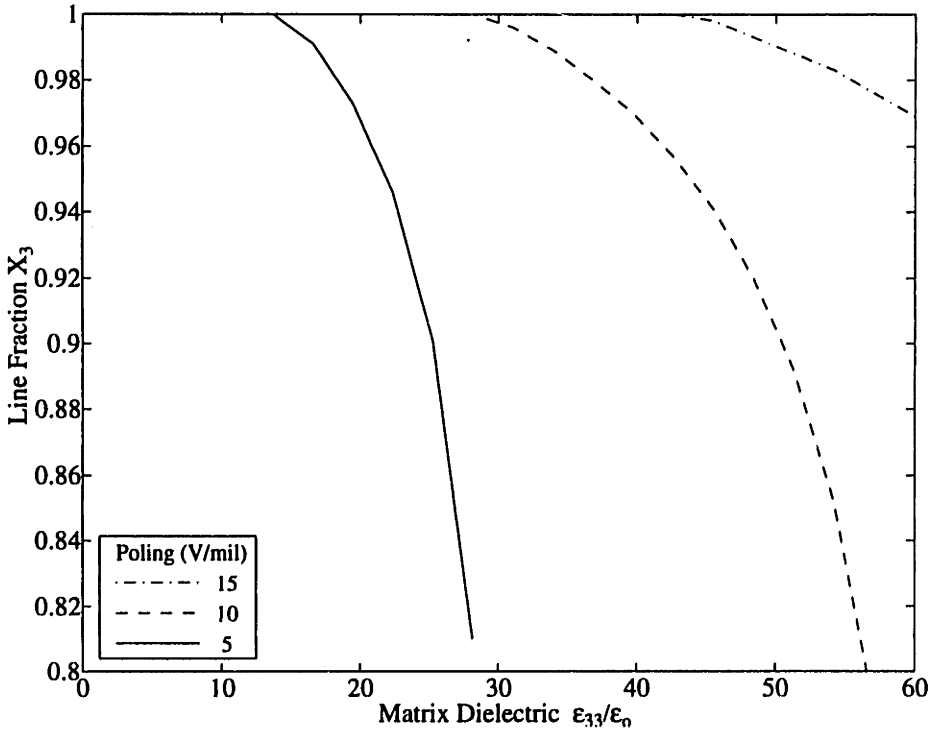

Figure 4.3: Design curves for PFCs showing regions of successful poling for several piezoceramic coercive fields. Generated from Numerical Uniform Fields (NUF).

matrix dielectric and quite low line fractions. One common conclusion from each of these curves is that it will definitely be necessary to increase the matrix dielectric from its pure epoxy level.

A mismatch of another sort is present in the composite. This stems from the existence of another phase in the matrix - small inclusions of air, also called voids. These voids are either originally present in the matrix, induced into the material by mixing, or caused by the formation of gas as a result of cure. To understand the effects of voids, reference can be made to the various transport models derived for inclusions in a dielectric, briefly described in section 1.3.3. Of note is the paper by Polder and Van Santen [49]. Using the model of an isolated particle in an effective homogeneous material, they derive the effective dielectric for spherical inclusions as:

$$\varepsilon^{eff} = \varepsilon^{m}\left(1+3v_{v}\frac{\varepsilon^{v}-\varepsilon^{m}}{\varepsilon^{v}+2\varepsilon^{m}}\right) \tag{4.1}$$

where m and v denote the matrix and void. The only restriction is that v_v, the volume fraction of voids, must be small. This will definitely be true for voids in a polymer matrix. Next, they present the electric field in an empty spherical hole for a medium with effective dielectric constant, ε^{eff}:

$$E^{v} = \frac{3\varepsilon^{eff}}{2\varepsilon^{eff}+1}\overline{E} \tag{4.2}$$

Since the volume fractions of voids will be small, it is evident from equation (4.1) that $\varepsilon^{eff} \approx \varepsilon^{m}$. From equation (4.2), given that polymers have relative dielectric between 3 and 6, that:

$$\frac{E^{v}}{\overline{E}} \approx \frac{3}{2} \tag{4.3}$$

Thus, there is an intensified field within the void. This effect, combined with the low dielectric strength of air, may cause localized breakdown of the material at high electric field levels. Such high field levels may be necessary for poling of the composite material. As a result, manufacturing for various dielectric mismatches must be done to minimize the occurrence of voids, and Chapter 6.0 outlines some methods by which this is accomplished. Even with these steps taken, voids still exist to some extent.

4.3 High Dielectric Particulate Inclusions

Just as the addition of high dielectric fibers will produce an effective dielectric for the composite above that of the matrix alone, the addition of high dielectric particles into the matrix should do the same. The key difference in the introduction of this new phase to the

matrix material will be its size. If the particulate filler used is small enough, its spatial scale will be far finer than that of the microstructure of the fibers. Given such a fine scale, the resulting medium can be viewed simply as a homogeneous matrix material with new effective properties. Thus, the composite modeling and optimization further divides into modeling and optimizing of the matrix material, which will itself be a composite material. The addition of the particulate now allows tailoring of the stiffness and dielectric properties. However, it will soon be apparent that the result is a tradeoff, as more particulate increases both the stiffness and dielectric, and reduces the ease of manufacturing.

Naturally, a first step in understanding the effects of particulate filler is to utilize modeling methods to determine the effective material constants. A large number of models are available and were briefly described in section 1.3.3. Since the particulate composite has 0-3 connectivity, the response of the composite is not dominated by the filler phase in any one direction. Should the filler be piezoelectric, this electric-mechanical coupling may be ignored for relatively low fractions of filler. Thus, the independent models for mechanical and electrical effective properties will suffice here.

4.3.1 Effective Permittivity for Particulate Composites

For the case of effective permittivity (dielectric), the work of Hashin [52] is chosen. This work is one of the clearest presentations of the conductivity problem, presenting the problem based on a Self Consistent approach. He shows the solution for the most general case, and specializes to other cases whose solutions were reached by other researchers as well. Important discussions on geometry and good comparisons to previous research complete the work.

The representative volume element is similar to that for the Self Consistent Model presented in Chapter 3.0, where a representative particle is surrounded by a matrix sheath, encapsulated by an infinite effective media. Solution of the harmonic equation in each of these phases, subject to consistent field boundary conditions, yields the effective material constants. By examining two special cases of material connectivity, Hashin produces the best upper and lower bounds for a "statistically homogeneous and isotropic two phase material of arbitrary phase geometry":

$$\text{(Lower)} \qquad \varepsilon_L^{eff}(v_1, v_2) = \varepsilon_1 \left(1 + \frac{v_2}{\frac{\varepsilon_1}{\varepsilon_2 - \varepsilon_1} + \frac{v_1}{3}} \right) \tag{4.4}$$

$$\text{(Upper)} \qquad \varepsilon_U^{eff}(v_1, v_2) = \varepsilon_2 \left(1 + \frac{v_1}{\frac{\varepsilon_2}{\varepsilon_1 - \varepsilon_2} + \frac{v_2}{3}} \right) \tag{4.5}$$

The terms v_1, v_2 represent the volume fractions of phase 1 and 2, respectively. The equations presented are actually special cases of a more general framework, where for the present discussion, Hashin has assumed that the ratio

$$c' = \frac{a^3}{b^3} \tag{4.6}$$

is equal to the volume fraction of particulate, v_2.

The lower bound (4.4) corresponds to the case where particulate (phase 2) is completely surrounded by matrix (phase 1), shown in Figure 4.4. This case pertains to composites where the percentage of particulate is not so high as to create high dielectric paths between the far field potentials. The upper bound (4.5), on the other hand, describes the other extreme of complete particulate connectivity, where the matrix (phase 1) is completely surrounded by particulate (phase 2). This case is not shown, but represents composites with very high particulate volume fractions. The equation for this case (Eqn 4.5) is simply a reversal of material phases from the first equation (Eqn 4.4).

An intermediate curve is given if the following assumption is made:

$$c' = \frac{a^3}{b^3} = 1 \tag{4.7}$$

This is the boundary value problem for an infinite medium that contains a single particle inclusion. Hashin remarks that this special case of the present work has been reported previously by Landauer [30], and results in the following implicit expression for the effective dielectric:

$$\text{(Middle)} \qquad v_1 \frac{\varepsilon_1 - \varepsilon^{eff}(v_2,1)}{\varepsilon_1 + 2\varepsilon^{eff}(v_2,1)} + v_2 \frac{\varepsilon_2 - \varepsilon^{eff}(v_2,1)}{\varepsilon_2 + 2\varepsilon^{eff}(v_2,1)} = 0 \tag{4.8}$$

This curve begins tangent to the lower bound at low volume fraction of filler and finishes tangent to the upper bound at high volume fractions. If the ratio of dielectric between the two phases is not too large, the two bounds are relatively close, and describe a small region. Such an example is given in Figure 4.5 where the dielectric mismatch is only 1:10. For large dielectric mismatch, as in this problem, these bounds are very far apart. These bounds are the best possible, however, given information only on the volume fractions. There exists a certain arbitrariness represented by the parameter c', whose nature Hashin admits is unknown. Further information on the phase geometry is needed.

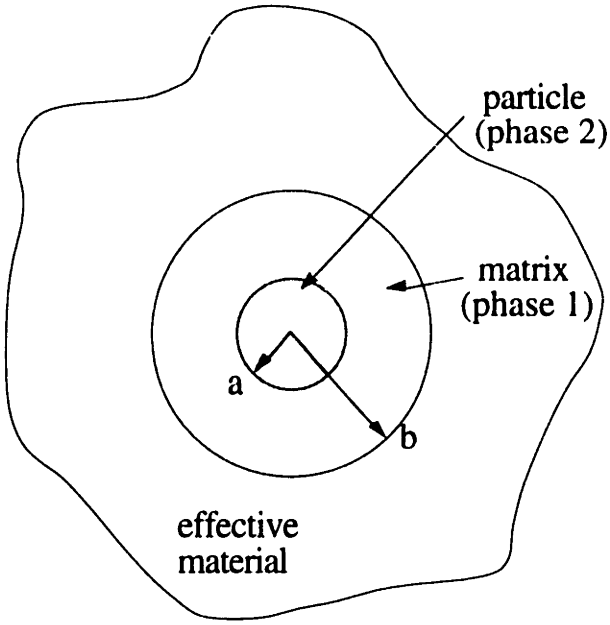

Figure 4.4: Representative volume element for Self Consistent approach by Hashin [52]

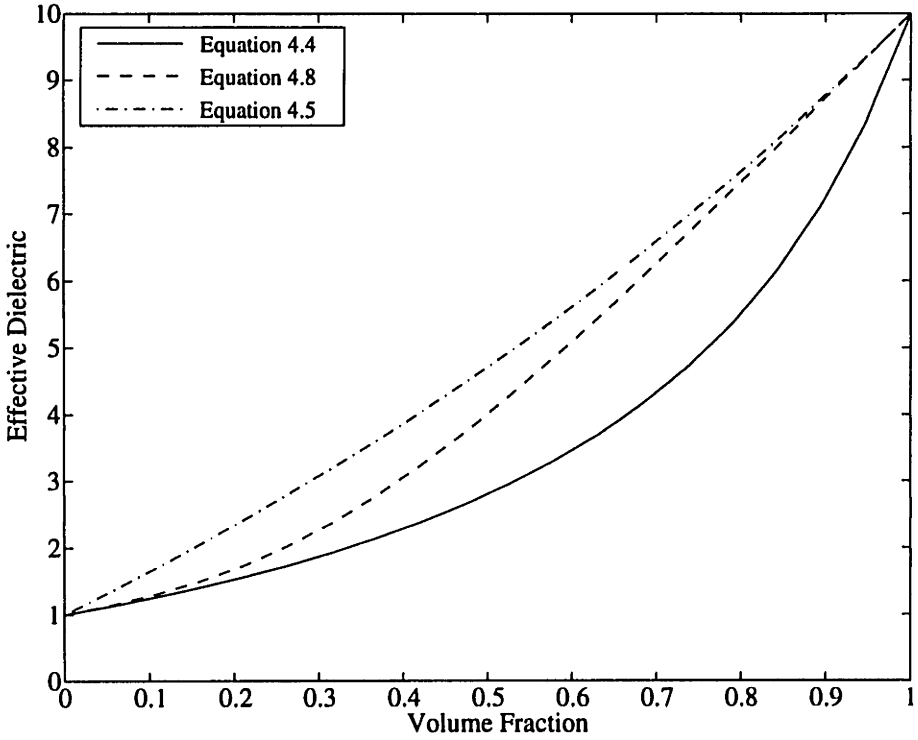

Figure 4.5: Prediction of effective dielectric for a two phase particulate composite with dielectric mismatch of 1:10.

One might surmise that the parameter c′ may actually represent the connectivity and could be statistically founded. For small volume fractions, low probability exists of high dielectric paths between the potentials, and the effective dielectric will be that of the lower bound. As the volume fraction increases, so does the probability of connectivity, until a 'critical volume fraction' is reached, whereby the effective dielectric more closely follows the upper bound. Several works [62,63], have been published that attempt to predict critical volume fractions based on particulate geometry and statistical analysis. However, the volume fractions used here will be low enough so as to permit comparison to the lower and intermediate bounds presented in this work.

4.3.2 Effective Modulus for Particulate Composites

Not only do the addition of high dielectric particles affect the permittivity, but if the stiffness is significantly different from that of the matrix, the overall stiffness will be affected. This is likely the case here, as all high dielectric materials are typically ceramic or metal, with much higher stiffness than the polymer. The discussion of effective properties for stiffness is very similar to that of dielectric and deals with both bounding and approximate solutions. Again, the difficulty of specifying phase geometry creates difficulty with determining accurate predictions.

The work of Paul [64] is described by Jones [23] as being one of the first to use variational techniques to examine the bounds of multi-phase materials. The work uses the minimum potential and minimum complementary energy approaches to form the upper and lower bounds on the moduli of isotropic 2 phase media (i.e. particulate composites). Interestingly enough, the two bounds are virtually the same as the Mechanics of Materials solutions for the longitudinal and transverse moduli of fibrous composites[13]:

$$\text{(Lower)} \qquad E \geq \frac{E_m E_d}{\nu_m E_d + \nu_d E_m} \tag{4.9}$$

$$\text{(Upper)} \qquad E \leq \nu_m E_m + \nu_d E_d \tag{4.10}$$

A further solution is one that follows in the same spirit as the Combination Model in section 3.3.3. This method applies the Mechanics of Materials approach to a cube of matrix material containing a cubic inclusion. The same assumptions of uniform fields are used, and the same inconsistency among the fields exist, due to the assumption of equal strains in the material phases. The model is similar to the Combination Model presented in this work, except that there is no direction where the inclusion material has connectivity. The effective Young's Modulus is easy to derive, and is reported in Jones (pg 122):

---

[13] When the assumption of equal Poisson's Ratios is made

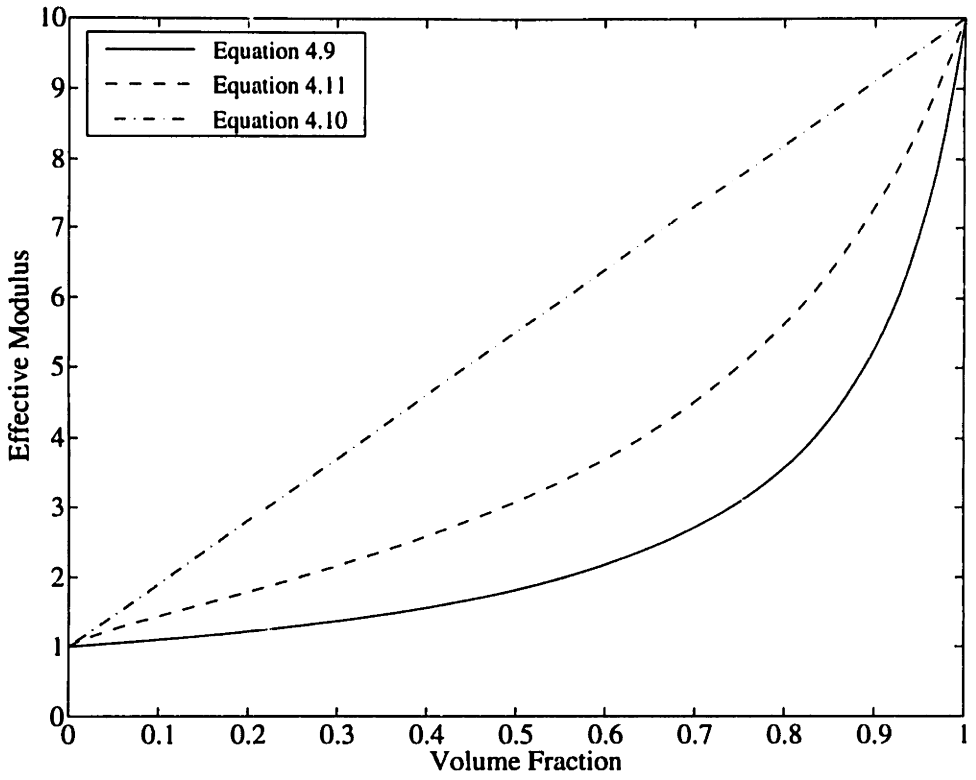

Figure 4.6: Prediction of effective Young's modulus for a two phase particulate composite with modulus mismatch of 1:10.

$$\text{(Middle)} \qquad E = \frac{E_m + (E_d - E_m)v_d^{2/3}}{E_m + (E_d - E_m)v_d^{2/3}(1 - v_d^{1/3})} E_m \tag{4.11}$$

The three curves are compared in Figure 4.6 for a stiffness mismatch of 10. Note that for all of these solutions, no information is provided on the aspects of phase geometry. For mechanical properties, the term contiguity is often used to describe the likelihood of particle interaction equivalent to connectivity in discussions of conductivity problems. Only more complicated models, such as the semi-empirical methods of Halpin-Tsai [65] for fibrous composites take this effect into account. However, also like the conductivity problem, the volume fractions used here will be low enough that the present models will suffice.

4.4 Experimental Methods for High Dielectric Particulate Matrix

The material chosen for the high dielectric was a piezoceramic, type PZT 5H. This ceramic has one of the highest dielectric constants of the piezoelectric family ($\varepsilon_{33}^{T} = 3400$), and is easily obtainable in very fine powder form. Very fine metallic powder or graphite

(carbon black) could also have been used, as its dielectric is essentially infinity, and a wide body of literature is available on its use in materials for electrical purposes. However, since these materials are actually conductive, there is the added danger of dielectric breakdown. The more such powder is added, the lower the dielectric strength of the resulting matrix material. The critical volume fraction at which the effective dielectric sharply increases is also likely to signify a sharp drop in resistivity. Furthermore, the model does not easily distinguish between materials with dielectric 500 times that of the matrix, and materials with infinitely higher dielectric. With respect to the original matrix, piezoceramic appears to have infinite dielectric.

The manufacturing setup is shown in Figure 4.7. Three specimens were manufactured in each lot (batch) to ensure redundancy in manufacturing and measurement techniques. Aluminum mold pieces were bonded to aluminum/mylar electrode material with double-sided tape to contain the epoxy flow within the mold. The two part epoxy matrix was first mixed in the proper ratio of 4:1 (part A to part B), followed by the addition of the required amount of piezoelectric filler[14]. After mixing the epoxy and filler together, the mixture was placed in the mold and covered with a top electrode and cover plate. The epoxy was cured for 1 hour at 65 °C under low pressure (approximately 15 psi) using applied weight. Following the cure, the specimens were cut from the mold and dimensions measured with a micrometer and calipers. The thickness was measured in three places using micrometers with 0.001 mm precision, and the width and length were measured in two places using calipers with 0.02 mm precision. Capacitance was measured and the dielectric calculated from

$$\frac{\varepsilon}{\varepsilon_0} = \frac{Ct}{\varepsilon_0 A} \tag{4.12}$$

where C is the capacitance, t the thickness, A the area, and ε_0 the permittivity of free space (8.85e-12 F/m).

The results are shown in graphical form in Figure 4.10. These values are the data shown as 'without dispersant'. The amount of piezoceramic was varied from 20% to 80% by weight (3.38% to 35.86% by volume). Due to its high density (7800 kg/m^3), high mass ratios of PZT only correspond to moderate volume fractions. However, amounts much above this were impossible, as mixing became difficult and the resulting material would be useless as a matrix for manufacturing with fragile PZT fibers.

The addition of piezoceramic filler was able to increase the effective dielectric significantly, from approximately 6 with pure epoxy to 27 with 80 wt% of filler (36 vol%),

---

[14] PZT 5H Powder, Lot 128B, Morgan-Matroc, average dia=1.10 μm

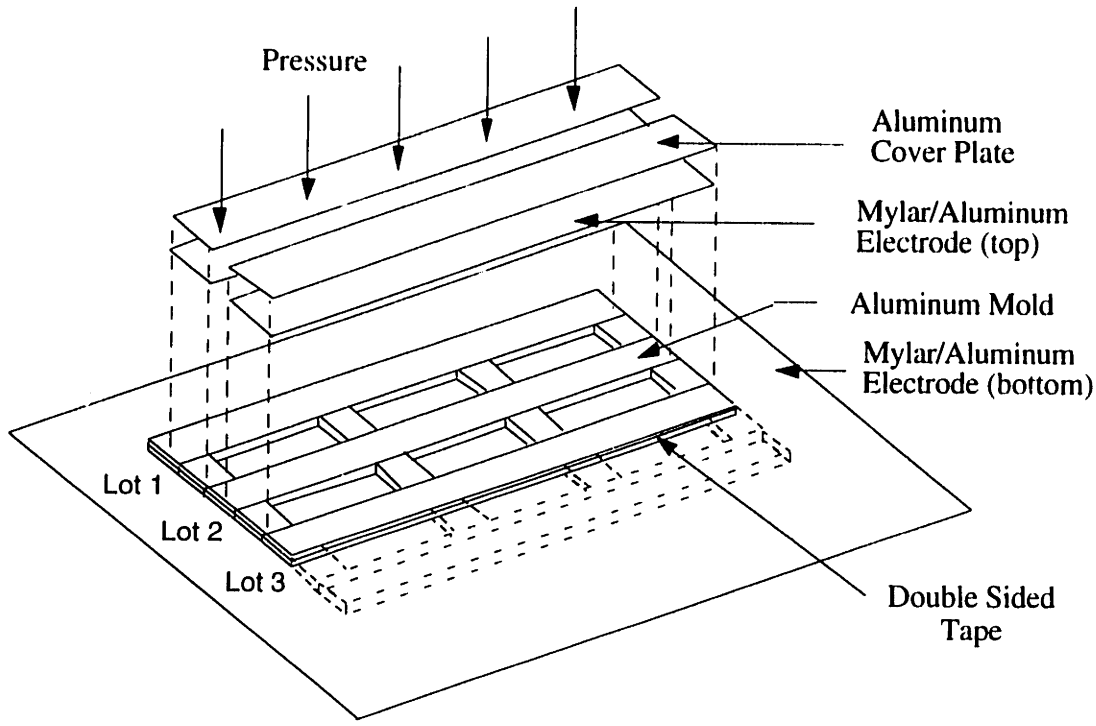

Figure 4.7: Manufacturing setup for particulate/epoxy study

an increase of 4.5 times. However, the values are perhaps not as high as expected when comparing with the models presented. Values of 30 vol% of filler is likely to be near to the critical fraction [63], and a more dramatic rise in dielectric should perhaps occur. Instead, the values seem to follow a path just slightly above the lower bound (Eqn 4.4).

Measurements of the mechanical properties were done using a tensile testing machine[15] and data acquisition system[16]. The tests were conducted under displacement control with the slow extension speed of 0.2 mm/min (0.008 in/min). This was used to avoid matrix viscoelastic effects. The test machine load cell provided the load data, while the strain information was provided by a strain gage measurement system[17]. Specimens were cut to a width of approximately 5 mm, just wide enough to apply a single strain gage to the specimen. This was done to ensure an accurate assessment of the average strain field across the specimen. The test length was approximately 30 mm.

The benefit of an increase in dielectric also brought an increase in stiffness. This is shown in Figure 4.11. The matrix Young's Modulus is increased from 2800 MPa with pure epoxy to 7800 MPa at 80 wt% (36 vol%) filler loading, an increase of 2.8 times. The

[15] Model 4505, Instron, 100 Royall St, Canton, MA 02021

[16] Labview for Macintosh, National Instruments, 6504 Bridge Point Parkway, Austin, TX 78730

[17] Model 2210, Measurements Group Inc., PO Box 27777, Raleigh NC 27611

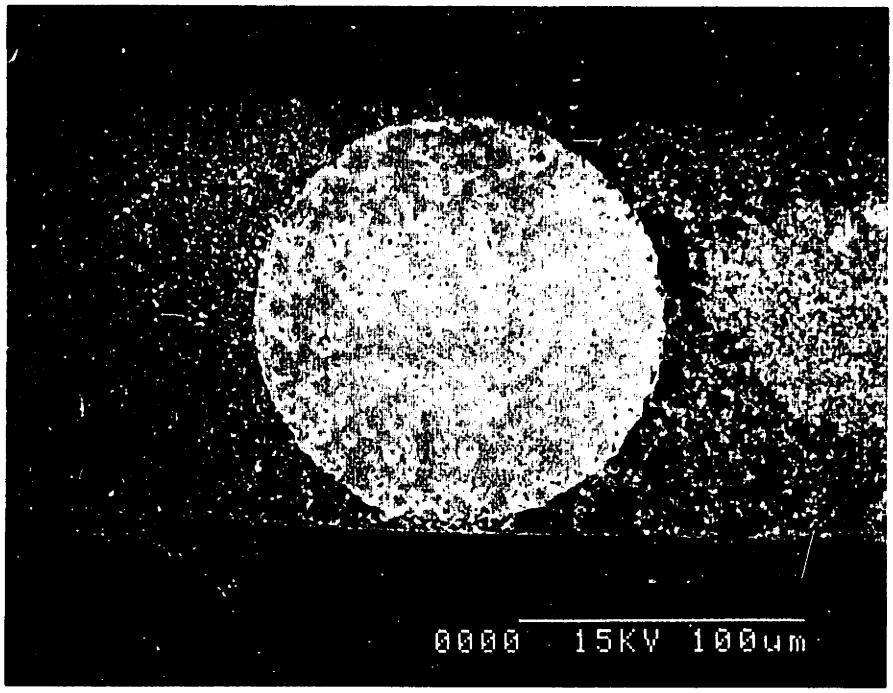

Figure 4.8: SEM Photo of PZT fiber composite with particulate filler in epoxy matrix, exhibiting poor dispersion properties

general trend of stiffness with volume fraction seems to follow equation (4.11), describing the cubic inclusion model.

In addition to an increase in stiffness and dielectric, the matrix material became much harder to process due to the much increased viscosity, particularly at high particle fractions. This naturally will make the fiber composite manufacturing more difficult in terms of matrix flow, compaction, and void removal. After cure, the matrix was far more brittle, less conformable, and susceptible to easy fracture. Although these attributes will not affect the fiber composite performance directly, they will play a large role in the quality of the final composite.

Many of the difficulties mentioned above, both electrical and mechanical, may possibly be explained by interfacial effects. Virtually all models assume perfect matrix-filler bonding and do not consider the possibility of poor adhesion or additional chemical components separating the filler and matrix, such as water. Furthermore, if the particles are to behave, at least in a statistically averaged sense, as individual inclusions with a representative amount of surrounding matrix, then they must be properly dispersed. Dispersing of particles involves the separation of filler particles such that they do not tend to aggregate and form larger secondary particles. Evidence of poor dispersion is seen in Figure 4.8. This SEM photograph shows a piezoelectric fiber surrounded by filler/epoxy matrix. Notice that the particles tend to form clusters and do not move well into confined

areas (around fiber). The next section discusses methods for improving the dispersion characteristics of filler/epoxy systems.

4.5 Effect of Surface Modifying Agents On Effective Properties

4.5.1 Surface Modifying Agents

Surfation, as defined by [66], is "the result of the chemical reaction of an organo-compound with a filler, pigment, or reinforcement surface to permanently alter the organophilic nature of the surface." Thus, surface modifying agents are those compounds that change the chemical nature of a filler system that is to be used in an aqueous media.

The body of literature and extent of patents on surface modifying agents is huge. This is typically because the choice of surfactant will be extremely application-dependent, and many specific types have been developed. Surfactants can be classed through the nature of their primary purpose, surface interaction mechanisms, and active groups to name a few. However, two very broad classifications based on interaction mechanisms are often made. These are coupling agents and dispersing agents.

Coupling Agents

Coupling agents, of which organofunctional silanes are the most widely utilized are used primarily to reduce the degradation of properties associated with the introduction of filler into a media. Normally, when mineral fillers are added to a polymer without surface treatment there can be serious embrittlement of the material, degradation of strength, and increased moisture sensitivity. This increased moisture sensitivity may result in a loss of strength in the composite and deterioration of electrical properties [67].

If the filler surface is first treated with an organo-functional silane, there is significant improvement in flexural strengths and toughness, and better retention of these properties over time, even when subject to adverse environmental effects. The basis of the interactions is a silicon atom to which is attached a hydrolyzable group (such as chloride, methoxy, ethoxy, etc.). This group reacts with water on the surface of the filler material and becomes highly reactive, and in a chemical structure that will bond to the filler. The nature of the bond is a covalent one, and leaves the filler with a surface treatment that contains a long molecular chain. These structures typically promote entanglement with the polymer chains of the matrix material and may also be involved in cross linking or even strong covalent bonding with reactive sites on the polymer. Such reactions provide the

composite with dramatically improved interfacial adhesion, resulting in the aforementioned improvements in properties.

Dispersing Agents

Dispersing agents are different from coupling agents in the interfacial mechanisms and the primary purpose they serve, even though the consequences of using dispersants are very similar to coupling agents. Unlike coupling agents, dispersants are not focused on the adhesion between filler and matrix, or the improvement of mechanical properties. Rather, as the name suggests, dispersants serve to disperse, or separate, filler particles from one another in an aqueous system. They are often used to reduce the viscosity and stabilize mixtures, improving the flow properties for various spraying and coating applications. A common application that relies heavily on the dispersion of fine pigments is household latex paint. Dispersing agents keep the particles dispersed, allowing higher concentrations, uniform color, and low viscosity.

For the present work, a dispersing agent was chosen for its ability to separate particle filler, and more nearly approach the conditions assumed in micro modeling. As it turns out, the dispersant chosen has attributes not only typical of dispersants, but also those of coupling agents that promote adhesion and reduce embrittlement.

4.5.2 Wetting and Dispersing

Reference [68] offers the following definition:

> "Wetting, by itself, generally means the spreading of one substance, usually a liquid, over a substrate such as a solid....Dispersion is really the mechanical process of moving pigment or inert particles apart. The term "wetting and dispersion" refers to the displacement of air or moisture from pigment particle surfaces to facilitate mechanical separation of the primary particles, distribute the pigment particles, and to keep the pigment particles from coming back together immediately."

The need to consider these processes may be understood by a description of the physical chemistry at the filler surface [66]. Most inorganic fillers have very high surface energy (which is often measured by surface tension and the difficulty of wetting the material) due to an imbalance of bonding forces at the surface. Surfaces such as these are very receptive to moisture (hydrophilic) and water tends to adsorb, reducing the surface

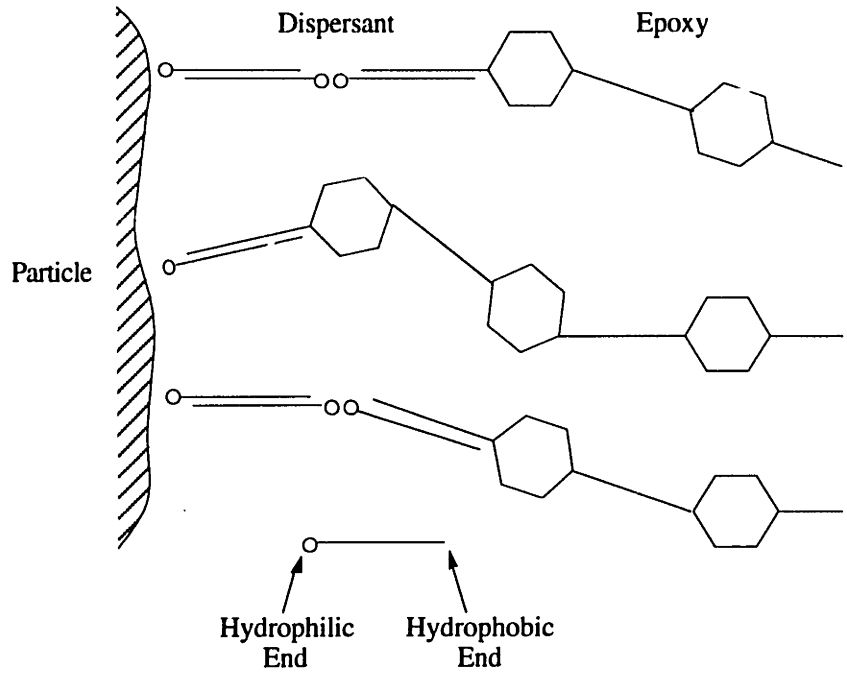

Figure 4.9: Interaction of the dispersing agent with epoxy polymer chains and the filler particle surface

energy of the particle. However, as the particle size decreases, the activity at the surface increases proportional to particle area. Very small particle have little mass, and the van der Waals[18] forces are quite large between the particles. As a result, small particles tend to adhere to others, creating larger effective particle diameters.

These groups of particles (secondary particles) are usually held together weakly by the moisture, and are only primary particles that have contact along edges or at points. Tertiary particles are those that have face to face contact and cannot usually be separated, except by using large amounts of energy that will often break the original crystal structure of the primary particle. The key then, is the separation of these secondary particles into the original form of primary particles. Highly polar polymers are able to displace air and adsorbed water from filler surfaces, but require a lot of time and energy to do so. Nonpolar or slightly polar polymers (such as epoxy) cannot easily perform this function, so that use of a dispersing agent is very important Thus, the main function of the dispersing agent is to decrease the time and energy for the complete dispersion process.

There is a large number of available dispersants, some of which overlap in function and mechanism with coupling agents. Of five major classes [68], probably the most common is of bifunctional form, and is the type used here. These bifunctional dispersants

[18] Sum of dipole, dispersion, and hydrogen bonding.

do not directly reduce surface tension, but facilitate wetting and dispersion by having two chemical groups with very different tasks. One end is hydrophilic and readily adsorbs to the surface of the filler at edges, corners, and surfaces. The second end, a hydrophobic tail, orients itself away from the particle and either bonds readily with the polymer through polymerization, or is entangled in the polymer chains. This is depicted in Figure 4.9. The added attraction of bifunctional dispersants, then, is the promotion of adhesion in addition to the primary function of dispersion.

The exact nature of the surface chemistry is controversial. Methods of bonding include covalent, ionic, chemisorption, van der Waals, and other related chemical bonding. The significance of each depends not only on the exact constituents that react, but also on the various opinions of the reactions that take place at interfacial sites. Perhaps the most widely accepted theory for intermolecular interactions in solution and at interfaces has been the Donor-Acceptor Theory (or Acid-Base Interactions),described in Ref[69]. Fowkes [70,71] has been a strong proponent of this theory, and has shown that the forces of attraction "operate only when the acidity of one phase can interact with the basicity of the other phase." His experiments showed that acidic polymers adsorb only on basic fillers and not at all on acidic fillers, and that basic polymers adsorb on acidic fillers and not at all on basic fillers. Thus, another way to perceive the function of a dispersant or coupling agent is to view it as a means to change the particle acidity/basicity to better interact with the polymer. Electrons transfer from the basic phase to the acidic one, causing an attraction between the two materials similar to a hydrogen bond in nature.

The actual ability to disperse comes from the fact that each particle is now surrounded by dispersing agent with like orientation. Previously, the particles had localized build-up of charges with opposing polarities, causing attraction. The introduction of dispersant now creates filler with particles that have little affinity for one another. A difficulty arises with the introduction of excess dispersant, because the availability of unused sites can cause the phenomena known as bridging. This is also known as flocculation and is characterized by particles closely joined by bridges of solvent (in this case dispersant). This will cause higher viscosity and poor adhesion, and should be avoided.

4.5.3 Experimental Results

The dispersing agent Hypermer KD-2[19] was chosen for the high-dielectric particulate study. This is a polymeric dispersant made specifically for ceramic filler

[19] Supplied by Surfactants Group, ICI Americas, Inc., Wilmington, DE 19897.

Table 4.1: Initial Study of Mixing Order on Matrix Dielectric

Batch #	Mixing Order	% PZT	% Disp.	% Epoxy	$\frac{\varepsilon_{33}}{\varepsilon_0}$
1	A→B→DISP→PZT	80	4	16	33.7
2	A→DISP→B→PZT	80	4	16	33.2
3	A→DISP→PZT→B	80	4	16	32.9
4	A→PZT→DISP→B	80	4	16	31.4

applications. This particular agent is actually made for polar solvents (epoxy is slightly polar), and is basic with a hydrophilic tail. The exact amount needed is difficult to assess, but 2% of dispersant by weight to the filler has been suggested as the theoretical mono-layer coverage [72]. Instead, the larger amount of 5% by weight (20:1 for PZT:dispersant) was chosen due to the uncertainties in possible competitive reaction with the epoxy. There is the possibility that the amino group of the dispersant will occupy some of the available sites in the polymer. This is not easily analyzed because the exact structure of the agent is proprietary. The competitive reaction is likely, however, as the dispersant is post-added to the system. Preliminary work showed a significant increase in dielectric with 5% by weight compared to 2% by weight when the dispersant was post-added.

Two initial studies were done to investigate the effects of manufacturing procedures with dispersant on the matrix dielectric. The first involved the order in which various components of the matrix system were added. Four lots, each of three samples, were manufactured according to the method outlined in section 4.3, with the exception of dispersant. All four batches comprised PZT 5H particulate (80% by weight), epoxy parts A and B (16% by weight), and dispersant (4% by weight). Note that the amount of dispersant to PZT filler is still 5% by weight. Table 4.1 summarizes the dielectric for four different mixing orders. In each case, the dispersant is post-added, that is, the PZT filler comes in contact with the epoxy system prior to the dispersant. At each step, the solution was mixed by hand for one minute, except at the introduction of the particulate, where the solution was mixed for five minutes by hand. Only a small difference in dielectric was found for the first three batches (1-3), indicating that if a competitive reaction takes place between the epoxy and dispersant, it is due to part A of the epoxy[20]. The last batch (#4) shows a significant difference, probably due to the fact that it was virtually impossible to

[20] Epoxy mix ratio is 4:1 (part A to B), thus part A had to be present to provide adequate solvent for the filler.

Table 4.2: Initial Study of Moisture Effects on Matrix Dielectric

Batch #	Mixing Order	% PZT	% Disp.	% Epoxy	$\frac{\varepsilon_{33}}{\varepsilon_o}$
5	A→DISP→PZT→B	75	3.75	21.25	23.7
6	A→DISP→PZT(dried)→B	75	3.75	21.25	23.9
7	(PZT+DISP)→A→B	78.75		21.25	21.4

thoroughly mix all of the PZT into only part A. Some of the dispersant had to be added just to finish the first step. Overall, not much variation in dielectric was found (6.8% maximum variation) for the different mixing patterns.

The second initial study investigated the effect of moisture and filler pre-treatment. Again, batches of three samples were manufactured using the same methods as above, except that the amount of PZT was lowered to 75% by weight of the total solution. Batch #5 served as the control and was mixed in the same order as batch #3. Batch #6 was pre-dried in an oven at 230°F for one hour to remove moisture. Following the drying, this batch was immediately mixed in the same manner as Batch #5. Both of these batches again had a dispersant-to-filler ratio of 5% by weight. Batch #7 used pre-treated filler mixed with the epoxy. The pretreatment was accomplished by mixing one gram of dispersant with nine grams of alcohol, to which 10 grams of PZT filler was subsequently added. After the alcohol had evaporated, the treated filler was mixed with the epoxy such that the total PZT/Dispersant fraction was 78.75%.

Little difference is seen between the dielectric of batches 5 and 6. Thus, the dispersant is able to remove the water left on the particle surface so that it appears electrically the same as pre-dried filler. The pre-treatment process of batch 7 actually lowered the dielectric, compared to the previous batches. In hindsight, it is unlikely that only the necessary amount of dispersant was attached to each particle. Instead, the excess dispersant deposited itself to each filler particle, causing poor dispersion and electrical properties. Batches of pre-treated filler with less dispersant should be examined in a further study to more conclusively examine pre- versus post-adding.

The next step was to evaluate the overall effect of the dispersing agent on the electrical, mechanical, and rheological properties of the filler/epoxy system. Batches with dispersant were made in the same manner as previously described, with the same mixing order as batch #2 (pt.A → pt.B → dispersant → PZT). The batches were again mixed by hand for one minute between each step, except for after the addition of PZT, when the

solution was mixed for 5 minutes. After cure, the specimens were removed from the mold, sanded, and the dimensions measured.

Scanning Electron Micrographs show the effect of dispersant on filler dispersion in a fiber composite application, shown in Figure 6.3 (Chapter 6.0). Note the better separation of the particles, indicated by the apparent increase in particle density. The particles were also able to get into the regions close to the fiber more often. However, in some instances, it still appears as though regions of high pressure force the particles to evacuate these areas. The better dispersion was also felt physically, as the addition of the dispersant had an effect on the rheology of the mixture. The viscosity of the mixture was definitely reduced, but this was never quantified by measurements. The most obvious effect was the smoothness of mixture compared to the very grainy texture of the previous mixtures without dispersant. Filler fractions above 80 wt% were never attempted, although this may have given an indication as to whether the dispersant would allow higher particulate loading. After cure, the change in specimen brittleness was remarkable, reflected in much higher flexural strengths. Previous batches without dispersant easily cracked during cutting or fractured when bending moments were applied.

The effect on the measured mechanical properties was far less noticeable. Although only two specimens were tested, it seems that the dispersant had little effect on the Young's modulus. This is shown in Figure 4.11. The specimens with dispersant have approximately the same modulus as those without. For the use of coupling agents, rather than dispersants, several references [66,73] report that an increase in Young's modulus is standard. However, the same has not been reported for particulate composites utilizing dispersants.

The effect on the measured dielectric properties is much more apparent. The more effective dispersion of the particles promotes better permittivity of the filler/matrix material. The dielectric of the specimens with dispersant was consistently higher (15% - 30%) than those without, for the tested volume fractions. The exact mechanism is unclear, but it may be due to a smaller average particle size which allows for a more uniform electric field distribution and smaller field concentrations around inclusions. Thus, the material appears more homogeneous. Another consideration may be the absence of water at the interfacial sites, which may impede the ability to transfer electrons between material phases.

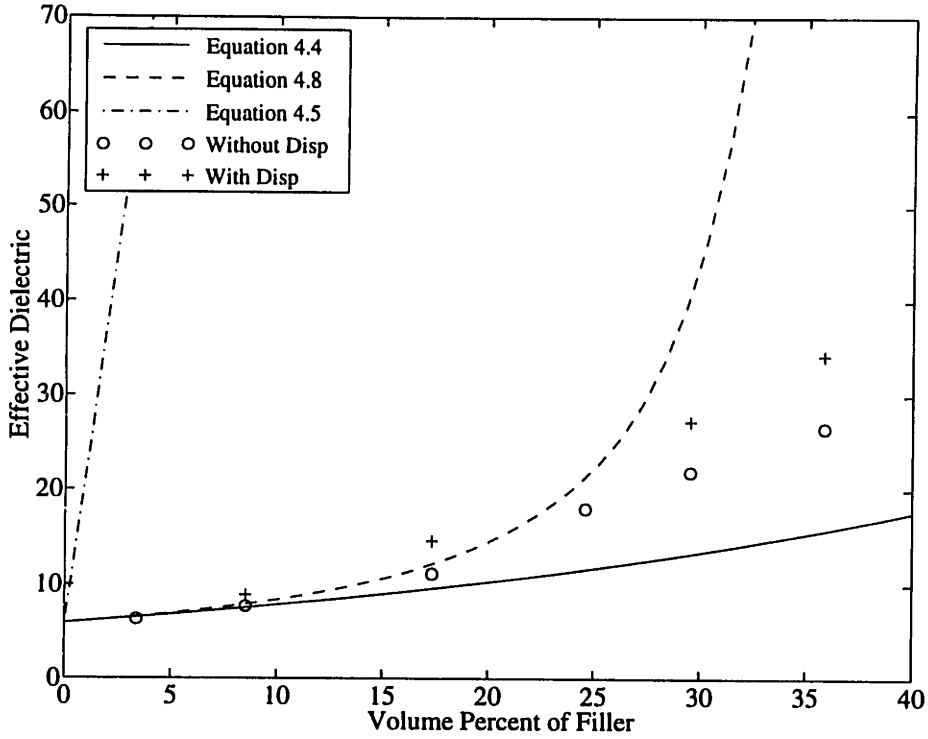

Figure 4.10: A comparison of experimental with predictions for effective dielectric for particulate/epoxy matrix system

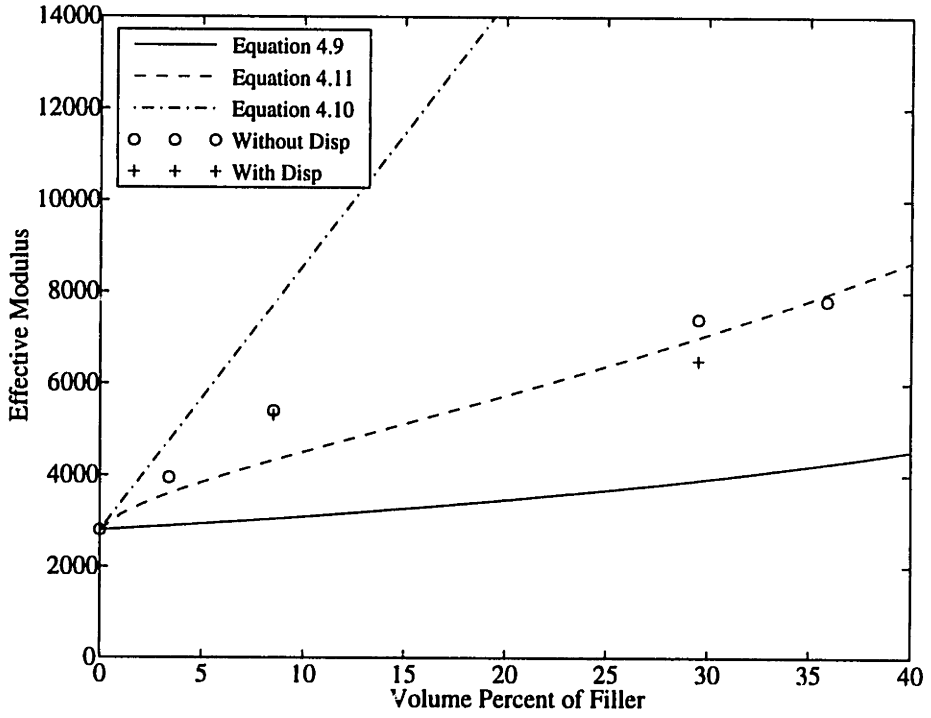

Figure 4.11: A comparison of experimental with predictions for effective Young's modulus for particulate/epoxy matrix system

Table 4.3: Material Properties of Filler/Epoxy Matrix Material

	s_{11}	s_{12}	s_{22}	s_{66}	c_{11}	c_{12}	c_{22}	c_{66}	$\frac{\varepsilon_{33}}{\varepsilon_o}$
New Matrix	154	-46.2	154	400	8.74	3.75	8.74	2.50	27.3

(Units: s_{ij}: 10^{-12} m^2/N, c_{ij}: 10^9 N/m^2)

4.6 Summary

Since the introduction of the dispersing agent has had only beneficial results, it will be used in the manufacturing of the new particulate matrix material. It provides increased dielectric with lower viscosity and a much improved toughness. What remains is the determination of the appropriate amount of filler material to use. Referring back to Figure 4.2, it is obvious that the stiffness of the matrix will not be a governing factor in actuation capability. At the maximum particulate loading achieved (80 wt%), the stiffness increase was less than a factor of three, so that the fiber to matrix ratio is still at least 8:1. Since the dielectric ratio is 100:1, virtually no influence on the effective d_{31} will be seen for the new, stiffer matrix.

The question then becomes one of manufacturing. Higher concentrations of filler inevitably mean higher viscosities, even with good dispersion. Experimentally, a filler fraction of 75 wt% (29 vol%) has shown to be of low enough viscosity that good manufacturing can be achieved with fiber composites. For this fraction of filler, it is still possible to obtain compaction and uniformity under cure pressure, and the viscosity allows the application of the matrix to the brittle fibers without damage. The matrix properties for this percent of filler and appropriate dispersant level are summarized in Table 4.3. The results of the study in this chapter are now applied to manufacturing. The twist-extension laminate example, presented in the next chapter, will utilize this new matrix material for increased actuation capability. The manufacturing and testing for this laminate are then discussed in sections 6.5 and 7.4, respectively.

5.0 Mechanics of Anisotropic Actuation

5.1 Overview

Chapter 5.0 deals with the topic of anisotropy. Although mechanical and piezoelectric anisotropy exist in poled piezoelectrics, the standard applications can only make use of the actuator in the plane of isotropy. However, through various techniques (compositing, unique attachment schemes or interdigitated electrodes), it is possible to obtain anisotropy in the plane of interest. The anisotropy may be mechanical, electrical, or both. The benfits derived from such anisotropy has not been quantified previously, but is done so in this section. Augmented Classical Laminated Plate Theory (ACLPT) provides the vehicle for examining induced twist through anisotropic actuators. Induced-twist is recognized as an important parameter for high authority control of aeroelastic structures, and other applications where bend-twist coupling is of interest. The final section introduces the twist-extension coupled laminate which is referred to throughout the remaining chapters.

5.2 Design of an Anisotropic Actuator

5.2.1 Benefits of Anisotropic Actuators

The field of structural control using active materials has received much attention in recent years. A multitude of models have been developed for the actuation and sensing of beam [74], plate [14], and shell [75] structures that employ a variety of active elements. Experimental results in closed loop control of a variety of applications (see section 1.1) have verified these models and demonstrated the feasibility of active structural control using active materials. As the field has matured, attention has turned toward increasing the performance of these systems. However, the basic active materials have not changed in the past twenty years, so that increasing performance will rely on using current materials in unique ways, or combining materials to create new technologies.

One means of improving the level of structural control performance is the use of tailorable anisotropic actuator materials. Tailoring gives the designer added freedom to specify varying degrees of structural coupling. However, current methods of actuation and sensing that utilize piezoceramics must use monolithic ceramics that exhibit in-plane isotropy. Thus, it is impossible to distinguish and actuate any single component of in-plane strain with these ceramics. Present methods to induce anisotropy require a composite

host structure [14], or special piezoelectric attachment techniques [76] to produce the desired degree of coupling.

Piezoelectric fiber composites, however, have a large potential for independently controlling structural deflections in different directions. This arises from the ability to choose parameters at the material, lamina, and laminate levels of manufacture. Matrix and ceramic combinations, volume fractions, and ply angles all contribute to the tailorability of the actuator. As a result, the designer can minimize or maximize various coupling parameters that influence the structural behavior. Various torsional, bending, and extensional modes can now be separated, allowing for more efficient control of independent deflection shapes and the enhancement of control performance.

In some cases, material coupling may be quite beneficial. For example, standard graphite/epoxy materials have been used to modify aeroelastic characteristics of wings. In particular, careful orientation of the fiber direction couples wing-bending and torsional deflections, delaying divergence and increasing lift. Naturally, this technique could be extended to wings incorporating active elements. Ehlers and Weishaar [77] have demonstrated the role of elastic coupling in various aeroelastic structures such as forward and aft swept wings. They report that small amounts of coupling will reduce the actuator strength necessary to increase lift, while enhancing performance by using energy already present in the airstream.

5.2.2 Material Properties

One possibility for tailoring at the laminate level includes placing the principal actuator axes in directions other than the global structural axes. Since the problem is solved in the global coordinates, it is necessary to rotate the material properties to align with these directions. Consider the in-plane rotation about the 3-axis of a $[+\theta]$ angle laminate from

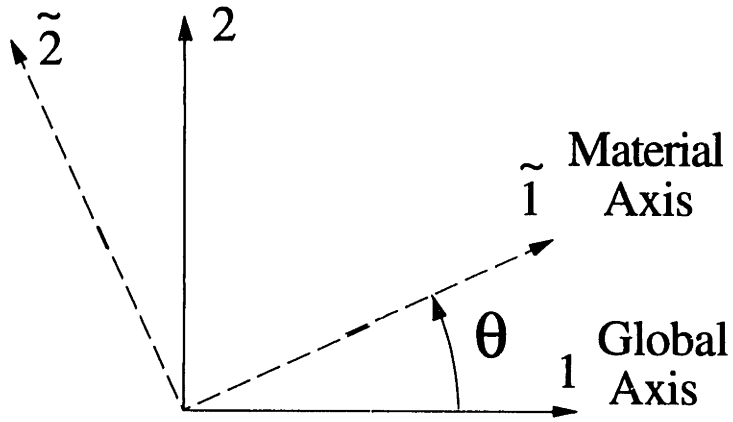

Figure 5.1: Axes definitions for laminated structure modeling

the material axes $(\tilde{1}-\tilde{2})$ into the global axes $(1-2)$, shown in Figure 5.1. The relationship between the field variables is:

$$\tilde{\mathbf{D}}=\mathbf{R}_E\mathbf{D} \quad \tilde{\mathbf{E}}=\mathbf{R}_E\mathbf{E} \quad \tilde{\mathbf{S}}=\mathbf{R}_S\mathbf{S} \quad \tilde{\mathbf{T}}=(\mathbf{R}_{S_t})^{-1}\mathbf{T} \tag{5.1}$$

where subscript 't' refers to matrix transpose. Rotations of the material properties about the 3-direction can be achieved using first and second order transformation matrices:

$$\mathbf{R}_S=\begin{bmatrix} \cos^2\theta & \sin^2\theta & \cos\theta\sin\theta \\ \sin^2\theta & \cos^2\theta & -\cos\theta\sin\theta \\ -2\cos\theta\sin\theta & 2\cos\theta\sin\theta & \cos^2\theta-\sin^2\theta \end{bmatrix} \quad \mathbf{R}_E=\begin{bmatrix} \cos\theta & \sin\theta & 0 \\ -\sin\theta & \cos\theta & 0 \\ 0 & 0 & 1 \end{bmatrix} \tag{5.2}$$

Simple matrix algebra brings about the rotated material matrix:

$$\begin{bmatrix} \varepsilon^S & \mathbf{e} \\ -\mathbf{e}_t & \mathbf{c}^E \end{bmatrix}_{\text{global}} = \begin{bmatrix} \mathbf{R}_{E_t}\tilde{\varepsilon}^S\mathbf{R}_E & \mathbf{R}_{E_t}\tilde{\mathbf{e}}\mathbf{R}_S \\ -\mathbf{R}_{S_t}\tilde{\mathbf{e}}_t\mathbf{R}_E & \mathbf{R}_{S_t}\tilde{\mathbf{c}}^E\mathbf{R}_S \end{bmatrix} \tag{5.3}$$

5.2.3 Anisotropy at the Lamina Level

The investigation of anisotropy at the lamina level considers the effects of parameter variations on the single-ply actuator. Anisotropy at this level may be present in the actuator material in one of two ways:

1. Mechanical anisotropy: shown in the stiffness constants $(\tilde{c}_{22} \neq \tilde{c}_{11})$,
2. Piezoelectric anisotropy: shown in the free-strain constants $(\tilde{d}_{32} \neq \tilde{d}_{31})$

The piezoelectric induced stress constant, $\tilde{e}_{ij}$, is an effective measure of anisotropy at the lamina level because it embodies both origins of anisotropy in a single constant:

$$\begin{aligned} \tilde{e}_{31} &= \tilde{c}^E_{11}\tilde{d}_{31}+\tilde{c}^E_{12}\tilde{d}_{32} \\ \tilde{e}_{32} &= \tilde{c}^E_{12}\tilde{d}_{31}+\tilde{c}^E_{22}\tilde{d}_{32} \end{aligned} \tag{5.4}$$

A large amount of induced stress anisotropy will exist when $\tilde{e}_{31}$ and $\tilde{e}_{32}$ are very different. Another measure of anisotropy becomes apparent if this lamina is rotated so that the principal axes are not coincident with the structural axes. In this case, an additional nonzero piezoelectric term is created:

$$\begin{aligned} \mathbf{e} &= \mathbf{R}_{E_t}\tilde{\mathbf{e}}\mathbf{R}_S \\ e_{31} &= \tilde{e}_{31}\cos^2\theta+\tilde{e}_{32}\sin^2\theta \\ e_{32} &= \tilde{e}_{31}\sin^2\theta+\tilde{e}_{32}\cos^2\theta \\ e_{36} &= \cos\theta\sin\theta(\tilde{e}_{31}-\tilde{e}_{32}) \end{aligned} \tag{5.5}$$

The extra term, e_{36}, is the piezoelectric induced shear stress term created through a rotation of the lamina. Its existence depends on the presence of anisotropy and the ply angle. This single term can be used to represent all the effects at the ply level that contribute to anisotropic behavior. Thus, maximizing its magnitude maximizes the anisotropy of the lamina. The maximum values are reached at ply angles of ±45°. This is easily understood since the ply rotation is completely analogous to a Mohr's circle transformation of stresses, where the maximum shear stress is always realized at this angle. Note that $\tilde{e}_{31}$ and $\tilde{e}_{32}$ may have opposite signs. Recent work by Hagood et. al. [42] on Interdigitated Electrode piezoceramics (IDE) has shown that this type of free-strain anisotropy is possible.

5.2.4 Anisotropy at the Laminate Level

The ultimate objective for piezoelectric fiber composites is their introduction into a laminated, built-up active structure for control. Thus, it will be important for design purposes to predict overall structural properties and response to various loading conditions. Classical Laminated Plate Theory lends itself well to design studies of laminated structures, and has already proven its value when augmented with actuator-induced forces and moments to extend the analysis to active structures [14,75]. A caveat of the theory is its limitation to a local description of the plate behavior. That is, it does not capture variations in loading or structural geometry within the plane of the structure. Nonetheless, it *is* able to provide accurate predictions of macroscopic deformations for several important cases, and allows for the examination of important laminated structure parameters.

A typical laminated plate section is shown below in Figure 5.2. Axes coincident with those described in the previous section are maintained. Possible loading conditions include edge moments M_1, M_2, and M_6, and in-plane forces N_1, N_2, and N_6. The underlying assumption of this theory is the manner in which the deformations of the typical section are characterized. These are the remaining Kirchoff assumptions for plate structures, and closely parallel the Bernoulli-Euler derivation for beams Jones[23]:

1. The strains are assumed continuous between lamina boundaries so there is no slip between plies.
2. Plane sections perpendicular to the midplane remain plane and perpendicular to the midplane after extension and bending.

The second assumption above is equivalent to requiring that the out of plane shear strains (S_4,S_5) be zero. i.e. no shear deformation - only pure bending. The result of such assumptions is to allow the laminate to be treated as a single material, whose properties are based on some collection of the individual ply properties. Thus, the problem is actually the formulation of the laminate constitutive equations, where kinematic quantities are related to force quantities, given certain assumptions on the strain deformation fields.

To formulate these relations, the displacements of a point P in the material are examined when the material undergoes deformation (shown in Figure 5.3). For this point P at height x_3 from the midline, its displacement may be described by:

$$\begin{aligned} u_1 &= u_1^o - x_3 \frac{\partial u_3^o}{\partial x_1} \\ u_2 &= u_2^o - x_3 \frac{\partial u_3^o}{\partial x_2} \end{aligned} \tag{5.6}$$

where subscript 'o' denotes displacements of the midplane. Introduction into the strain-displacement relations provides:

$$\begin{aligned} S_1 = \frac{\partial u_1}{\partial x_1} \quad &\rightarrow \quad \frac{\partial u_1^o}{\partial x_1} - x_3 \frac{\partial^2 u_3^o}{\partial x_1^2} \\ S_2 = \frac{\partial u_2}{\partial x_2} \quad &\rightarrow \quad \frac{\partial u_2^o}{\partial x_2} - x_3 \frac{\partial^2 u_3^o}{\partial x_2^2} \\ S_6 = \frac{\partial u_1}{\partial x_2} + \frac{\partial u_2}{\partial x_1} \quad &\rightarrow \quad \left(\frac{\partial u_1^o}{\partial x_2} + \frac{\partial u_2^o}{\partial x_1} \right) - 2x_3 \frac{\partial^2 u_3^o}{\partial x_1 \partial x_2} \end{aligned} \tag{5.7}$$

The first term of each strain represents the strain at the midplane, while the x_3 dependent term describes the curvature, so that the above may be written:

$$S_i = S_i^o + x_3 \kappa_i \qquad (i = 1,2,6) \tag{5.8}$$

To relate the applied loads (resultant forces and moments) to the internal states of stress, it is necessary to carry out equilibrium through a summation of forces across the laminate thickness. The resultant forces (N_i) and moments (M_i) per unit length are given by:

$$N_i = \int_{-h/2}^{h/2} (T_i) dx_3 \qquad M_i = \int_{-h/2}^{h/2} (T_i x_3) dx_3 \qquad (i = 1,2,6) \tag{5.9}$$

where 'h' refers to the laminate thickness. The stresses may be rewritten using the constitutive equations given in (2.23). Representing all components together in matrix form allows easier manipulation of terms:

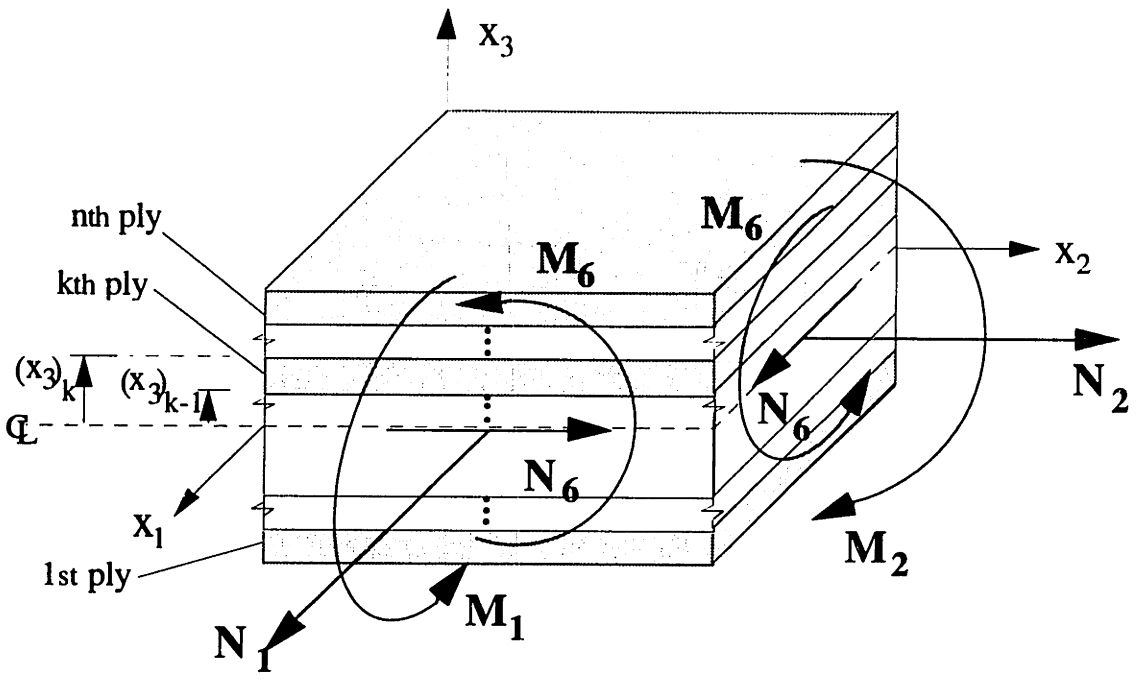

Figure 5.2: Classical Laminated Plate Theory definitions

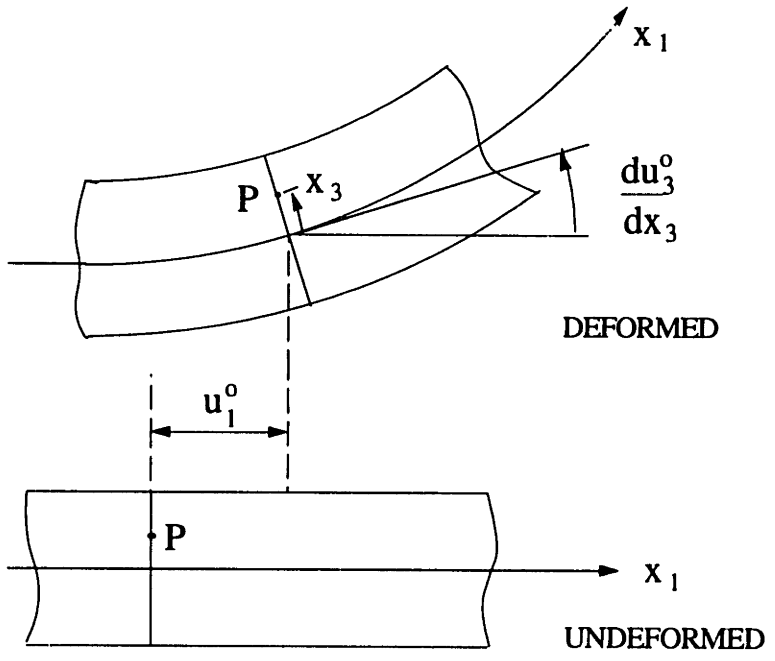

Figure 5.3: Definitions of Kirchoff deformation in laminated structures

$$N = \int_{-t/2}^{t/2} (-e_t E + c^E S) dx_3 \qquad M = \int_{-t/2}^{t/2} (-e_t E + c^E S) x_3 dx_3$$
$$(i = 1,2,6) \tag{5.10}$$

Using the assumed strain fields gives,

$$N = -e_t E \int_{-t/2}^{t/2} dx_3 + c^E S^o \int_{-t/2}^{t/2} dx_3 + c^E K \int_{-t/2}^{t/2} x_3 dx_3$$
$$M = -e_t E \int_{-t/2}^{t/2} x_3 dx_3 + c^E S^o \int_{-t/2}^{t/2} x_3 dx_3 + c^E K \int_{-t/2}^{t/2} x_3^2 dx_3 \tag{5.11}$$

Performing the integration may be divided into a discrete summation over the laminates 1 to n, leaving,

$$\mathbf{N} = -\mathbf{N}^A + [\mathbf{A}]\mathbf{S}^o + [\mathbf{B}]\boldsymbol{\mathcal{K}}$$
$$\mathbf{M} = -\mathbf{M}^A + [\mathbf{B}]\mathbf{S}^o + [\mathbf{D}]\boldsymbol{\mathcal{K}} \tag{5.12}$$

where $\mathbf{N}^A$ and $\mathbf{M}^A$ represent the actuator induced forces and moments. The stiffness terms are

$$[\mathbf{A}] = \sum_{k=1}^{n} (\mathbf{c}^E)_k \left((x_3)_k - (x_3)_{k-1}\right)$$
$$[\mathbf{B}] = \frac{1}{2} \sum_{k=1}^{n} (\mathbf{c}^E)_k \left((x_3)_k^2 - (x_3)_{k-1}^2\right) \tag{5.13}$$
$$[\mathbf{D}] = \frac{1}{3} \sum_{k=1}^{n} (\mathbf{c}^E)_k \left((x_3)_k^3 - (x_3)_{k-1}^3\right)$$

and the actuator induced forces and moments are

$$\mathbf{N}^A = \sum_{k=1}^{n_A} (\mathbf{e}_t \mathbf{E}_3)_k \left((x_3)_k - (x_3)_{k-1}\right)$$
$$\mathbf{M}^A = \frac{1}{2} \sum_{k=1}^{n_A} (\mathbf{e}_t \mathbf{E}_3)_k \left((x_3)_k^2 - (x_3)_{k-1}^2\right) \tag{5.14}$$

The number of total laminates is 'n', and the number of active laminates is 'n_A'. Use of equations (5.12) requires knowledge of two of the three possible loading cases (either mechanical forces, total strains, or actuator forces). The loading conditions easiest to implement from a practical standpoint are those of a free[21] expansion where the resultant mechanical loads are zero, and the field voltage applied to the actuators is known. In such

[21] 'free' in the sense of no net applied mechanical loading. Actuator is not undergoing free strain.

a case, the equations (5.12) can be inverted to solve for the resulting strains and curvatures, which are easily measured through conventional methods.

$$\begin{Bmatrix} \mathbf{S}^{o} \\ \boldsymbol{\mathcal{K}} \end{Bmatrix} = \begin{bmatrix} \mathbf{A} & \mathbf{B} \\ \mathbf{B} & \mathbf{D} \end{bmatrix}^{-1} \begin{Bmatrix} \mathbf{N}^{A} \\ \mathbf{M}^{A} \end{Bmatrix} \tag{5.15}$$

Solution for the midplane strains and curvature strains will provide information on the global laminate deformations. Such information can be used to examine the twist, extension, and bending that can be obtained for an applied electric field and particular structural parameters.

5.3 A Twist-Extension Coupled Laminate Example

A simple laminate case has been chosen for the purpose of comparing the various actuators. Absolute conclusions on the actuator types cannot be drawn from any one case, because the performance is application-dependent. However, the analysis of this case does provide excellent insight into the fundamentals of anisotropic actuation, allowing easier application to other laminates and loading cases.

The laminate chosen for this study is $[45_A/0_S/-45_A]$, an antisymmetric angle-ply laminate. For positive actuation on both active laminae (i.e. applied electric field coincident with poling direction), the result will be a coupled extension and twist deformation. A ±45° angle was chosen to maximize the piezoelectric stress constant e_{36},. An extension-twist coupled laminate is also amenable to experimental verification. Since nominally no bending takes place, clamping will not compromise the actuation, allowing the CLPT model to accurately predict the twist while neglecting end effects.

Calculation of the A, B, D matrices shows a form typical of antisymmetric angle-ply laminates:

$$\begin{Bmatrix} N_1^A \\ N_2^A \\ N_6^A \\ M_1^A \\ M_2^A \\ M_6^A \end{Bmatrix} = \begin{bmatrix} A_{11} & A_{12} & 0 & 0 & 0 & B_{16} \\ A_{12} & A_{22} & 0 & 0 & 0 & B_{26} \\ 0 & 0 & A_{66} & B_{16} & B_{26} & 0 \\ 0 & 0 & B_{16} & D_{11} & D_{12} & 0 \\ 0 & 0 & B_{26} & D_{12} & D_{22} & 0 \\ B_{16} & B_{26} & 0 & 0 & 0 & D_{66} \end{bmatrix} \begin{Bmatrix} S_1^o \\ S_2^o \\ S_6^o \\ \mathcal{K}_1 \\ \mathcal{K}_2 \\ \mathcal{K}_6 \end{Bmatrix} \tag{5.16}$$

This matrix identifies the coupling present between various deformation modes and represents the passive properties of the laminate. Thus, these parameters are independent of mechanical or actuator imposed loads. The above matrix shows that coupling does indeed exist between extension loads $[N_1, N_2]$ and twist curvature $[\mathcal{K}_6]$, due to the 'B' terms. These terms also couple shear loads $[N_6]$ and bending curvatures $[\mathcal{K}_1, \mathcal{K}_2]$.

The mechanical loads may be applied completely independent of the material properties of the laminate chosen, implying that any loading combination $[N_i, M_i]$ is valid. However, actuator induced loads are dependent on the material configuration chosen for the laminate, for it is the very lay-up used that determines the possible induced moments and forces. For this particular case with positive actuation on each actuator,

$$N_6^A = M_1^A = M_2^A = 0 \tag{5.17}$$

These induced loads are zero because the antisymmetric nature of this laminate balances the induced shear forces and applied bending moments. The remaining loads and deformations may be shown as the reduced system:

$$\begin{Bmatrix} N_1^A \\ N_2^A \\ M_6^A \end{Bmatrix} = \begin{bmatrix} A_{11} & A_{12} & B_{16} \\ A_{12} & A_{22} & B_{26} \\ B_{16} & B_{26} & D_{66} \end{bmatrix} \begin{Bmatrix} S_1^o \\ S_2^o \\ \kappa_6 \end{Bmatrix} \tag{5.18}$$

Since the antisymmetric ply angle chosen is ±45°, several additional geometrical symmetries exist. Positive actuation on both actuators also results in symmetry of actuator induced forces:

$$A_{11} = A_{22} \quad B_{16} = B_{26} \quad N_1^A = N_2^A \tag{5.19}$$

Inverting the above relations (5.18) and solving for the twist curvature yields:

$$\kappa_6 = \frac{-2B_{16}N_1^A + (A_{11} + A_{12})M_6^A}{-2B_{16}^2 + D_{66}(A_{11} + A_{12})} \tag{5.20}$$

where the following geometric and actuator terms are given with the plane stress material constants expressed in the local (ply) coordinates:

$$\begin{aligned} A_{11} + A_{12} &= \left(t_S(\tilde{c}_{11} + \tilde{c}_{12}) + t_A(\tilde{c}_{11}^E + 2\tilde{c}_{12}^E + \tilde{c}_{22}^E)\right) \\ B_{16} &= \frac{1}{4}(\tilde{c}_{11}^E - \tilde{c}_{22}^E)\left(t_A t_S + t_A^2\right) \\ D_{66} &= \frac{1}{4}\left((\tilde{c}_{11}^E - 2\tilde{c}_{12}^E + \tilde{c}_{22}^E)\left(\frac{t_A t_S^2}{2} + t_A^2 t_S + \frac{2t_A^3}{3}\right) + \frac{t_S^3}{6}(\tilde{c}_{11} - \tilde{c}_{12})\right) \\ N_1^A &= E_3 t_A(\tilde{e}_{31} + \tilde{e}_{32}) \quad M_6^A = \frac{1}{2}E_3(\tilde{e}_{31} - \tilde{e}_{32})(t_A t_S + t_A^2) \end{aligned} \tag{5.21}$$

It is easy to see the important terms that contribute to the twist curvature, $[\kappa_6]$. The twist moment, M_6, directly induces twist and is dependent on the existence of piezoelectric stress anisotropy ($\tilde{e}_{31} \neq \tilde{e}_{32}$), as discussed in the section on anisotropy at the lamina level. If stiffness isotropy also existed ($\tilde{c}_{11}^E \neq \tilde{c}_{22}^E$), the term B_{16} would be zero, and the twist would simply be a function of M_6^A and D_{66}. Twist can also be generated by the

actuator induced extensional force N_1^A because it is coupled through the B_{16} term. This term does not depend on piezoelectric induced-stress anisotropy, but requires stiffness anisotropy in order to exist.

It is important to note that these constants cannot be independently specified and that c_{ij}^E and e_{ij} are interrelated. For this reason, it is difficult to draw conclusions about the contributions of the individual terms when both effects are present. Thus, actuation will be compared on the basis of stiffness, c_{ij}^E, and piezoelectric free-strain constants, d_{ij}. These constants are also easier to measure, and the free-strain d-constants are a better understood quantity. However, the concept of induced stress remains essential in the discussion of actuators, and will be dealt with further.

Replacing the e_{ij} constants with those of equation (5.4), and nondimensionalizing with respect to actuator quantities yields an expression for nondimensional twist curvature:

$$\frac{K_6 t_A}{\Lambda_{MON}} = \frac{\Lambda_{ACT}}{\Lambda_{MON}} \frac{(T+1)\left(4R_A(1-\zeta)(1-R_A\upsilon_{12A}^2)+2T\psi(1+\upsilon_{12})(C_B-R_A(1-\upsilon_{12A})(1+\zeta))\right)}{-(T+1)^2(1-R_A)^2+2\left(C_E+T\psi(1+\upsilon_{12})\right)\left(C_B(\frac{T^2}{2}+T+\frac{2}{3})+T^3\psi\frac{(1-\upsilon_{12})}{6}\right)} \tag{5.22}$$

where the nondimensionalized ratios are defined as

$$T=\frac{t_S}{t_A} \quad \psi=\frac{\tilde{c}_{11}}{\tilde{c}_{11}^E} \quad R_A=\frac{\tilde{c}_{22}^E}{\tilde{c}_{11}^E} \quad \zeta=\frac{\tilde{d}_{32}}{\tilde{d}_{31}} \quad \Lambda=\tilde{d}_{31}E_3 \tag{5.23}$$
$$C_E=2R_A\upsilon_{i2A}+R_A+1 \quad C_B=-2R_A\upsilon_{12A}+R_A+1$$

The terms R_A and ζ are the ratios of transverse to longitudinal properties in the actuator, for stiffness and piezoelectric free strain, respectively. T is the ratio of substrate thickness (t_S) to actuator thickness (t_A), while ψ provides information on the relative stiffness of the actuator and substrate materials. Quantities C_B and C_E are the non-dimensional stiffness terms derived from the bending (D_{66}) and extensional ($A_{11}+A_{12}$) groups in the original equation (5.20). It is important to note the significance of the Λ terms. Λ is the commonly used free-strain actuation term ($\tilde{d}_{31}E_3$), where Λ_{MON} refers to the actuation capability of a monolithic piezoceramic. The term Λ_{ACT} takes into account the possibility that a particular actuator may have a different free-strain actuation capability than a monolithic piece of the same material (PZT type). One such case is the interdigitated electrode piezoceramics where the poling direction is actually along the geometric 1-axis used here.

Investigating the effects of anisotropy on the twist can be done by varying one parameter, while the others are held constant. In particular, the effect of the stiffness and piezoelectric anisotropy ratios on the twist curvature will be shown as a function of

thickness ratio (T). The laminae stiffness ratio (ψ), will be assumed to have the value of one. Stiffer substrate materials will only slightly increase the curvature twist. For the most part, the larger induced actuator stresses will be offset by the larger geometric terms (B_{16}, D_{66}, etc.).

Figure 5.4 examines the effect of free-strain anisotropy on the nondimensionalized twist curvature. In general, larger free-strain anisotropy enhances the twist. The exception is the case of ideal stiffness anisotropy ($R_A = 0$). This curve shows that if the transverse stiffness is zero, it is impossible to induce any transverse actuator stress loads ($\tilde{e}_{32} = 0$), and thus, the twist is independent of $\tilde{d}_{32}$ and ζ. Therefore, a fundamental limit on actuation potential exists for actuators with high levels of stiffness anisotropy. Furthermore, without a substrate material, the twist caused by the extensional induced loads ($2B_{16}N_1^A$) exactly cancels the twist caused by the twist moment term ($(A_{11} + A_{22})M_6^A$) in the numerator of equation (5.20).

The four graphs in Figure 5.4(a-d) show the progression of twist for decreasing levels of stiffness anisotropy. The last graph is the special case of stiffness isotropy ($R_A = 1$). For this special case:

$$\frac{\kappa_6 t_A}{\Lambda_{MON}} = \frac{(T+1)(1-\zeta)(1-\upsilon_{12A})}{(1-\upsilon_{12A})(T^2+2T+\frac{4}{3})+\frac{\psi T^3(1-\upsilon_{12})}{6}} \qquad (5.24)$$

Interdigitated piezoceramics (IDE) are an example of this special case. Note that the substrate with optimal thickness is actually no substrate at all. The stiffness of the system increases in a cubic manner with substrate thickness, while actuation authority increases only linearly with thickness (increasing the moment arm). Since the actuators in this special case have adequate transverse stiffness, ($R_A = 1$), they need not rely on the substrate to provide stiffness for inducing stress. Instead, each actuator pushes against the transverse stiffness of the opposing actuator.

Figure 5.5 examines the effect of stiffness anisotropy on the curvature twist at various levels of piezoelectric free-strain anisotropy. As expected, for a particular free-strain anisotropy, increasing levels of stiffness anisotropy enhance the twist. For very high levels of free-strain anisotropy ($\zeta = -0.5$), this enhancement is small, and is similar to the discussion above, for the case when $R_A = 0$.

The four graphs in Figure 5.5(a-d) show the progression of twist for decreasing levels of free-strain anisotropy. The last graph is the special case of equation (22) for $\zeta = 1$ (free-strain isotropy):

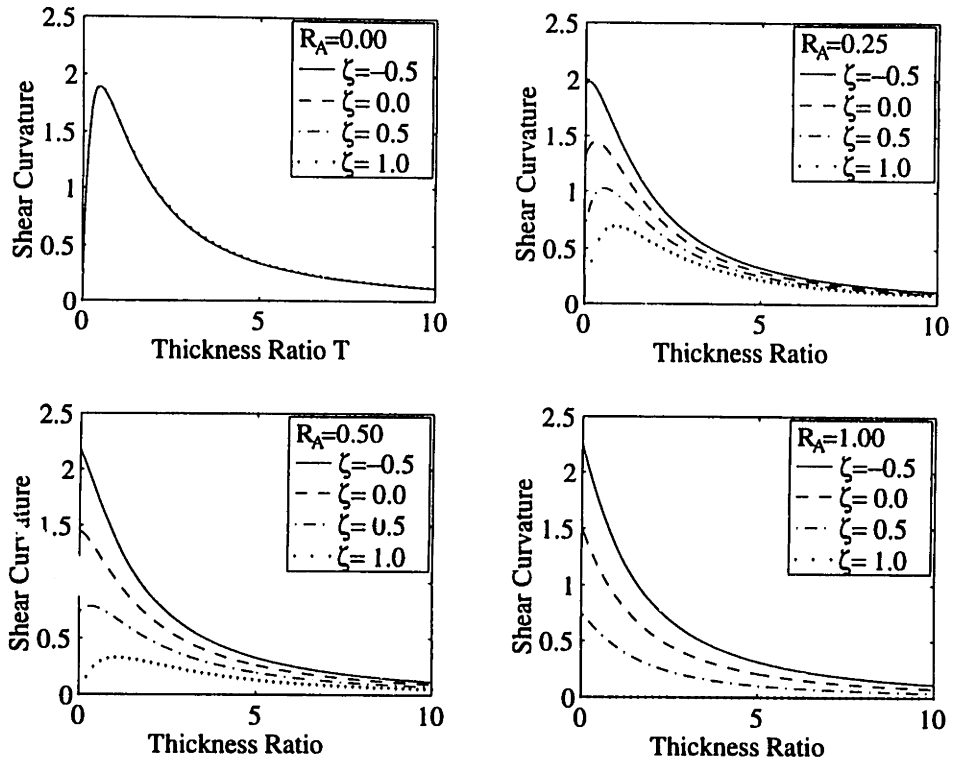

Figure 5.4: Actuator with free-strain anisotropy for various stiffness ratios

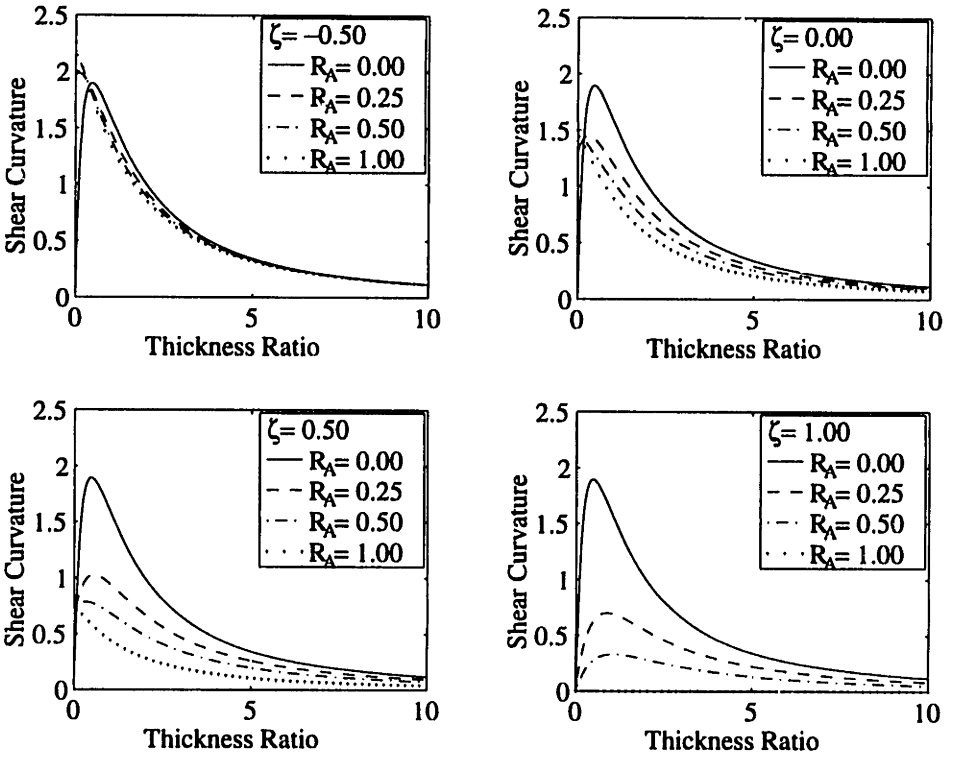

Figure 5.5: Actuator with stiffness anisotropy for various free-strain ratios

$$\frac{\kappa_6 t_A}{\Lambda_{MON}} = \frac{2T\psi(T+1)(1+\upsilon_{12})(1-R_A)}{-(T+1)^2(1-R_A)^2 + 2\left(C_E + T\psi(1+\vartheta_{12})\right)\left(C_B\left(\frac{T^2}{2}+T+\frac{2}{3}\right)+T^3\psi\frac{(1-\upsilon_{12})}{6}\right)}$$

(5.25)

Directionally Attached Piezoceramics [76] are an example of actuators employing stiffness anisotropy with isotropic piezoelectric free strain. An interesting aspect of this special case is again the reliance of twist on the presence of a substrate material. For the special case of no substrate ($t_S = 0$) and stiffness anisotropy only ($\zeta = 1$), the two numerator terms in (5.20) again exactly cancel one another. This effect is echoed in equation (5.25) for T=0. Thus, there is an optimal substrate thickness for an anisotropically stiff laminate having isotropic free-strain actuation.

5.4 Anisotropic Actuator Comparison for a Twist-Extension Laminate

Up to this point, discussion has been limited to the examination of generic actuators, and the effect of stiffness and free-strain anisotropy on laminated structure actuation. Several different types of anisotropic actuators based on piezoceramic materials exist, and have already been referred to in section 5.3. This next section details the attributes of each of these actuators, and is an excerpt from Ref[80]. The purpose is to facilitate a comparison of the fundamental differences in the types of available actuators. The understanding gained from such a comparison can then be extended to other cases of actuation and laminates.

5.4.1 Piezoelectric Fiber Composites

For the present comparison, the properties used are those of the current material systems and manufacturing capabilities. Bulk piezoelectric properties for 5H-type PZT are

Table 5.1: PFC Plane Stress Material Properties

	c_{11}^E	c_{12}^E	c_{22}^E	c_{66}^E	e_{31}	e_{32}	$\frac{\varepsilon_{33}^S}{\varepsilon_o}$
Fibers	66.2	19.2	66.2	23.5	-23.4	-23.4	1950
Matrix	3.74	1.12	3.74	1.31	0	0	27.3

(Units: s_{ij}^E: 10^{-12} m^2/N, c_{ij}^E: 10^9 N/m^2, d_{ij}: 10^{-12} m/V, e_{ij}: N/Vm)

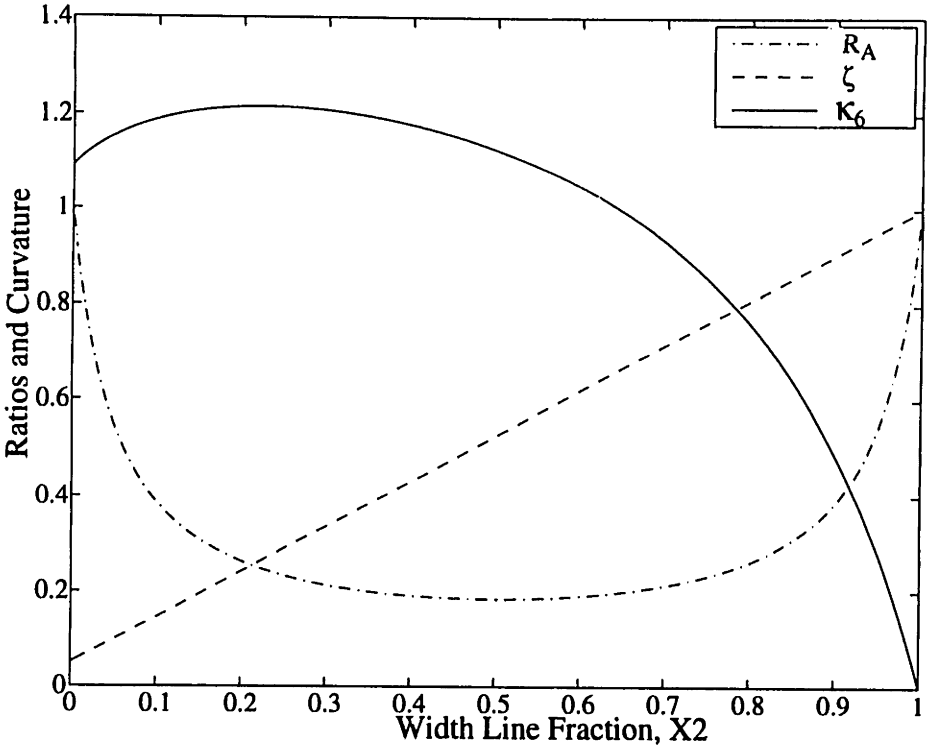

Figure 5.6. PFC design curves of anisotropy ratio and nondimensionalized curvature (for T=0.5)

used for the fibers, and the measured properties are used for the particulate-loaded epoxy. These are given in Table 5.1. The closed form combination model presented in section 3.3 is used to generate predictions for the actuator parameters. The maximum through-thickness line fraction (X_3) that has been experimentally achieved is 0.98. The width line fraction (X_2) is a free parameter that may be chosen to tailor the composite properties. Figure 5.6 shows the model predictions for ζ and R_A for a range of X_2 based on the properties given. Nondimensional twist curvature is also shown for a constant thickness ratio of 0.5. This serves only to illustrate the general trend with X_2. An X_2 of 0.5 (equal spacing of fibers and matrix across the width) provides high anisotropy and stiffness, and is chosen for the comparison. In this case, the composite piezoelectric free-strain and stiffness anisotropies are 0.52 and 0.18, respectively. Actuation capability of the PFC actuators is taken to be that of monolithic piezoceramics, as the maximum free strain level in the longitudinal direction is not changed[22].

[22] d_{31} is not the same as that for monolithic ceramic, but the same level of free strain may be reached by applying higher field levels. Thus Λ is the same as that for monolithic ceramic.

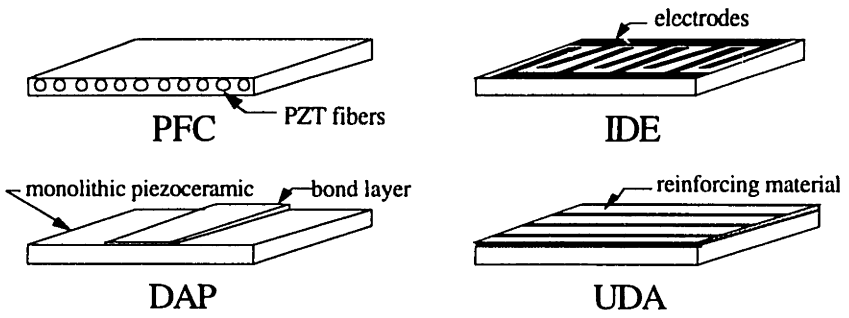

Figure 5.7. Anisotropic actuators compared in this analysis

5.4.2 Other Anisotropic Actuators

An Interdigitated Electrode (IDE) piezoceramic directed toward structural actuation was introduced by Hagood et. al. [42]. As shown in Figure 5.7, this novel electrode pattern is comprised of electrode fingers with alternating polarities, on both sides of the piezoceramic. As a result, the majority of electric field components are actually in the plane of the actuator, so that poling is in-plane, rather than through the thickness. This creates a high level of free-strain anisotropy because the two free-strain piezoelectric constants are of opposite sign. The model predicts a free-strain anisotropy ratio of ζ=-0.5, although experimentally, much higher values were seen due to material nonlinearities and electric field geometric effects. Not only is high anisotropy caused by this electrode pattern, but the in-plane polarization also increases the actuation capability to 1.8 times that of the monolithic piezoceramic. However, these actuators have nearly isotropic stiffness.

The introduction of Directionally Attached Piezoceramics (DAP) is attributed to Barrett [76]. The concept, shown in Figure 5.7, incorporates monolithic piezoceramic actuators bonded in special attachment patterns. The bond pattern is typically along a thin line, creating high longitudinal stiffness, but very low transverse stiffness. Barrett reports large levels of stiffness anisotropy (as large as 1/50 to 1/80), but has been limited by practical constraints to values of R_A between 1/7 and 1/20. A value of 1/20 is assumed for the comparison. Since the free-strain piezoelectric constants remain the same in the two directions, the DAP elements are actuators that can be thought of as demonstrating stiffness anisotropy only. The actuation capability of the DAP element is that of the monolithic piezoceramic.

To complete the comparison of actuators, a hypothetical Unidirectional Actuator (UDA) is proposed. This actuator is comprised of a monolithic piezoceramic bonded to an ideal, anisotropically stiff reinforcement material. As an example, this reinforcement

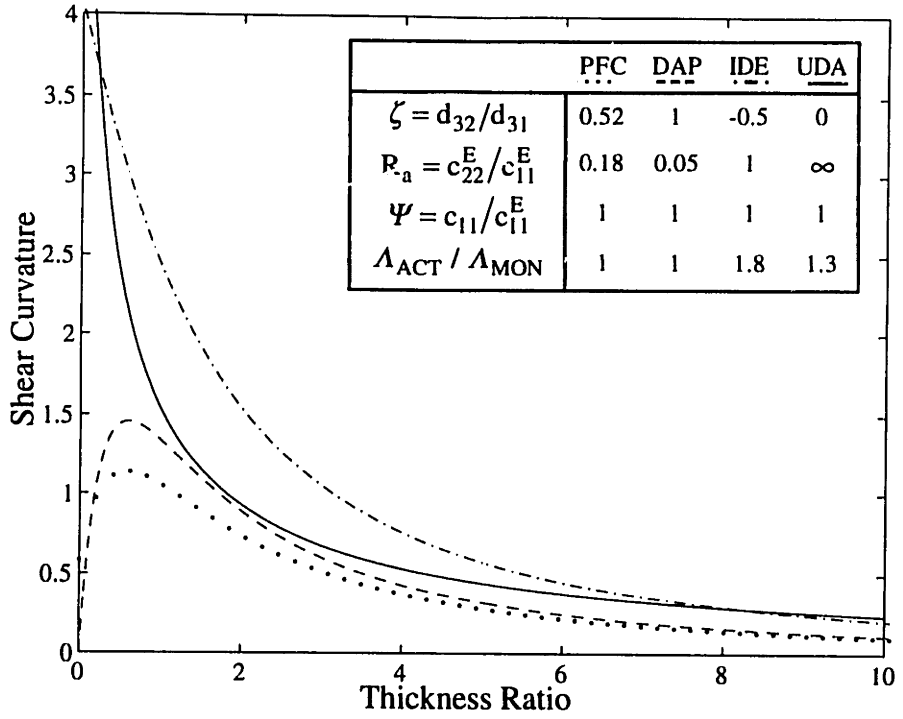

Figure 5.8. Comparison of nondimensionalized curvature vs. thickness ratio for four actuators

material could be composed of extremely stiff fibers embedded in a very soft matrix. The limiting case would be an actuator with an infinite transverse stiffness, giving a stiffness ratio (R_A) of infinity. In addition to creating high stiffness anisotropy, the actuation in the transverse direction would be zero, making the free-strain ratio (ζ) zero. The transverse clamping effect also serves to enhance the longitudinal free-strain piezoelectric constant ($\tilde{d}_{31}$) by a Poisson's term, so that the actuation capability of the UDA is approximately 1.3 times that of a monolithic piezoceramic.

5.4.3 Comparison

It is now possible to compare the various actuator types for this antisymmetric laminate case. Comparison is made on the basis of similar substrate materials (ψ=1 in each case), but each with its individual actuation capability. The comparison is shown in Figure 5.8, in the same format as the previous graphs with nondimensional twist curvature versus thickness ratio. Values of the actuator parameters are summarized in the figure.

The figure exemplifies the rather different characteristics of each actuator. For thin substrates ($T \rightarrow 0$), the IDE and UDA actuators provide very high levels of twist, while

the PFC and DAP elements are unable to produce much twist due to their dependence on the substrate to induce transverse stress loads. Slightly thicker substrate materials result in a dramatic drop in twist for the IDE and UDA actuators, while the PFC and DAP elements provide twist that reaches a peak at approximately T=0.5. Medium size substrates (1<T<5) will have the most twist when IDE actuators are incorporated, although the differences in twist become less apparent between the four types. Finally, as the substrate reaches larger thicknesses (T>10), the twist approaches zero for all actuators. The differences in actuators at this point (T~10) can be attributed to the different actuation capabilities (Λ_{MON}), and to the fact that the UDA twist approaches zero as 1/T, while the other three approach zero as $1/T^2$.

5.5 Summary

This chapter was an investigation into the mechanics of actuation in structures that incorporate anisotropic actuators. It provided a strong motivation for the use of tailorable actuators, especially in structures with isotropic substrates. Anisotropic actuators are able to directly induce shear stress loads, so that twist deformations are possible, even on an isotropic host. This study highlighted the difference in the possible origins of actuator anisotropy, and showed how they contribute to the *overall* actuation anisotropy. The introduction of the concept of induced stress in structures provided a convenient means for evaluating how a particular actuator will perform.

A twist-extension coupled laminate provided the basis for an actuator comparison, and was developed from Classical Laminated Plate Theory with induced stress actuator terms. The comparison of the actuators showed fundamental differences in the manner in which actuators are able to induce stress loads. These differences are not only exemplified through the models, but may be logically understood through the induced-stress concepts.

This chapter has laid the groundwork for an experimental study of laminated structures using piezoelectric fiber composites. Future sections will show the manufacture and testing of a twist-extension coupled laminate, and results will be compared to the theory developed in this chapter.

6.0 Manufacturing Piezoelectric Fiber Composites

6.1 Overview

There has been little previous research into manufacturing of piezoelectric fiber composites (compared to other composites), and virtually none of the established methods pertain to the current application of structural actuation. Thus, there is a need to establish a manner for manufacturing that reliably produces piezoelectric fiber composites with known properties and physical attributes. At this initial stage, the more immediate goal is to develop methods for making mono-layer piezoelectric composites that may serve to validate the model predictions. This first step will help provide an expanded knowledge of the manufacturing process that will contribute to more refined techniques in the near future.

This chapter begins with a description of manufacturing objectives for conformable mono-layer fiber composites. Some preliminary investigations into manufacturing provide an understanding of the requirements for a successful composite specimen. These are expanded to create a manufacturing procedure outlined in Section 6.3. Here, the mold setup, lay-up techniques, and curing process are described, and similarities between these methods and those for standard graphite/epoxy composites is discussed. Finally, the sample preparation for experiments is explained, including electroding and polarization techniques. The last section, 6.5, describes the more recent techniques used to manufacture the extension-twist coupled laminate, including improvements developed in the standard methods of lay-up, cure, and electroding.

6.2 Manufacturing Objectives and Requirements

The primary objective was to produce conformable single-fiber layer composites to allow comparison of experimental effective properties to those predicted in the various analytical models. these composites were to be manufactured by hand, using individual piezoelectric fibers and a two part epoxy resin system for the matrix material. Manufacturing techniques would borrow from those developed for graphite/epoxy composite manufacturing.

Other secondary objectives for manufacturing become apparent when the geometry of the composite specimens are considered. Since the thickness of each specimen will be one fiber layer, the usual reliance on statistical averaging to reduce the effect of inhomogenities no longer holds, and specimen uniformity cannot be ignored. In order to get a reasonably accurate representation of the overall composite properties, it is important

to have uniformity in several aspects. First, it is necessary to have uniform spacing of fibers, so that the measurement of properties is location -independent. Uniform thickness across the specimen was also important for this reason, and uniform thickness along the fiber length was imperative due to the two dimensional nature of the models.

Spacing and line fractions were dictated by other important requirements. Maximum levels of actuation can be accomplished for maximum through-thickness line (X_3) fractions. Minimum amounts of low dielectric matrix in series with the piezoelectric will allow significant field in the fiber for both poling and actuation. Eventually, the use of multi-fiber layer composites at high volume fractions will result in random, high-dielectric pathways across the thickness, known as contiguity, or percolation effects. Such effects will reduce the need for ultra-high X_3 fractions, although high volume fractions will always be advantageous in terms of actuation capability. In the other direction, spacing of the fibers, represented by the transverse line fraction (X_2), will largely affect the transverse properties and act as a property tailoring parameter. The discussions in anisotropic actuation (Chapter 5.0) cover this in more detail. For the purposes of manufacturing, this value is varied to compare trends in properties for experiment and models.

Several other objectives dealt with the process of manufacturing itself. One of these was void content. Often, gas is trapped in the resin due to handling or mixing, or forms when the heat of cure is applied. Following cure, these trapped gases leave bubbles known as voids throughout the matrix system. Voids represent weak spots, both mechanically and electrically (detailed in section 4.2.2). High void concentrations would render the specimen useless, by making the necessary poling voltage impossible to achieve due to arcing cross the voids. Finally, it was important to minimize fiber breakage. Although none of the key mechanisms occurring in fibrous composites is load transfer, longitudinal stiffness and actuation (occurring though the fibers) is greatly reduced for even small amounts of epoxy in series with the fibers.

Preliminary manufacturing provided several insights that contributed to the final manufacturing technique. Surface tension of the fiber/epoxy system was very high, so that the fibers tended to be drawn tightly together, creating overlapping and difficulties with specifying fiber spacing. A top surface in the mold reduced surface tension, and provided better uniformity in specimen height. A low viscosity epoxy system was also important in reducing the surface tension problem, and improved the flow characteristics, reducing fiber damage. This also enabled easy removal of voids with applied vacuum and moved excess epoxy away from the composite, increasing the through-thickness line fraction (X_3). Finally, a very slow cure process at room temperature eliminated void build-up due to gas formation.

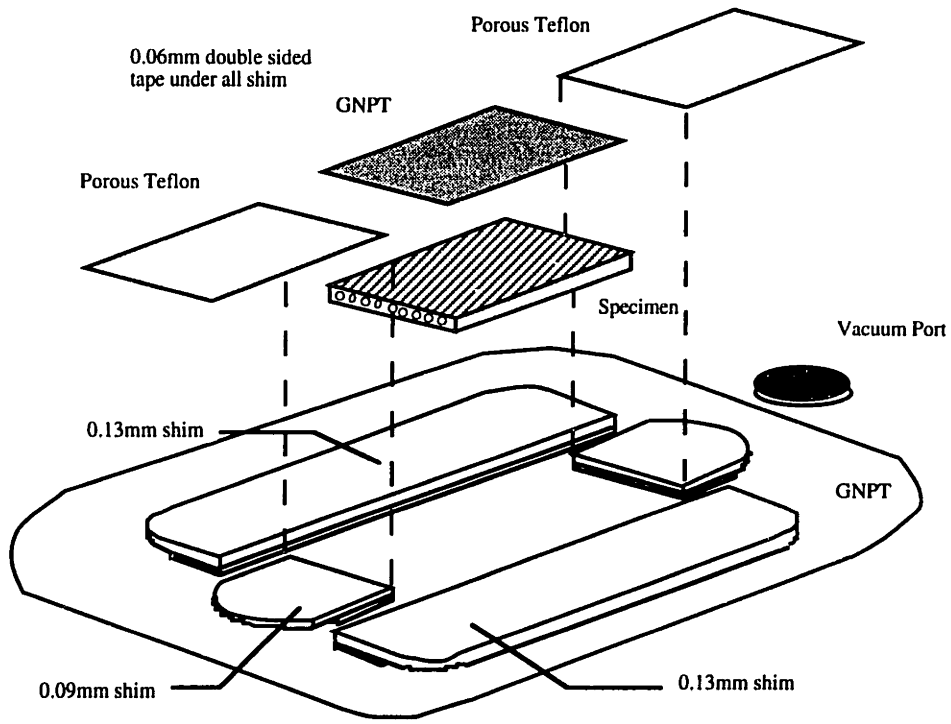

Figure 6.1: Experimental setup for the manufacturing of piezoelectric fiber composites

6.3 PFC Characterization - Manufacturing Methods

Techniques and materials standard to the curing of graphite/epoxy composites were used as a basis for developing the manufacturing process. The setup is shown in Figure 6.1. The entire mold was assembled on an aluminum cure plate that included fittings for a vacuum system. Guaranteed non-porous Teflon (GNPT) formed the top and bottom surfaces of the mold to facilitate specimen removal after the cure. Mold side and end pieces were manufactured for each cure from stainless steel shim stock, and coated with mold release. The thickness of mold pieces could be changed to allow variations in epoxy flow and direction. The standard setup used, shown in the figure, consisted of thinner (0.09 mm) shim stock at the ends to facilitate the flow of excess epoxy away from the specimen, along the fiber direction. The sizes chosen were found to work well with the fiber diameter supplied.

The mold pieces were attached to the Teflon base using 0.06 mm double sided tape. This ensured no resin leaked out from beneath the mold, and that any excess epoxy had to travel out above the end pieces, and in the fiber direction. In this way, there would never be a shortage of epoxy for the specimen. Porous Teflon lead away from the mold to the

vacuum port, and acted as a path for liquid or gas. This provided maximum vacuum to the specimen while creating a reservoir for the excess epoxy.

Following the above preparations, a low temperature-cure epoxy[23] was mixed, and a thin layer laid into the mold. Piezoelectric fibers of 120 micron diameter[24] were cut to length and straightened by hand. These were laid individually into the mold at measured intervals, and held in place with the thin epoxy layer. Following the fiber lay-up, a covering layer of epoxy was applied sparingly to the fibers. The GNPT top was set onto the specimen, and the entire assembly was sealed with vacuum tape and bagging materials. Full vacuum and added pressure (approximately 15 psi, applied with weights) was applied to the specimen. This condition was held at room temperature for 12 hours, until the epoxy was fully set, and the danger of void formation by heat was passed. The specimen was then heated to 65 °C for one hour to ensure the epoxy had fully occurred (complete cross linking) and the maximum properties were achieved. The sample was kept under vacuum and pressure during this step. A scanning electron microphotograph of an initial specimen with relatively low X_3 is shown in Figure 6.2.

Ten samples in total were manufactured, each 1.5 inches (38 mm) in length and 1 inch (25 mm) wide. Each specimen had a thickness very close to that of the fiber diameter, so that X_3 was approximately 0.98. The transverse line fraction X_2 was varied among the specimens between 0.15 and 0.57. Several specimens were not used due to poor uniformity or damage during handling.

6.4 PFC Characterization - Sample Preparation

Following the cure, the specimen was allowed to fully cool before proceeding. The specimen was removed from the mold, and the dimensions measured. The width and length were measured using calipers with 0.01 mm precision, and the thickness was measured using micrometers with 0.002 mm precision. The sample was lightly sanded to increase surface roughness and ceramic connectivity between the electrode faces, and electroded with 2000 Å to 3000 Å of pure silver. Silver was chosen for its high conductivity (compared to aluminum), and its good adhesion (as compared to gold). Electroding was done with an electron beam evaporator[25] , operating at low power to reduce the heat generated. Sputtering vapor deposition techniques proved impossible as the heat generated caused damage to the matrix and tended to warp the specimen.

---

[23] EPO-TEK 301 epoxy, Epoxy Technologies Inc., 14 Fortune Drive, Billerica, MA. 01821

[24] PZT Fibers, CeraNova Corporation, 14 Menfi Way, Hopedale, MA. 01747

[25] Microelectronics Technology Central Facility, MIT, Cambridge, MA. 02139

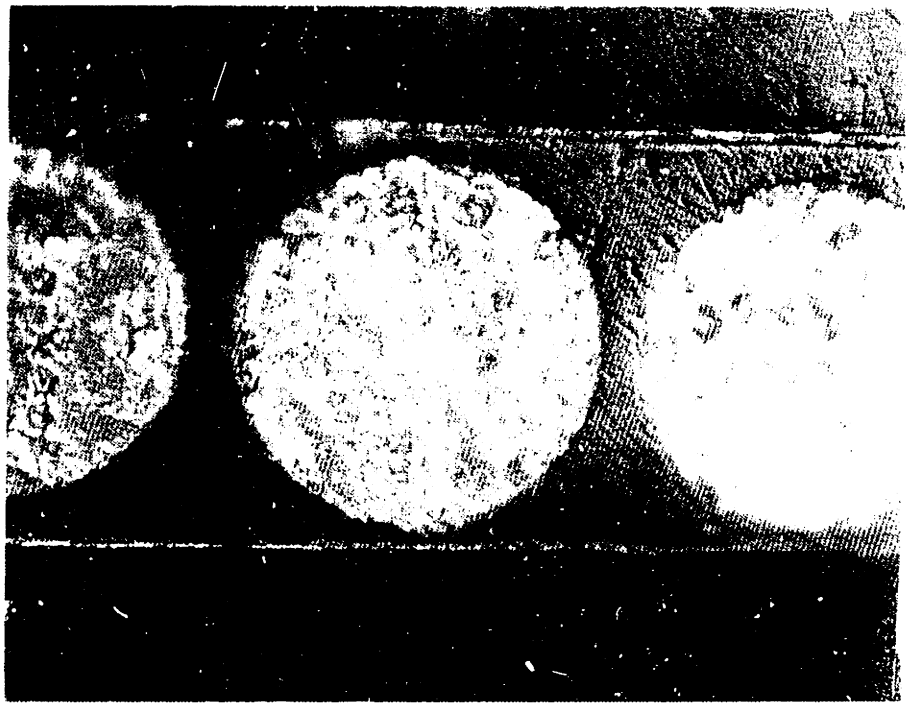

Figure 6.2: Photograph of early specimen with relatively large thickness line fraction (magnified 300x)

Poling of each specimen was performed in a heated, silicon oil environment[26]. The presence of oil acted as an electrical insulator, and reduced the opportunity for electrical breakdown (arcing) around the edges of the specimens. The oil was also heated to 80C to add internal energy to the material dipoles, and enable easier alignment with the applied field direction. For each specimen, the dc field of approximately 80 volts/mil (32 kV/cm) was applied for 15 minutes at this temperature. Then, the specimen was removed, cooled, and the electric field removed. Removing the field prior to cooling the specimen would otherwise result in a loss of polarization.

6.5 Manufacturing for a Twist-Extension Coupled Laminate

Up to this point, the techniques outlined have been used in the manufacturing of the composite specimens for comparison of effective properties with models. More recently, improved methods have been used for manufacturing of piezoelectric fiber composites. They include improvements in lay-up and cure methods, various new electroding techniques, and the introduction of the improved matrix material to the composite. These methods were utilized for the manufacture of the specimens used for the twist-extension coupled laminate example, and are outlined here.

---

[26] Exacal EX-250HT Bath, Neslab Instruments Inc., 25 Nimble Hill Road, Newington, NH 03801

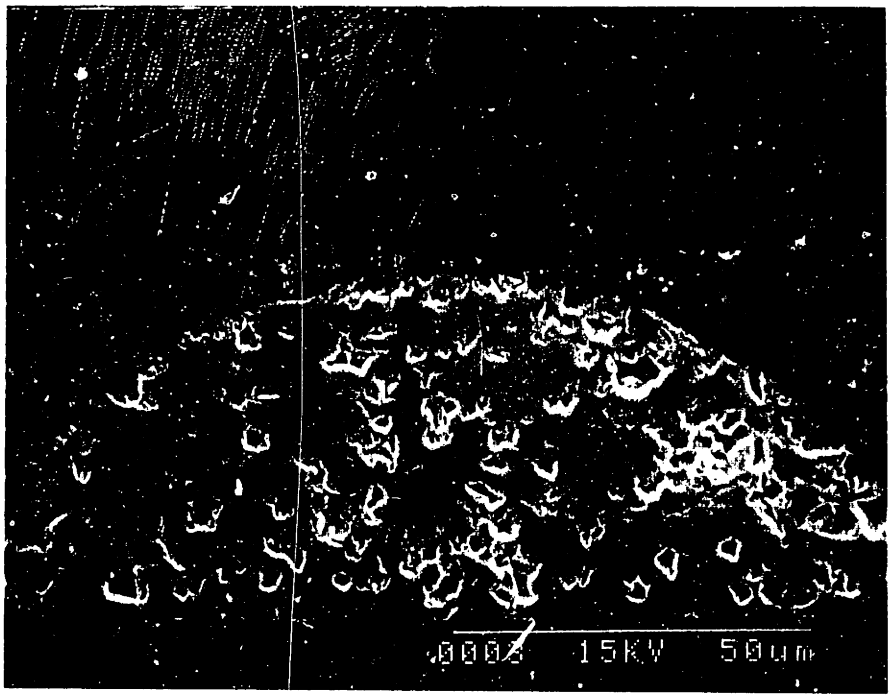

Figure 6.3: SEM Photo of PZT fiber composite with particulate filler in epoxy matrix, with copper/kapton interlaminar electrodes.

The first change involved the techniques used for the lay-up of piezoceramic fibers. Previously, a thin layer of epoxy was spread into the mold as the first step, and used to hold the fibers in place during the lay-up. With this method, it was often difficult to maintain uniform spacing of the fibers. Instead, a very thin strip (~1 mm) of double-sided tape was positioned at each end of the mold, next to the end mold pieces shown in Figure 6.1. The fibers could then be laid into place precisely, with each fiber end adhering to the tape. In this way, a more uniform spacing could be achieved, and this spacing would be maintained when the matrix material was applied. This was necessary due to the introduction of the much more viscous filler/epoxy matrix for this application.

A 15 mm by 94 mm strip was laid up by hand, using 170 micron fibers oriented at 45 degrees. The matrix used for the twist-extension laminate contained 75 wt% of PZT filler and 3.75 wt % dispersant. The methods for manufacturing the matrix were outlined in section 4.5.3, and the properties were summarized in section 4.6. This matrix was spread evenly onto the fibers, and the specimen prepared for vacuum in the usual manner. Curing, however, was now done in an autoclave curing system[27] so that vacuum and 80 psi additional pressure could be applied to the composite. This increased the compaction,

[27] Model BAC 35, Baron-Blakeslee, TELAC, MIT

reduced excess epoxy, and gave excellent specimen uniformity in thickness. After cure, the composite was slowly cooled, removed from the mold, and the dimensions measured.

Three types of interlaminar electrodes have been investigated. One type, shown in the photograph of Figure 6.3, is 0.0005 inch Kapton with a 2500 Å layer of sputtered copper which is bonded onto the active subply at the time of cure. This material is easily etched and has the potential for use as a patterned electrode. The second type involves manufacturing the PFC's without electrodes, lightly sanding to increase surface roughness, and depositing a 3000 Å silver layer on each surface through a thermal-vapor deposition process. This is the original process used in the manufacturing of specimens for the effective property study (section 6.3). The third type is similar, except that air-dried silver paint is applied by hand. The present laminate application employs this method of electroding.

In order to achieve the maximum piezoelectric properties of the composite, it is important to ensure complete poling. The specimens used for effective property measurements , detailed in section 6.4, were sanded enough so that the tops of fibers were exposed to the sputtered electrodes. As section 7.3 will show, this permitted a low coercive field for poling equal to that of bulk PZT 5H ceramic. In more recent applications, where the specimens are only very lightly sanded, or specimens utilize thin film polyimide electrodes, this will not be the case. In these cases, there will not be direct connectivity between ceramic and electrodes. Instead, it will be necessary to measure or predict the coercive field for the specimens. An excellent indication of the degree of ceramic connectivity is effective dielectric, and a simple relation between effective dielectric and coercive field likely exists. In fact, it is easy to show using the methods in the Closed Form Combination Model, that the field within the fiber can be expressed as a function of fiber volume fractions v_2 and v_3, and the effective dielectric ε_{33}^{eff}:

$$\frac{E_3^f}{\overline{E}_3} = \frac{\varepsilon_{33}^m (v_2^f + v_3^m v_2^m) - v_3^m \varepsilon_{33}^{eff}}{\varepsilon_{33}^m v_3^f v_2^f} \qquad (6.1)$$

As an example, for a through thickness fraction of $v_3 = 0.95$ and a width fraction of $v_2 = 0.50$, the effective dielectric $\varepsilon_{33}^{eff}/\varepsilon_o$ predicted by the Closed Form model is 248. Using equation 6.1, the field reaching the fiber is found to be only approximately 15% of the applied field. This is a large reduction, and would require a field of 46 kV/cm (117 volts/mil) just to reach the coercive field within the PZT 5H[28]. Fortunately, there is a means to lower the coercive field by raising the temperature of the piezoceramic material. This allows for easier movement of the crystal dipoles, effectively reducing the coercive

[28] Given that the coercive field for PZT 5H is assumed to be 17.5 volts/mil at room temperature

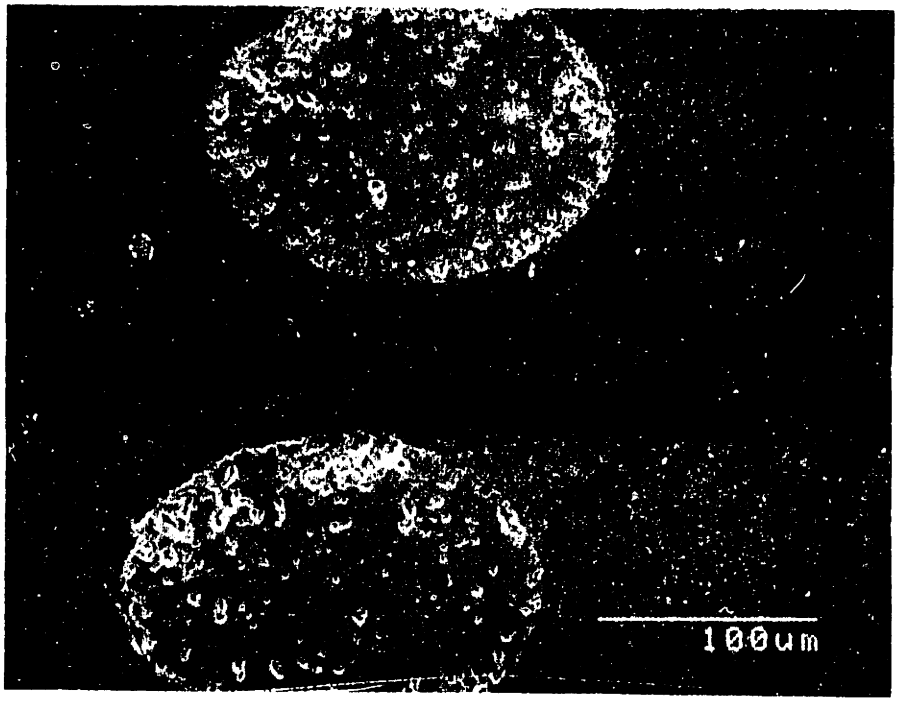

Figure 6.4: SEM Photo of 45° PZT fiber composite ply laminated to steel substrate

field. The difficulty of this process, however, is the current inability to predict the piezoceramic response in the nonlinear regime (i.e. at poling field levels) and its dependence on temperature. Work is currently being done to investigate this issue [81].

The most accurate and direct method to obtain the coercive field is through experiment, and is the means used here. For a new specimen, it is possible to determine the coercive field by measuring the butterfly or hysteresis (polarization) curves at the desired temperature. The coercive field is the value of field at strain reversal on the butterfly curve, or the value of field at the axis crossing on the polarization curve. The points tend to correspond very well for a particular piezoceramic specimen [81], although the polarization method is preferred because it is generally more accurate and does not require application of a strain gage to the specimen.

After poling, and prior to any further steps, the composite was aged for 72 hours to eliminate the possibility of any time-dependent polarization effects. The composite was cut into two pieces, each of which were bonded to a 0.025 mm (1 mil) stainless steel substrate, with the poling directions oriented outward. The plies were bonded to the steel substrate using an epoxy adhesive (Young's Modulus of 2.8 GPa) and cured at room temperature to avoid possible depolarization. The resulting bond layers measured approximately 0.01 mm (<0.5 mil). A photograph of a section of the assembly is shown in Figure 6.4. Testing of the specimen is described in section 7.4.

6.6 Summary

Chapter 6.0 dealt with the second of two original subtasks for piezoelectric fiber composites: To develop the ability to manufacture conformable active composites that incorporate transversely aligned piezoelectric fibers. A hand lay-up technique was developed for manufacturing mono-fiber layer composites from individual PZT fibers and a two part epoxy resin system. These methods involved procedures that were applied in an attempt to create a uniform, reliable, and conformable actuator with good actuation properties. Curing under vacuum and incorporating materials form standard graphite/epoxy manufacturing helped to reach this goal. These standard techniques were used to manufacture the specimens used for experimentally evaluating the effective material properties. More recent techniques were applied to the manufacture of the specimens for the laminated structure in the anisotropic actuation study, and incorporated the improved matrix material from Chapter 4.0. The next chapter picks up the discussion, with the test procedures and results for the manaufactured specimens.

7.0 Experimental Methods and Results

7.1 Overview

The value of experimental results lies not only in the verification of analytical models, but also in an increased understanding of the material systems and processes being used. Experiments often bring to light various aspects that may not have been considered when dealing with the purely analytical results. Such aspects include issues of practicality and manufacturability that may limit the range of possible performance. Another issue is the acceptance of various assumptions in the analysis that may not be well founded. Such an example is the assumption that the fiber properties were those of the bulk ceramic. Results found during the effective property experiments indicate that this may not be the case, and prompted further investigation into material property characterization.

The major objective of experimental methods, however, is for the verification of the analytical models developed for the particular system. This chapter describes the experimental procedures undertaken and presents the results for the study of piezoelectric fiber composites. Section 7.2 details the methods for obtaining the effective material constants, including the compliance, dielectric, and piezoelectric free-strain. The results of those tests are given in section 7.3. An adaptation of the Discrete Uniform Fields (DUF) model is also presented in order to account for the current geometry of the experimental specimens. The final section, section 7.4, describes the experimental results for the twist-extension coupled laminate.

7.2 PFC Characterization - Experimental Procedures

In order to compare experimental results with those predicted by the model, it is necessary to carefully consider the manner in which these results are obtained. Not only is it necessary to measure the electrical, mechanical, and coupling properties, but they must also be measured under the correct boundary conditions. Fortunately, the constitutive equations have been chosen in the form most amenable to experimental verification, given in equation 2.37 and repeated here:

$$\begin{Bmatrix} D_3 \\ S_1 \\ S_2 \\ S_6 \end{Bmatrix} = \begin{bmatrix} \varepsilon_{33}^T & d_{31} & d_{32} & 0 \\ d_{31} & s_{11}^E & s_{12}^E & 0 \\ d_{32} & s_{12}^E & s_{22}^E & 0 \\ 0 & 0 & 0 & s_{66}^E \end{bmatrix} \begin{Bmatrix} E_3 \\ T_1 \\ T_2 \\ T_6 \end{Bmatrix} \tag{7.1}$$

The mechanical properties, represented by short-circuit compliances (s_{ij}^E) are easily measured for mechanical loads when the electrodes are shorted. The electrical

properties, represented by the free-dielectric (ε_{33}^T), are easily measured for electrical loads when no stress is applied. Finally the coupling terms, represented by the piezoelectric free strain constants (d_{ij}), are measured by obtaining free strain when an electrical load is applied. It is important to note that all the properties to be obtained are plane stress properties. These are the most relevant, as virtually all applications will include thin planar structures. However, since this constitutive equation is in compliance form, these properties are also those for the full three dimensional representation of the material.

For measurement of the electrical and piezoelectric properties, the specimens were held at point contact with a spring grip mechanism, whose grips also delivered electric potential. The dielectric (ε_{33}^T) was measured at zero stress

$$\overline{T}_1 = \overline{T}_2 = \overline{T}_6 = 0 \qquad \rightarrow \qquad \overline{D}_3 = \varepsilon_{33}^T \overline{E}_3 \tag{7.2}$$

The measurement was taken with a digital multimeter in the form of capacitance, from which the dielectric could be calculated:

$$\varepsilon_{33}^T = \frac{C^T t}{A} \tag{7.3}$$

where C^T is the capacitance at zero stress, t is the specimen thickness, and A is the specimen area. Reporting of the data is actually done in the form of the dielectric relative to vacuum:

$$K_{33}^T = \frac{\varepsilon_{33}^T}{\varepsilon_o} = \frac{C^T t}{A\varepsilon_o} \tag{7.4}$$

The term ε_o is the permittivity of free space (8.85 e^{-12} F/m). The piezoelectric free strain constants (d_{31}, d_{32}) were also found by applying electric field to the specimen at zero stress, and measuring the resulting strain:

$$\overline{T}_1 = \overline{T}_2 = \overline{T}_6 = 0 \qquad \rightarrow \qquad \begin{aligned} \overline{S}_1 &= d_{31}\overline{E}_3 \\ \overline{S}_2 &= d_{32}\overline{E}_3 \end{aligned} \tag{7.5}$$

Electric field was applied up to the poling voltage (32 KV/cm), in the direction of poling. Strains were measured using a strain gage system[17], where gages were aligned with the longitudinal and transverse (1 and 2) directions, as shown in Figure 7.1. Values for the property constants were calculated from the strain-electric field slope at zero field, in order to obtain the low-field values. Sinusoidal voltage tests were also carried out to characterize the poling attributes of the composites. Curves of varying electric field versus strain well into the nonlinear response region are a useful indication of polarization trends. Comparisons of the classic "butterfly curve" with those of the monolithic piezoceramic lend insight into the relative coercive fields, and are discussed in the next section.

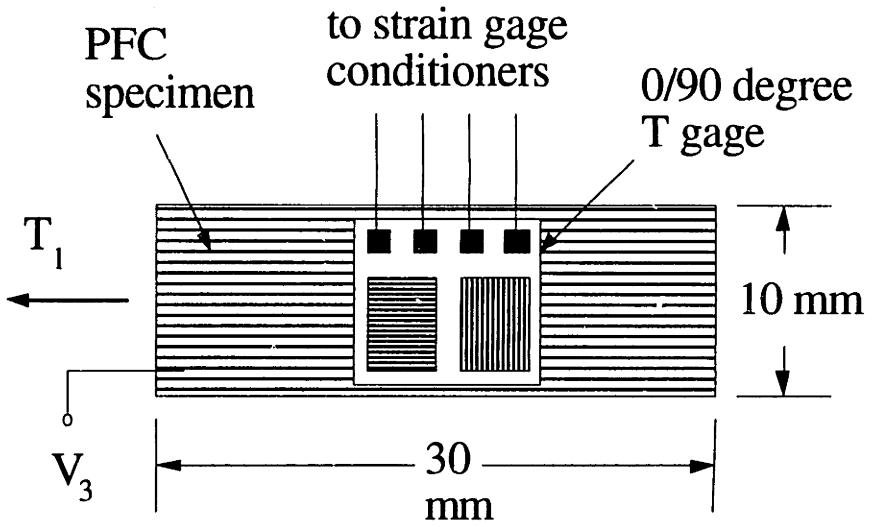

Figure 7.1: Specimen dimensions and strain gage placement for experiments

Tensile tests were conducted to determine the effective compliance properties. Specimens were tested by applying mechanical loads in the longitudinal direction, and measuring strain in the longitudinal and transverse directions. All other stresses were zero, and the electrodes were shorted to achieve the short circuit condition:

$$\overline{T}_2 = \overline{T}_6 = \overline{E}_3 = 0 \quad \rightarrow \quad \begin{aligned} \overline{S}_1 &= s_{11}^E \overline{T}_1 \\ \overline{S}_2 &= s_{12}^E \overline{T}_1 \end{aligned} \tag{7.6}$$

The transverse compliance was not found at this time. Stainless steel tabs were bonded to each end of the specimens using cyanacrolate adhesive. These tabs served as points for gripping the specimens in the testing machine. A small scale test machine[29] with pneumatic grips was used to apply the load, while a strain gage system again provided the strain data. Each specimen was cut to a narrow strip (approximately 10 mm x 30 mm), to ensure a uniform stress (and therefore strain) distribution across the specimen.

7.3 PFC Characterization - Experimental Results

Manufacturing provided highly conformable piezocomposites of line fractions X_2 varying from 0.15 to 0.57, and testing provided the effective material constants that characterize the material.

---

[29] Instron Model 4201, Instron, 100 Royall St., Canton, MA 02021

The first data to be evaluated were the AC test curves. Figure 7.3 shows the strain response of a typical specimen along the fiber direction for a sinusoidal voltage input. Surprisingly, this response is very close to that of a monolithic piezoceramic, and is often termed the "butterfly" curve. This curve shows the poling/depoling trend typical of sinusoidal inputs at voltages above the coercive field. More remarkably, the coercive field necessary to depole the specimen is low, at about 70 Volts, or 15 Volts/mil. Such low coercive field levels show that most of the electric field is actually reaching the ceramic, indicating some connectivity in the 3-direction. This is likely the case, as sanding prior to electroding removed the thin layer of epoxy above the fibers. Also, if most of the field is reaching the piezoelectric then the strain-to-voltage constant, d_{31}, should be very close to that of the monolithic ceramic. This is also predicted by the two *Uniform Fields* models for even low values of v_2^p when $v_3^p = 1$.

In actuality, the experimental values for effective d_{31} are much lower than the d_{31} of the ceramic alone, suggesting an apparent inconsistency between the data and models. However, it is proposed that the difference is not an inconsistency, but rather a result of the analysis that models round fibers as square. Even with some connectivity in the 3-direction, the majority of the fiber actually has matrix above and below, which prevents much of the electric field from reaching it. This effectively creates a "dead zone" of inactive fiber. The reduction in d_{31} is due not only to the inactivity of these portions, but also to their high stiffness. Resulting actuation is less than that which would occur if the inactive section was replaced with pure epoxy, representing a square fiber.

The discretized combination model approach can be used to model this phenomenon after making a small alteration. If it is assumed that some small portion of the fiber top, of length "t," was removed during sanding, then the actual specimen is that shown in Figure 7.2. Only a minor modification to the previous discretized method need be introduced. The method presented in equations 3.72-75 remain the same with the exception that the slices of matrix and fiber are added to a column of matrix *and* column of fiber in equation 3.75.

This model is used for comparison to the experimental data, shown in Figures 7.3 to 7.8. Graphs show the effective properties versus width line fraction X_2 for a "t"-value of 0.1 (10%). The value for "t" was chosen by varying "t" until the best fit was obtained for the effective relative dielectric ($K_{33}^{eff} = \varepsilon_{33}^{eff}/\varepsilon_o$) data, shown in Figure 7.4. As discussed in section 5.5, the dielectric is a good indicator of the thickness in an average sense. This is especially important in the current specimens because variations in thickness below the ability to measure accurately can greatly affect the properties. Uniformity in manufacture would need to be on the order of microns for reliable a priori predictions.

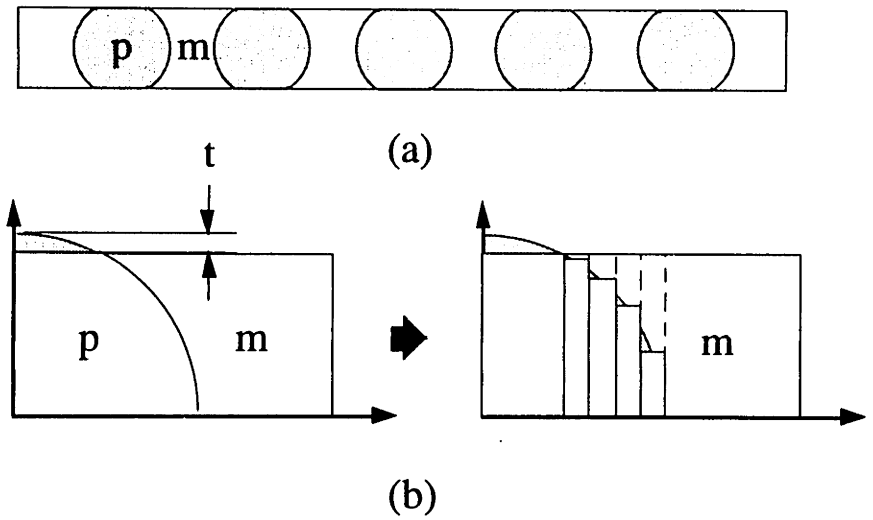

Figure 7.2: Modifications to the discretized model for accurate specimen representation.

For this value of "t", the strain-to-voltage data is compared to the model. Reasonable agreement is seen in the d_{31} constant with points on either side of the predicted response (Model 1). The lower curve (Model 2), shown for comparison, is a prediction by the discretized model if all the slices are replaced by pure matrix. This illustrates the effect of the inactive part of the fiber.

The d_{32} data, however, shows a striking departure from the model values. While the model predicts negative values, d_{32} experimentally assumes low positive values. This discrepancy is most likely caused by the assumption of uniform strains in the 3-direction. The d_{32} effect causes a high strain in the fiber which is probably localized around the fiber area only. However, the model assumes that the matrix and fiber actually have the same strain in the 3-direction, causing significant stresses to build up to satisfy this condition. This affects the 2-direction through the mechanical Poisson's ratio, and contributes to the effective d_{32}. A first order approximation for modeling this phenomena is to release the matrix from the piezoceramic by treating the matrix as transversely isotropic (using the equations developed for the piezoceramic throughout this paper) and setting its s_{23} $(= s_{13})$ to zero. This is equivalent to removing the stresses in the 3-direction that would otherwise keep the strains in the two phases equal. The result is a marked change in the predicted 32

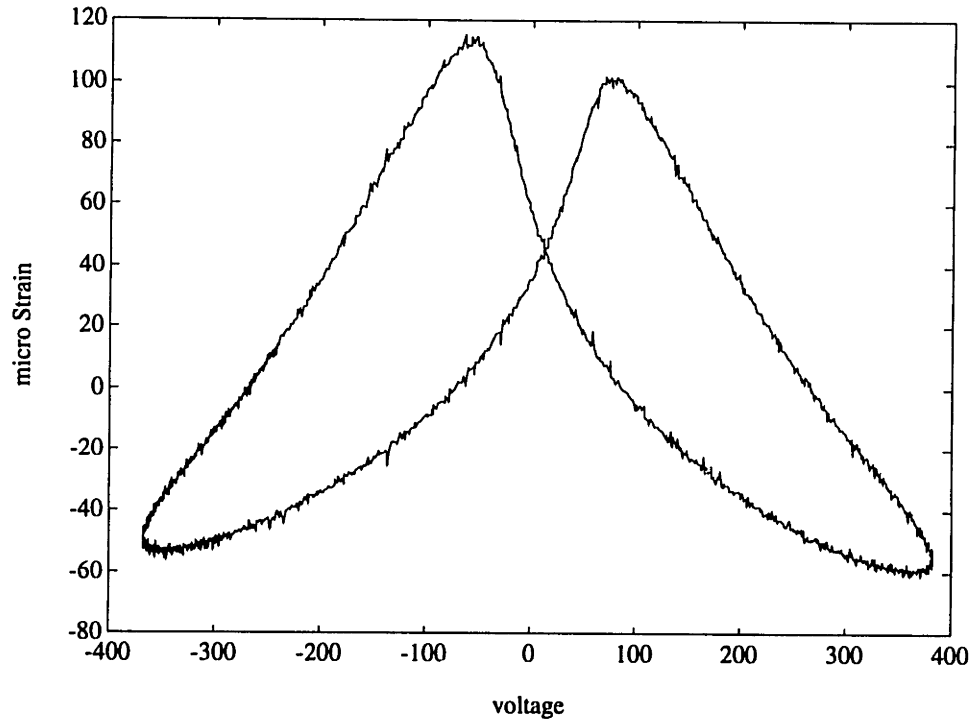

Figure 7.3: Typical strain response along the fibers for a sinusoidal voltage input (0.3 Hz)

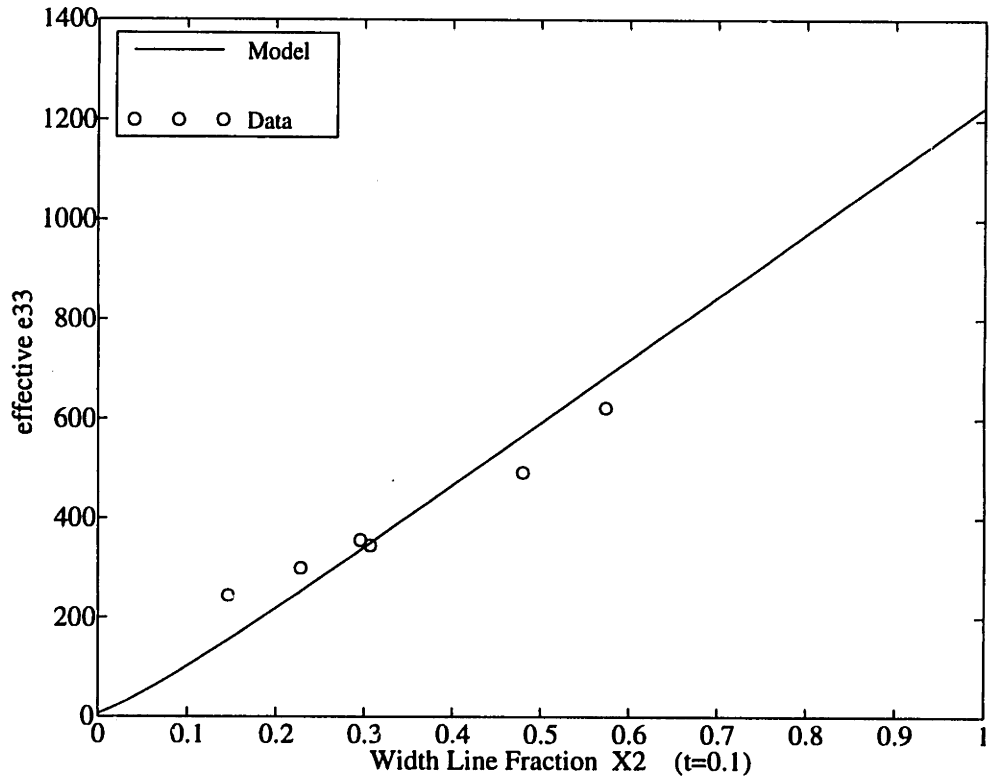

Figure 7.4: Comparison of experimental $\varepsilon_{33}^{eff}/\varepsilon_0$ with discretized Uniform Fields model

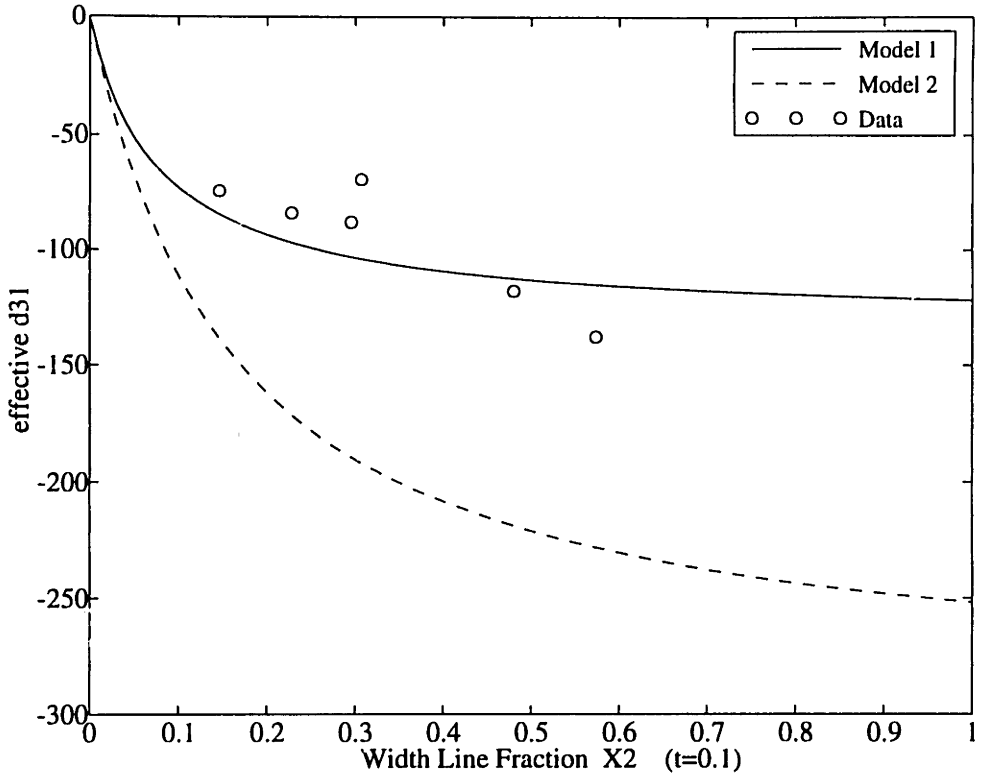

Figure 7.5: Comparison of experimental d_{31}^{eff} with discretized Uniform Fields model

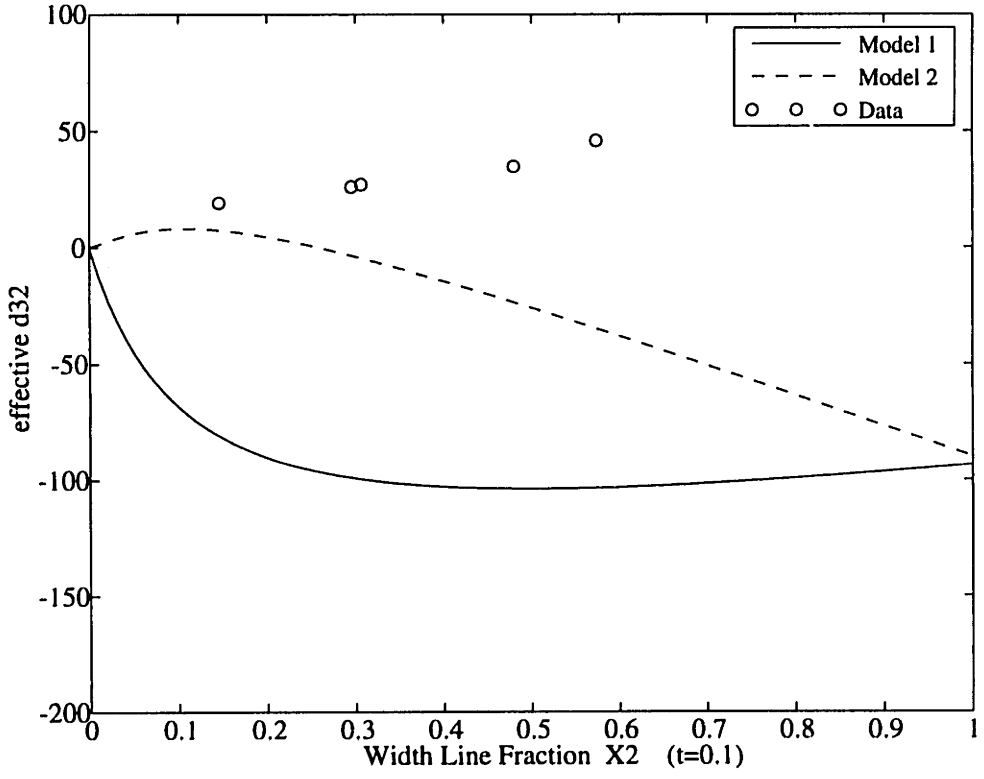

Figure 7.6: Comparison of experimental d_{32}^{eff} with discretized Uniform Fields model

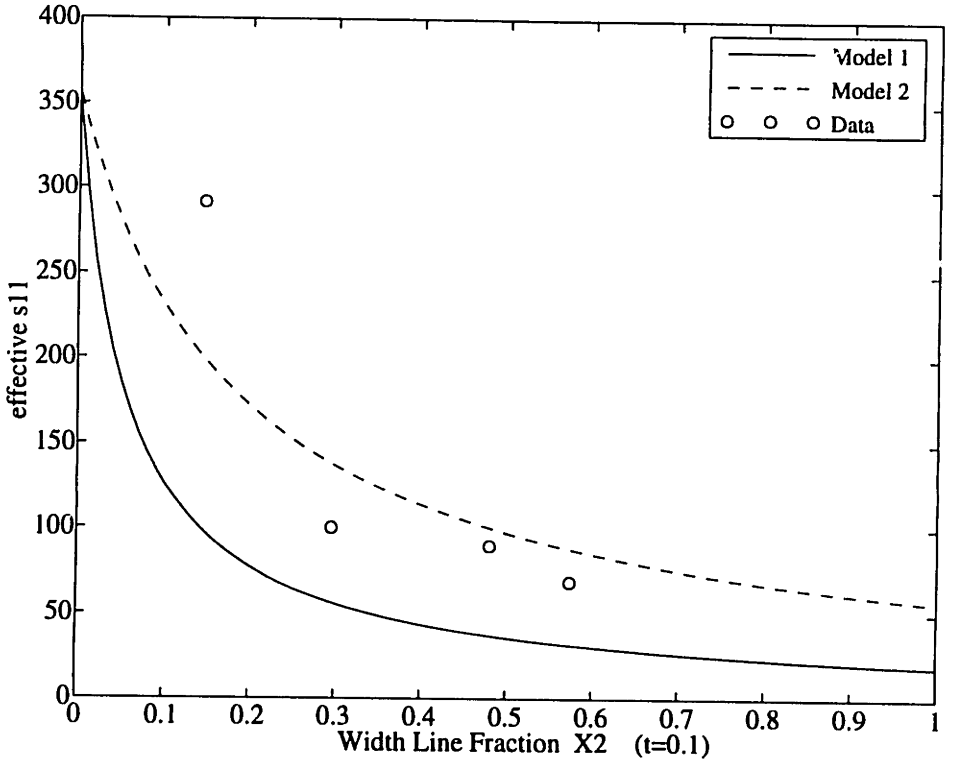

Figure 7.7: Comparison of experimental s_{11}^{eff} with discretized Uniform Fields model

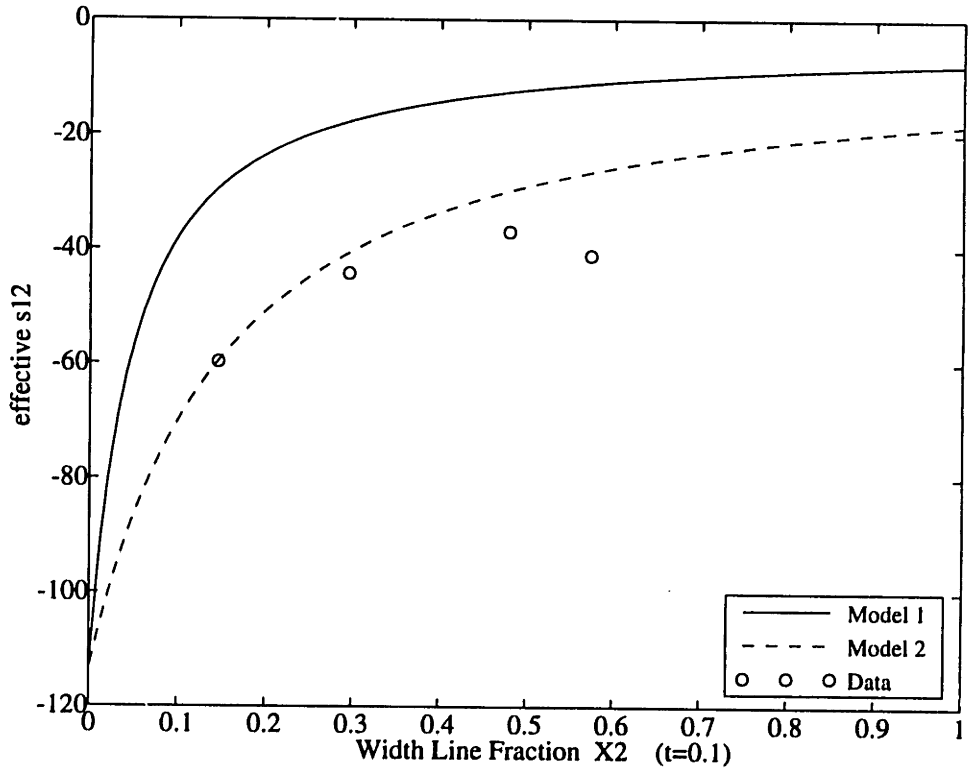

Figure 7.8: Comparison of experimental s_{12}^{eff} with discretized Uniform Fields model

strain-to-voltage constant, shown by the dashed line in Figure 7.6, and hints at the trend given by the experimental data. Smaller such trends were also seen in the Self Consistent and Finite Element models (section 3.6, comparison), even when the matrix and fiber were coupled in the 3 direction.

The figures for effective s_{11}^{eff} and s_{12}^{eff} show the experimental compliances higher than those predicted by the model (Model 1). Typically, longitudinal properties are expected to be in good agreement. A likely explanation for the discrepancy was a difference between the stiffness of piezoceramic fibers and bulk ceramic. Model 1 assumes bulk properties for the fiber in the discretized model. An investigation was carried out to characterize the piezoceramic fibers, but due to the difficulty of the fineness and brittle nature of the fibers has not been conclusive as of yet. However, initial results seem to indicate that the fibers may be almost a factor of two *less* stiff than the bulk ceramic [82]. For the sake of comparison, the model prediction for such fiber properties are included, and shown as Model 2. This provides much better agreement with the experimental results.

7.4 Results for a Twist-Extension Coupled Laminate

This section describes the testing performed for the laminated structure incorporating piezoelectric fiber composite actuators. Following the final manufacture, the capacitance was measured and the dielectric constant was found to be 154. The width (X_2) and the thickness (X_3) line fractions measured after manufacture were 0.78 and 0.84, respectively. From this dielectric constant, and the measured value for X_2, it was possible to calculate an averaged value for X_3, and use this to calculate all the composite properties. This is the single most accurate method to evaluate the through-thickness line fraction (X_3). Small nonuniformities in thickness, sanding and fiber waviness, and the limitations on measurement accuracy make it virtually impossible to measure the true X_3 for a mono-fiber layer composite. Properties of the composite were predicted using the Closed Form Combination Model derived in section 3.3.4, and are summarized in Table 7.1.

Table 7.1: Manufactured Laminate Properties

MEASURED			CALCULATED				
X_2	X_3	$\frac{\varepsilon_{33}^T}{\varepsilon_o}$	X_3	$R_A = \frac{c_{22}^E}{c_{11}^E}$	$\zeta = \frac{d_{32}}{d_{31}}$	$\psi = \frac{c_{11}}{c_{11}^E}$	T
0.78	0.84	154	0.86	0.43	0.80	3.53	0.125

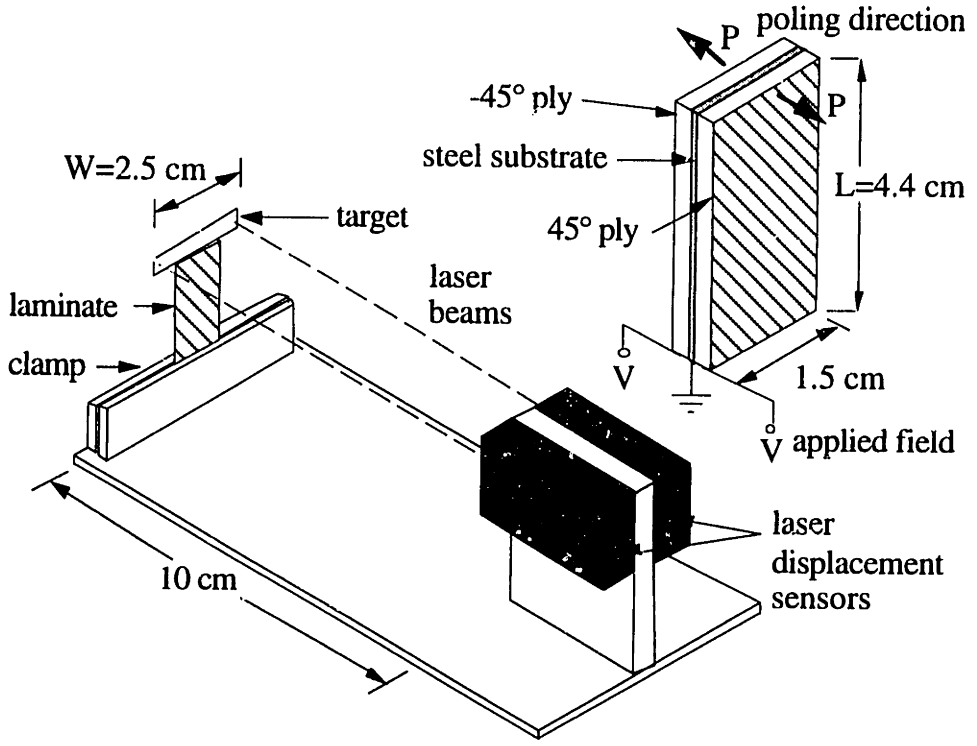

Figure 7.8: Experimental set-up for twist-extension coupled laminate

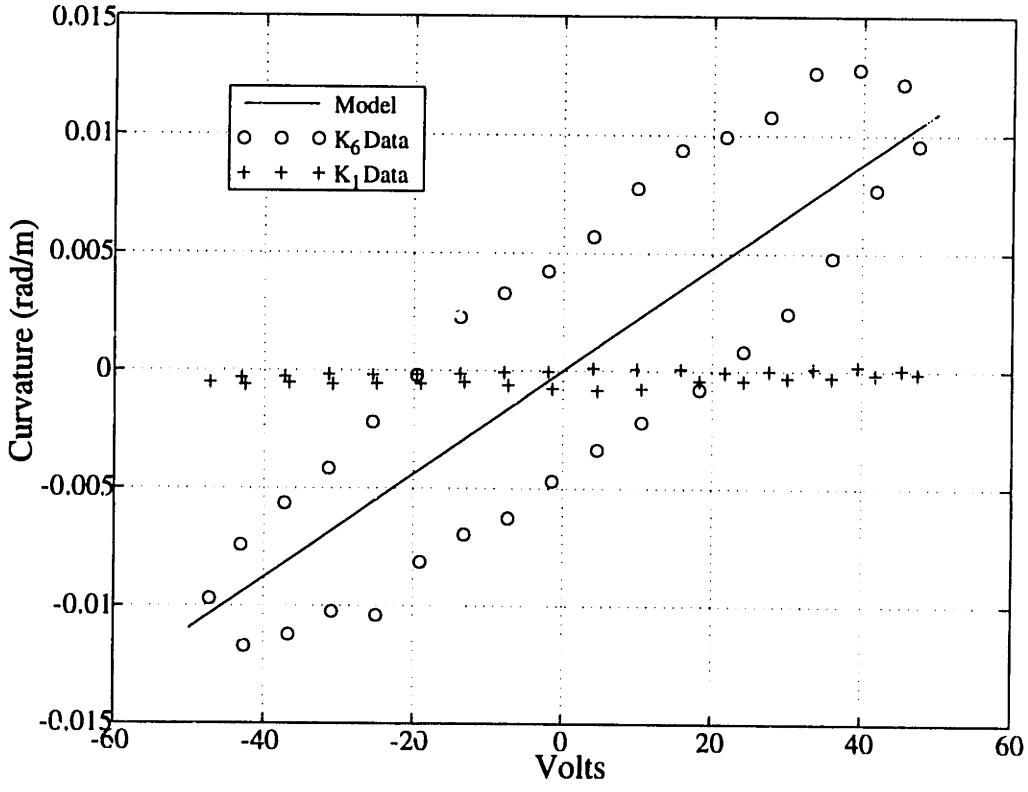

Figure 7.9: Comparison of data with model for twist-extension coupled laminate

The experimental setup is shown in Figure 7.9. The $[45_A/0_S/-45_A]$ laminate was clamped at its base, and fitted with a laser target. The active plies were actuated quasi-statically (0.005 Hz) to eliminate the majority of viscoelastic effects that may have been present from the matrix material. Actuation was in-phase, with a 100 volt peak-to-peak (0.5 kV/cm) triangular waveform. Tip displacements were measured using two laser displacement sensors[30], with 10 micron resolution. The differential outputs provided twist information, and average outputs provided bending information. Using this information and the laminate dimensions, the resulting twist and bending curvatures were calculated:

$$\kappa_6 = 2\kappa_{12} = \frac{2(D_1 - D_2)}{LW} \qquad \kappa_1 = \frac{(D_1 + D_2)/2}{L^2} \qquad (26)$$

Measurements D_1 and D_2 are the laser displacements, and L and W are the active length and width shown in Figure 7.9. Comparison of the experimental curvature strains with the CLPT model is given in Figure 7.10, where a single entire loop is shown. Excellent agreement is seen for both curvatures. The small magnitude of κ_1 shows that almost pure twist actuation was obtained. Deviation from the model is observed at higher field levels, as nonlinear effects become more important. Viscoelastic properties of the matrix material also play a role.

7.5 Summary

Chapter 7.0 described the experimental work carried out in the development of piezoelectric fiber composites. This work served two main purposes. It provided experimental values for the effective material parameters so that comparisons could be made with the developed models. It also examined the experimental response of the first laminated structure incorporating PFCs. Excellent agreement between the observed and the predicted curvatures showed that Classical Laminated Plate Theory was a valuable tool in examining these structures. This increased confidence also in the micro models from which the effective material properties were based. Finally, these experiments showed the feasibility of piezoelectric fiber composites for structural actuation.

---

[30] LB-70/LB-11 Proximity Sensors, Keyence Corporation

8.0 Conclusions and Recommendations

This chapter highlights the conclusions generated from the development of piezoelectric fiber composites for structural actuation. These conclusions draw from the insights learned both at the material, and at the structural levels. The upcoming sections follow the course of development that occurred in this study and this document, progressing from modeling to manufacturing, and to the application of the material to structures. The final section summarizes the accomplished work and makes recommendations for future research in this area.

8.1 Micro Electromechanical Models

Several micro-electromechanical models were advanced for the prediction of effective ply properties of a piezoelectric/matrix actuator material using a *Uniform Fields* approach. These models include a fully coupled numerical combination model, and a closed form combination model solution, the second of which lacked the induced stress terms but compared very well to the first model in the material regimes considered. A general methodology was also developed, so that materials of any connectivity could be analyzed through individual cases. These cases could then be combined to give the combination model for that material. In particular, these models were applied to the case of piezoelectric fiber composites with the fibers oriented in the plane. Finally, a discretized method was developed from this general approach which allowed for discretely varying fields across the volume element. An additional benefit derived from the model is the ability to model circular fibers, and adapt the scheme to approximate the actual experimental composite geometry.

Two elasticity models were also developed that allow continuous field variations within one or more material phases. The basis of the first of these elasticity models was developed from first principles using equations of elasticity and electrostatics. The two governing differential equations are shown to be coupled through the mechanical-electrical coupling present in the piezoelectric material. Assumptions applied to the governing equations led to the Self Consistent model which solved a boundary value problem to calculate the effective material constants. An approximate elasticity solution of the fully coupled equations was achieved by applying a Finite Element method.

Comparison of the five models provided excellent insight into the issues that dominate the response of the PZT fiber composite system. A high dielectric matrix system with low stiffness, and a very high through-thickness fiber line fraction is necessary to achieve substantial actuation. All of the models predict these trends, and compare very

well. The Self Consistent method agrees extremely well with the Finite Element method, especially for fiber volume fractions below 0.5. This is due primarily to the ability of these models to allow varying field distributions. At higher volume fraction, the best comparison with the Finite Element model is seen with the Discrete Uniform Fields model, which is best able to capture the modeled geometry at maximum volume fractions.

8.2 Optimizing Matrix Materials

A study was undertaken to examine the possibilities of modifying the properties of the matrix material to better serve the needs of the PZT fiber composite system. The issues of compliance and dielectric mismatch were discussed, and related to the goal of high composite actuation capability. The objective became to develop a matrix of high dielectric with compliance that remained low enough that the PZT fibers would not be significantly clamped. To accomplish the increase in dielectric, a fine PZT particulate filler was added to the epoxy. Predictions of increased dielectric and stiffness were made using simple uncoupled models for particulate systems. A substantial increase in dielectric was experimentally found, with the dielectric increasing 4-5 times over the pure epoxy for a filler fraction of 35%. An increase in stiffness was also found, as predicted by the models. A large difficulty arises from the *unpredicted* effects of particulate filler: serious embrittlement, lowered flexural strength, and much higher viscosity. The cause of these effects was attributed to interfacial phenomena at the filler-epoxy boundary, including adsorbed water and poor surface bonding chemistry.

The effect of surface modifying agents on the effective properties was next examined. A polymer dispersant was used as an agent to improve filler-matrix adhesion, by replacing water at the interface. Electrical properties of the composite were found to improves considerably, with the dielectric further increasing by 15-30% over the filler systems without dispersing agents. Little or no change was observed on the Young's Modulus of the matrix. The chemical additive also allowed for a better dispersion of particles, and reduced the incidence of aggregation into larger particle systems. An improvement in viscosity was qualitatively observed, and would allow introduction of the new matrix into the brittle fiber systems without damage. A final benefit of the agent was a tremendous reduction in brittleness of the matrix material after cure.

8.3 Manufacturing and Materials

Several methods of manufacturing were investigated toward producing conformable piezoelectric fiber composites. All of the methods used thus far involved hand lay-up of single PZT fibers into a mold designed for the particular shape and size of the specimen.

This is unlikely to change until the time comes when the technology exists for producing continuous PZT fibers. Cure materials and procedures have also been standard throughout the methods, and derive their origins from the curing of graphite/epoxy composite panels. This includes the use of a mold top and vacuum during cure to provide specimen uniformity and better compaction. The vacuum also helped reduce voids and remove excess epoxy, which could be collected in the porous cure materials. These procedures provided the specimens used for the effective property study.

As the manufacturing process became better understood, the techniques became more advanced. An autoclave system provided a better control over the cure process and allowed extra pressure on the composite, which was needed after the addition of the particulate-doped matrix. Different methods of electroding were also examined. The first specimens were sanded, exposing the piezoelectric and providing ceramic connectivity between the electrode faces. Electrodes were then deposited through a vapor deposition process. This method worked well and provided high actuation capability for the composites, and a maximum strain level comparable to that for monolithic PZT. Thin film polyimide electrodes were also examined, and this process holds promise for the advancement of PFC's to integrated composite structures. Difficulties lie in adhesion to the specimen at elevated temperatures, and the inability to pre-sand the specimens, thereby reduced the actuation capability. Nonetheless, such materials may hold the key to advanced manufacturing of piezoelectric fiber composites.

8.4 Mechanics of Anisotropic Actuation

The move to applications was undertaken to better understand the issues relating to structures, and to test the concept of piezoelectric fiber composites as structural actuators. This was accomplished through an investigation into the actuation of laminated structures with anisotropic active materials, and provided a motivation toward using tailorable anisotropic actuators such as PFCs. The study found that actuator anisotropy, which stems from different in-plane stiffness or actuation properties, contributes to an actuator's ability to induce unequal in-plane stress loads. The presence of this anisotropy in actuators enables shear stress to be induced for ply orientations not aligned with the principal ply axes. The incorporation of several of these active plies into laminated structures introduces the possibility of twist deformation in isotropic substructures. The predictions for this study were easily and effectively modeled using an augmented Classical Laminated Plate Theory which included actuator induced-stress terms, and the effective material properties from the Uniform Fields models.

A twist-extension coupled, antisymmetric laminate was chosen as an example for the study of induced twist. Induced twist was described as a function of structure thickness and actuator material anisotropies. Comparison of four separate actuators highlighted the fundamental difference between stiffness anisotropy and free-strain anisotropy effects. Actuators that have a relatively low transverse stiffness, such as PFC and DAP elements, are unable to induce large transverse loads without a substrate material to provide the structural stiffness. Optimizing the twist actuation requires a particular substrate-to-actuator thickness ratio. Actuators that have high transverse stiffness, such as the IDE and UDA, do not require substrate materials to induce high levels of twist. High levels of free-strain anisotropy enhance the twist actuation in these cases. Actuators that have very high stiffness anisotropy, such as DAP elements, would not benefit from added free-strain anisotropy. PFC's have the additional freedom of tailoring material geometry so that the optimum levels of anisotropy may be used for a particular set of material properties.

In order to demonstrate twist actuation in isotropic substrates, a $[45_A/0_S/-45_A]$ laminate was manufactured and tested. This laminate incorporated PFC actuators to induce the actuation loads. Excellent agreement was found between the experimental response and the response predicted through the CLPT model. The results show the feasibility of modeling PFC laminates with laminated plate theory, and further demonstrates the opportunities for anisotropic actuation using this new type of actuator.

8.5 Summary and Recommendations

This thesis has described the work undertaken toward the goal of large scale structural actuation and sensing using piezoelectric fiber reinforced composite plies. The subtasks identified in this study, composite property predictions and manufacturing technology development, have been carried out in order to meet this goal. Modeling of composites through micro electromechanical approaches has been well established, and the mechanics of these composites are now understood. These models are able to make reliable predictions for the effective mechanical, electrical, and coupled composite properties, and highlight the predominant effects that contribute to increased actuation capability. A means for piezoelectric fiber composites manufacturing was also developed, based on an extension of knowledge learned through graphite/epoxy composite manufacturing. These techniques have been advanced so that mono-fiber layer composites may be manufactured for the experimental characterization of composite properties and for initial use in laminated active structures.

The future directions will involve improvements aimed at the material level and at the structural level. Increased actuation performance will be the focus of the material level

investigations. Improvements should be made in the manufacturing process that will allow consistent composite quality with higher actuation. This will involve a better understanding of cure kinetics to optimize temperature, time, and pressure for increased compaction and higher through thickness fiber fractions. Further optimization of the matrix should also be pursued with the goal of higher dielectric and lower viscosity in mind. This may be possible by investigating other surface modifying agents for a better match with the present filler/epoxy system. An substantial improvement in dielectric may be achieved by an application of electrophoresis techniques to the manufacturing methods. In this way, it may be possible to create high dielectric pathways between the electrodes and the fibers, more uniformly distributing the electric field lines.

Future work will also continue to improve piezoelectric fiber composites toward structural applications. The present work has shown that high twist actuation is achieved in thin structures with transversely stiff actuators, whereas high actuation capabilities discern the actuators used with thicker structures. Interdigitated electrode piezoceramics have these characteristics and demonstrate good twist actuation throughout the range of structure sizes. However, issues of conformability, reliability, and the benefit of tailoring still point to piezoelectric fiber composites as an attractive alternative to monolithic ceramics. The next step will be to combine these two technologies. The use of etched copper/Kapton electrodes will permit interdigitated electrodes on piezoelectric fiber composites. This new approach, in conjunction with improved matrix material properties, has the potential to make piezoelectric fiber composite actuators extremely advantageous for structural control applications.

References

[1]Hagood, N.W. and von Flotow, A.H., "Damping of Structural Vibrations with Piezoelectric Materials and Passive Electrical Networks," *Journal of Sound and Vibration*, April-May, 1991.

[2]Anderson, E.H., Hagood, N.W., and Goodliffe, J.M., "Self-Sensing Piezoelectric Actuation: Analysis and Application to Controlled Structures," AIAA Paper No. 92-2645, *AIAA Conference on Structures, Structural Dynamics, and Materials*, Dallas, TX, April 13-15, 1992.

[3]Forward, R.L. and Swigert, C.J., "Electronic Damping of Orthogonal Bending Modes in a Cylindrical Mast-Theory," *Journal of Spacecraft and Rockets*, January-February, 1981.

[4]Fanson, J.L. and Caughey, T.K., "Positive Position Feedback Control for Large Space Structures," *AIAA Journal*, Vol. 28, No. 4, pp. 717-724, April 1990.

[5]Hanagud, S., Obal, M.W., and Calise, A.J., "Optimal Vibration Control by the Use of Piezoceramic Sensors and Actuators," *Proceedings 28th AIAA/ASME/ASCE/AHS Structures, Structural Dynamics, and Materials Conference*, AIAA Paper No. 87-0959, pp. 987-997, Monterey, California, April 1987.

[6]Hagood, N.W., Chung, W.H., and von Flotow, A.H., "Modelling of Piezoelectric Actuator Dynamics for Active Structural Control," *Journal of Intelligent Material Systems and Structures*, Vol. 1, No. 3, pp. 327-354, July 1990.

[7]Hagood, N.W., Crawley, E.F., de Luis, J., and Anderson, E.H., "Development of Integrated Components for Control of Intelligent Structures," *Smart Materials, Structures, and Matematical Issues*, Technomic Publishing Co., pp. 80-104, 1989.

[8]Lazarus, K. and Crawley, E.F., "Multivariate High-Authority Control of Plate-Like Active Structures," AIAA Paper No. 92-2529, *AIAA Conference on Structures, Structural Dynamics, and Materials*, Dallas, TX, April 13-15, 1992.

[9]Ehlers, S.M. and Weisshaar, T.A., "Static Aeroelastic Behavior of an Adaptive Laminated Piezoelectric Composite Wing," AIAA Paper No. 90-1078, *Proceedings of the 31st AIAA./ASME/ASCE/AHS Structures, Structural Dynamics, and Materials Conference*, Long Beach, CA, April 1990.

[10]Pines, D. and von Flotow, A.H., "Active Control of Bending Wave Propagation at Acoustic Frequencies," *Journal of Sound and Vibration*, In Press, 1990.

[11]Rogers, C.A. and Fuller, C.R., "Recent Advances in Active Control of Sound and Vibration," *Proceedings of the VPI and SU Conference on Recent Advances in Active Control of Sound and Vibration*, Blacksburg, VA, April 1991.

[12]Crawley, E.F. and de Luis, J., "Use of Piezoelectric Actuators as Elements of Intelligent Structures," *AIAA Journal*, Vol. 25, No. 10, 1987.

[13]Warkentin, D.J. and Crawley, E.F., "Prospects for Electronic Component Distribution in Intelligent Structures," *ADPA/AIAA/ASME/SPIE Conference on Active Materials and Adaptive Structures*, Alexandria, VA, Nov. 5-7, 1991.

[14]Crawley, E.F.and Lazarus, K., "Induced Strain Actuation of Isotropic and Anisotopic Plates", AIAA Journal, Vol. 29, No. 6, June 1991, pp. 944-951.

[15]Barrett, R., "Aeroservoelastic DAP Missile Fin Development", *Third International Conference on Adaptive Srtuctures*, 1992.

[16]Yoshikawa, S., Selvaraj, U., Brooks, K.G., and Kurtz, S.K., "Piezoelectric PZT Tubes and Fibers for Passive Vibrational Damping," *IEEE ISAF '92*, Greenville, SC, Aug. 31-Sept. 3, 1992.

[17]Blackwood, G.H. and Ealey, M.A., "Electrostricitve Behavior in Lead Magnesium Niobate (PMN) Actuators. Part 1: Materials Perspective", Smart Materials and Structures, No. 2, pp 124-133, 1993.

[18]Berlincourt, D., "Transducers Using Forced Transitions Between Ferroelectric and Antiferroelectric States", *IEEE Transactions on Sonics and Ultrasonics*, Vol. SU-13, No.4, pp. 116-125, October 1966.

[19]Ghandi, K. and Hagood, N.W., "Shape Memory Ceramic Actuation of Adaptive Structures", to be published in *Proceedings of 35th AIAA./ASME/ASCE/AHS Structures, Structural Dynamics, and Materials Conference*, Hilton Head, NC, 1994.

[20]Newnham, R.E., Bowen, L.J., Klicker, K.A., Cross, L.E., "Composite Piezoelectric Transducers", *Materials Engineering*, No. 2, pp 93-106, 1980.

[21]Smith, W.A., "The Role of Piezocomposites in Ultrasonic Transducers", *Proceedings of the 1989 IEEE Ultrasonics Symposium*, Montreal, Quebec, October 1989.

[22]Waller, D.J. and Safari, A., "Piezoelectric Lead Zirconate Titanate Ceramic Fiber/Composites", *Journal of the American Ceramic Society*, No. 6, Vol. 75, 1992.

[23]Jones, R.M., *Mechanics of Composite Materials*, Hemisphere Publishing Corporation, New York, 1975.

[24]Hermans, J.J., "The Elastic Properties of Fiber Reinforced Materials when the Fibers are Aligned", *Pro. Konigl. Nedel. Akad. van Wetenschppen*, Amsterdam, B70(1):1-9, 1967.

[25]Hashin, Z.and Rosen, B.W., "The Elastic Moduli of Fiber Reinforced Materials", *Journal of Applied Mechanics*, 31, 1-9, 1964.

[26]Whitney, J.M. and Riley, M.B., "Elastic Properties of Fiber Reinforced Materials", *AIAA Journal*, No. 9, Vol. 4, 1966.

[27]Farmer, J.P., "Heat Transfer in an Anisotropic Thermosetting Advanced Composite During its Cure", S.M. Thesis, MIT, January 1993.

[28]Thornborough, J.D. and Pears, C.D., *ASME Paper 65-WA/HT4*, 1965.

[29]Rayleigh, L., :On the Influence of Obstacles Arranged in Rectangular Order upon the Properties of a Medium", *Philosophical Magazine*, 34:481, 1892.

[30]Landauer, R., "The Electrical Resistance of Binary Metallic Mixtures", *Journal of Applied Physics*, Vol. 23, pg 779, 1952.

[31]Kerner, E.H., "The Electrical Conductivity of Composite Media",*Proceedings of the Physics Society* (B), Vol. 69, pg 808, 1956.

[32]Hashin, "Assessment of the Self Consistent Scheme Aproximation: Conductivity of Particulate Composites", *Journal of Composite Materials*, Vol. 2, 1968.

[33]Farmer, J.D. and Covert, E.E., "Transverse Thermal Conductance of Thermosetting Composite Materials During Their Cure", *Proceedings of 34th AIAA./ASME/ASCE/AHS Structures, Structural Dynamics, and Materials Conference*, La Jolla, CA., April 1993.

[34]Hashin, Z. and Shtrikman, S., "A Variational Approach to the Theory of the Effective Magnetic Permeability of Multiphase Materials", *Journal of Applied Physics*, No. 10, Vol. 33, pp 3125-3131, 1962.

[35]Han, L.S. and Cosner, A.A., "Effective Thermal Conductivities of Fibrous Composites", *Journal of Heat Transfer*, Vol. 103, May 1981.

[36]Banno, H.," Recent Developments of Piezoelectric Ceramic Products and Composites of Synthetic Rubber and Piezoelectric Ceramic Particles", *Ferroelectrics*, Vol. 50, pp 3-12, 1983.

[37]Smith, W.A. and Auld, B.A., "Modeling 1-3 Composite Piezoelectrics: Thickness-Mode Oscillations", *IEEE Transactions on Ultrasonics, Ferroelectric, and Frequency Control*, 1990.

[38]Pak, Y.E., "Circular Inclusion Problem in Antiplane Piezoelectricity", submitted to *International Journal of Solids and Structures.*

[39]Honein, T., Honein, B., Honein, E., Herrmann, G., "On Piezoelectric Circular Inclusions", *Mechanical Modeling of New Electromagnetic Materials*, ed: R.K.T. Hsieh, Elsevier Science Publishers, 1990.

[40]Sottos, N., *Proceedings of the ASME Winter Annual Meeting*, New Orleans, November 1993.

[41]Collins, S.A., Miller, D.W., and von Flotow, A.H., "Piezopolymer Spatial Filters for Active Structural Control", *Proceedings of the VPI and SU Conference of Recent Advances in Active Control of Sound and Vibration*, Blacksburg, VA, April 1991.

[42]Hagood, N.M., Kindel, R., Ghandi, K., and P. Gaudenzi, 1993. "Improving Transverse Actuation of Piezoceramics using Interdigitated Surface Electrodes." SPIE Paper No. 1917-25, *Proceedings of the 1993 North American Conference on Smart Structures and Materials*, Albuquerque, NM.

[43]Tiersten, H.F., *Linear Piezoelectric Plate Vibrations*, Plenum Press, New York, 1969.

[44]IEEE Std 176-1978, *IEEE Standard on Piezoelectricity*, The Institute of Electrical and Electronics Engineers, 1978.

[45]Xu, Y.H., *Ferroelectric Materials and Their Applications*, Elsevier Science Publishing Company, Amsterdam, 1991.

[46]Lines, M.E. and Glass, A.M., *Principles and Applications of Ferroelectric and Related Materials*, Clarendon Press, Oxford, 1977.

[47]Timoshenko, S.P. and Goodier, J.N., *Theory of Elasticity*, 2nd Edition, McGraw-Hill, New York, 1951.

[48]Lekhnitskii, S.G., *Theory of Elasticity of an Anisotropic Body*, Mir Publishers, Moscow, 1981.

[49]Polder, D. and Van Santen, J.H., "The Effective Permeability of Mixtures of Solids", Physica XII, No. 5, pp 257-271, 1946.

[50]Hill, R., "A Self Consistent Mechanics of Composite Materials", *Journal of Mechanics and Physics of Solids*, Vol. 13, pp. 213-222, 1965.

[51]Hershey, A.V., "The Elasticity of an Isotropic Aggregate of Anisotropic Cubic Crystals", *Journal of Applied Mechanics*, Vol. 21, pp. 236-240, 1954.

[52]Hashin, Z., "Assessment of the Self Consistent Scheme Approximation: Conductivity of Particulate Composites", *Journal of Composite Materials*, Vol. 2, pp. 284-300, 1968.

[53]Hill, R., "Theory of Mechanical Properties of Fibre-Strengthened Materials: I. Elastic Behavior", *Journal of Mechanics and Physics of Solids*, Vol. 12, pp. 199-212, 1964.

[54]Hashin, Z., "Analysis of Composite Materials-A Survey", *Journal of Applied Mechanics*, Vol. 50, pp. 481-505, 1983.

[55]Eshelby, J.D., "The Determination of the Field of an Ellipsoidal Inclusion and Related Problems", *Proceedings of the Royal Society*, London, Vol. A, No. 241, pp. 376-396, 1957.

[56]Gaudenzi, P. and Bathe, K.J., "An Iterative Finite Element Procedure for the Analysis of Electroelastic Materials", *Proceedings of the Fourth International Conference on Adaptive Structures*, Paper 93-04-06, Cologne, FRG, 1993.

[57]Allik, H. and Hughes, T.J.R., "Finite Element Method for Piezoelectric Vibration", *International Journal for Numerical Methods in Engineering*, Vol. 2, pp. 151-157, 1970.

[58]Cook, R.D., Malkus, D.S., Plesha, M.E., *Concepts and Applications of Finite Element Analysis*, 3rd Edition, John Wiley & Sons, New York, 1989.

[59]*Ansys Engineering Analysis System Theoretical Manual*, Swanson Analysis Systems Inc., Houston, PA, 1989.

[60]Flinn, R.A. and Trojan, P.K., Chapter 9: Plastics(High Polymers): Structures and Properties, *Engineering Materials and Their Applications*, 3rd Edition, Houghton Mifflin Co., Boston, 1986.

[61]Bent, A.A. and Castro, Z., Unpublished results for the coercive field of PZT 5H type ceramics versus temperature, August 1993.

[62]Rushau, G.R. and Newnham, R.E.,"Critcal Volume Fractions in Conductive Composites, Journal of Composite Materials, Vol. 26, No. 18, 1992.

[63]Sax, J. and Ottino, J.M., "Modeling of Transport of Small Molecules in Polymer Blends: Application of Effective Medium Theory", *Polymer Engineering and Science*, Vol. 23, No. 3, February, 1983.

[64]Paul, B., "Prediction of Elastic Constants of Multiphase Materials", Trans Metallurgical Society of AIME, Vol. 218, pp. 36-41, February, 1960.

[65]Halpin, J.C. and Tsai, S.W., "Effects of Environmental Factors on Composite Materials", *AFML-TR 67-423*, June, 1969.

[66]Ferrigno, T.H., "Principles of Filler Selection and Use", from *Handbook of Fillers for Plastics*, ed: H.S. Katz and J.V. Milewski, Van Nostrand Reinhold Company, New York, 1987.

[67]Berger, S.E. and Petty, H.E., "Organofunctional Silanes", from *Handbook of Fillers for Plastics*, ed: H.S. Katz and J.V. Milewski, Van Nostrand Reinhold Company, New York, 1987.

[68]Vash, R., "Wetting and . ·nersing", in *Handbook of Coatings and Additives*, ed: Call.., E.J., Marcel Dekker, New York, 1987.

[69]Fowkes, F.M., "Acid-Base Interactions", from *Encyclopedia of Polymer Science and Engineering*, Vol. S(supplement), John Wiley & Sons, New York.

[70]Fowkes, F.M., "Acid-Base Interactions in Polymer Adhesion", from *Physiochemical Aspects of Polymer Surfaces*, Vol.2, ed: K. Mittal, Plenum Press, New York, 1981.

[71]Fowkes, F.M, Dwight, D.W., Manson, J.A., Lloyd, T.B., Tischler, D.O., Shah, B.A., "Enhancing Mechanical Properties of Polymer Composites by Modification of Surface Acidity or Basicity of Fillers", *Material Research Society Proceedings*, Vol. 119, 1988.

[72]Hibbert, P., Personal Communication, ICI Surfactants, ICI Americas Inc., Wilmington, DE, September, 1993.

[73]Pleuddemann, E.P., Interfaces in Polymer Matrix Composites, in *Composite Materials*, Ed: L.J. Broutman and R.H. Krock, Vol. 6, Academic Press, New York, 1974.

[74]Crawley, E.F. and Anderson, E.H., "Detailed Models of Piezoceramic Actuation of Beams.", *Journal of Intelligent Material Systems and Structures*, 1:4-25, 1990.

[75]Jia, J. and Rogers, C.A., "Formulation of a Laminated Shell Theory Incorporating Embedded Distributed Actuators.", *Adaptive Structures*, AD-Vol. 15, Ed: B.K. Wada, ASME, NY, 1989.

[76]Barrett, R.M., "Modeling Techniques and Design Principles of a Low Aspect Ratio Active Aeroservoelastic Wing." Paper No. 1917-10, *Proceedings of the 1993 North American Conference on Smart Structures and Materials*, Albuquerque, NM, 1993.

[77]Ehlers, S. M. and Weisshaar, T. A. "Effect of Adaptive Material Properties on Static Aeroelastic Control." AIAA Paper No. 92-2526, *Proceedings of the 33rd AIAA Structures, Structural Dynamics, and Materials Conference*, Dallas, TX, 1992.

[78]Skinner, D.P., Newnham, R.E., and Cross, L.E. "Flexible Composite Transducers." *Material Research Bulletin*, 13:599-607, 1978.

[79]Hagood, N.W. and A. A. Bent "Development of Piezoelectric Fiber Composites for Structural Actuation." AIAA Paper No. 93-1717, *Proceedings of the 34th AIAA Structures, Structural Dynamics, and Materials Conference*, La Jolla, CA, 1993.

[80]Bent, A.A., Hagood, N.W., Rodgers, J.P., "Anisotropic Actuation with Piezoelectric Fiber Composites", *Proceedings of the Fourth International Conference on Adaptive Structures*, Paper 93-04-36, Cologne, FRG, 1993.

[81]Chan, K., "Nonlinear Modeling Aspects of Piezoceramic Materials", S.M. Thesis, MIT, January 1994.

[82]Bent, A.A. and Cohen, L., Unpublished results for the stiffness characterization of fine piezoceramic fibers, December 1993.

Appendix A: Nomenclature

The folowing nomenclature is used throughout this manuscript:

s_{ij}^{E}	ijth piezoceramic compliance, short circuit condition
d_{ij}	ijth piezoceramic voltage-to-strain coeficient
ε_{ij}^{T}	ijth piezoceramic dielectric, constant stress conditions
s_{ij}	ijth matrix compliance
ε_{ij}	ijth matrix dielectric
S_i	ith direction material strains
T_i	ith direction material stress
D_i	ith direction electrical displacement
E_i	ith direction electric field
p	piezoceramic material phase superscript
m	matrix material phase superscript
v_i^p	volume fraction of piezoceramic in ith direction
A	superscript for fully coupled case A material combination
B	superscript for fully coupled case B material combination
A'	superscript for closed form case A material combination
B'	superscript for closed form case B material combination
A	reorganized matrix of constitutive constants for case A
B	reorganized matrix of constitutive constants for case B
eff	superscript for closed form combination model

Note that 'p' and 'f' are used interchangeably for the piezoceramic (fiber) phase

Appendix B: Uniform Fields Formulations

The terms of the reorganized constitutive equations for Case A (equation 3.9) are as follows:

$$a_{11} = \frac{s_{11}^E \varepsilon_{33}^T - d_{31}^2}{(s_{12}^E - s_{11}^E)(-\varepsilon_{33}^T (s_{12}^E + s_{11}^E) + 2d_{31}^2)}$$

$$a_{12} = \frac{s_{12}^E \varepsilon_{33}^T - d_{31}^2}{(s_{12}^E - s_{11}^E)(-\varepsilon_{33}^T (s_{12}^E + s_{11}^E) + 2d_{31}^2)}$$

$$a_{13} = \frac{s_{13}^E \varepsilon_{33}^T - d_{31} d_{33}}{(s_{12}^E - s_{11}^E)(-\varepsilon_{33}^T (s_{12}^E + s_{11}^E) + 2d_{31}^2)}$$

$$a_{15} = \frac{d_{31}}{-\varepsilon_{33}^T (s_{12}^E + s_{11}^E) + 2d_{31}^2} \qquad a_{35} = \frac{-d_{33}(s_{12}^E + s_{11}^E) + 2d_{31} s_{13}^E}{-\varepsilon_{33}^T (s_{12}^E + s_{11}^E) + 2d_{31}^2}$$

$$a_{33} = \frac{(s_{12}^E + s_{11}^E)(d_{33}^2 - s_{33}^E \varepsilon_{33}^T) + 2(s_{13}^{E\,2} \varepsilon_{33}^T - 2d_{31} d_{33} s_{13}^E + s_{33}^E d_{31}^2)}{(s_{12}^E - s_{11}^E)(-\varepsilon_{33}^T (s_{12}^E + s_{11}^E) + 2d_{31}^2)}$$

$$a_{44} = \frac{1}{s_{66}^E} \qquad a_{55} = \frac{-(s_{12}^E + s_{11}^E)}{-\varepsilon_{33}^T (s_{12}^E + s_{11}^E) + 2d_{31}^2}$$

The terms of the reorganized constitutive equations for Case B (equation 3.24) are as follows:

$$b_{11} = \frac{s_{33}^E}{s_{33}^E s_{11}^E - s_{13}^{E\,2}} \qquad b_{12} = \frac{-s_{12}^E s_{33}^E + s_{13}^{E\,2}}{s_{33}^E s_{11}^E - s_{13}^{E\,2}} \qquad b_{13} = -\frac{s_{13}^E}{s_{33}^E s_{11}^E - s_{13}^{E\,2}}$$

$$b_{15} = \frac{d_{33} s_{13}^E - d_{31} s_{33}^E}{s_{33}^E s_{11}^E - s_{13}^{E\,2}} \qquad b_{22} = \frac{(s_{11}^{E\,2} - s_{12}^{E\,2}) s_{33}^E + 2(s_{12}^E - s_{11}^E) s_{13}^{E\,2}}{s_{33}^E s_{11}^E - s_{13}^{E\,2}}$$

$$b_{33} = \frac{s_{11}^E}{s_{33}^E s_{11}^E - s_{13}^{E\,2}} \qquad b_{23} = \frac{s_{13}^E (s_{11}^E - s_{12}^E)}{s_{33}^E s_{11}^E - s_{13}^{E\,2}} \qquad b_{44} = s_{66}^E$$

$$b_{25} = \frac{(-d_{31} s_{33}^E + d_{33} s_{13}^E)(s_{12}^E - s_{11}^E)}{s_{33}^E s_{11}^E - s_{13}^{E\,2}} \qquad b_{35} = \frac{d_{31} s_{13}^E - d_{33} s_{11}^E}{s_{33}^E s_{11}^E - s_{13}^{E\,2}}$$

$$b_{55} = \frac{\varepsilon_3^T (s_{33}^E s_{11}^E - s_{13}^{E\,2}) + (-s_{33}^E d_{31}^2 - s_{11}^E d_{33}^2 + 2d_{31} d_{33} s_{13}^E)}{s_{33}^E s_{11}^E - s_{13}^{E\,2}}$$

The remaining effective property terms for the fully coupled case B combination of piezoceran

$$s_{22}^B = \frac{f_{12}(f_{12} f_{33} + f_{13} f_{23}) + f_{22}(f_{11} f_{33} - f_{13}^2) + f_{23}(f_{11} f_{23} + f_{12} f_{13})}{(f_{11} f_{33} - f_{13}^2)}$$

$$d_{32}^{B} = \frac{f_{14}(f_{12}f_{33} + f_{13}f_{23}) + f_{24}(f_{11}f_{33} - f_{13}^2) - f_{34}(f_{11}f_{23} + f_{12}f_{13})}{(f_{11}f_{33} - f_{13}^2)}$$

$$\varepsilon_{33}^{B} = \frac{f_{34}(f_{11}f_{34} - f_{13}f_{14}) + f_{44}(f_{11}f_{33} - f_{13}^2) - f_{14}(f_{13}f_{34} - f_{14}f_{33})}{(f_{11}f_{33} - f_{13}^2)}$$

where, for the b_{ij} given above:

$$f_{ij} = v_2^p b_{ij}^p + v_2^m b_{ij}^m$$

Appendix C: Self Consistent Fields Formulations

The terms of the A and D matrices from equation 3.126 are as follows:

$$A_{11} = X_2\beta_{11}^m - \beta_{12}^m + \beta_{11}^f + \beta_{12}^f \quad A_{12} = X_2\beta_{11}^m - \beta_{12}^m + \beta_{12}^f + \beta_{22}^f \quad A_{13} = \beta_{15}^f + \beta_{56}^f$$

$$A_{21} = -X_1\beta_{11}^m + \beta_{12}^m + \beta_{11}^f - \beta_{12}^f \quad A_{22} = X_1\beta_{11}^m - \beta_{12}^m + \beta_{12}^f - \beta_{22}^f \quad A_{23} = \beta_{15}^f - \beta_{56}^f$$

$$A_{31} = \beta_{15}^f \qquad A_{32} = \beta_{16}^f \qquad A_{33} = -X_5\beta_{44}^m + \beta_{55}^f$$

$$A_{44} = 2X_1\beta_{11}^m - 2\beta_{12}^m - \beta_{66}^f \qquad A_{45} = -\beta_{14}^f$$

$$A_{54} = \beta_{14}^f \qquad A_{55} = -X_5\beta_{44}^m + \beta_{44}^f$$

$$D_{11} = 2\beta_a^m - \beta_a^f - \beta_b^f \quad D_{21} = \frac{2\beta_{11}^m}{1 - v_f} \quad D_{21} = \frac{2\beta_{11}^m}{1 - v_f}$$

$$D_{21} = -\beta_a^f + \beta_b^f \quad D_{22} = (1 - X_1)\beta_{11}^m \quad D_{23} = -(1 - X_1)\beta_{11}^m$$

$$D_{31} = -\beta_c^f \qquad D_{34} = -\frac{2\beta_{44}^m}{1 - v_f}$$

The effective material constants may be expressed in terms of the C matrix in equation 3.128, t strain material constants, and the fiber volume fraction:

$$\beta_a^{eff} = X_4C_{11} + X_3C_{21} + \beta_a^m \qquad \beta_b^{eff} = X_3C_{11} + X_4C_{21} + \beta_a^m$$

$$\beta_{56}^{eff} = X_3C_{12} + X_4C_{22} \qquad \beta_{15}^{eff} = X_4C_{12} + X_3C_{22}$$

$$\beta_{11}^{eff} = X_4C_{13} + X_3C_{23} + X_5 \qquad \beta_{12}^{eff} = X_3C_{13} + X_4C_{23} - X_3 + \beta_{12}^m$$

$$\beta_{22}^{eff} = X_3C_{14} + X_4C_{24} + X_5$$

$$\beta_c^{eff} = v_f(C_{12}\beta_a^f + C_{22}\beta_b^f + C_{32}\beta_c^f) + C_{12}(X_6\beta_a^m + X_7\beta_b^m) + C_{22}(X_7\beta_a^m + X_6\beta_b^m)$$

$$\beta_d^{eff} = v_f(C_{11}\beta_a^f - C_{21}\beta_b^f - C_{31}\beta_c^f) + C_{11}(-X_6\beta_a^m - X_7\beta_b^m)$$
$$+ C_{21}(-X_7\beta_a^m - X_6\beta_b^m) + \beta_d^f v_f + \beta_d^m(1 - v_f)$$

where

$$X_1 = -\frac{v_f^3 + 5v_f^2 + 7v_f + 3}{(1-v_f)^3} \quad X_2 = \frac{v_f + 1}{1 - v_f}$$

$$X_3 = \frac{v_f(v_f^2 + 4v_f + 3)}{(1-v_f)^3}\beta_{11}^m \quad X_4 = -\frac{v_f(3v_f^2 + 5)}{(1-v_f)^3}\beta_{11}^m \quad X_5 = \frac{2v_f^3 + 3v_f^2 + 2v_f + 1}{(1-v_f)^3}\beta_{11}^m$$

$$X_6 = \frac{v_f(2v_f^2 + 3v_f - 4)}{2(v_f^2 + 2v_f - 1)} \quad X_7 = \frac{v_f(v_f + 2)}{2(v_f^2 + 2v_f - 1)}$$

Appendix D: FEM Analysis File

```
/COM,ANSYS REVISION 4.4   UP437 A125    15.1614    8/11/1993
/COM      FILE: PFCa18.dat
/COM Last Revision: Dec. 27, 1993
/prep7
/show,x11
/PNUM,KPOI,1
/PNUM,LINE,1
/PNUM,AREA,1
/PNUM,VOLU,1
/TITLE,Piezoelectric Fiber Composite
KAN,0
KAY,10,1
ET,1,98
/COM
/COM                    * Fiber - Full 3D properties
/COM
c11=79.4e9
c12=32.4e9              * (All c's used only for matrix defn)
c44=23.5e9              * NOTE: Ansys has c44 what should be c66
K33T=3400               * (K33T - not used except for matrix defn)
NL,1,271,127e9,80.2e9,84.7e9
NL,1,277,127e9,84.7e9
NL,1,282,117e9
NL,1,286,23.5e9
NL,1,289,23e9
NL,1,291,23e9
NL,1,145,-6.5,-6.5,23.3
NL,1,103,15e-9          * (K11S=1700)
NL,1,157,15e-9
NL,1,211,13e-9          * (K33S=1470)
NL,1,138,17.0
NL,1,143,17.0
/COM
/COM                  * Matrix
/COM
```

```
Re=100                  * Dielectric Ratio
Rc=20                   * Stiffness Ratio
c11m=c11/Rc
c12m=c12/Rc
c66m=c44/Rc
K33m=K33T/Re*8.85e-12
NL,2,103,K33m
NL,2,157,K33m
NL,2,211,K33m
NL,2,271,c11m,c12m,c12m
NL,2,277,c11m,c12m
NL,2,282,c11m
NL,2,286,c66m
NL,2,289,c66m
NL,2,291,c66m
NL,2,145,-0.0000065,-0.0000065,0.0000233   * Tiny matrix piezoelectric const
NL,2,138,0.000017
NL,2,143,0.000017
Xf=0.98                 * Line Fraction of Fiber
E3=100                  * Electric Field (volts/mil)
V3=(E3/25.4*1e6)            * Voltage across 1 m thickness
dep=0.10                * Depth of Model
Ax=1*1
Ay=dep*1
Az=dep*1
K,1                         * Keypoints
K,2,,Xf
K,3,,1
K,4,,1,0.5
K,5,,1,1
K,6,,0.5,1
K,7,,0,1
K,8,,Xf
KGEN,2,1,8,,-dep
A,1,2,10,9
VROTAT,1,,,,,,1,9,-90,4             * Volumes
VATT,1,,1
V,2,3,4,17,10,11,12,18
V,17,4,5,19,18,12,13,20
V,19,5,6,21,20,13,14,22
V,21,6,7,23,22,14,15,24
VLSEL,VOLU,5,8
VATT,2,,1
VLALL
KDVS,ALL,0.2            * Element Size Specs
KDVS,6,0.15
```

```
KDVS,14,0.15
KDVS,7,0.1
KDVS,15,0.1
/COM KDVS,19,0.15
/COM KDVS,20,0.15
/COM KDVS,23,0.1
/COM KDVS,24,0.1
LDVA
VMESH,1,8                    * Mesh
CPSIZE,398
NSEL,Z,0                     * Select nodes for wavefront reordering
WSTART,ALL
WAVES
/COM
/COM    Load Case #1 Boundary Conditions and Loading - Apply E Field
/COM
NSEL,Z,0                     * Apply ground electrode electrical BC
NT,ALL,VOLT,0
NSEL,Z,1                     * Apply top electrode electrical BC
NT,ALL,VOLT,V3
CP,3,UZ,ALL                  * Couple top face nodes in Z
NSEL,X,0                     * Couple front face nodes in X
CP,1,UX,ALL
*GET,N1,NMIN
NSEL,Y,1                     * Couple right face nodes in Y
/COM CP,2,UY,ALL
*GET,N2,NMIN
NSEL,X,-dep          * Apply symmetry to back face nodes in X
SYMBC,0,1,ALL
NSEL,Y,0                     * Apply symmetry to left face nodes in Y
SYMBC,0,2,ALL
NSEL,Z,0                     * Apply symmetry to bottom face nodes in Z
SYMBC,0,3,ALL
NALL
LWRITE
/COM
/COM     Load Case #2 Boundary Conditions and Loading - Apply Ux Displ
/COM
D,N1,UX,0.01                 * Apply front face displacement Ux
NSEL,Z,1,0
NT,ALL,VOLT,0                * Apply Short-Circuit Conditions
NALL
LWRITE
/COM
/COM    Load Case #3 Boundary Conditions and Loading - Apply Uy Displ
/COM
```

```
DDELE,N1,UX                * Remove front face displacement Ux
NALL
NSEL,Y,1
CP,2,UY,ALL
D,N2,UY,0.1          * Apply right face displacement Uy
NALL
LWRITE
AFWRITE
FINISH
/COM          *** Solution Phase ***
/INPUT,27
FINISH
/COM                 *** Post Process ***
/POST1
NFILE
/COM
SET,1,3              *** First Loadcase ***
NSEL,Z,1
FSUM
*GET,chg1,FSUM,AMPS
NALL
*GET,ux1,UX,N1
*GET,uy1,UY,N2
/COM
SET,2,3                *** Second Loadcase ***
*GET,ux2,UX,N1
NSEL,X,0
FSUM
*GET,fx2,FSUM,FX
Tx=fx2/Ax
*GET,uy2,UY,N2
/COM
SET,3,3                *** Third Loadcase ***
*GET,ux3,UX,N1
NSEL,Y,1
FSUM
*GET,fy3,FSUM,FY
Ty=fy3/Ay
*GET,uy3,UY,N2
/OUTPUT,Const
K33=chg1/Az/V3
d31=ux1/dep/V3
d32=uy1/V3
s11=ux2/dep/Tx
s12a=uy2/1/Tx
s12b=(ux3/dep)/Ty
```

```
s22=(uy3/1)/Ty
/OUTPUT
/SHOW,Plots,,1              *** Plotting ***
/VUP,1,Z
/VIEW,1,2,2,1
/TYPE,1,4
NALL
SET,1,3
/CONTOUR,1,,AUTO
/CLABEL,1,-1
PLNSTR,VOLT
PLNSTR,SIGE,0
FINISH
```